

The role of the telomere bouquet in controlling
spindle pole body composition in
fission yeast meiosis

Cécile Bez

University College London

and

Cancer Research UK London Research Institute

PhD Supervisor: Dr Julia Promisel Cooper

A thesis submitted for the degree of

Doctor of Philosophy

University College London

September 2011

Declaration

I Cécile Bez confirm that the work presented in this thesis is my own. Where information has been derived from other sources, I confirm that this has been indicated in the thesis.

Abstract

The telomere bouquet is a highly conserved structure specific to meiotic prophase in which the telomeres are gathered to a limited region of the nuclear periphery. In a number of organisms including fission yeast, the bouquet is tethered to the spindle pole body (SPB) or centrosome. The meiosis-specific factors Bqt1/Bqt2 function as a bridge to connect the telomere proteins Taz1/Rap1 to the SPB. Deletion of any of these elements disrupts the bouquet, leading to defective spindle formation and aberrant meiosis (Tomita and Cooper, 2007). The aim of this thesis was to determine the molecular basis for control of the meiotic spindle by the telomere bouquet. We asked the question: how does the meiotic SPB differ in the presence and absence of bouquet function? Using methods to quantify SPB component levels via fluorescence microscopy in live cells, we found that bouquet-defective strains show a slight elevation of the level of Pcp1, an SPB component, but such elevation is not enough to confer bouquet-mutant phenotypes in bouquet-proficient backgrounds. Indeed, our data suggest that in the absence of the bouquet, SPB duplication occurs properly and with normal timing. However, we observed that the separation of the duplicated SPBs is markedly abnormal, as the duplicated SPBs fail to remain apart and at least one of them often becomes dislodged from the nucleus. Moreover, the γ -tubulin complex fails to localise to both spindle poles. Hence, the duplicated SPBs fail to properly recruit the γ -tubulin complex. We thus investigated the molecular mechanism underlying control of γ -tubulin complex recruitment by the bouquet. Our findings allow us to propose a model that explains the different types of spindle defects seen in the absence of the bouquet.

Acknowledgement

First of all, I would like to thank my supervisor Julie for her guidance and patience throughout my PhD and also for always trying to teach us how to use our brain.

Next I want to thank all the present and past lab members Alex, Chris, Devanshi, Jessica, Kazu, Luis, Michael, Ofer, Pierre-Marie, Sophie, Thomas, Vitalik and Yuan for making the lab a stimulating but yet fun place to work. A special thanks to Jessica for always giving me THE good advice even when it is not what I want to hear, to Alex, thanks to whom I have realised that I can also “teach” what I have learnt and for his refreshing enthusiasms, to Yuan for being most of the time on another planet but without whom the lab would have never be the same and of course to Pierre-Marie pour son Amitié, son aide précieuse et son incroyable capacité à me “supporter” même en version Calimero et Petit Pimousse...

I am also more than grateful to Kazu for his precious supervision and extreme patience with ALL my questions during the initial step of my PhD and far beyond his time in the lab. Thank you Kazu!!!

I would also like to thank my thesis committee Frank Uhlmann and Jacky Hayles for their input and support as well as all the yeast labs – The Toda lab, the Uhlmann Lab and the Hayles lab for the their insightful scientific and non scientific discussions... Particularly Isabelle for simply being the “Queen” of the microscope room and for her endless efforts to make the “machine” behave as we want and not as they want...

MERCI du plus profond de mon cœur à mes parents sans qui je n’en serais pas là aujourd’hui, pour leur inconditionnelle confiance en moi et pour être TOUJOURS présent pour moi.

Finally, a very special thanks to you know who for you know what... et bien plus encore.

Table of Contents

Abstract	3
Acknowledgement	4
Table of Contents	5
Table of figures	8
List of tables	10
Abbreviations	11
Chapter 1. Introduction	13
1.1 Telomere	13
1.1.1 Definition	13
1.1.2 Canonical roles of the telomere	13
1.1.3 Another role for telomeres	14
1.1.4 Fission yeast telomeres	14
1.2 Meiosis	17
1.2.1 Definition	17
1.2.2 Specific features	17
1.3 Meiosis and telomere bouquet in fission yeast	21
1.3.1 Introduction to Fission yeast meiosis	21
1.3.2 Bouquet formation	25
1.3.3 Bouquet stage and nuclear movements	29
1.3.4 Telomere firework and meiosis progression	30
1.3.5 The roles of the telomere bouquet	31
1.4 MTOC: The centrosome	34
1.4.1 Definition	34
1.4.2 Centrosome and cell cycle	35
1.4.3 Centrosome and meiosis	38
1.5 MTOC: The Spindle pole body	39
1.5.1 Definition	39
1.5.2 Fission Yeast SPB and cell cycle	41
1.5.3 Fission yeast SPB and meiosis	45
1.6 Microtubule assembly	48
1.6.1 Microtubule	48
1.6.2 Microtubule nucleation: the γ -tubulin complex	49
1.6.3 γ TuC Recruitment to MTOCs	55
1.7 Aim of the study	58
Chapter 2. Materials and Methods	59
2.1 Strains list	59
2.2 Strains list by figure	62
2.3 Strains list by table	63
2.4 Media and Reagents list	64
2.4.1 Media	64
2.4.2 Reagents	64
2.5 Strain growth and maintenance	65
2.5.1 Classic growth conditions	65
2.5.2 Strains containing plasmid	65

2.5.3	Strains with <i>nmt</i> promoter	66
2.5.4	For meiosis	66
2.5.5	Selective media	66
2.5.6	Frozen stock	67
2.6	Creating strain.....	67
2.6.1	Gene targeting	67
2.6.2	Random spores analyses	67
2.6.3	Pcp1-2 copies	68
2.6.4	Diploids	69
2.7	Yeast transformation	69
2.8	Genomic DNA preparation	70
2.9	PCR	71
2.9.1	Routine	71
2.9.2	For gene targeting	72
2.9.3	For cloning	72
2.10	Meiosis synchronisation	73
2.10.1	Nitrogen starvation.....	73
2.10.2	Counting number of nuclei per ascus	74
2.11	Protein extraction	75
2.11.1	Trichloroacetic acid (TCA)	75
2.11.2	For two-dimensional protein gel electrophoresis (2D-PGE)	76
2.12	Two-dimensional protein gel electrophoresis	77
2.12.1	First dimension isoelectric focusing	77
2.12.2	Second dimension SDS-PAGE.....	78
2.13	Western blotting.....	78
2.14	Fluorescence microscopy.....	79
2.15	Fluorescence signal quantitation	80
Chapter 3.	Measurement of SPB component intensities in live cells	81
3.1	Aim	81
3.2	Introduction of quantitation method	82
3.2.1	Western blotting or fluorescence microscopy?	82
3.2.2	What defines the signal to be quantified?	82
3.2.3	Total SPB intensity quantitation	83
3.2.4	Issues of normalisation	87
3.3	Analysis of Pcp1 intensity measurement in live cells	91
3.3.1	Pcp1 accumulation in WT meiosis is a dynamic process	91
3.3.2	Bouquet disruption results in mildly altered Pcp1 levels but does not affect its timing of accumulation	93
3.4	Pcp1 level manipulation	98
3.4.1	Choice of Pcp1 over-expression strategy	98
3.4.2	Can the small difference in Pcp1 intensity between WT and <i>bqt1Δ</i> cells explain the <i>bqt1Δ</i> phenotypes?	103
3.5	Pcp1 is representative of SPB behaviour	108
3.5.1	Pcp1 and Sid4 colocalise throughout meiosis in <i>bqt1Δ</i> cells	108
3.5.2	Pcp1 and Sid4 accumulation profiles are similar in <i>bqt1Δ</i> cells	109
3.6	Overview	113
Chapter 4.	Separation of the duplicated SPB is abnormal in bouquet deficient cells	114

4.1 Aim	114
4.2 Separation of the duplicated SPB is abnormal in bouquet deficient cells	115
4.3 Overview	120
Chapter 5. The bouquet is required for γ-TuC localisation to SPBs	121
5.1 Aim	121
5.2 In absence of the bouquet, the γ -TuC localises unevenly between duplicated SPB.....	122
5.3 Presence of γ -TuC at the SPB correlates with spindle formation ...	130
5.4 Alp4 over-expression does not rescue bouquet phenotypes	134
5.4.1 Plasmid based Alp4 over-expression	134
5.4.2 Genomic integration based Alp4 over-expression	135
5.5 Overview	142
Chapter 6. γ-TuC recruitment to the meiotic SPB	143
6.1 Aim	143
6.2 Pcp1 participates in γ -TuC recruitment to the meiotic SPB	144
6.3 SPBs fail to interact properly with the membrane in absence of bouquet.....	149
6.4 Overview	153
Chapter 7. Biochemical approach to assess modification of SPB components in meiosis.....	154
7.1 Aim	154
7.2 Meiosis synchronisation	155
7.2.1 Strategy	155
7.2.2 Bouquet phenotypes are similar in azygotic and zygotic meiosis....	158
7.3 Pcp1 characterisation.....	162
7.3.1 Improvement of protein extraction from meiotic samples	162
7.3.2 Pcp1 profile analysed by western blot through meiosis.....	163
7.3.3 Pcp1 post-translational modifications analysed by 2D -PGE.....	167
7.4 Alp4 characterisation	169
7.4.1 Alp4 profile analysed by western blot throughout meiosis.....	169
7.4.2 Alp4 post-translational modifications analysed by 2D -PGE.....	171
7.5 Overview	176
Chapter 8. Discussion and future perspectives.....	177
8.1 Implications of the similarities of the SPB cycle in presence and absence of the bouquet.....	178
8.2 Implications of SPB separation defects	179
8.3 How can the bouquet influence γ -TuC localisation?.....	180
8.4 What is/are the feature(s) of the telomere bouquet necessary to control the meiotic spindle?	182
References	187

Table of figures

Figure 1.1 Structure of <i>Schizosaccharomyces pombe</i> telomeres	16
Figure 1.2 Zygotic and Azygotic meiosis progression in fission yeast.....	23
Figure 1.3 Nuclear reorganisation upon meiotic induction.....	24
Figure 1.4 Telomere bouquet formation and composition in fission yeast.....	28
Figure 1.5 Defective meiotic spindle in the absence of the bouquet	33
Figure 1.6 Centrosome structure	37
Figure 1.7 SPB cycle in fission yeast.....	42
Figure 1.8 Schematic representation of the γ -tubulin small complex (γ -TuSC) and γ -tubulin ring complex (γ -TuRC).....	52
Figure 1.9 The different types of MTOCs in fission yeast.....	54
Figure 3.1 Example of WT meiosis.....	85
Figure 3.2 Schematic diagram of Total SPB intensity quantitation method.....	86
Figure 3.3 Comparison of normalisation methods.....	88
Figure 3.4 Values of Pcp1 intensity are variable from experiments but in a consistent way.....	90
Figure 3.5 Pcp1 accumulation in WT meiosis is a dynamic process.....	92
Figure 3.6 Pcp1 levels changes with the same timing in WT and <i>bqt1</i> Δ cells...	94
Figure 3.7 Pcp1 over-expression.....	100
Figure 3.8 Expression of 2 copies of <i>pcp1</i>	102
Figure 3.9 WT <i>versus bqt1</i> Δ present the same difference of Pcp1 intensity than WT <i>versus pcp1-2copies</i>	104
Figure 3.10 <i>pcp1-2copies</i> has no defect in meiosis sporulation.....	105
Figure 3.11 The small difference of Pcp1 intensity between WT and <i>bqt1</i> Δ is not biologically significant.....	106
Figure 3.12 <i>pcp1-2copies</i> displays small supernumerary Pcp1 dots during SPB separation.....	107
Figure 3.13 Pcp1 and Sid4 colocalise at the SPB throughout meiosis in WT .	110
Figure 3.14 Pcp1 and Sid4 colocalise at the SPB throughout meiosis in <i>bqt1</i> Δ cells	111
Figure 3.15 Shape of Sid4 intensity profile is similar in WT and <i>bqt1</i> Δ cells ...	112
Figure 4.1 Example of SPB separation at MI but not at MII.....	116
Figure 4.2 Examples of SPB separation at MII only	117
Figure 4.3 Example of SPB that do not separate at all.....	118
Figure 5.1 Example of γ -TuC localisation throughout WT meiosis	124
Figure 5.2 Example of γ -TuC unequal separation at MII only	125
Figure 5.3 Example of γ -TuC unequal separation at MI and MII	126
Figure 5.4 Example of γ -TuC signal leaving the SPB	127
Figure 5.5 Example of spindle formation and γ -TuC localisation throughout WT meiosis	131
Figure 5.6 Examples of γ -TuC unequal localisation to duplicated SPBs	133
Figure 5.7 Alp4 expression under the control of <i>nmt1</i> promoter in repressed conditions does not rescue bouquet SPB defects	136

Figure 5.8 Alp4 expression under the control of <i>nmt1</i> promoter in repressed conditions does not rescue bouquet SPB defects	137
Figure 5.9 Strong Alp4 over-expression in WT cells shows severe meiotic defects	140
Figure 5.10 Strong Alp4 over-expression does not rescue bouquet SPB separation defects	141
Figure 6.1 Mild phenotypes of <i>pcp1-15</i> meiosis at 32°C	146
Figure 6.2 Strong phenotypes of <i>pcp1-15</i> meiosis at 32°C	147
Figure 6.3 Example of SPB insertion in the nuclear envelop in WT mitosis and meiosis	151
Figure 6.4 SPB detaches from the nuclear envelop in bouquet deficient cells	152
Figure 7.1 Example of meiosis synchronisation profile.....	157
Figure 7.2 Example of WT azygotic meiosis.....	159
Figure 7.3 Aberrant spindle formation and SPB separation in bouquet deficient azygotic meiosis	160
Figure 7.4 Comparison of zygotic and azygotic asci containing spores in bouquet deficient background.	161
Figure 7.5 Pcp1 is hypersensitive to proteases in meiotic extract.....	165
Figure 7.6 Pcp1 analysis by western blot does not reveal differences between WT and bouquet deficient cells	166
Figure 7.7 Pcp1 analysis by 2D-PGE does not reveal post-translational differences between WT and bouquet deficient cells	168
Figure 7.8 Alp4 analysis by western blot does not reveal differences between WT and bouquet deficient cells	170
Figure 7.9 Alp4-HA can be detected after 1D-PGE but not after 2D-PGE	175
Figure 8.1 Schematic representation of WT, circular and circular with internal telomere strains	184
Figure 8.2 Telomere clustering is not required for bouquet function	185

List of tables

Table 1.1 γ -tubulin complex components in several organisms	51
Table 3.1 P- value comparing Pcp1 intensity of WT and <i>bqt1</i> Δ cells at several key points of meiosis	95
Table 3.2 SPB duplication is not significantly affected in bouquet deficient cells	97
Table 4.1 Separation of the duplicated SPB is abnormal in bouquet deficient cells	119
Table 5.1 Alp4 localises unequally between duplicated SPBs in bouquet mutant	128
Table 5.2 Correlation between Alp4 unequal localisation to the SPB and SPB separation defects	129
Table 6.1 Pcp1 is involved in Alp4 recruitment at the meiotic SPB	148
Table 7.1 Summary of the experimental changes to try to detect Alp4 by 2D-PGE	174

Abbreviations

Δ	Gene deletion
1D-PGE	One-dimensional protein gel electrophoresis
2D-PGE	Two-dimensional protein gel electrophoresis
aa	Amino acid
AMTOC	Aberrant microtubule organisation centre
aur	Aureobasidin A
bp	Base pair
CFP	Cyan fluorescent protein
CO	Crossing-over
dNTP	Deoxyribonucleotide triphosphate
DSB	Double strand break
DTT	Dithiothreitol
EM	Electron microscopy
EMM	Edinburgh minimal medium
eMTOC	Equatorial microtubule organising centre
FSM	Forespore membrane formation
γ -TuC	γ -tubulin complex
γ -TuRC	γ -tubulin ring complex
γ -TuSC	γ -tubulin small complex
GFP	Green fluorescent protein
GTP	Guanosine triphosphate
HA	Hemagglutinin epitope
hyg	Hygromycin B
iMTOC	Interphase microtubule organising centre
INM	Inner nuclear membrane
kan	Kanamycin/geneticin
mCherry	Monomeric Cherry
MI	Meiosis-I

MII	Meiosis-II
MPF	Mitosis promoting factor
mRFP	Monomeric red fluorescent protein
MTOC	Microtubule organising centre
nat	Nourseothricin
NCO	Non crossing over
NE	Nuclear envelop
NEBD	Nuclear envelop breakdown
NHEJ	Non homologous end joining
nmt	No message in thiamine
NPC	Nuclear pore complex
O/N	Over night
OB-fold	Oligonucleotide/oligosaccharide binding-fold
ONM	Outer nuclear membrane
PBS	Phosphate buffered saline
PCM	Pericentriolar material
PCR	Polymerase chain reaction
PEG	Polyethylene glycol
pI	Isoelectric point
PMSF	Phenylmethylsulphonyl fluoride
Pnmt	No message in thiamine promoter
RT	Room temperature
SAC	Spindle assembly checkpoint
SC	Synaptonemal complex
SDS-PAGE	Sodium dodecyl sulfate polyacrylamide gel electrophoresis
SPB	Spindle pole body
TPE	Telomere position effect
ts	Thermo-sensitive
ye4s	Yeast extract with supplements

Chapter 1. Introduction

1.1 Telomere

1.1.1 Definition

Telomeres represent the extremities of linear chromosomes and comprise specific repetitive DNA sequences as well as specialised proteins. The DNA component is arranged in a double stranded region containing G-rich DNA repeats and a single stranded 3'overhang at the extreme tip of the G rich strand. Double stranded and single stranded regions are both bound in a specific manner by specialised telomere binding proteins which recruit by protein/protein interactions additional factors to form multi-subunit complexes (Dehe and Cooper, 2010, Jain and Cooper, 2010). In addition, telomeres have a heterochromatic nature responsible for the so-called telomere position effect (TPE). TPE results in reversible silencing of genes near telomeres (Nimmo et al., 1994, Gottschling et al., 1990).

1.1.2 Canonical roles of the telomere

The role of telomeres to protect the genome against genomic instability is shared by all eukaryotes, independently of the diversity in structure and composition of the telomeres.

Perhaps the most important function of telomeres is the so-called “capping function”. Telomeres disguise the ends of chromosomes to prevent them from being recognised as double strand break (DSB) by the DNA damage repair machinery. At internal regions, DSBs trigger a DNA damage response resulting in repair of the break. Such mechanism is essential to preserve genomic integrity but would be extremely deleterious if it were to happen at the end of linear chromosomes. Indeed, if repair mechanisms were active at telomeres they would

result in end-to-end fusions, which would create dicentric chromosomes, hence leading to aneuploidy after chromosomes segregation (Jain and Cooper, 2010).

The second extremely important role of telomeres is to ensure their own complete replication. The biochemical limitations of the canonical replication machinery lead to the “end replication problem”. The lagging strand machinery is not capable of fully replicating blunt ended molecules and telomere sequences are lost with successive rounds of replication. In addition, the leading strand machinery is not capable of fully duplicating a linear molecule with a 3′ overhang leading to the loss of the 3′ overhang. To circumvent these problems, telomerase evolved. Telomerase is a reverse transcriptase that uses its own RNA template to add telomeric repeats to the very end of telomeres. In association with 5′ resection, it restores the single stranded 3′ overhang of the telomeres as well as the lost repeats, thereby providing self-preservation mechanisms to telomeres (Jain and Cooper, 2010).

1.1.3 Another role for telomeres

Another very conserved role of the telomeres throughout the eukaryotic kingdoms yet extremely divergent from those observed in proliferative growth is their role in meiosis where they take the lead in the formation of the telomere bouquet (see section telomere bouquet).

1.1.4 Fission yeast telomeres

Cloning and sequencing of the fission yeast telomeres in 1980s by Sugawara and Szostak revealed at the end of each chromosome ~300 bp of degenerate telomere repeats ($G_{2-6}TTAC[A]$). In addition, on chromosome I and II, 19 kb of repetitive sequences named the sub-telomeric elements are present. On chromosome III, however, the rDNA repeats are localised adjacent to the telomeres toward the centromere. The heterochromatic nature of the telomere is conferred by the presence of hypermethylation on the histone H3 lysine9 (H3K9), hallmark of the heterochromatin and binding site of the chromo domain protein Swi6 (orthologue

of the heterochromatin protein-1 (HP1) (Nimmo et al., 1994, Ekwall et al., 1996, Nakayama et al., 2001, Kanoh et al., 2005). In addition, different protein complexes bind the fission yeast telomeres. Taz1 a Myb domain protein (Cooper et al., 1997) specifically binds the double stranded region of the telomeres. Rap1 and Rif1 are recruited to the double stranded region of the telomeres via direct interaction with Taz1 (Kanoh and Ishikawa, 2001), although Rap1 has also been visualised at a subset of telomeres in the absence of Taz1 (Chikashige and Hiraoka, 2001, Kanoh and Ishikawa, 2001). The 3' overhang is directly bound by the single strand binding protein Pot1 (Baumann and Cech, 2001) which contains oligonucleotide/oligosaccharide binding-fold (OB-fold) domains conferring high affinity and specificity for the telomeric single stranded G-strand (Gottschling and Zakian, 1986). Protein/protein interactions form the single strand complex composed of Pot1, Tpz1, Ccq1 and Poz1 where Poz1 bridges the single strand complex to the Taz1/Rap1 double strand complex (Figure 1.1). Together they perform the specific functions of the telomeres presented in the previous sections.

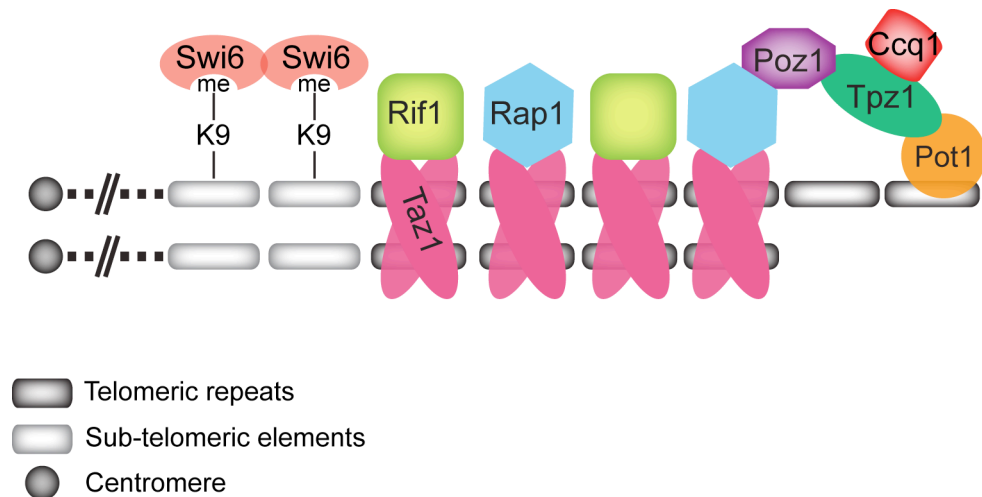


Figure 1.1 Structure of *Schizosaccharomyces pombe* telomeres

Taz1 binds the double stranded region of the telomeric repeats. Rap1 and Rif1 bind to the double stranded region of the telomeric repeats by interacting with Taz1. Pot1 binds the single stranded 3' overhang of the telomeric repeats and interact with Tpz1. Poz1 bridges the double strand binding complex Taz1/Rap1 to the single strand binding complex Pot1/Tpz1. The hallmark of heterochromatin Swi6 and methylation of Histone H3 lysine 9 (H3K9-me) are present at the sub-telomeric elements.

1.2 Meiosis

1.2.1 Definition

Meiosis is the special cell division that leads to the formation of the gametes or spores but its role goes beyond that since it also has the burden to introduce genetic diversity. Meiosis is therefore essential for organisms that undergo sexual reproduction and is a key mechanism of their evolution.

Meiosis is characterised by two consecutive rounds of chromosome division after only one round of DNA replication, thereby compensating for genome doubling after fertilisation. Thus a diploid cell will give rise to haploid gametes / spores at the end of the meiotic divisions. In order to achieve such challenging tasks, meiosis has developed specific features and differs from the mitotic cell cycle in many ways.

1.2.2 Specific features

Meiosis varies between mammals, plants, and yeast, yet specific features were developed and conserved through the eukaryotic kingdom to achieve its roles.

1.2.2.1 Homologous recombination and pairing

The first meiotic division is in charge of homologue segregation prior to a mitotic-like segregation of the sisters in meiosis-II (MII). First of all, homologues have to pair in order to insure that each daughter cell obtains one chromosome of each pair after MI instead of a random segregation. Homologous pairing involves homologue search and recognition and culminates in most organisms in formation of a tripartite proteinaceous complex between the homologues, the synaptonemal complex (SC). Homologous pairing takes place during meiotic prophase and is intimately linked with homologous recombination; however, it can be achieved dependently or independently of recombination depending on the organism. In budding yeast and mice, SC establishment and repair of the DSBs

are concomitant and DSBs are required for faithful chromosomes synapsis (Giroux et al., 1989, Romanienko and Camerini-Otero, 2000) conversely, in *C.elegans* and in female drosophila, DSB formation is not essential for homologue pairing and SC formation (Dernburg et al., 1998, McKim et al., 1998) but SC assembly is important for faithful recombination (Colaiacono et al., 2003, Liu et al., 2002).

Homologous recombination is one of the key events of meiosis, and has several roles. First, it introduces genetic diversity; second, it prepares cells for meiosis-I (MI) segregation. After DNA replication, DSBs are generated early during meiotic prophase by the endonuclease Spo11 (Keeney et al., 1997) along the four chromatids of each chromosome, initiating meiotic recombination (Borde et al., 2000). DSBs are repaired in meiosis using the homologue as predominant template rather than the sister chromatid as opposed to non-meiotic DSBs. The repair of a break using the homologue as template can either be executed in a non-crossover (NCO) or a crossover (CO) manner; however, only the resolution of the double Holliday junction (repair intermediate) in a CO manner will result in non sister chromatid exchange. The physical manifestation of a CO between homologues in meiosis can be cytologically visualised and is named the chiasma. In organisms containing a synaptonemal complex, a mechanism known as CO interference ensures that COs occur far apart enough on the chromosome in order to obtain at least one CO per chromosome pair. Fission yeast lacks both the SC and CO interference (Bahler et al., 1993, Kohli and Bahler, 1994). Nonetheless, it is very important that each pair of chromosomes do get a crossover as this is necessary for proper segregation of the homologues in MI; in fission yeast, it appears that a assurance of at least one CO per chromosome is accomplished by making a large number of DSBs and COs in each chromosome. In addition, presence of at least one CO per chromosome pair is also ensured by another mechanism named crossover homeostasis that was first described in budding yeast (Martini et al., 2006) but is also present in *C.elegans* (Youds et al., 2010) and fission yeast (Kan et al., 2011). Crossover homeostasis favours CO at the expense of NCO in situations where fewer DSBs are generated.

1.2.2.2 First meiotic division: the reductional division

After pairing, in order to achieve segregation per se, cells have developed specific mechanisms to prevent precocious sister chromatid segregation and promote kinetochore mono-orientation, monopolar attachment and proper alignment of the homologues on the metaphase plate [reviewed in (Sakuno and Watanabe, 2009)]. Specific meiotic cohesin complexes establish sister chromatid cohesion along the arms of the chromosomes and at the centromere. To ascertain sister chromatid separation only at MII, cohesin is cleaved by the endopeptidase separase and removed from chromosomes in a stepwise manner, first along the arms to allow homologues segregation at MI to take place and second at centromeres only in MII to allow sister separation (Buonomo et al., 2000, Kitajima et al., 2003). Essential to this sequential process is the protection of the pericentromeric cohesin at MI by the action of shugoshin and protein phosphatase 2A (Sgo1-PP2A) complex. At the pericentromeric region, during MI, Sgo1-PP2A complex antagonise the action of cohesin kinases that promotes the cleavage of the cohesin by separase (Kitajima et al., 2006, Ishiguro et al., 2010). Together with chiasmata, these meiotic features generate the tension required for the spindle to separate the homologues.

1.2.2.3 The telomere bouquet

Another specific feature of meiosis is the formation of the telomere bouquet. The telomere bouquet is the name given to the polarised chromosomal arrangement where telomeres cluster at the nuclear periphery, usually near the centrosome if present. It is a conserved feature of meiosis, having first been observed in salamander meiosis by Gustave Eisen in 1900 (Scherthan, 2001). During early prophase, telomeres attach to and move along the inner face of the nuclear envelope (NE), to gather and form the telomere bouquet (Hiraoka and Dernburg, 2009). This arrangement is transient and ends with the dispersion of the telomeres. Despite being very well conserved, studies from human, mouse, plants and yeast show that the mechanisms leading to bouquet formation and dispersion

are relatively diverse [reviewed in (Harper et al., 2004) and (Scherthan, 2007)]. In addition, even in organisms such as the worm *C.elegans* which lack the bouquet, recent studies showed that a bouquet-like mechanism involving specific regions of each chromosome known as pairing centres (MacQueen et al., 2005) takes place at the same time as the bouquet in other organisms and requires similar machinery (Hiraoka and Dernburg, 2009). Considering the near-ubiquity of the telomere bouquet, it seems natural to believe that it must play a very important role in meiosis. In addition, because the bouquet is initiated prior to or concomitantly with pairing and recombination events, and the polarised, aligned configuration taken by the chromosomes during the bouquet stage seems intuitively capable of assisting the homologous search, it has been widely proposed that the role of the bouquet is to promote those processes [reviewed in (Harper et al., 2004) and (de La Roche Saint-Andre, 2008)]. Because in most organisms, meiosis occurs at a specific time in specific cells and tissues, many of the molecular components of the bouquet remain to be identified, and it is not an easy task to study the function of the bouquet. Studies from yeast and plants, however, where specific bouquet components have been identified and mutants that fail to form a bouquet have begun to be defined (Cooper et al., 1998, Nimmo et al., 1998, Trelles-Sticken et al., 2000, Golubovskaya et al., 2002). Moreover, detailed studies in fission yeast have identified additional unanticipated roles of the bouquet (Tomita and Cooper, 2007). The role(s) of the telomere bouquet in fission yeast will be further discussed in the following section.

1.3 Meiosis and telomere bouquet in fission yeast

1.3.1 Introduction to Fission yeast meiosis

Fission yeast cells live and proliferate naturally as haploids, and only under starvation conditions do haploid cells of opposite mating type induce the pheromone pathway. They mate and form a zygote, which will undergo sexual development (zygotic meiosis), the end product being an ascus with four haploid spores (Yamamoto, 1996). Therefore, in order to proceed through meiosis, fission yeast cells have first to undergo conjugation and karyogamy (Figure 1.2A). Alternatively, in the laboratory, fission yeast can be grown as diploids, and as for haploid cells, nitrogen starvation initiates meiosis progression; under these circumstances, meiosis is referred to as azygotic meiosis (Figure 1.2B).

Upon nitrogen starvation and pheromone pathway activation, tremendous nuclear reorganisations give rise to formation of the telomere bouquet (Chikashige et al., 1997). The centromeres, which were gathered at the spindle pole body (SPB centrosome equivalent in yeast; see below) throughout mitotic interphase, switch their positions with the telomeres to form the telomere bouquet (Funabiki et al., 1993) (Figure 1.3). The bouquet in fission yeast results in very tight colocalisation between the SPB and the telomeres, resulting in a more compact focus compared to the bouquet in other organisms; it is also much less transient, lasting throughout meiotic prophase. In zygotic meiosis, telomere clustering at the SPB is already observed in haploid nuclei prior to karyogamy. During karyogamy, which appears to be led by the SPB and associated with small movements of the nucleus, homologous chromosome association begins at telomeres (Chikashige et al., 1994). After complete fusion of the two parental nuclei the nucleus in the bouquet configuration undergoes long oscillatory nuclear movements during which homologous searching, pairing and recombination are taking place. The movements are led by the SPB and mediated by astral microtubules (Ding et al., 1998); the nucleus pulls back and forth in the cell adopt an elongated shape named the horsetail shape (Chikashige et al., 1994). Similarly, azygotic meiotic

nuclei also form the telomere bouquet upon pheromone induction and adopt the horsetail shape, leading to prophase chromosomal movements, also known as horsetail movements (Chikashige et al., 1994). During prophase, two events in addition to homologous pairing and recombination are essential for faithful chromosome segregation: SPB maturation and kinetochore remodelling are taking place during the bouquet stage; these will be considered below. At the end of prophase, the horsetail movements stop, the nucleus localises in the centre of the cell and after chromosome condensation MI segregation starts followed by MII and spore formation (Figure 1.2).

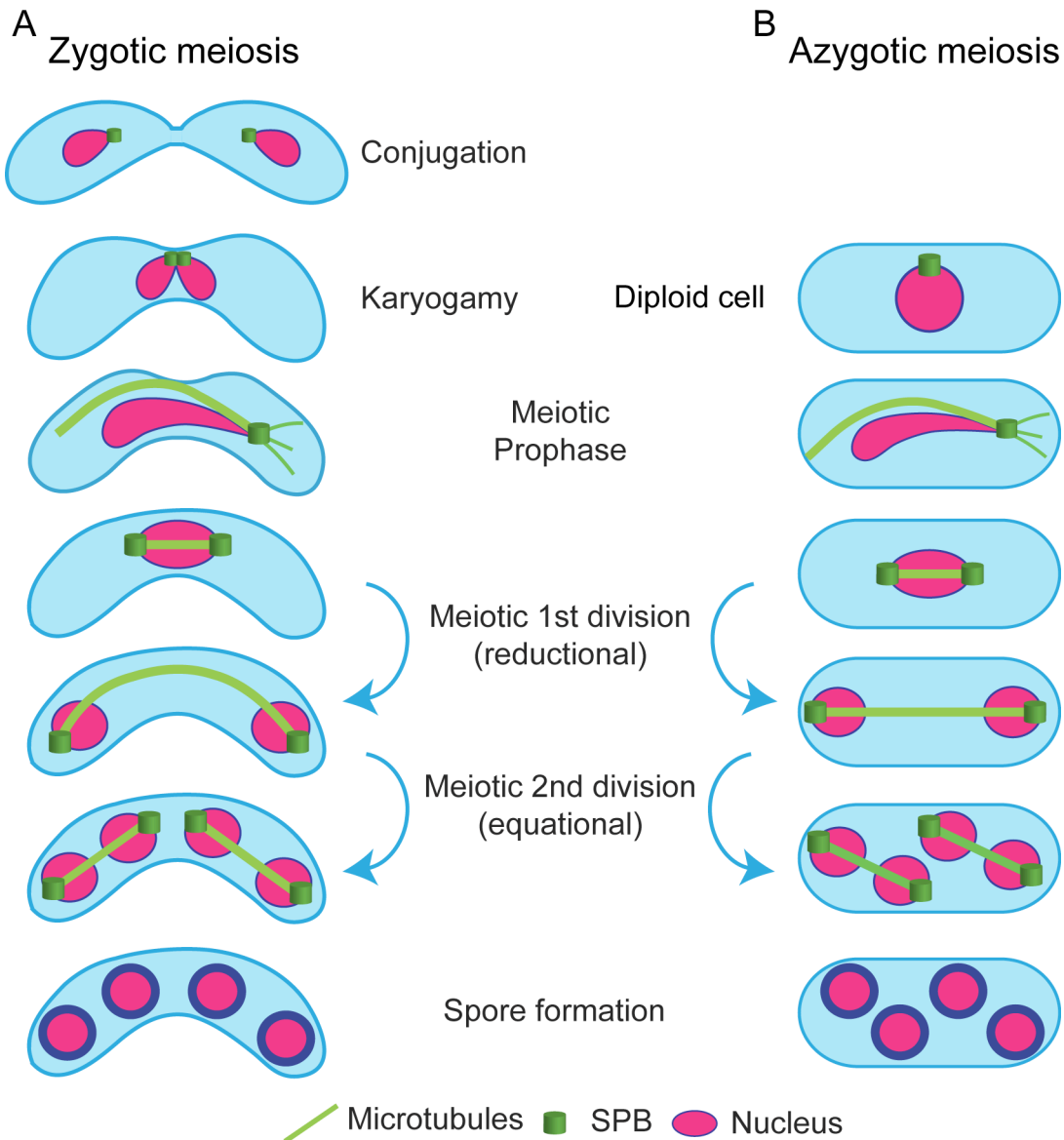
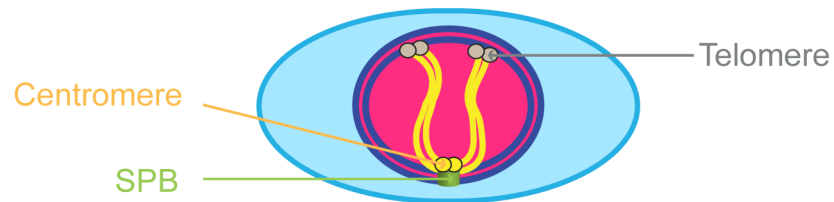



Figure 1.2 Zygotic and Azygotic meiosis progression in fission yeast

After meiotic induction during zygotic meiosis, conjugation of haploids cells with their nucleus in bouquet configuration is followed by karyogamy, which initiates at the SPB. After meiotic induction during azygotic meiosis, the bouquet is formed and cells enter meiotic prophase. For both zygotic and azygotic meiosis, during prophase, the nucleus is pulled back and forth by the array of astral microtubules nucleated at the SPB and adopts the horsetail shape. The bouquet stage persists throughout meiotic prophase and is present during pre-meiotic S phase, chromosomes pairing and homologous recombination. At the onset of MI the telomere bouquet is dissolved and MI proceed with segregation of the homologues by nucleation and elongation of the nuclear spindle. After MI the SPBs duplicate, separate and form MII nuclear spindles that separate the sisters. The last step of meiosis consists in formation of an ascus with four spores.

Vegetative growth



Pheromone pathway
&
Nitrogen Starvation



Bouquet stage

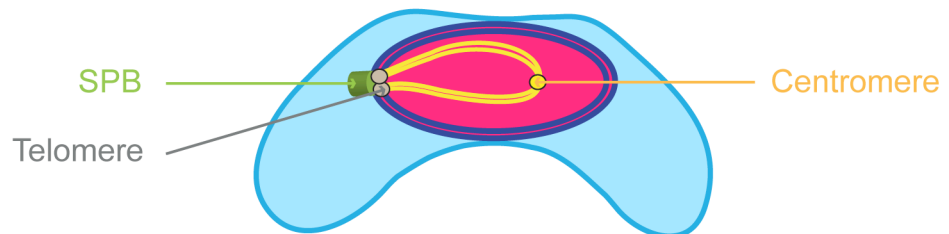


Figure 1.3 Nuclear reorganisation upon meiotic induction

In vegetatively growing cells, the telomeres are anchored at the nuclear periphery while the centromeres are clustered at the SPB, upon meiotic induction, telomeres and centromeres switch position, the telomeres are gathered at the SPB to form the telomere bouquet.

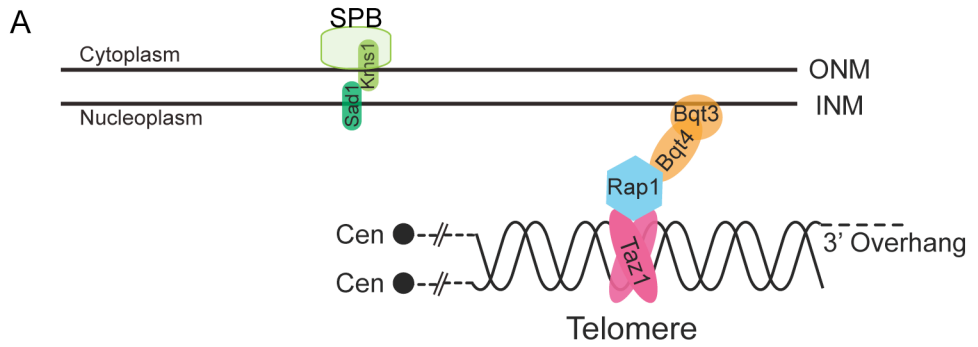
1.3.2 Bouquet formation

In mitotic interphase, centromeres are gathered at the SPB whereas telomeres are localised at the nuclear periphery (Funabiki et al., 1993) (Figure 1.3). The mechanism by which centromeres are localised at the SPB during mitotic interphase is controversial. A newly characterised inner nuclear membrane (INM) Ima1 has first been described as part of a protein network that links the centromeric DNA to the NE and microtubules (King et al., 2008), however recent study strongly argue against this model (Hiraoka et al., 2011). As opposed to centromeres, the mechanism by which telomeres are tethered to the periphery is well documented. Mitotic telomeres are anchored by direct interaction of the telomeric protein Rap1 with the INM component Bqt4 which interacts with another INM protein Bqt3 (Chikashige et al., 2009) (Figure 1.4A). The function of telomere localisation at the NE in mitosis remains unknown whereas it becomes important in meiosis to prevent telomeres from delocalising from the NE in order to achieve efficient bouquet formation (Chikashige et al., 2009). Upon pheromone induction, centromeres are released from the SPB (Asakawa et al., 2005) and meiosis specific proteins are expressed, of which Bqt1 and Bqt2 are necessary for bouquet formation (Chikashige et al., 2006, Martin-Castellanos et al., 2005, Tang et al., 2006). Both Bqt1 and Bqt2 interact with the telomeric protein Rap1 at telomeres. Bqt1 bridges the telomere complex with the SPB by direct interaction with the SPB component Sad1 (Chikashige et al., 2006, Hagan and Yanagida, 1995) (Figure 1.4B). Sad1 is a member of the SUN-domain family, and interacts with the SPB component Kms1 (Shimanuki et al., 1997, Niwa et al., 2000), which has a putative KASH domain (Starr and Fischer, 2005). SUN-domain proteins are generally thought to be restricted to the INM and have at least one transmembrane domain in addition to a SUN-domain at their C-terminal, which localises in the space between the INM and the ONM and seem to play roles in anchoring other proteins to the NE (Hiraoka and Dernburg, 2009). In addition, SUN-domain proteins have been shown to interact via their SUN-domain with transmembrane proteins bearing a KASH-domain to mediate functions in

chromosomes organisation and dynamics [reviewed in (Tzur et al., 2006)]. KASH-domain proteins share a short KASH domain (~30aa) of weak conservation at their C-terminal and have been shown to interact with the cytoskeleton via their N-terminal [reviewed in (Starr and Fischer, 2005)]. The SUN-KASH complex formed by Sad1-Kms1 appears to be responsible for guiding the telomeres from their peripheral loci to the SPB, where they gather and form the telomere bouquet (Chikashige et al., 2006) (Figure 1.4C). The forces required to mediate such movements have not been described yet. Reconstitution of the Sad1/Bqt1-2/telomere complex in mitotic cells is not enough to promote bouquet formation (Chikashige et al., 2006) hence, additional meiotic specific factors are most likely to be involved in bouquet formation. Since Kms1 has been reported to interact with dynein microtubule motors (Miki et al., 2004), dynein seemed like a good potential candidate. However only small defects in telomeres clustering are observed in dynein mutants (Miki et al., 2002). Therefore, it is possible to speculate that the machinery providing the forces used to mediate telomere clustering is meiosis specific and involves more than one microtubule motor.

In addition to the proteins directly involved in bouquet formation, some aspects of the heterochromatic nature of the telomere seem also implicated in telomere SPB association. Both the histone methyltransferase Clr4 and Rik1 which is another factor necessary for methylation of the H3K9 and subsequent binding of chromodomain proteins including Swi6, Chp1 and Chp2 (Ekwall et al., 1996, Nakayama et al., 2001, Thon and Verhein-Hansen, 2000) are required for telomere clustering (Tuzon et al., 2004). Swi6 itself however is not required (Tuzon et al., 2004).

Vegetative growth

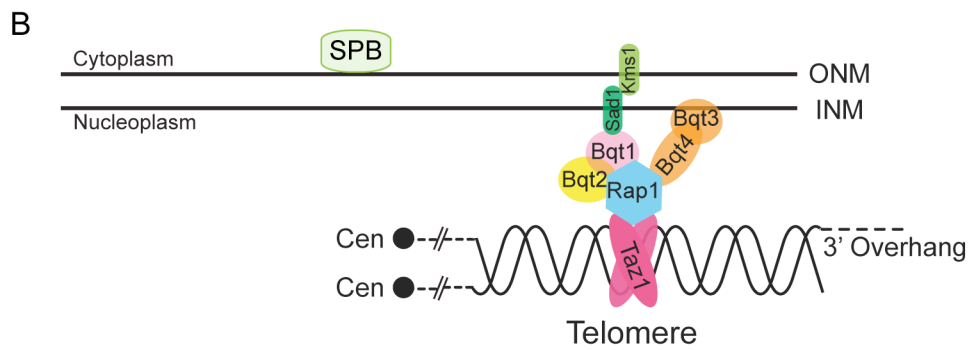


↓

Pheromone pathway
&
Nitrogen Starvation

↓

Meiosis



↓

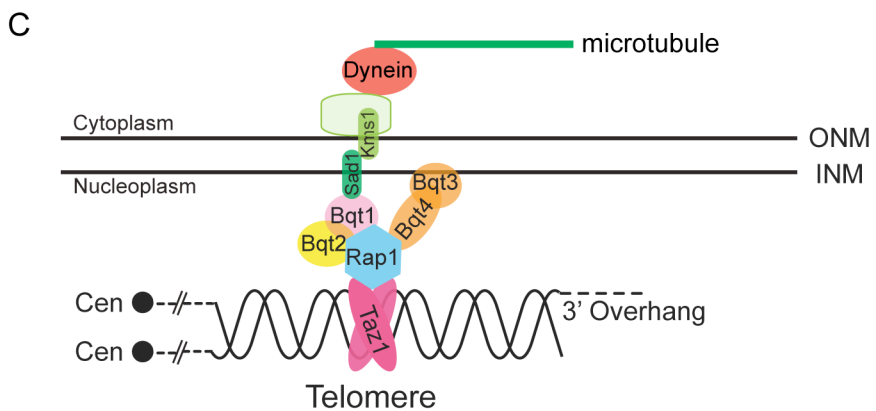


Figure 1.4 Telomere bouquet formation and composition in fission yeast

(A) In vegetatively growing cells, the telomeres are anchored at the nuclear periphery by interaction between the telomeric protein Rap1 and the components of the INM Bqt4 which interacts with another INM component Bqt3. (B) Upon meiotic induction, meiotic specific proteins Bqt1 and Bqt2 are expressed, and together form a complex with the telomeric protein Rap1 at telomeres. The SPB components Sad1 anchored in the INM and Kms1 anchored in the ONM form a SUN/KASH complex, which relocate to telomeres by interaction between Sad1 and Bqt1. Sad1/Kms1 complex is responsible for guiding the telomeres through the NE to the SPB to form the telomere bouquet. The forces required for this process have not been described yet. (C) The gathering of the telomeres at the SPB is accompanied by oscillatory nuclear movements, mediated by dynein motors and microtubules.

Deletion of the telomeric protein Rap1 (Chikashige and Hiraoka, 2001) or the meiotic specific proteins Bqt1 and Bqt2 (Chikashige et al., 2006) completely abolishes the formation of the bouquet while some residual colocalisation between the telomeres and the SPB have been monitored following deletion of the specific telomere binding protein Taz1 (Cooper et al., 1998). This remaining bouquet formation could be attributed to Rap1 binding activity at telomeres independent of Taz1 (Chikashige and Hiraoka, 2001, Kanoh and Ishikawa, 2001). In addition, deletion of Bqt4 also reduces greatly but does not abolish bouquet formation, meaning that anchoring of the telomeres at the periphery is required but that a subset of telomeres are still able to reach the SPB without it. Finally, *kms1Δ* cells have also shown bouquet disruption although telomeres and SPB remain colocalised while defects arise from severe SPB dispersion itself. Analyses of strains lacking Taz1, Rap1, Bqt1 or Bqt2 consistently show reduced level of homologous recombination as well as very low spore viability (Cooper et al., 1997, Nimmo et al., 1998, Chikashige et al., 2006, Martin-Castellanos et al., 2005, Tomita and Cooper, 2007). In addition, *taz1Δ* strains have been shown to also have a reduced level of homologue pairing along chromosomes arms but not at the centromeres (Ding et al., 2004). These findings support the general assumed role of the bouquet in promoting homologous pairing and recombination by increasing homologue proximity and chromosome alignment.

1.3.3 Bouquet stage and nuclear movements

Nuclear oscillation is a conserved feature of the bouquet stage and has been studied in several organisms including *S.cerevisiae* (Conrad et al., 2008) maize (Sheehan and Pawlowski, 2009) and mouse spermatocytes (Morelli et al., 2008). Fission yeast, however, illustrates a dramatic prolonged version of those movements as they last for approximately two hours through the entire prophase period. While *S.cerevisiae* meiotic chromosome movements are actin mediated (Kozul et al., 2008), in fission yeast an array of astral microtubules emanating from the SPB pulls the nucleus back and forth, generating the horsetail shape

(Ding et al., 1998). The movements are mediated by meiosis specific dynein motors (Yamamoto et al., 1999, Miki et al., 2002) and the physical mechanisms underlying those movements have been nicely described (Vogel et al., 2009). In addition, a meiotic specific protein Hrs1/Mcp6 (Saito et al., 2005) that interacts with SPB components has been shown to stabilize the nucleation of the minus end of the microtubules at the SPB (Tanaka et al., 2005).

Studies of deletion of proteins involved in horsetail movement, including mutants of the light or heavy chain of the dynein motors as well as Hrs1/Mcp6, reported reduced levels of homologous pairing [along the arms of the chromosomes and at centromeres (Ding et al., 2004)] and recombination (Yamamoto et al., 1999, Miki et al., 2002, Ding et al., 2004, Niccoli et al., 2004, Saito et al., 2005). However, mutants disrupting only the horsetail movements show only mild defects in spore viability and number of spores by ascus. It has been proposed that the role of the movements in fission yeast is comparable to that of the SC in other organisms (Ding et al., 2004).

1.3.4 Telomere firework and meiosis progression

At the end of prophase, the horsetail movement stops, the nucleus resumes a central position in the cell and prepares for MI division. The exact timing of the following events is not completely established but the suspected sequential events are as follows: at the onset of MI, the telomeres leave the SPB in a concerted manner – this event has been dubbed telomere fireworks. Telomere fireworks occur within minutes of separation of the duplicated SPBs and the onset of spindle elongation (Tomita and Cooper, 2007). In the meantime, the kinetochores are captured by the spindle microtubules and, by the end of MI centromeres resume their positioning at the SPB to start MII division similarly to a mitotic division. The transition between meiotic prophase and onset of MI is under the control of the transcription factor Mei4 (Shimoda et al., 1985, Horie et al., 1998) which generates a transcriptional wave (Mata et al., 2002) but is also involved in a feedback system controlling early meiotic gene repression (Mata et al., 2007).

One very important target of Mei4 with respect to entry into MI is the phosphatase Cdc25, by regulating *cdc25* expression level Mei4 coordinates the onset of MI (Murakami-Tonami et al., 2007). It has been shown that cells arrest prior to bouquet dissolution in a *mei4Δ* strain (Kakui et al., 2011); therefore, the mechanisms involved in telomere fireworks are probably governed by the transcriptional wave or the negative feedback loop influenced by Mei4.

1.3.5 The roles of the telomere bouquet

Identification of separate molecular components involved in bouquet formation and in the nuclear movements associated with the bouquet stage allows the distinction between the roles of the bouquet per se and the roles of the nuclear oscillations since the bouquet is present in mutant where the movements are abolished. As intuitively speculated, both the bouquet and movements appear to be important for homologue pairing as well as for recombination (de La Roche Saint-Andre, 2008). However, mutants that impair bouquet formation all have defects in spore formation while mutants affecting horsetail movements present a spore formation close to WT, meaning that the reduction in pairing and recombination encountered in bouquet mutants cannot account for the severe defects in spore formation. Therefore, looking for an additional role of the bouquet, Tomita & Cooper found that the telomere bouquet controls the meiotic spindle (Tomita and Cooper, 2007). In the absence of the bouquet, SPBs appear brighter and sometimes delocalised from the NE, and spindle formation is defective. Spindle defects range from monopolar, multipolar, weak and collapsing to absent spindles (Figure 1.5). Careful analyses showed that deletion of any of the components involved in bouquet formation, Taz1, Rap1 or Bqt1 (hereafter referred to as bouquet mutants) present the same defects. Because *taz1* and *rap1* deletions have been shown to be prone to telomere fusion mediated by non homologous end joining (NHEJ) in G1 arrested cells (Ferreira and Cooper, 2001), and that meiosis is directly preceded by a G1 arrest phase, analyses of *taz1Δ* and *rap1Δ* strains were performed in conjunction with *lig4* deletion to circumvent NHEJ-

related problems. *taz1Δlig4Δ* cells, however, present weaker phenotypes than *rap1Δlig4Δ* or *bqt1Δ* probably because of Rap1 binding to telomere independently of Taz1 (Chikashige and Hiraoka, 2001, Kanoh and Ishikawa, 2001). Therefore, *bqt1* deletion appears as the most penetrant mutant to study bouquet disruption phenotypes. The spindle and SPB defects observed in bouquet mutants were also shown to be independent of horsetail movements and recombination (Tomita and Cooper, 2007,) since strains deleted for *rec12* (the Spo11 homologue) (De Veaux et al., 1992) or *dhc1* (dynein heavy chain) did not present any defects in spindle formation. In addition, bouquet mutants combined with *dhc1Δ* present the same phenotypes as bouquet mutants alone (Tomita and Cooper, 2007) meaning that the pulling forces exerted on the SPB during movement while the SPB is not anchored to the telomeres are also not responsible for the spindle and SPB defects. Therefore, the defects observed at the SPB and spindle level when the bouquet is disrupted are really due to the lack of “communication” between SPB and telomeres during the bouquet stage. Moreover, the same phenotypes are observed when using a mutant allele of Taz1 that locates to the SPB but fails to bind DNA; in this mutant, the protein complex involved in bouquet formation (i.e. Taz1, Rap1, Bqt1, Bqt2) is present at the SPB without attached telomeres (Tomita and Cooper, 2007). It is thus reasonable to think that some factor brought by the telomeric chromatin itself during the bouquet stage influences proper SPB and spindle behaviour.

Furthermore, it is also conceivable considering the tight timing between telomere fireworks and MI progression that dissolution of the telomere bouquet triggers to some extent SPB separation and spindle formation. Therefore, in bouquet mutants the lack of either bouquet or dissolution could impair SPB separation and spindle formation. Investigation of the molecular mechanisms involved in bouquet dissolution could also shed light on bouquet function.

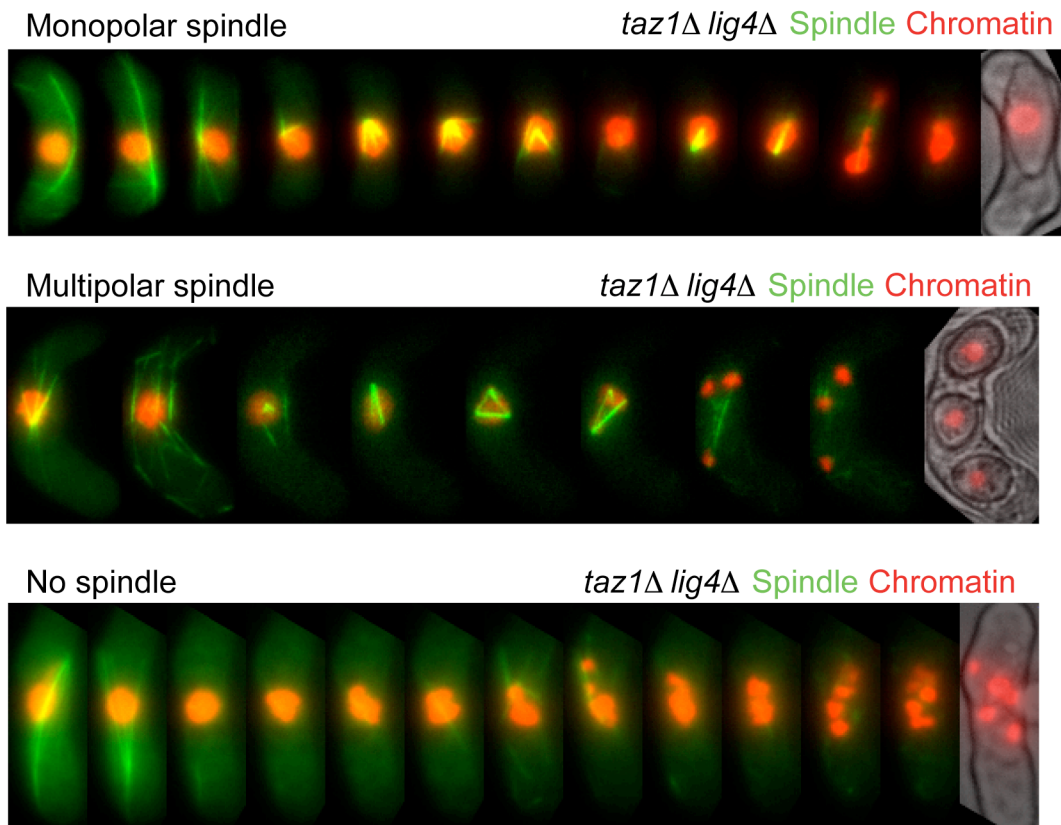


Figure 1.5 Defective meiotic spindle in the absence of the bouquet

Series of frames from *taz1Δ lig4Δ* meiosis movies acquired by fluorescence microscopy in live cells. Spindle and chromosomes were observed via ectopically expressed GFP-Atb2 and endogenously tagged Hht1-mRFP respectively. In the absence of the bouquet, different spindle defects have been observed. An example of a monopolar spindle is shown in the upper panel, a multipolar spindle in the middle panel and absence of spindle in the lower panel. Chromosomes segregation defects and aberrant spore formation are also observed. Adapted from Tomita and Cooper, 2007 with permission from Elsevier.

1.4 MTOC: The centrosome

1.4.1 Definition

The centrosome is an organelle of metazoan cells that is, unlike other organelles, devoid of a membrane. It has first been observed and characterised by Theodore Boveri, at the end of the 19th century, who raised a lot of questions that remain today. Centrosomes represent the major microtubule organising centre (MTOC) in animal cells and as such, are essential for cytoplasmic as well as for spindle microtubule nucleation, and in spatial organisation inside the cell. Centrosomes are therefore at the centre of many cellular functions such as cell motility, polarity, adhesion and cell cycle progression.

Centrosomes are localised near the nucleus and are composed of a pair of centrioles, the mother (the older) and the daughter, surrounded by an electron-dense matrix known as pericentriolar material (PCM). The canonical centriole is a barrel-shaped structure constituted of nine triplets of microtubules (doublet or singlet in some organisms) arranged in a ninefold axis of symmetry. In the centrosome the two centrioles are perpendicularly organised from each other at the proximal end and are connected by interconnecting fibres that are distinct from the PCM. In addition the mother centriole presents some appendages (Bornens, 2002) (Figure 1.6).

As MTOCs, centrosomes functions involve their aptitude to nucleate, anchor and release microtubules. Those functions are mediated through the centrioles and the PCM. On the one hand, the PCM serves as a docking platform and recruits hundreds of proteins including the machinery necessary for nucleation of the microtubule (Gould and Borisy, 1977). In addition, its composition and size vary with the cell cycle, following the so-called centrosome maturation. In order to prepare for mitosis, the PCM expands to increase its microtubule nucleation capacity necessary for the formation of efficient mitotic spindles. On the other hand, centrioles confer centrosome stability, dynamicity and the capacity to

duplicate. In addition, centrioles are also required for PCM formation (Bobinnec et al., 1998, Bettencourt-Dias et al., 2005, Basto et al., 2006). Finally, both PCM and the appendages of the mother centriole anchor microtubules.

1.4.2 Centrosome and cell cycle

1.4.2.1 Centrosome duplication

During the cell cycle, centrosomes follow a cycle of duplication and separation very much like the replication of DNA in S phase and subsequent chromosome segregation in mitosis. Like DNA replication, centrosome duplication is taking place once and only once per cell cycle (Tsou and Stearns, 2006, Nigg, 2006). The centrosome duplication cycle is tightly regulated to avoid centrosome amplification since abnormality in centrosome number and structure is often observed in cancer cells and associated with genomic instability (Zyss and Gergely, 2009). At the heart of centrosome duplication lies the control of centriole number (Cunha-Ferreira et al., 2009). The centrosome duplication cycle is divided in several steps (Kuriyama and Borisy, 1981, Chretien et al., 1997), first the mother and daughter centrioles disengage at the end of M phase, beginning G1 of the next cycle in a form that allows duplication of each centriole; this step has been described as the licensing step for duplication and requires the action of separase and shugoshin (Tsou and Stearns, 2006, Wang et al., 2008). However, the two centrioles remain connected *via* the newly established interconnecting fibres (Bahe et al., 2005). During S phase, the daughter centriole (procentriole) nucleates and elongates orthogonally to each existing centriole until they reach full length in G2 (Cunha-Ferreira et al., 2009). Finally the two newly formed centrosomes will have to separate for proper spindle formation.

1.4.2.2 Centrosome separation and nuclear envelop breakdown

In metazoa, the nuclear envelope is composed of the inner and outer nuclear membranes, the nuclear pore complex, and the nuclear lamina. In addition to its obvious function in creating a physical barrier that separates the events taking

place in the nucleoplasm from those occurring in the cytoplasm, the NE also plays many roles in the cell including chromatin organisation inside the nucleus and gene expression regulation. After centrosome duplication, concomitantly with centrosome separation, a breakdown of the NE (NEBD) occurs. NEBD allows the interaction between the chromosomes and the microtubules emanating from the centrosome and subsequent bipolar spindle formation.

In prometaphase, the NEBD starts with the partial disassembly of the nuclear pore complex (Lenart et al., 2003) which leads to an increase in NE permeability; this first step is followed by the depolymerisation of the nuclear lamina (Gerace and Blobel, 1980) which compromises the integrity of the NE and contributes to NE disintegration. Complete NEBD is facilitated by the action of microtubules and dynein motors that are pulling away and clearing off the NE from the chromatin (Beaudouin et al., 2002, Salina et al., 2002). The remains of NE are then recycled via the endoplasmic reticulum (Kutay and Hetzer, 2008). During NEBD, separation of the centrosomes is performed in three steps. The first step is related to centriole duplication since it involves the disengagement of the mother and daughter centrioles. The second step consists of the removal in late G2 of the remaining connections (the interconnecting fibres) between the disengaged duplicated centrioles, a step which is in part triggered by phosphorylation of the linker proteins (Yang et al., 2006). The third and final step is the physical separation of the two newly formed centrosomes to each pole of the future metaphase plate. This last step necessitates the action of the cytoskeleton machinery such as plus end and minus end-directed motors to generate opposite forces and push apart the centrosomes, as well as interactions between astral microtubules and the cell cortex (Lim et al., 2009, Tanenbaum and Medema, 2010). These steps seem to be controlled by the activity of key kinases of the cell cycle such as Cdk1 and Polo (Lim et al., 2009, Blangy et al., 1995, Lane and Nigg, 1996).

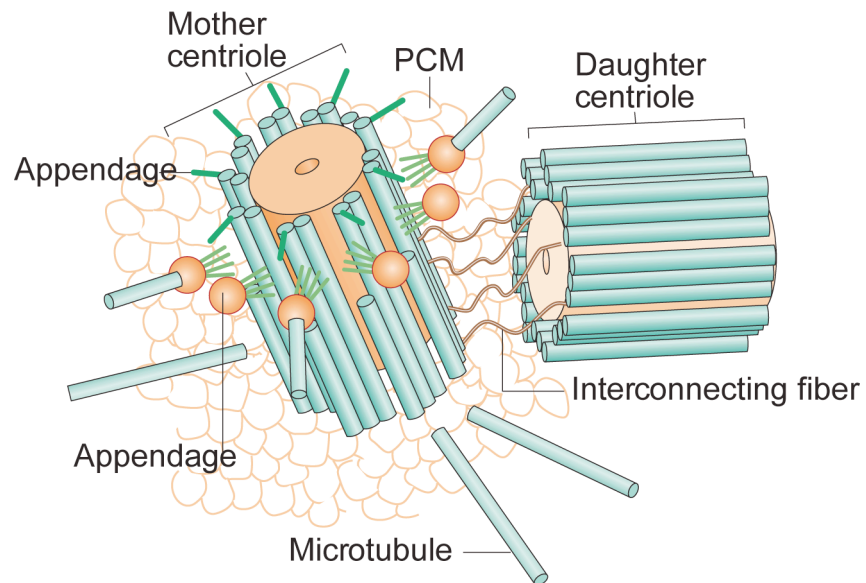


Figure 1.6 Centrosome structure

The centrosome is composed of a pair of centriole, each with nine triplets of microtubules and a pericentriolar matrix (PCM). The centrioles are orthogonally arranged one from another and are connected by the interconnecting fibre. The mother centriole also presents some appendages, which are anchoring the microtubules. The PCM serves a recruiting platform for the nucleation of the microtubules. Adapted by permission from Macmillan Publishers Ltd: (Bettencourt-Dias and Glover, 2007), copyright (2007)

1.4.2.3 Centrosome: Not just a MTOC

In addition to its role as a MTOC the centrosome appears to be implicated in many cellular processes (Doxsey et al., 2005a) including DNA damage response (Brown and Costanzo, 2009, Loffler et al., 2007), cytokinesis (Piel et al., 2001, Gromley et al., 2003), asymmetric cell division (Cheng et al., 2008), and very importantly cell cycle progression itself (Doxsey et al., 2005b). The influence of the centrosome on the G2 to M phase transition seems to be exerted through the localisation and regulation of the kinases known to play a role in cell cycle progression such as Cdk1 (Kramer et al., 2004).

1.4.3 Centrosome and meiosis

Despite the pioneering work on centrosome research being performed from sea urchin eggs, the centrosomes of gametes are much less well understood than the centrosome of somatic cells. Behaviour of the meiotic centrosome varies greatly depending on organism, but most of all between male and female meiosis. Male meiosis is achieved with the presence of the canonical centrosome while female meiosis in many species, including *Drosophila*, *C.elegans*, *Xenopus*, chicken, mice, human and other mammals, is acentrosomal (reviewed in (Manandhar et al., 2005)). In acentrosomal meiosis, the pair of centrioles is lost before the oocyte enters meiosis and spindle formation is achieved without canonical centrosomes, leading to a spindle organisation different from that of mitotic spindles – acentrosomal meiosis will be expanded upon in section 1.6.2.3. Male meiosis, despite being accomplished with the presence of centrosomes, varies from mitosis with respect to centriole duplication. While mitotic centriole duplication is tightly regulated and like DNA replication happens once and only once per cell cycle (Tsou and Stearns, 2006), meiosis being the product of two consecutive divisions without intervening DNA replication involves uncoupling of the centriole and chromosome cycle and therefore occurs twice. Hence, some aspects of

centrosome regulation in meiosis are most likely to differ from mitosis (Peters et al., 2010).

1.5 MTOC: The Spindle pole body

1.5.1 Definition

The spindle pole body (SPB) is the centrosome equivalent in yeast. SPBs and centrosomes share the same functions and many proteins localising to the centrosome are conserved and can be found at the SPB; however, their structure and size are extremely different. Despite their differences, functional studies of the SPB have been instrumental in the understanding of centrosome functions.

A major difference regarding centrosome and SPB lies in their relationship with the NE. While in metazoa there is a breakdown of the NE in order to enable spindle microtubules and chromosomes interactions, there is no such NEBD in yeast. Both mitotic and meiotic divisions undergo a closed division, meaning that the SPB had to develop an alternative strategy to allow microtubules and chromosomes to interact. The budding yeast SPB is embedded in the NE throughout the cell cycle thereby enabling formation of cytoplasmic microtubules from one side of the SPB and spindle microtubules from the other side. The fission yeast SPB is cycling in and out of the NE with the cell cycle (Ding et al., 1997) (this aspect of the fission yeast SPB will be further discussed in the next section).

In contrast to fission yeast, the structure, composition and phosphoproteome of the budding yeast SPB has been extensively characterised (Jaspersen and Winey, 2004, Muller et al., 2005, Keck et al., 2011). The budding yeast SPB is a disc-shaped organelle with a diameter of approximately 100nm (Byers and Goetsch, 1974). Its size varies proportionally to the DNA content since diploid and tetraploid cells have SPBs with a diameter of 200 nm and 400 nm respectively (Byers and Goetsch, 1975b). The dynamic evolution of the SPB size with the cell cycle and the DNA content is believed to be required to increase microtubule nucleation capacity, in order to segregate efficiently the chromosomes during

mitosis. The budding yeast SPB is composed of three layers of electron-dense material as shown by electron microscopy (EM). The outer plaque facing the cytoplasm and the inner plaque facing the nucleoplasm are respectively associated with cytoplasmic and spindle microtubules. The central plaque that spans the NE serves as a connecting point with the NE and also presents an appendage, the half-bridge, on one of its ends (Byers and Goetsch, 1974, Byers and Goetsch, 1975a, Moens and Rapport, 1971, Robinow and Marak, 1966). Cryo-electron microscopy and electron tomography reveal two additional layers localised between the outer and the central plaque, which have been named the first and the second intermediate layers (IL1 and IL2). In addition, the half-bridge was determined to be a multi-layered structure connected to the central plaque and the intermediate layers (Bullitt et al., 1997, O'Toole et al., 1999). The half-bridge plays a crucial role in SPB duplication since the new SPB assembles from a satellite localised at the distal end of the extended half-bridge in the cytoplasm, while the old SPB remains inserted into the NE (Byers and Goetsch, 1975b, Adams and Kilmartin, 1999). The new SPB and the bridge connecting the new SPB to the old one will then be inserted into the NE in order to assemble the nuclear plaque of the SPB (Jaspersen and Winey, 2004). The insertion step requires local formation of a fenestra in the NE (Winey et al., 1993, Schramm et al., 2000, Araki et al., 2006, Kupke et al., 2011).

The fission yeast SPB is much less studied than its budding yeast counterpart; however, it is approximately the same size and is also a disc-shaped organelle constituted of three plaques (Ding et al., 1997). The half-bridge appendage is also present, although its localisation seems slightly different from that of budding yeast, probably because of their different interaction with the NE (Ding et al., 1997). Nevertheless in both yeasts, the half-bridge plays a crucial role in SPB duplication and shares some components (Paoletti et al., 2003, Adams and Kilmartin, 2000, Kilmartin, 2003).

1.5.2 Fission Yeast SPB and cell cycle

1.5.2.1 SPB duplication

As for the centrosome in metazoa, the yeast SPB is under cell cycle control and therefore duplicates once and only once per cycle. In fission yeast, the SPB is found through most of interphase in the cytoplasm immediately adjacent to the NE. A finely fibrous material between the SPB and the NE has been observed, suggesting the existence of a connection with the NE during interphase (Tanaka and Kanbe, 1986, Ding et al., 1997) (Figure 1.7a). Duplication occurs in a stepwise manner. First, a new SPB forms adjacent to the old one at the distal end of the half-bridge; at that stage, SPBs are not yet competent for spindle microtubule nucleation (Ding et al., 1997, Uzawa et al., 2004) (Figure 1.7b). The second step consists of the maturation of the duplicated SPB, which last until mitosis begins. The first step of the maturation process encompasses the invagination of the NE and the accumulation of darkly staining material in the newly formed pocket beneath the SPBs (Ding et al., 1997, Uzawa et al., 2004) (Figure 1.7c). The second step consists of the insertion of the duplicated SPBs connected by the bridge in the fenestra formed in the NE (Figure 1.7d). SPB insertion in the NE is directly followed by the separation of the duplicated SPBs and the formation of the mitotic spindle. Timing of SPB duplication is a very controversial subject, since an apparent discrepancy exists between two published observations. Using exponentially growing cells and cells synchronised in early G2 by elutriation, SPB duplication has first been described to happen late in the cell cycle at the G2/M transition (Ding et al., 1997). However a more recent study using different conditional mutants to stop and release cells at several points in the cell cycle, reports SPB duplication to happen at the G1/S transition (Uzawa et al., 2004).

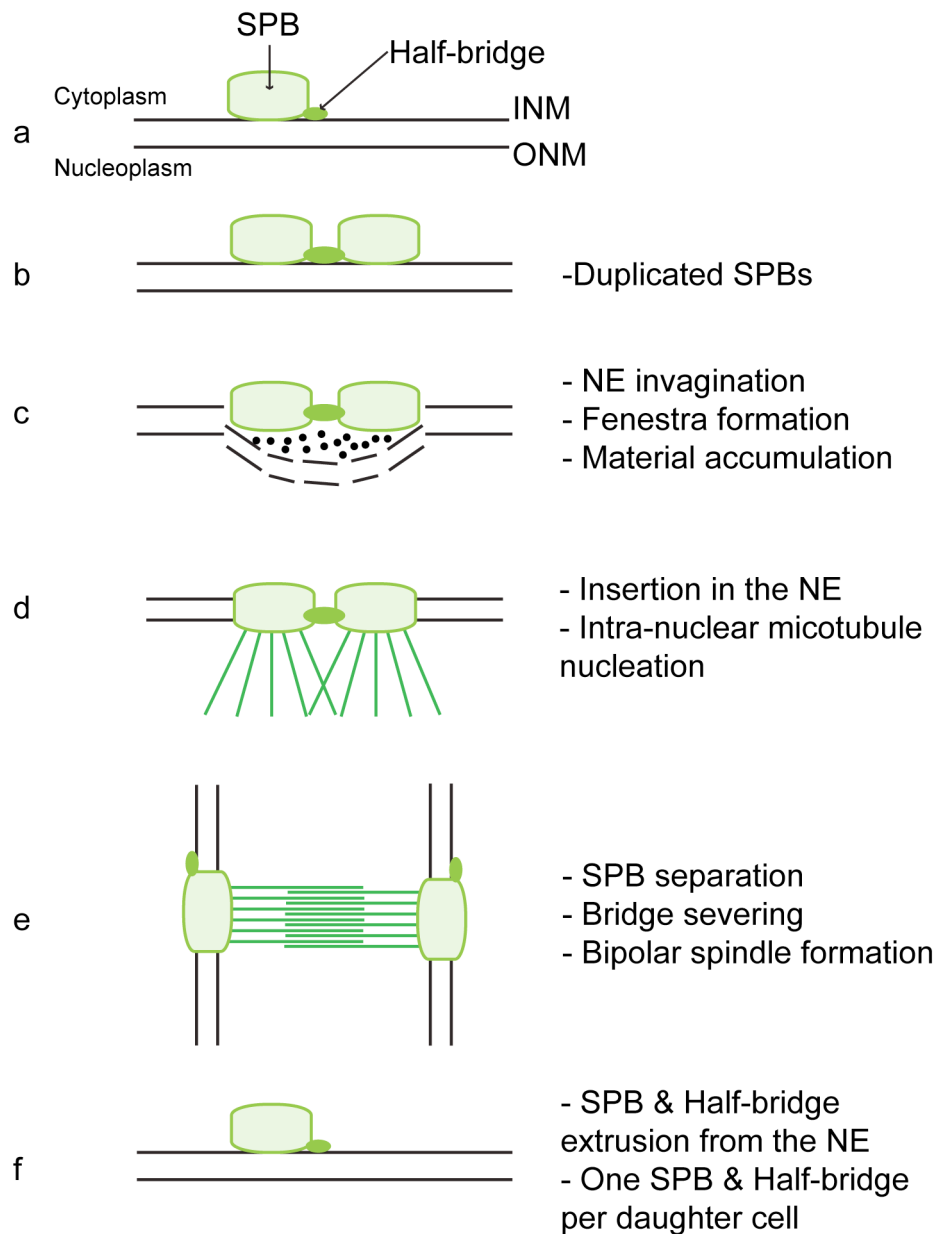


Figure 1.7 SPB cycle in fission yeast

(a) After mitotic division, the SPB with its half-bridge is on the cytoplasmic side of the NE. (b-c) SPB duplication occurs in two steps. (b) First during G1/S a new SPB forms adjacent to the old one at the distal end of the extended half-bridge. (c) Second after having passed S phase and until G2/M the SPBs mature and a fenestra is created by invagination of the NE beneath the SPBs. (d) The SPBs finally insert in the fenestra and are competent for nuclear microtubule nucleation. (e) Insertion in the fenestra is immediately followed by bipolar spindle formation, SPBs separation and severing of the bridge. (f) At the end of mitosis, the SPB with its half-bridge is extruded from the NE and resume its positioning on the cytoplasmic side of the NE.

1.5.2.2 SPB insertion in the nuclear envelope

Insertion of the SPB in the NE requires a membrane anchoring system as well as an activation step linked to mitotic commitment.

The anchoring step requires the nuclear pore complex component Cut11 (West et al., 1998). *cut11* is an essential gene that encodes a transmembrane protein with seven putative membrane-spanning domains at its N-terminus and stands as the functional homologue of Ndc1 in *S.cerevisiae* (West et al., 1998, Winey et al., 1993) and NDC1 in human (Stavru et al., 2006). In addition to its constitutive localisation to the nuclear pore complex, Cut11 also localises to the SPB in a cell cycle dependent manner (i.e. at the time when SPB inserts in the NE) (West et al., 1998). Analyses of a thermo-sensitive allele of Cut11 (*cut11.1*) by electron microscopy (EM) show that the mother SPB is poorly attached to the NE while the daughter SPB fails completely to be anchored; this situation results in monopolar spindle formation, disruption of the integrity of the NE and chromosome missegregation (West et al., 1998, Tallada et al., 2009).

The step of SPB activation, necessary for proper insertion of the SPB in the NE, is mediated by the essential SPB component Cut12, which localises to the inner plaque of the SPB throughout the cell cycle (Bridge et al., 1998). Analyses of a thermo-sensitive allele of Cut12 (*cut12.1*) by EM showed the exact same phenotypes as those of *cut11.1* and the combination of both *cut11.1* and *cut12.1* is synthetic lethal, meaning that Cut11 and Cut12 work in different pathways to ensure insertion of the duplicated SPB in the NE. However, unlike Cut11, Cut12 does not have any transmembrane domain and has been shown to support SPB insertion by promoting local activation of the maturation promoting factor (MPF) rather than by playing a physical role (Tallada et al., 2009). In line with this idea, constitutive activation of the MPF (Daga and Jimenez, 1999, Tallada et al., 2007) rescues the SPB insertion defect of the *cut12.1* mutant but not that of *cut11.1*. The MPF in fission yeast is composed of the catalytic subunit Cdc2 and the regulatory

subunit cyclin B encoded by *cdc13* (Hagan et al., 1988). Regulation of MPF activity is achieved *via* the balanced activity of the inhibitory kinase Wee1 and the activating phosphatase Cdc25 (Nurse, 1990). In addition, a feedback loop where Cdc25 and Wee1 are further activated and repressed respectively establishes complete and irreversible commitment to mitosis. Plo1 kinase localises to the SPB from the G2/M transition (Mulvihill et al., 1999) and seems to be implicated in the feedback loop (Hagan, 2008). In addition, genetic studies showed that Cut12 promotes mitotic entry by activation of Plo1 kinase. Nevertheless, Cut12 and Plo1 localise independently to the mitotic SPB (Bridge et al., 1998, Mulvihill et al., 1999, MacIver et al., 2003, Petersen and Hagan, 2005). Another essential SPB core component, Pcp1 (Flory et al., 2002), which localises to the inner face of the SPB, is also involved in Plo1 kinase recruitment to the mitotic SPB (Fong et al., 2010). A thermo-sensitive allele of Pcp1 (*pcp1-18*) that fails to recruit Plo1 to the mitotic SPB confers defects in SPB insertion reminiscent of those of *cut11.1* and *cut12.1* as shown by EM. Taken together, these data highlight the complexity and the different levels of regulation required for proper insertion of the mitotic SPB in the NE as well as the tight relationship between the SPB and MPF.

1.5.2.3 Separation of the duplicated SPBs

After insertion in the NE and activation of the MPF, the SPBs are competent for spindle microtubule assembly (Figure 1.7d); each SPB starts to nucleate intranuclear microtubules and then separates in different fenestrae with severing of the bridge and formation of the bipolar spindle (Ding et al., 1997) (Figure 1.7e). The molecular details involved in these processes have not been extensively characterised. However, the kinesin-related Cut7 protein has been shown to participate to the initial step of microtubule interdigitation (Hagan and Yanagida, 1990, Hagan and Yanagida, 1992). Separation of the budding yeast SPBs however, has been more characterised (Lim et al., 2009). Similarly to centrosome separation, SPB separation in budding yeast requires the action of opposing forces

generated by plus and minus end-directed kinesin motors (Saunders et al., 1997) as well as proteins showing microtubule bundling activity in order to generate shearing forces and break the inter SPB bridge (de Gramont et al., 2007). In addition, master regulators of the cell cycle such as the yeast equivalent of Cdk1 (Cdc28) and Polo kinase (Cdc5) have also been implicated (Crasta et al., 2006, Crasta et al., 2008). Therefore, physical separation of the duplicated SPBs and severing of the bridge are two processes directly intertwined with spindle formation and microtubule elongation since spindle formation requires SPB separation and that SPB separation requires spindle formation.

At the end of mitosis, the SPB with its half-bridge is extruded from the NE and resumes its position at the cytoplasmic side of the NE. Each daughter cell possesses one SPB and one half-bridge (Figure 1.7f).

1.5.3 Fission yeast SPB and meiosis

During meiosis the SPB plays many roles (Figure 1.2). First, it leads the way in the conjugation process, fusing first during karyogamy prior to nuclear envelope fusion (Hirata and Tanaka, 1982, Chikashige et al., 1994, Tange et al., 1998); second, it organises the microtubule array required to orchestrate the horsetail movements while playing a key role in the formation of telomere bouquet. Then, it nucleates the meiotic spindle at MI and MII and finally actively participates in spore formation. Despite the diversity and the importance of the functions carried out by the SPB throughout meiosis, very little is known about its maturation and organisation compared to the mitotic SPB; nevertheless, several studies have revealed some specificities of the meiotic SPB.

Kms1 is a constitutive SPB component present both in vegetative cells and during sexual differentiation; however, while it is dispensable in cycling cells, in meiosis it is required for both karyogamy and to maintain the structural integrity of the SPB. This is indicative of different roles of Kms1 at the SPB in meiosis *versus* mitosis (Shimanuki et al., 1997, Niwa et al., 2000).

Another example of meiotic specificity of the SPB stems from the presence of the meiotic SPB component Hrs1/Mcp6p during prophase. Hrs1 is required during prophase to remodel the microtubules to form the astral microtubule arrays necessary to mediate the vigorous horsetail movements (Tanaka et al., 2005, Saito et al., 2005).

In addition, SPB maturation appears, at least to some extent, to be differentially regulated in comparison to mitosis (Jin et al., 2005). For instance, transcription of the gene encoding Pcp1, is upregulated at the onset of MI like many other SPB components (Mata et al., 2002). The transcription factor Dot2 has been reported to negatively regulate Pcp1 transcription until the onset of MI (Jin et al., 2005). Dot2 is the homologue of the human transcription factor EAP30 that is part of a complex that regulates RNA polymerase II activity (Schmidt et al., 1999). In *dot2* mutant cells, Pcp1 protein level is increased; such increase leads to the formation of aberrant microtubule organising centres and correlates with spindle defects as well as chromosome missegregation (Jin et al., 2005). Therefore, specific meiotic SPB maturation processes and the control of SPB component levels appear extremely important.

Finally, perhaps the major and most documented role of the meiotic SPB involves spore formation. Prior to spore formation, the SPB is structurally modified and the layers of the outer plaque are formed. The accumulation of components of the forespore membrane formation (FSM) starts at the SPB at prophase-II by contacts between the FSM with the outermost layer of the SPB (Tanaka and Hirata, 1982, Hirata and Shimoda, 1994, Nakamura et al., 2008). The initiation of the FSM elongation starts during the metaphase-II to anaphase-II transition, and its expansion lasts until closure of the FSM 20 min after the end of MII (Nakamura et al., 2008). The last step of spore formation is the accumulation of spore wall components between the outer and inner membrane of the FSM. FSM formation requires specific SPB components and the general secretion machinery for fusion with vesicles derived from the endoplasmic reticulum and the Golgi apparatus

(reviewed in (Shimoda, 2004)). Interestingly, the initiation of spore formation coincides with, and seems linked with, the loss of the nucleocytoplasmic permeability barrier, which occurs specifically at the onset of anaphase II in the absence of physical breakdown of the NE (Asakawa et al., 2010, Arai et al., 2010). Therefore, spore formation appears tightly linked to meiosis itself; however, studies have shown that there is no “checkpoint-like” control coordinating meiosis and FSM formation (Nakamura et al., 2008). This observation reinforces the differences with mitotic division where a checkpoint is present to coordinate cytokinesis with chromosome segregation (McCollum and Gould, 2001).

Despite the differences presented above, meiotic and mitotic SPBs share the same SPB core components and are mostly similar in structure. During meiotic prophase, the SPB is adjacent to the NE on the cytoplasmic side (resembling its interphase location) prior to its integration in the NE during MI (Hirata and Tanaka, 1982). However, whether duplication and insertion follow the same regulation as for the mitotic SPB is not known. The nuclear pore complex component Cut11, which is essential for proper insertion of the mitotic SPB, also colocalises with the meiotic SPB at the time of meiotic division, but not during conjugation or ascus maturation. This observation suggests that Cut11 could play a similar role in mitosis and meiosis (West et al., 1998). However, during meiosis, SPBs have to duplicate a second time between MI and MII in order to segregate the sister chromatids during the two MII divisions. Whether the SPB is also cycling in and out of the NE between MI and MII has not yet been documented.

1.6 Microtubule assembly

1.6.1 Microtubule

The second player in addition to the MTOC essential for the formation of the spindle is the microtubules themselves.

Each microtubule polymer comprises thirteen parallel protofilaments arranged in a pseudo-helix of around 25 nm in diameter. Each protofilament is composed of $\alpha\beta$ -tubulin heterodimers. Polymerisation of the linear protofilament is a unidirectional process, which creates a polarised protofilament where α -tubulin is found at one end, referred to as the minus end, and β -tubulin at the other end, referred to as the plus end (Mitchison, 1993, Nogales et al., 1999).

Microtubules are highly dynamic structures and alternate constantly between polymerisation and depolymerisation states in a process referred to as dynamic instability (Mitchison and Kirschner, 1984). This cycle of growth and shrinkage is dependent on hydrolysis of GTP bound by the tubulin heterodimers. Since microtubules are capped *in vivo* at their minus ends, instability occurs mainly at their plus ends. The dynamic property of the microtubules is at the centre of the diverse cellular functions achieved by the microtubules. Indeed, it enables them to reach, for example, for the kinetochore during chromosome segregation. To amplify their functions, microtubules can associate with different microtubules associated proteins (MAPs) such as motors, plus end trackers or proteins showing bundling activity and many more (Wade, 2009).

1.6.2 Microtubule nucleation: the γ -tubulin complex

1.6.2.1 Across species

In vitro, in presence of high concentrations of purified tubulin, microtubules can self-assemble. However, the kinetics *in vivo* are much less favourable for self-assembly and microtubule assembly is performed at the MTOC where microtubules are anchored by their minus ends while their plus ends are free to extend. Despite their diversity in shape, size and occurrence, a universal feature of MTOCs is the presence of γ -tubulin, which serves as the nucleation point for microtubules (Job et al., 2003). γ -tubulin is the third member of the tubulin family and shares on average 30% homology with α and β -tubulin, depending on the organism (Oakley and Oakley, 1989, Burns, 1995). However, it is not assembled with α and β -tubulin in the protofilaments; instead, it binds the minus end of the microtubule (Zheng et al., 1995) (Wiese and Zheng, 2000). Since its discovery in *Aspergillus nidulans* (Oakley et al., 1990), studies in various systems have shown that γ -tubulin is conserved in all eukaryotes (Oakley and Oakley, 1989, Horio et al., 1991, Zheng et al., 1991, Stearns et al., 1991, Liu et al., 1994, Spang et al., 1996).

In vitro and *in vivo* studies revealed that γ -tubulin functions together with other proteins in a complex named the γ -tubulin complex (γ -TuC) to accomplish its microtubule nucleation function. The other proteins of the complex are related to each other and also are evolutionary conserved (see Table 1.1 for correspondences in different species). A substantial amount of work in many organisms has shown that the γ -TuC can exist in two distinct complexes of different sizes which localise to both the centrosome/SPB and the cytoplasm (Stearns and Kirschner, 1994, Zheng et al., 1995, Vardy and Toda, 2000, Murphy et al., 2001, Oegema et al., 1999). The smaller complex, γ -tubulin small complex (γ -TuSC) is composed of two subunits of γ -tubulin and one of each γ -tubulin interacting protein GCP2 and GCP3, the orthologues of Alp4 and Alp6 in fission yeast (Murphy et al., 1998, Vardy and Toda, 2000) (Figure 1.8). The larger

complex was first visualised as a ring by EM analysis (Zheng et al., 1995) (Moritz et al., 2000), and was therefore named the γ -tubulin ring complex (γ -TuRC). The γ -TuRC is composed of several copies of the γ -TuSC in association with three to four additional subunits, for which the stoichiometry is not known, GCP4-5 and 6 (orthologue of Gfh1, Mod21 and Alp16 in fission yeast) (Fujita et al., 2002, Venkatram et al., 2004, Murphy et al., 2001, Fava et al., 1999, Anders et al., 2006) (Figure 1.8). Budding yeast, however, possesses only the γ -TuSC containing the γ -tubulin interacting proteins Spc97 and Spc98 (Knop et al., 1997, Geissler et al., 1996). Nevertheless, recent structural studies have shown that in *S.cerevisiae*, the γ -TuSC assembles a ring like structure reminiscent to that of the γ -TuRC (Kollman et al., 2010). This finding reinforces greatly the hypothesis that the γ -TuC function as microtubules templates to nucleate the thirteen protofilaments found in microtubules *in vivo*.

In most organisms, the components of the γ -TuSC have been shown to be essential for spindle assembly whereas depletion or deletion of the additional components present in the γ -TuRC have been reported to mainly affect the fidelity of the process by compromising microtubule nucleation activity (Anders et al., 2006, Fujita et al., 2002, Verollet et al., 2006). Nevertheless, *in vitro* studies have shown that γ -TuRC is thirty times more efficient than γ -TuSC in microtubule nucleation (Oegema et al., 1999). In addition, electron tomography revealed that γ -TuRC but not γ -TuSC is present at microtubule ends (Moritz et al., 1995, Moritz et al., 2000). Therefore, it is proposed that the additional components present in the γ -TuRC enhance microtubule nucleation activity and confer some specificity (Oegema et al., 1999) (Vogt et al., 2006).

Fission yeast	Human	<i>Drosophila melanogaster</i>	Budding yeast
Gtb1	γ -tubulin (2 genes)	γ -tubulin 23C γ -tubulin 37CD	Tub4
Alp4	GCP2	Dgrip84	Spc97
Alp6	GCP3	Dgrip91	Spc98
Gfh1	GCP4	Dgrip75	-
Mod21	GCP5	Dgrip128	-
Alp16	GCP6	Dgrip163	-
?	GCP-WD	Dgp71WD	-

Table 1.1 γ -tubulin complex components in several organisms

The three first rows: components of the γ -TuSC and the following rows the additional components present in the γ -TuRC. “-“ orthologue not present. “?” Not enough information to determine the presence of an orthologue. Adapted from Wiese and Zheng, 2006.

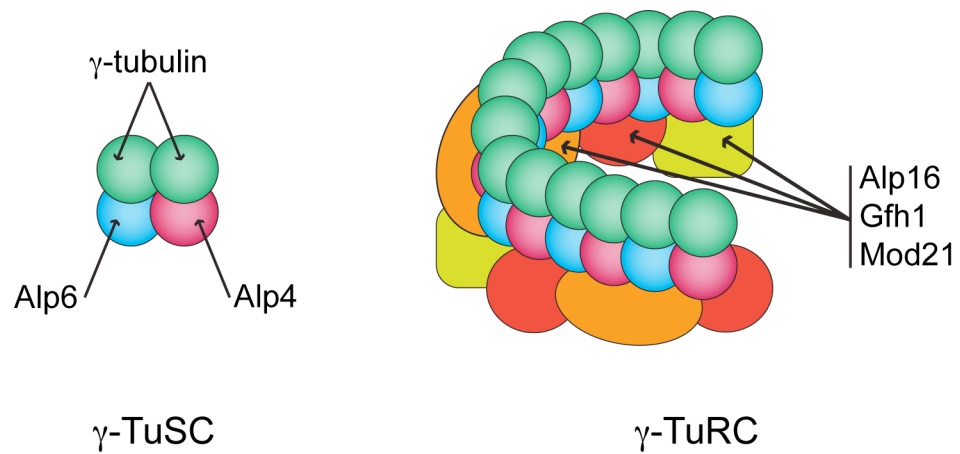


Figure 1.8 Schematic representation of the γ -tubulin small complex (γ -TuSC) and γ -tubulin ring complex (γ -TuRC)

The γ -TuSC is composed of two subunits of γ -tubulin and one of each γ -tubulin interacting proteins Alp4 and Alp6. The γ -TuRC contains between six and seven γ -TuSC and additional subunits of Alp16, Gfh1 and Mod21 for which the stoichiometry is not known.

1.6.2.2 Fission yeast γ -TUC

During mitosis, spindle and cytoplasmic microtubules are solely nucleated from the SPB; however, in interphase and during mitotic exit, additional distinct MTOCs can be found (reviewed in (Sawin and Tran, 2006)) (Figure 1.9). In interphase, cytoplasmic microtubules bundles are organised at multiples sites from the nuclear periphery but also from microtubules themselves and within the cytoplasm; these nucleation sites have been dubbed the iMTOC for interphase microtubule organising centres. At the time of mitotic exit, a third type of MTOC, the equatorial MTOC (eMTOC) organises a distinct microtubule structure named the post anaphase array (Heitz et al., 2001). Interestingly, despite their differences, all three MTOCs found in fission yeast recruit the entire γ -TuC (γ -TuRC) (Anders and Sawin, 2011) and depend on the presence of the γ -TuC for their activity, reinforcing the ubiquitous role of the γ -TuC in microtubule nucleation. However, as shown by EM immunocytochemistry analyses, despite most of the γ -tubulin being found in the nucleus in close proximity to the SPB (Ding et al., 1997), its microtubule nucleation capacity remains low until its activation in mitosis (Masuda et al., 1992).

Characterisation of the components of the two forms of the γ -TuC showed that the components of the γ -TuSC (Gtb1, Alp4 and Alp6) are essential for cell viability (Horio et al., 1991, Vardy and Toda, 2000) while the extra components found in the γ -TuRC (Gfh1, Mod21 and Alp16) are not (Fujita et al., 2002, Venkatram et al., 2004, Anders et al., 2006). In addition, while conditional alleles of the components of the γ -TuSC confer defects in nucleation of all microtubules, deletion of Gfh1, Mod21 or Alp16 only affect cytoplasmic microtubules. Furthermore, genetic manipulation of the *alp4* gene (γ -TuSC component) revealed distinct functions for the cytoplasmic and the nucleoplasmic fraction of the γ -TuC (Masuda et al., 2006). These differences highlight the complexity of the spatial and temporal regulation of the γ -TuC.

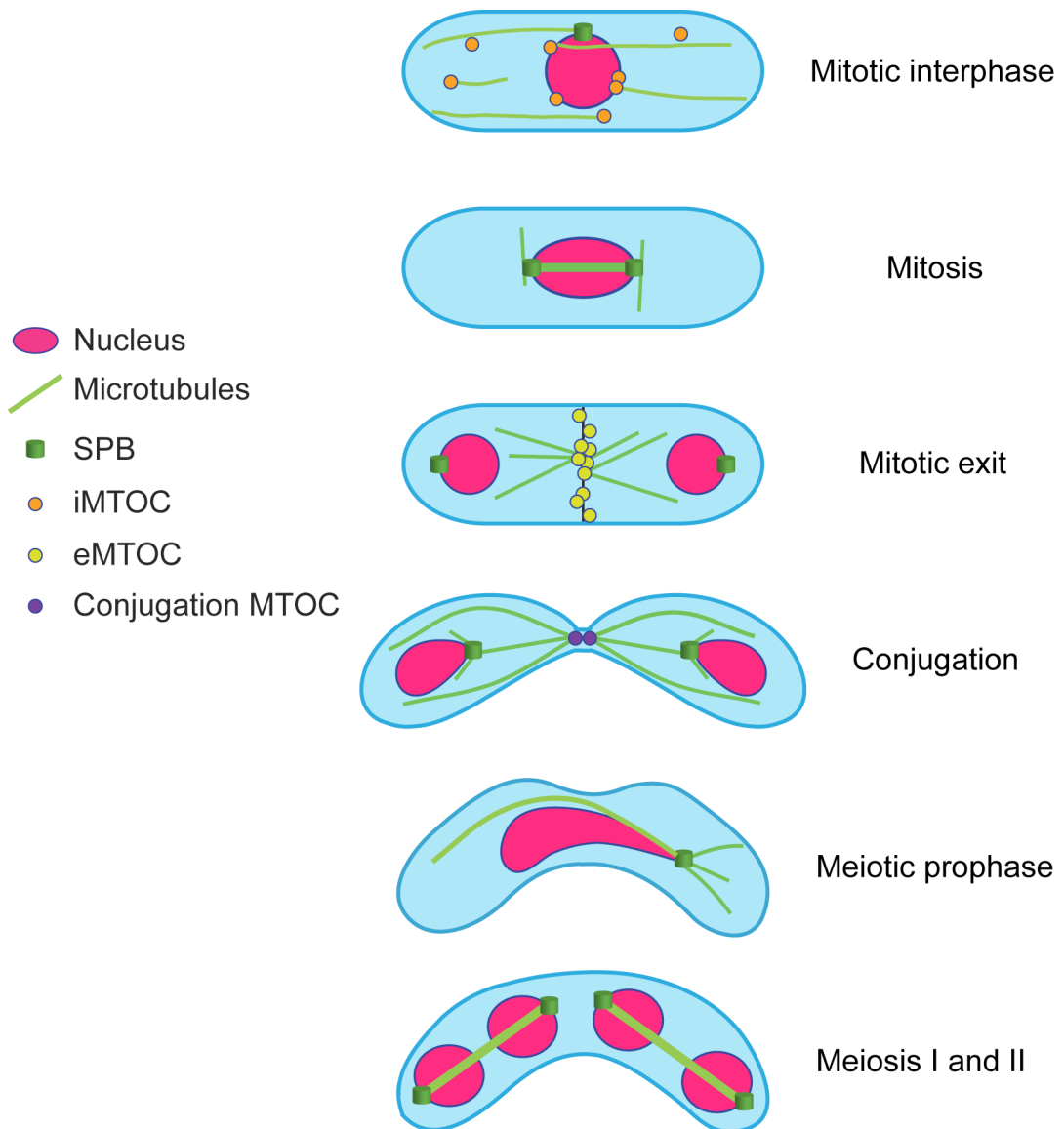


Figure 1.9 The different types of MTOCs in fission yeast

During mitotic interphase, microtubules bundles are nucleated from the cytoplasmic side of the SPB and the iMTOC that includes, the nuclear periphery, the microtubules themselves and sites within the cytoplasm. During mitosis, astral microtubules and spindle microtubules are nucleated from the cytoplasmic and nucleoplasmic side of the SPB respectively. During mitotic exit a post-anaphase array of microtubules is nucleated from the eMTOC at the site of cell division. During conjugation, microtubules are nucleated from the SPBs and from a MTOC localised in the projection tip. During meiotic prophase, microtubules are nucleated from the cytoplasmic side of the SPB that present some specificity at that stage. During MI and MII the nuclear spindles are nucleated from the nucleoplasmic side of the SPBs.

In addition, although very much less studied, specificities also arise at the meiotic MTOCs, as the SPB during meiotic prophase nucleates specific arrays of astral microtubule responsible for the oscillatory movements of the nucleus (Ding et al., 1998) and a MTOC distinct from the SPB has been observed during conjugation (Petersen et al., 1998) (Figure 1.9).

1.6.2.3 Acentrosomal microtubule nucleation

As mentioned in section 1.4.3, chromosome segregation during female meiosis is achieved by acentrosomal spindle assembly. Studies of mouse oocytes have shown that MTOCs containing γ -tubulin and pericentrin can self-organise and replace centrosome function to assemble spindle microtubules (Schuh and Ellenberg, 2007). In addition, recent studies of *Drosophila* oocytes highlight the importance of γ -tubulin in acentrosomal meiosis (Hughes et al., 2011), thereby reinforcing the importance of the γ -tubulin complex in nucleation of the microtubules from diverse MTOCs. Furthermore, studies in *Xenopus* oocyte extracts have implicated chromatin in organisation of acentrosomal spindle microtubules (Heald et al., 1996), using mechanisms that seems to require at least to some extent the presence of γ -tubulin (Mahoney et al., 2006).

1.6.3 γ TuC Recruitment to MTOCs

1.6.3.1 Across species

γ -TuC recruitment to centrosomes dramatically increases prior to mitosis and correlates with centrosome maturation and expansion of the PCM. The PCM creates a fibrous matrix that serves as a docking platform for the proteins involved in microtubule anchor and nucleation (Bornens, 2002). Several proteins have been implicated in γ -TuC recruitment to the centrosome including proteins from the pericentrin family: pericentrin, AKAP 450/CG-NAP and CDK5RAP2 in human (Zimmerman et al., 2004, Takahashi et al., 2002, Fong et al., 2008), centrosomin and CP309 in *Drosophila* (Mahoney et al., 2006, Zhang and Megraw, 2007, Kawaguchi and Zheng, 2004). Proteins of the pericentrin family are large coiled-

coil proteins with a centrosomin motif (Zhang and Megraw, 2007) at their N-termini and calmodulin-binding domain at their C-termini (Flory et al., 2002). Two members of the pericentrin family are present in fission yeast, Pcp1 and Mto1 (detailed in the next section), yet the most characterised member of the pericentrin family is the budding yeast SPB component Spc110 (Kilmartin et al., 1993, Mirzayan et al., 1992). Spc110 is essential for cell viability and thermo-sensitive mutants confer compromised SPB integrity and severe defects in spindle assembly (Sundberg and Davis, 1997, Sundberg et al., 1996, Kilmartin and Goh, 1996). Functional analyses of the different domains of the protein revealed that the coiled-coil domain is essentially a spacer element (Kilmartin and Goh, 1996) between the centrosomin motif 1 at the N-terminus which interacts with the γ -TuC (Knop and Schiebel, 1997) and the calmodulin-binding domain at the C-terminus which stabilises the protein (Stirling et al., 1994). The calmodulin-binding domain is also speculated to be an auto-inhibitory domain regulated by calmodulin binding (Geiser et al., 1993). In addition, since the budding yeast SPB is embedded in the nuclear envelope throughout the cell cycle, another essential SPB component Spc72 (which does not belong to the pericentrin family) is required to recruit the γ -TuC to the cytoplasmic side of the SPB (Knop and Schiebel, 1998). Moreover, in vertebrates γ -TuC recruitment to the centrosome requires the additional γ -TuRC component, NEDD/GCP-WD (Luders et al., 2006, Haren et al., 2006, Verollet et al., 2006).

1.6.3.2 In fission yeast

The two members of the pericentrin family in fission yeast, Mto1 and Pcp1, are required for γ -TuC recruitment to distinct MTOCs. Mto1 together with Mto2 form a complex that regulates γ -TuC localisation to the iMTOC, eMTOC and the cytoplasmic side of the interphase and mitotic SPB; however, neither Mto1 nor Mto2 is essential (Sawin et al., 2004, Venkatram et al., 2004, Samejima et al., 2005, Venkatram et al., 2005). The Mto1 N-terminal harbors a centrosomin 1

motif important for interaction with the γ -TuC while the C-terminus is important for localisation to the different MTOCs (Samejima et al., 2010).

Pcp1, like its budding yeast orthologue Spc110, is required for the recruitment of the γ -TuC during mitosis and spindle microtubule nucleation (Fong et al., 2010). Upon mitotic entry, insertion of the SPB in the NE allows interaction between Pcp1 and the nuclear fraction of γ -TuC (Ding et al., 1997). Interestingly, the thermo-sensitive allele of *pcp1* defective in γ -TuC recruitment to the mitotic SPB carries a mutation in the centrosomin motif 1 (Fong et al., 2010). As mentioned above, in addition to its role in γ -TuC recruitment, Pcp1 has also been shown to participate in the recruitment of Plo1 kinase to the mitotic SPB (Fong et al., 2010) (see 1.5.2.2). Nonetheless, neither Pcp1 nor Mto1 are required for localisation of the γ -TuC underneath the SPB during interphase (Fong et al., 2010), suggesting that another yet unknown mechanism is involved in γ -TuC recruitment.

The γ -TuC is also required in meiosis to nucleate the spindle microtubules as well as the array of microtubules required for horsetails movements (Tange et al., 2004, Tanaka et al., 2005). During prophase, γ -TuC recruitment to the cytoplasmic side of the SPB depends on Hrs1/Mcp6; however, while the γ -TuC fails to localise to the SPB in *hrs1* Δ prophase cells, its localisation to the SPB resumes at the onset of meiosis, meaning that like in vegetatively growing cells, the γ -TuC is differentially recruited to the cytoplasmic and nucleoplasmic sides of the SPB (Tanaka et al., 2005).

1.7 Aim of the study

As presented in section 1.3, an unexpected function of the telomere bouquet has been discovered (Tomita and Cooper, 2007). In addition to its role in facilitating homologue pairing and recombination, the bouquet also controls the meiotic spindle. In bouquet deficient cells, when the telomeres do not contact the SPB during prophase, the behaviour of the SPB and spindle are impaired from the onset of MI onwards, leading to chromosomes mis-segregation. This finding raises the question: “how does the telomere bouquet control the meiotic spindle?” Because the bouquet influences events that take place not during the bouquet stage but immediately after the bouquet stage, we hypothesise that the bouquet leaves a “mark” on the SPB during their period of contact. We therefore investigated the difference(s) between an SPB that has been contacted by the telomere and an SPB that had no contact with telomeres during the prophase stage.

Chapter 2. Materials and Methods

2.1 Strains list

JCF N°	Mating type	Genotype	Source
4785	h ⁹⁰	<i>ade6-M210 leu1 ura4 hht1-mRFP:his3+MX6 pcp1-GFP:kanMX6::leu1+</i>	Lab stock
5281	h ⁹⁰	<i>leu1 ura4 hht1-mRFP:his3+MX6 pcp1-GFP:kanMX6::leu1+ bqt1::hygMX6</i>	Lab stock
2098	h ⁹⁰	<i>ade6-M216 leu1 ura4 his3 pcp1::kanMX6-Pnmt81-GFP-pcp1</i>	This study
2097	h ⁹⁰	<i>ade6-M216 leu1 ura4 his3 pcp1::kanMX6-Pnmt41-GFP-pcp1</i>	This study
2099	h ⁹⁰	<i>ade6-M216 leu1 ura4 his3 pcp1::kanMX6-Pnmt1-GFP-pcp1</i>	This study
4575	h ⁹⁰	<i>ade6-M210 leu1-32 ura4-D18 his3-D1 hht1-mRFP:kanMX6</i>	Lab stock
7241	h ⁹⁰	<i>ade6-M210 leu1-32 ura4-D18 his3-D1 hht1-mRFP:kanMX6 aur1:Pcp1-GFP</i>	This study
7238	h ⁹⁰	<i>ade6-M210 leu1 ura4 hht1-mRFP:his3+MX6 pcp1-GFP:kanMX6::leu1+ aur1:Pcp1-GFP</i>	This study
7182	h ⁹⁰	<i>ade6-M210 leu1 ura4 sid4-mRFP:hygMX6 pcp1-GFP:kanMX6</i>	This study
7186	h ⁹⁰	<i>leu1 ura4 sid4-mRFP:kanMX6::leu1+ pcp1-GFP:kanMX6 bqt1::hygMX6</i>	This study
2529	h ⁹⁰	<i>leu1 ura4 his3 hht1-mRFP:his3+MX6 sid4-GFP:kanMX6::leu1+</i>	Lab stock
2530	h ⁹⁰	<i>leu1 ura4 his3 hht1-mRFP:his3+MX6 sid4-GFP:kanMX6::leu1+ bqt1::hygMX6</i>	Lab stock

JCF N°	Mating type	Genotype	Source
7169	h ⁹⁰	<i>leu1 ura4 sid4-mRFP:hygMX6 alp4-GFP:kanMX6</i>	This study
7173	h ⁹⁰	<i>leu1 ura4 alp4-GFP:kanMX6 sid4-mRFP:kanMX6::leu1+ bqt1::hygMX6</i>	This study
7204	h ⁹⁰	<i>leu1 sid4-mRFP:hygMX6 alp4-GFP:kanMX6 atb2:Pnmt1:mRFP-atb2:LEU2</i>	This study
7208	h ⁹⁰	<i>leu1 ura4-D18 alp4-GFP:kanMX6 sid4-mRFP:kanMX6::leu1+ bqt1::hygMX6 atb2:Pnmt1:mRFP-atb2:LEU2</i>	This study
7213	h ⁹⁰	<i>leu1 ura4 his3 lys1:Pnmt1:GFP-atb2 hht1-mRFP:kanMX6 pREP1-leu</i>	This study
7214	h ⁹⁰	<i>leu1 ura4 his3 lys1:Pnmt1:GFP-atb2 hht1-mRFP:kanMX6 pREP1-alp4+-Leu</i>	This study
7215	h ⁹⁰	<i>leu1-32 ura4-D18 lys1:Pnmt1:GFP-atb2 bqt1::hygMX6 pREP1-alp4+-Leu</i>	This study
7216	h ⁹⁰	<i>leu1-32 ura4-D18 lys1:Pnmt1:GFP-atb2 bqt1::hygMX6 pREP1-leu</i>	This study
7246	h ⁹⁰	<i>ade6-M210 leu1 ura4 his3 hht1-mRFP:his3+MX6 pcp1-GFP:kanMX6::leu1 alp4::kanMX6-Pnmt1-GFP-alp4</i>	This study
7247	h ⁹⁰	<i>ade6-M210 leu1 ura4 his3 hht1-mRFP:his3+MX6 pcp1-GFP:kanMX6::leu1+ bqt1::hygMX6 alp4::kanMX6-Pnmt1-GFP-alp4</i>	This study
4548	h ⁹⁰	<i>leu1 ura4 his3 lys1:Pnmt1:GFP-atb2 sid4-mRFP:kanMX6</i>	Lab stock
7218	h ⁹⁰	<i>pcp1-ts15-HA::hygMX6 sid4-mRFP::natMX6 aur1-Pnda3-GFP-atb2</i>	This study
5700	h ⁹⁰	<i>leu1 ura4 his3 hht1-CFP:his3+MX6 sid4-mRFP:kanMX6::leu1+ cut11-3xPK-GFP:ura4+</i>	Lab stock
5699	h ⁹⁰	<i>leu1 ura4 his3 hht1-CFP:his3+MX6 sid4-mRFP:kanMX6::leu1+ bqt1::hygMX6 cut11-3xPK-GFP:ura4+</i>	Lab stock

JCF N°	Mating type	Genotype	Source
7161	h ⁺ /h ⁻	<i>ade6-M210/ade6-M216 leu1/leu1</i> <i>lys1:Pnmt1:GFP-atb2/lys1:Pnmt1:GFP-atb2</i> <i>hht1-mRFP:kanMX6::leu1+</i> <i>hht1mRFP:kanMX6::leu1+</i> <i>sid4-GFP:kanMX6/sid4-GFP:kanMX6</i>	This study
7163	h ⁺ /h ⁻	<i>ade6-M210/ade6-M216 leu1/leu1</i> <i>lys1:Pnmt1:GFP-atb2/lys1:Pnmt1:GFP-atb2</i> <i>hht1-mRFP:kanMX6::leu1+</i> <i>hht1-mRFP:kanMX6::leu1+</i> <i>sid4-GFP:kanMX6/sid4-GFP:kanMX6</i> <i>bqt1::hygMX6/bqt1::hygMX6</i>	This study
7133	h ⁺ /h ⁻	<i>ade6-M210/ade6-M216</i> <i>pcp1-13xmyc-kanMX6/pcp1-13xmyc-kanMX6</i>	This study
7137	h ⁺ /h ⁻	<i>ade6-M210/ade6-M216</i> <i>pcp1-13xmyc-kanMX6/pcp1-13xmyc-kanMX6</i> <i>bqt1::hygMX6/bqt1::hygMX6</i>	This study
4390	h ⁺ /h ⁻	<i>ade6-M210/ade6-M216</i>	Lab stock
8479	h ⁺ /h ⁻	<i>ade6-M210/ade6-M216</i> <i>bqt1::hygMX6/bqt1::hygMX6</i>	Lab stock
7197	h ⁺ /h ⁻	<i>ade6-M210/ade6-M216</i> <i>alp4-HA-kanMX6/alp4-HA-kanMX6</i>	This study
7198	h ⁺ /h ⁻	<i>ade6-M210/ade6-M216</i> <i>alp4-HA-kanMX6/alp4-HA-kanMX6</i> <i>bqt1::hygMX6/bqt1::hygMX6</i>	This study
6914	h ⁹⁰	<i>ade6-M210 leu1 his3 taz1-YFP:kanMX6</i> <i>hht1-CFP:hygMX6 sid4-mCherry:natMX6</i> <i>trt1::his3+ atb2:Pnmt1:mRFP-atb2-LEU2</i>	Lab stock
6915	h ⁹⁰	<i>ade6-M210 leu1 ura4::telomere(500bp) his3</i> <i>taz1-YFP:kanMX6 hht1-CFP:hygMX6</i> <i>sid4-mCherry:natMX6 trt1::his3+</i> <i>atb2:Pnmt1:mRFP-atb2-LEU2</i>	Lab stock

Note:

leu1 is *leu1-32*, *ura4* is *ura4-D18* and *his3* is *his3-D1*

2.2 Strains list by figure

	Figures	Strains JCF N°
Chapter 3	1	4785
	2	-
	3	4785
	4	4785, 5281
	5	4785
	6	4785, 5281
	7	4785, 5281, 2098, 2097, 2099
	8	4785, 4575, 7241
	9	4785, 5281, 7238
	10	4785, 4575, 5281, 7238, 7241
	11	4785, 7238
	12	4785, 7238
	13	7182
	14	7186
	15	2529, 2530
Chapter 4	1	5281
	2	5281
	3	5281
Chapter 5	1	7169
	2	7173
	3	7173
	4	7173
	5	7204
	6	7208
	7	7213, 7214, 7216, 7215
	8	7246, 7247
	9	7246
	10	7247
Chapter 6	1	7218
	2	7218
	3	5700
	4	5699

	Figures	Strains JCF N°
Chapter 7	1	4390
	2	7161
	3	7163
	4	7169, 7163, 5281
	5	7133, 7137, 4390, 8479
	6	7197, 7198
	7	7197, 7198
	8	7197, 7198
	9	7197
Chapter 8	1	-
	2	6914, 6915

2.3 Strains list by table

	Figures	Strains JCF N°
Chapter 3	1	4785, 5281
	2	5281
Chapter 4	1	5281
Chapter 5	1	7173
	2	7173
Chapter 6	1	7218, 4548
Chapter 7	1	7197

2.4 Media and Reagents list

2.4.1 Media

Name	Components
YE4S	0.5% yeast extract, 3% glucose, 250 mg/ml uracil, adenine, histidine, leucine
YE	0.5% yeast extract, 3% glucose
EMM	14.7 mM potassium hydrogen phthalate, 15 mM Na ₂ HPO ₄ , 93.5mM NH ₄ Cl, 2% w/v glucose, salt stock, vitamin stock, mineral stock
EMM-N ⁻	Same as EMM without NH ₄ Cl
EMM-N ⁻ -low glucose	Same as EMM without NH ₄ Cl + 0.5% glucose
ME	3% (w/v) Bacto-malt extract, 250 mg/ml uracil, adenine, histidine, leucine, pH 5
YFM	YE5S + 15% glycerol

2.4.2 Reagents

Name	Components
TAE	0.08 M Tris acetate, 2 mM Na ₂ EDTA
6x DNA Loading Dye (for 50ml)	30% glycerol (15 ml), 60 mg bromophenol blue, 60 mg xylene cyanol, 6 mM EDTA (600 µl 0.5 M)
Breaking Buffer (Smash Prep Buffer)	2% Triton X-100, 1% SDS, 100 mM NaCl, 10 mM Tris-HCl pH 8.0, 1 mM Na ₂ EDTA pH8.0
TE	10 mM Tris-HCl, pH 7.5, 1 mM EDTA
LiAc-TE	100 mM lithium acetate pH 7.5, 10 mM Tris.HCl, 1mM EDTA pH 7.5
40% PEG-LiAc-TE	40% polyethylene glycol 4000, 100 mM lithium acetate pH 7.5, 10 mM Tris.HCl pH 7.5, 1 mM EDTA

Name	Components
Transfer Solution	1x Transfer Buffer (NUPAGE Invitrogen), 10% IMS
PBS	170 mM sodium chloride, 3 mM KCl, 10 mM Na ₂ HPO ₄ , 2mM KH ₂ PO ₄
PBST	PBS + 0.1% Tween-20
Milk Solution	PBST + 5% milk powder
Protein Buffer	1x LDS Sample Buffer (NUPAGE invitrogen), $\frac{1}{4}$ volume 1 M Tris-base and $\frac{1}{2}$ volume ddH ₂ O
Sample Preparation solution (2D-PGE)	7 M urea, 2 M thiourea, 4% (w/v) CHAPS, 2% IPG buffer, 40 mM DTT
Equilibration Buffer (2D-PGE)	6 M urea, 75 mM Tris-HCL pH 8.8, 29.3% (v/v) glycerol, 2% (w/v) SDS, 0.002% (w/v) bromophenol blue

Notes:

Components for the 2D-PGE solutions were when possible PlusOne Reagents (GE Healthcare)

2.5 Strain growth and maintenance

2.5.1 Classic growth conditions

Strains were revived and grown at 32°C in standard rich media YE4S (see 2.2), in liquid culture media or on 2% agar plates according to described methods (Moreno et al., 1991).

2.5.2 Strains containing plasmid

In order to maintain a plasmid in fission yeast, constant selection for the appropriate marker is required (see 2.3.5). Strains containing plasmid were thus grown at 32°C in selective media in liquid culture media or on 2% agar plates.

2.5.3 Strains with *nmt* promoter

nmt promoter is a promoter repressed in the presence of thiamine (Maundrell, 1990), cells harbouring an *nmt* promoter construct were grown depending on the requirement of the experiment, in presence of thiamine (15 μ M), in low thiamine (0.050 μ M) or without thiamine. (Note: thiamine only needs to be added in EMM and EMM variant media, YE4S, YE and ME already contain thiamine).

2.5.4 For meiosis

To induce meiosis, h^{90} or pair of h^- and h^+ strains vegetatively growing at 32°C on plates, were plated on ME (nitrogen source free media) plate at 25°C (see 2.2). Ascii formation occurs after 2 days incubation. Live analysis was carried out approximately 9 hours after meiosis induction.

2.5.5 Selective media

Selective medias were made by adding various amounts of drugs to YE4S liquid media bottle or melted and cooled bottle of agar media.

Name	Components
Hygromycin B	YE4S + 300 μ g/ml hygromycin B (Roch)
G418	YE4S +150 μ g/ml geneticin G418 (Gibco)
Aureobasidin A	YE4S + 0.5 μ g/ml aureobasidin A (Takara bio)
clonNat	YE4S + 100 μ g/ml nourseothricin (Werner Bio-agents)

Selective medias for auxotrophic marker were made by adding to EMM liquid media bottle or melted and cooled bottle of agar media the appropriate supplements to a final concentration of (225 mg/ml)

2.5.6 Frozen stock

Frozen stock of strains were made in YFM media and stored a -80°C according to described methods (Moreno et al., 1991).

2.6 Creating strain

2.6.1 Gene targeting

Gene deletion, N- and C-terminal tagging, and promoter replacement at endogenous loci were performed by the one-step gene insertion method (Bahler et al., 1998). The kanMX6 cassette was switched when needed to hygMX6 (Sato et al., 2005), (Hentges et al., 2005), his3⁺ or leu⁺. The cassette are then named his3⁺MX6 and kanMX6::leu1⁺. 100pb oligonucleotides are designed with 80 bp of homology with the flanking sequences of the insertion site at the endogenous locus to promote insertion, and 20 bp of homology with the cassette to amplify the plasmid template by PCR.

2.6.2 Random spores analyses

Most strains used in this study were constructed by random spore analysis.

Protocol:

1. h⁹⁰ or strains of opposing mating type with different genotypes were patched on ME plate to induce meiosis
2. Incubated at 25°C for 2 to 3 days
3. Incubated for at least 8 hours at RT on a rotating wheel in presence of 0.5% of Helix Pomatia Juice (Pall Biosepra), to break down the cell wall and free the spores.
4. Spores were then pelleted
5. Re-suspended in 1 ml of ddH₂O

- Platted on appropriate selective plates (~200 spores/plates) in order to select only the spores with the required genotype

2.6.3 Pcp1-2 copies

To create the strain harbouring two copy of *pcp1* gene, the strategy was to insert into the genome of a wt or a *pcp1-GFP* strain an extra GFP tagged copy of *pcp1* under the control of its own promoter and terminator.

The *aur1* locus was used as a marker to insert the different *pcp1* constructs as strains used in the laboratory harbour a mutation in the *aur1* gene preventing them to grow in the presence of aureobasidin.

Construct name	<i>pcp1</i> endogenous locus	<i>aur1</i> locus
P/P_{gfp}	<i>pcp1</i>	<i>pcp1-GFP</i>
P_{gfp}/P_{gfp}	<i>pcp1-GFP</i>	<i>pcp1-GFP</i>

- pcp1* with its own promoter and terminator was cut out of a plasmid from a genomic library (kind gift from Takashi Toda) using EcoRV and SacI restriction enzymes
- Cloned into pCST159 = (pAur1-Pcp1)
- After PCR on genomic DNA C-terminal part of *pcp1-GFP* was sub-cloned into pAur1-Pcp1M = (pAur1-Pcp1-GFP) using PstI and EcoRV restriction enzymes
- Construct were verified by sequencing
- Transformation in appropriate yeast strain after linearization of the pAur1-Pcp1-GFP with SwaI restriction enzyme was used to create the construct P/P_{gfp} and P_{gfp}/P_{gfp}

2.6.4 Diploids

In order to isolate diploids, the advantage of complementation of *ade6-M210* and *ade6-M216* mutations at the *ade6* locus was used. Both of these mutations confer respectively a red/pink colour when grown on low adenine media (YE). But the presence of both allele together in a diploid confer white colour.

To isolate diploids:

1. Strains of opposite mating type harbouring the different mutation at the adenine locus were patched for mating on ME plates for 10 to 12 hours at 25°C.
2. Re-streaked on EMM without adenine at 32°C
3. White colony soon after their appearance were picked and transferred on YE plate to verify their diploid state
4. Transferred on YE4S plate to use for experiments and to create a frozen stock
5. In parallel, transferred on ME plate and incubated O/N at 25°C to verify the capacity of the diploids to sporulate

2.7 Yeast transformation

Prior to transformation, transforming DNA was prepared by PCR amplification or plasmid digestion and then purified.

1. 20 ml of exponentially growing cells in YE4S media were pelleted
2. Pellet was washed twice in 1 ml of LiAc-TE
3. Re-suspended in ~80 µl of LiAc-TE, 100 µl of the concentrated cells was used for transformation

4. 2 μ l of salmon sperm carrier DNA boiled for 5 min and then chilled on ice and 10 μ l of transforming DNA were added to the 100 μ l of concentrated cells and incubated for 10 min at RT
5. 260 μ l of 40% PEG-LiAc-TE was added, mixed by gentle pipetting, the cell mix was then incubated at 32°C for 45 min
6. 43 μ l of pre warmed DMSO was added
7. Cells were heat-shocked at 42°C for 5 min
8. Pelleted, washed twice in 1 ml of ddH₂O and re-suspended in 500 μ l of YE4S media
9. For drug selection, the 500 μ l of cells were allowed to recover for 4 hours at 32°C in 5 ml of YE4S media
10. After recovery, cells were pelleted and re-suspended in 400 μ l of ddH₂O
11. 200 μ l was plated on YE4S media containing the adapted drug
12. Transformants were picked, re-streaked onto selective media and their genotype verified by PCR and/or microscopy

2.8 Genomic DNA preparation

1. 10 ml of culture grown to saturation were pelleted and washed with ddH₂O
2. Supernatant was discarded and pellet re-suspended in residual solution by brief vortexing
3. 200 μ l of smash prep buffer were added along with 200 μ l phenol:chloroform:isoamyl alcohol 25:24:1 (v/v) and ~0.3 g of acid washed beads
4. The mixture was vortexed for 3-4 min
5. 200 μ l of TE (pH8) was added and tubes centrifuged for 5 min
6. The aqueous layer was transferred to a new tube, 1 ml of 96% ethanol was added and mixed by inversion

7. Tubes were centrifuged for 2 min and the supernatant discarded
8. The pellet was re-suspended in 400 µl of TE plus 3 µl of 10 mg/ml RNaseA and incubated for 5 min at 37°C
9. 10 µl of 4 M ammonium acetate was added along with 1 ml of 96% ethanol and mixed by inversion
10. Tubes were centrifuged for 2 min and the supernatant discarded
11. Pellet was air dried or vacuum dried at RT and then re-suspended in 50 µl of TE, for PCR purposes the 1/40 dilution in TE was prepared

2.9 PCR

PCR was performed with different conditions and enzymes depending on the nature of the experiments.

2.9.1 Routine

For strains tagging or deletion verification, PCR was carried out using Expand long template PCR system (Roche) using the following conditions.

Components	Final concentration or volume
Buffer N°1 10x	1x
Mgcl2 (25 mM)	2.5 mM
dNTP mix (100 mM)	2.5 mM (each)
Primers (Forward and Reverse)	0.5 mM (each)
Polymeras	0.2 µl
DNA template	1 µl
ddH ₂ O	to a final volume of 20 µl

In most cases the programme used was as follow, annealing temperature and extension time were modified as required.

1. 94°C for 5 min
2. 94°C for 15 sec
3. 53°C for 30 sec
4. 68°C for 2.5 min
5. go to step (2) 30 more times
6. 68°C for 7 min
7. Store at 4°C

2.9.2 For gene targeting

For gene targeting, PCR was carried out with the same conditions as for routine PCR (see 2.7.1) but in a final volume of 100 μ l.

The programme used was as follow.

1. 94°C for 2 min
2. 94°C for 30 sec
3. 50°C for 2min
4. 68°C for 5 min
5. go to step (2) 4 more times
6. 94°C for 30 sec
7. 55°C for 1 min
8. 68°C for 5 min
9. go to step (6) 30 more times
10. 68°C for 10min
11. Store at 4°C

2.9.3 For cloning

For cloning purposes in order to minimise the introduction of mutation, PCR was carried out using Vent DNA polymerase system (NEB) using the following conditions.

Components	Final concentration or volume
ThermoPol Reaction Buffer (10x)	1x
MgSO ₄ (100 mM)	10 mM
dNTP mix (100 mM)	2.5 mM (each)
Primers (Forward and Reverse)	0.5 mM (each)
Polymerase	0.5 µl
DNA template	1 µl
ddH ₂ O	to at final volume of 50 µl

The following programme was used

1. 94°C for 5 min
2. 94°C for 15 sec
3. 52°C for 30 sec
4. 68°C for 4 min
5. Increase by 10 sec every cycle and go to step (2) 35 more times
6. 68°C for 7 min
7. Store at 4°C

2.10 Meiosis synchronisation

2.10.1 Nitrogen starvation

Nitrogen starvation was used to induce meiosis. Diploid cells were used, as conjugation of haploid strain is a limiting factor to synchronise cells in meiosis.

1. Diploid cells were woken-up from frozen stock, check for sporulation efficiency by patching on ME plate O/N at 25°C
2. Cells of O/N liquid culture in EMM to OD = 0.4-0.6 were harvested by centrifugation

3. Washed twice with EMM-N⁻low glucose
4. Re-suspended to OD = 0.2 in EMM-N⁻low glucose
5. Incubated at 30°C at 100 RPM
6. 1 ml aliquot were taken at different time point depending on the experiment requirement for further counting number of nuclei per ascus (see 2.8.2)
7. If used for 2D-PGE or western blot experiments respectively, 50 ml or 15 ml aliquot were harvested by centrifugation at different time point depending on the experiment requirement
8. Washed with PBS containing PMSF (1 mM) and protease cocktail inhibitor (SetIII Calbiochem)
9. Cells pellet were then frozen in liquid nitrogen and store at -80°C

2.10.2 Counting number of nuclei per ascus

To determine the level of synchrony, number of nuclei / ascus were counted throughout meiosis using DAPI staining.

1. 1 ml aliquot was taken at different time point depending on the experiment requirement
2. Cells were pelleted at maximum speed
3. Quickly fixed in 500 µl of 70% ethanol kept at 4°C
4. Washed once in 1 ml of PBS
5. Rehydrated in 500 µl of PBS (at that stage, cells can be stored at 4°C for maximum 5 days)
6. Cells were then pelleted at maximum speed in microcentrifuge
7. Re-suspended in 3 µl of VECTASHIELD mounting media with DAPI (Vector Laboratories)

- 1.5 μl were mounted between polysine pre-coated adhesive slide (VWR international) and 22x22 mm cover glasses (Menzel-Glaser) and imaged with a fluorescence microscope Zeiss Axioplan 2 microscope (Carl Zeiss Micromaging) with an attached CCD camera (Hamamatsu). Images were captured and analysed using Volocity software (Improvision)

2.11 Protein extraction

2.11.1 Trichloroacetic acid (TCA)

For western purposes, proteins were extracted using TCA extraction method.

1. Cells pellet of 15 ml liquid culture of OD = 0.5 were re-suspended in 200 μl added with PMSF (1 mM) and 1x protease cocktail inhibitor (SetIII Calbiochem)
2. Acid washed glass beads were added up to the meniscus
3. The mixture was vortex for 1 min
4. Tubes were pierced at the top and the bottom and placed into a new tube
5. The suspension was recovered in the new tube by centrifugation at 3000 RPM for 1 min
6. Beads were washed with 100 μl of 20% TCA added with PMSF (1 mM) and 1x protease cocktail inhibitor (SetIII Calbiochem) and the wash added to the recovered suspension
7. The mix was centrifuged at 3000 RPM for 10 min at room temperature
8. Supernatant was discarded and the pellet re-suspended in 150 μl of protein buffer (see 2.2.2)
9. Sample was boiled for 5 min
10. Centrifuge for 10 min at 3000 RPM

11. The supernatant was transferred to a new tube (at that stage, the protein extract can be stored at -20°C, if stored at -20°C sample were re-boiled before loading)
12. 1 to 1.5 µl of 1 M DTT was added to 8 to 15 µl of protein extract (depending on experiments) and loaded onto NuPAGE 4-12% Bis-Tris acrylamide gradient gels with MOPS SDS running buffer (Invitrogen) using XCell SureLock electrophoresis system for mini gels (Invitrogen) and XCell4 SureLock for midi gels (Invitrogen)
13. After the run, protein gels were analysed by western blot (see 2.11)

2.11.2 For two-dimensional protein gel electrophoresis (2D-PGE)

For 2D-PGE, following meiosis synchronisation by nitrogen starvation proteins were extracted with specific 2D-PGE sample preparation solution (see 2.2.2).

All the steps were performed on ice or at 4°C

1. Pellet from 50 ml liquid culture stored at -80°C, was re-suspended in 300 µl of 20%TCA added with PMSF (1 mM) and 1x protease cocktail inhibitor (SetIII Calbiochem)
2. 300 µl of acid washed glass beads were added
3. Cells were broken-up using Fast-prep machine from 45 sec at 6.5 setting
4. Tubes were pierced at the top and the bottom and placed into a new tube
5. The suspension was recovered in the new tube by centrifugation at 3000 RPM for 10 min
6. The supernatant was discarded and the pellet re-suspended in 150 µl of 2D-PGE sample preparation solution added with 2% appropriate IPG buffer (GE Healthcare), 1x Nuclease Mix (GE Healthcare), PMSF (1 mM) and 1x protease cocktail inhibitor (SetIII Calbiochem)
7. Centrifuged for 10 min at 13200 RPM
8. The supernatant was transferred to a new tube and stored at -80°C

2.12 Two-dimensional protein gel electrophoresis

Two dimensional protein gel electrophoresis (2D-PGE) was performed as described in 2D Electrophoresis Handbook, Principles and Methods (GE Healthcare).

Prior to 2D-PGE, protein concentration of the protein extract obtain as in 2.9.2 were determined using 2D Quant Kit following manufacturer instructions (GE Healthcare). And required amount (depending on experiments) of protein extract was cleaned using 2D clean-up kit following manufacturer instructions (GE Healthcare) and re-suspended in 100 μ l of DeStreak Rehydration Solution (GE Healthcare) containing 0.5% appropriate IPG buffer.

2.12.1 First dimension isoelectric focusing

1. 24 cm long Immobiline DryStrip gel strips with an indicated immobilised pH gradient (GE Healthcare) were rehydrated for 24 hours in 450 μ l of DeStreak Rehydration Solution containing 0.5% appropriate IPG buffer.
2. Samples were cup-loaded on the opposite side of the predicted isoelectric point (pI) of the protein of interest on the 24 cm long gel stripe
3. The first dimension of the 2D-PGE that separates proteins depending on their pI was run on Ettan IPGphor II Manifold instrument (GE Healthcare) using the following running protocol

For 4-7pH 24cm long Immobiline DryStrip gel strips:

1. 0.5 kVh at 500 V
 2. 5.2 kVh gradient up to 1000 V
 3. 13.5 kVh gradient up to 800 V
 4. 45k Vh at 8000 V
4. As soon as the first dimension run was finished, gel strip were stored at -80°C or directly used for the second dimension SDS-PAGE

2.12.2 Second dimension SDS-PAGE

After being subjected to isoelectric focusing, the second dimension of a 2D-PGE separates proteins depending on their sizes by SDS-PAGE.

1. Gel strip, was first subjected to equilibration in Equilibration buffer containing 65 mM DTT for 15 min
2. Followed by a second equilibration step of 15 min in Equilibration buffer containing 135 mM iodoacetamide
3. 24 cm gel strip was then cut in 3 equal fragments and subjected to the second dimension using NuPAGE 4-12% Bis-Tris Zoom IPG well acrylamide gradient gels with MOPS SDS running buffer (Invitrogen) using XCell SureLock electrophoresis system (Invitrogen)
4. After the second dimension, 2D-PGE were analysed by western blot.

2.13 Western blotting

1. After SDS-PAGE, proteins were transferred in Transfer Solution to a polyvinylidene fluoride (PVDF) membrane (Bio-Rad) in a Mini Trans-Blot Cell for mini gels (Bio-Rad) and Trans-Blot Cell for midi gels (Bio-Rad), at 250 mA for 1 h at 4°C
2. Membrane was then blocked for 1 h or O/N in milk solution
3. Incubated for 1 h at RT in milk solution containing primary antibody (concentration is antibody dependant see table)

Primary Antibody	Concentration
Mouse Anti-Myc.9B11 (Cell Signalling)	1:4000
Rabbit Anti-Pcp1(Fong et al., 2010)	1:5000
Mouse Anti-HA.11 (Covance)	1:1000

4. Washed 3 times 10 min in milk solution
5. Incubated for 45 min at RT in milk solution containing secondary antibody

Secondary Antibody	Concentration
Sheep ECL Anti- mouse IgG Horseradish peroxidase linked whole antibody (GE Healthcare)	1:5000
Donkey ECL Anti-Rabbit IgG Horseradish peroxidase linked whole antibody (GE Healthcare)	1:5000

6. Washed 3 times 10 min in PBST
7. Proteins were detected using ECL Plus Western Blotting Detection Systems (GE Healthcare)

2.14 Fluorescence microscopy

Time-lapse live cell imaging was carried out in a temperature controlled Environmental Chamber with a DeltaVision Spectris (Applied Precision) comprising an Olympus IX71 wide-field inverted epifluorescence microscope, an Olympus UPlanSapo 100x NA 1.4 oil immersion objective, and a Photometrics CCD CH350 camera cooled (Roper Scientific) or a Cascade EMCCD 512B camera (Roper Scientific) (only for the experiment with membrane marker). Images were captured and analysed using SoftWoRx (Applied Precision).

1. Cells induced in meiosis (see 2.3.4) were adhered to a 35mm glass culture dish (MatTek) precoated with 0.2 mg/ml soybean lectin (Sigma) and immersed in EMM-N⁻ with required supplements plus 15 μ M thiamine for strains harbouring *Pnmt1-GFP-atb2* or *Pnmt1-mRFP-atb2* construct. When required, beads (TetraSpeck microspheres 1.0 μ m fluorescence

blue/green/orange/dark red, invitrogen) where mixed to the cells prior to adhesion to the culture dish.

- Images were taken with the following setting depending on experiments and channels (see table).

Exp. Name	Lapse Time (min)	Sample Thickness (µm)	Z spacing (µm)	Number of Z section	Exposure time (s)		
					GFP	mRFP	CFP
A	10	6.3	0.3	21	0.2	0.08	-
B	10	9.1	0.35	26	0.2	0.06	-
C	10	9.1	0.35	26	0.2	0.2	
D	10	9.1	0.35	26	0.2	0.2	0.2
E	5	8.1	0.3	27	0.5	0.08	-

Note:

A = Pcp1-GFP, Sid4-GFP quantitation experiments

B = Pcp1-2 Copies quantitation and Alp4 over-expression experiments

C = Pcp1-GFP Sid4-mRFP, Alp4-GFP Sid4mRFP co-localisation experiment, Alp4-GFP Sid4mRFP mRFP-tubulin experiment and Sid4-mRP GFP-tubulin experiment

D = Membrane visualisation experiment

E = Diploid analysis experiment

- Images were then deconvoluted and combined to form a 2D image using Maximum Intensity projection setting for aesthetic purposes and Sum Intensity projection setting for quantitation purposes
- Images were finally processed with Adobe Photoshop

2.15 Fluorescence signal quantitation

SPB signal quantitation was performed as described in Chapter 3 using Volocity software (Improvision) on deconvoluted 3D movies, projected in 2D images using Sum Intensity setting using SoftWoRx (Applied Precision).

Chapter 3. Measurement of SPB component intensities in live cells

3.1 Aim

The major goal of this work was to investigate the differences at the SPB level in presence or absence of bouquet function. In this chapter, we examine the quantity of SPB components using intensity measurement in live cells. We ask the question: Does the difference between WT and bouquet deficient SPB lie in the level of SPB components? The idea to explore the quantity of SPB components came from two different angles. First from previous work done in Julie Cooper's Lab (Tomita and Cooper, 2007) where imaging of the SPB by fluorescence microscopy in live cell gave the impression that SPBs were brighter in bouquet deficient strains than in WT. Second, a report in the literature (Jin et al., 2005) showed that substantial over-expression of Pcp1 leads to spindle defects and SPB fragmentation somewhat reminiscent of those observed in the absence of the bouquet. Hence, we wished to test the possibility that association of telomeres with the SPB is required to limit the accumulation of SPB components, perhaps ensuring that the SPB would commence proper duplication once a threshold level of Pcp1 (and/or other SPB components) was reached. In order to explore the quantity of SPB components, we first needed to choose the most appropriate measurement method.

3.2 Introduction of quantitation method

3.2.1 Western blotting or fluorescence microscopy?

The two techniques we envisaged were protein quantitation by western blotting and protein quantitation by fluorescence microscopy. In order to discriminate between these two methods, we evaluated the different parameters that could influence accuracy, taking into account the dynamics of the SPB and the considerable changes in SPB components levels through meiosis.

We chose to perform SPB quantitation by fluorescence microscopy in live cell for two major reasons. The first one concerns the very nature of the techniques while the second concerns the specific nature of bouquet deficient cells' phenotypes. As opposed to live microscopy where one can follow behaviour of individual cells and can easily distinguish between morphologically distinct phases, western blot analysis gives an overview of a mixed population at a certain time point. One way to counteract this problem would have been to work with synchronised cultures. However, we were dubious about utilising the standard methods of meiosis synchronisation in fission yeast (Nurse, 1985, Iino and Yamamoto, 1985, Chikashige et al., 2004). In addition, the penetrance of phenotypes induced by bouquet deficiency is only slightly more than half of the population (Tomita and Cooper, 2007), which means that the effect observed by western blot would be diluted by half. In contrast, by single cell observation and quantitation, we can categorise phenotypes and draw relevant correlations.

3.2.2 What defines the signal to be quantified?

As a previous study showed that substantial over-expression of Pcp1 leads to SPB and spindle defects (Jin et al., 2005), Pcp1 appeared a good SPB marker to test our hypothesis. Quantitation was thus conducted on cells where the gene encoding Pcp1 was GFP tagged at its endogenous locus; these cells also harbour histone H3 tagged at its endogenous locus with mRFP in order to easily visualise meiotic progression. In WT vegetatively growing cells, Pcp1-GFP signal is seen as

a dot localising to the SPB (Flory et al., 2002). Pcp1 signal is weak during meiotic prophase (weaker than in vegetatively growing cells) and appears as a SPB dot just prior to the end of the horsetail movements. We can then clearly follow the division of the signal in MI and again in MII, when the SPBs orient toward the tip of the cell (Figure 3.1). However, in *bqt1Δ* cells, the signal is highly disorganised (Tomita and Cooper, 2007).

We first thought to quantify the total Pcp1-GFP signal present in the cell. To do so, we needed to be able to easily determine the outline of the cells in a field including several cells or to image a field comprising only one cell. Both of these options were limiting and challenging. In contrast, quantifying Pcp1-GFP as the intensities of the bright Pcp1 foci that appear at the SPB was more feasible (and accurate; see below). In WT cells, it is easy to discern the SPB foci as the SPB duplicates twice during the course of meiosis. In *bqt1Δ* cells, while this regular pattern is often disorganised, it remains easy to distinguish by eye SPB bright foci over the background signal; moreover, as expanded upon later in this chapter, we have found that there are no or very few meiotic *bqt1Δ* cells with more than 4 SPB dots (Table 3.2). Therefore quantitation was performed using the sum of Pcp1 bright foci at each time point throughout meiosis.

3.2.3 Total SPB intensity quantitation

Total SPB signal quantitation was performed with Volocity software (Improvision) on deconvoluted 3D movies, projected in 2D images using the Sum Intensity setting of SoftWoRx (Applied Precision). Microscope and experimental settings were rigorously kept identical for each experiment that we wanted to compare (see materials and methods 2.12, 2.13).

In both WT and mutant cells, all Pcp1-GFP signals were selected by eye and summed to quantify the total SPB signal in one cell at one time point; this sum was called 'sum of signal'. In order to compensate for the background signal included in the areas selected, equivalent signal-free regions within the same cells

3. Measurement of SPB component intensities in live cells

were summed and called 'sum of background equivalent area'. In addition, to normalise for the inherent variability of every cell and every experiment, the average intensity for one pixel of background was calculated for every time point and called 'Average background' (Figure 3.2). Ultimately, the formula to calculate the total SPB signal intensity for one time-point is:

Total SPB signal intensity =

(Sum of signal – Sum of background equivalent area) / (Average background)

This approach was repeated for every time-point and the outcome displayed as a graph of Total SPB signal intensity in a given cell over time. Tomita & Cooper described that 55% of *bqt1Δ* cells have dysfunctional SPB where SPB signal is markedly disorganised throughout meiosis and fail to localise to opposite ends of the zygote at anaphase-I (Tomita and Cooper, 2007). Therefore, to assess whether SPB defects were associated with altered quantities of Pcp1, we compared WT cells to *bqt1Δ* cells with dysfunctional SPB; 'wt-like' *bqt1Δ* cells (those with no obvious phenotypic defects) were categorised separately. Although this last category could represent a great internal control, technical issues have prevented us from being able to collect enough data to be quantitative about it. Quantitation requires imaging of the entire volume of the cell. However, as cells are being filmed over several hours, the precise focal planes may change and it is not rare to lose some signal. This issue is most observed in cells where SPBs segregate properly, as proper segregation is associated with extensive movements of the SPBs in the cell volume. Cells chosen for quantitations were therefore, rigorously fully observed.

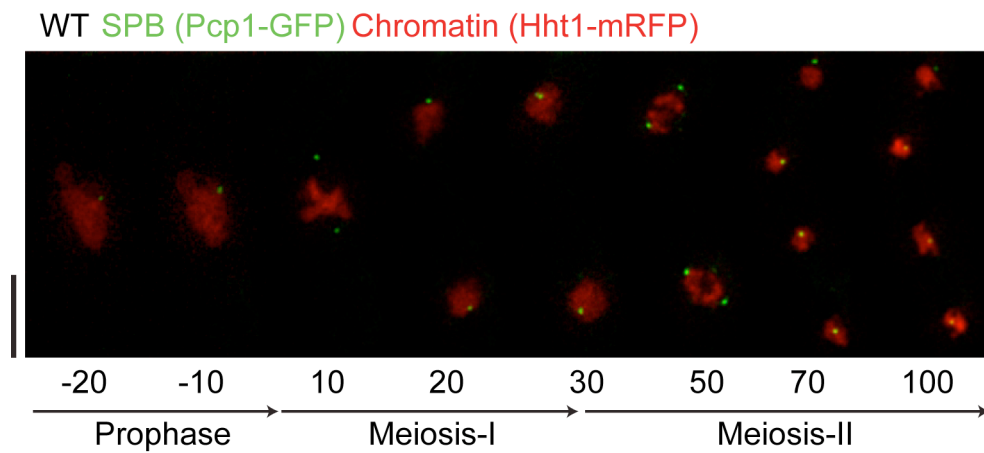
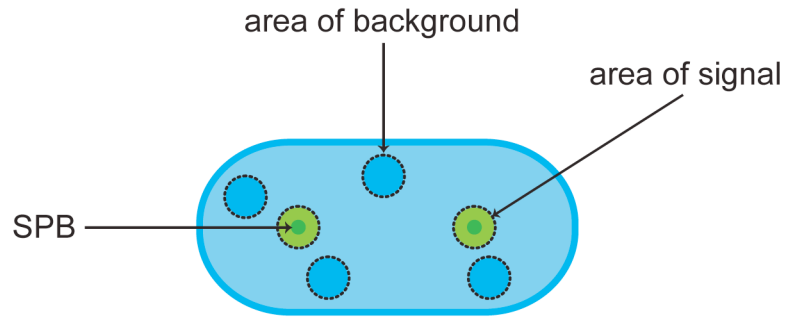


Figure 3.1 Example of WT meiosis

Series of frames from WT meiosis movie acquired by fluorescence microscopy in live cell. SPB and chromosomes were observed via endogenously tagged Pcp1-GFP and Hht1-mRFP respectively. Numbers under the frames represent the time in minutes. The stages of meiosis are indicated below. 0 min is the onset of MI. Scale bar equals 5 μ m. Meiosis-I stage illustrates how the SPB signal orients toward the tip of the cell during metaphase-I (10 min) and anaphase-I (20 min). Meiosis-II illustrates how the SPB signal orients toward the tip of the cell during metaphase-II (50 min).



Total SPB signal intensity =

$$(\text{Sum of signal} - \text{Sum of background equivalent area}) / \text{Average background}$$

$$= \text{[Two green circles]} + \text{[Four blue circles]} / 2$$

Figure 3.2 Schematic diagram of Total SPB intensity quantitation method
 Example of Pcp1 intensity quantitation for a cell with two SPBs. Area of signal describes areas comprising Pcp1-GFP signal. Area of background describes Pcp1-GFP signal free areas of the exact same size as the areas of signal. Average of background is determined for every cell at every time point and represents the average intensity for one pixel of background. Total SPB signal intensity represents total Pcp1-GFP signal at this time-point.

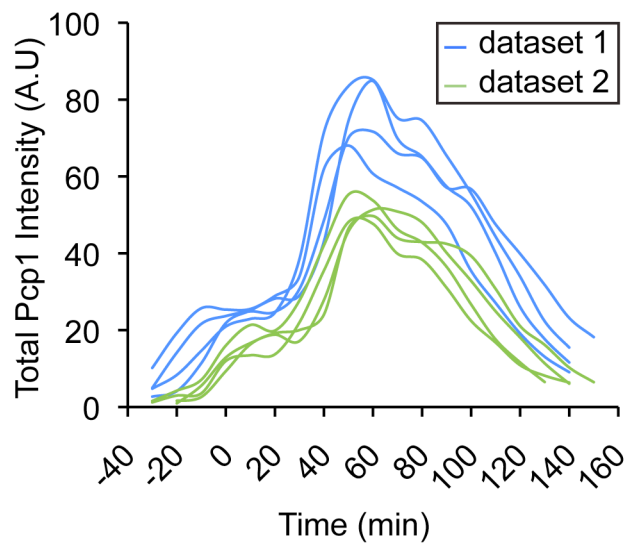
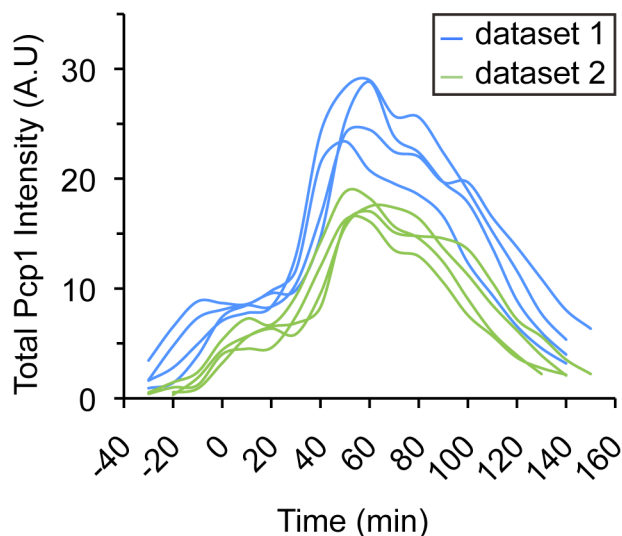
3.2.4 Issues of normalisation

To verify whether our method of normalisation indeed corrects for variations between different experiments due to external factors such as the stability of the lamp, we compared datasets obtained weeks apart (Figure 3.3). We observed that while films of WT cells captured over a given week yield very similar values, the range of the values is slightly wider when different weeks are compared (blue curves and green curves represent different weeks). We therefore tried to improve the normalisation using GFP-coated beads instead of the “Average background” described in the previous section. Beads were mixed with the cells and both were adhered to a culture dish, immersed in sporulation media and imaged. At each time point, an area containing a bead was selected as well as an equivalent signal-free region within the vicinity of the bead, and the intensity of the bead calculated as (signal of the bead – signal of the background). The resulting formula to calculate the total SPB signal intensity for one time-point is:

Total SPB signal intensity =

(Sum of signal – Sum of background equivalent area) / (Bead intensity)

Comparison of the datasets normalised using the beads versus the scaling factor reveals that the two methods yield similar results (compare Figure 3.3A and B). We nonetheless wanted to pursue the experiment with the GFP-coated beads and compare more datasets. Unfortunately, however, when we imaged a new batch of bead from the same company (using the same setting as for the cells), the bead signals were suprasaturated, thereby invalidating the use of the bead. Hence, increased intensity of the new beads was much higher than that of the old beads, so for the moment, we returned to use the scaling factor.

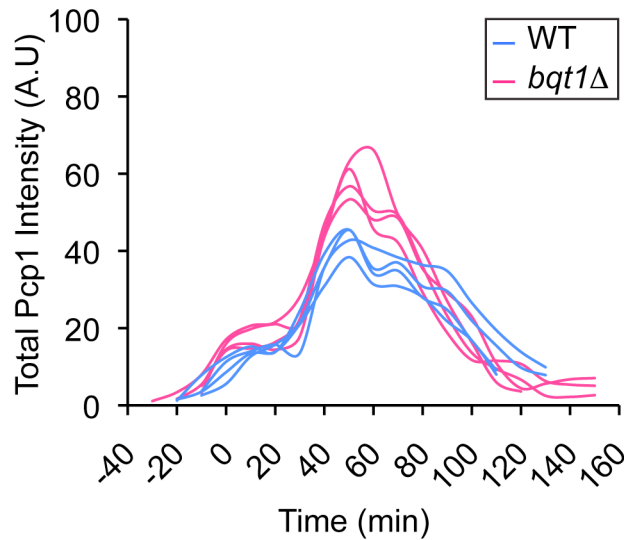
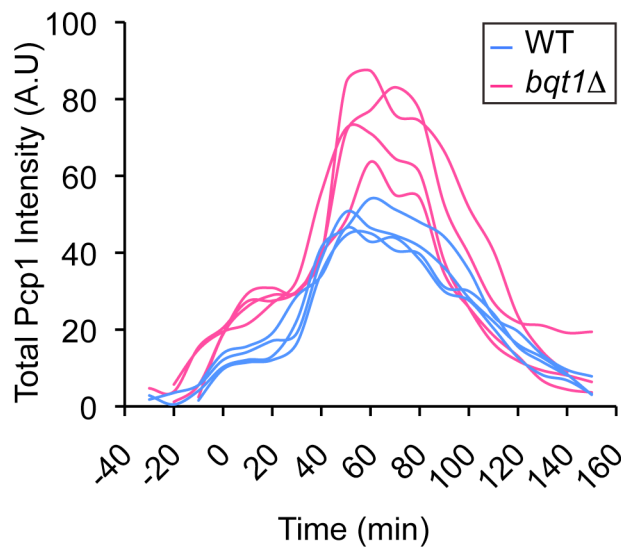
A Comparison of WT profiles normalised using the scaling factor**B** Comparison of WT profiles normalised using the beads**Figure 3.3 Comparison of normalisation methods**

(A-B) Superimposition of 4 curves from WT cells of Pcp1 intensity measurement from one dataset (blue) and 4 curves from WT cells of Pcp1 intensity measurement from another dataset (green). 0 min represent the onset of MI. (A) Normalisation of total pcp1 signal was performed using the scaling factor (B) Normalisation of total pcp1 signal of the exact same data as in (A) was performed using the bead. No differences were observed between the two methods of normalisation.

3. Measurement of SPB component intensities in live cells

While the normalisation mode did not appear to affect variations between experiments, series of films captured on different weeks did appear to vary slightly but systematically. To explore this effect further, we asked whether the relative results obtained (see below for extensive comparison) for WT and *bqt1Δ* were preserved between datasets imaged weeks apart (Figure 3.4). In this instance, a dataset refers to data collected for both WT and *bqt1Δ* in a single narrow window of time. We found that while two datasets imaged weeks apart have slightly different magnitudes of intensity (compare Figure 3.4A and B), the trends and relative intensity ranges between strains do not vary.

In conclusion, normalisation of the intensity obtained during experiments performed far apart in time is a major limitation in the number of cells includable in the statistics. Hence, we have always attempted to image cells for comparison within the narrowest possible window of time and whenever capturing data over multiple weeks, we take equal numbers of films of each different strain within *each* week. We are confident that data can be interpreted if all parameters are taken into account with methodical and thorough analysis.

A Comparison of WT and *bqt1* Δ Pcp1 intensity profiles (dataset 1)**B** Comparison of WT and *bqt1* Δ Pcp1 intensity profiles (dataset 2)**Figure 3.4 Values of Pcp1 intensity are variable from experiments but in a consistent way**

(A-B) Superimposition of Pcp1 intensity graphs of 4 WT cells (blue) and 4 *bqt1* Δ cells with a dysfunctional SPB (magenta). 0 min represent the onset of MI. (A) and (B) are two datasets where within each dataset, WT and *bqt1* Δ data were collected in a narrow window of time. Values between (A) and (B) are variable but *bqt1* Δ profiles have slightly higher intensities than WT, independently of the dataset.

3.3 Analysis of Pcp1 intensity measurement in live cells

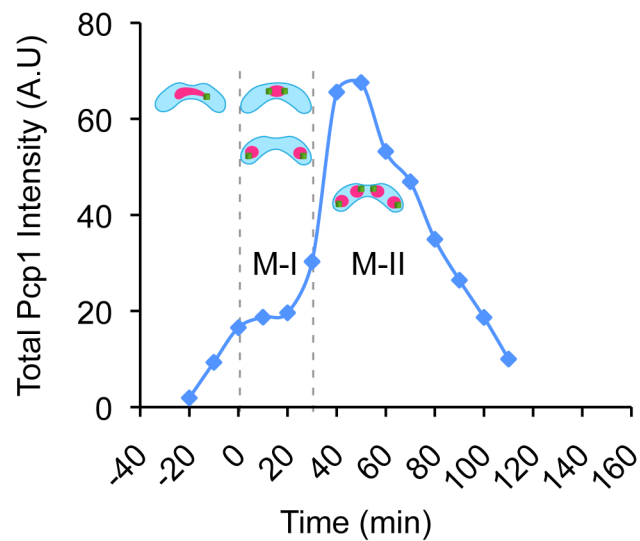
In order to determine whether the difference between WT and bouquet deficient SPB stems from altered levels of SPB components, we quantified the total SPB signal intensity in WT and *bqt1Δ* cells using the method explained in the previous section. We chose to pursue our studies using *bqt1Δ* cells since they sustain the most severe level of bouquet disruption without any of the general telomere phenotypes (e.g. telomere lengthening and deprotection) seen in the absence of Taz1 or Rap1 (Cooper et al., 1997, Kanoh and Ishikawa, 2001).

3.3.1 Pcp1 accumulation in WT meiosis is a dynamic process

We examined the Pcp1-GFP intensity profile for 22 WT cells. The shape of the curve obtained is highly dynamic, demonstrating the fine-tuning of SPB components levels through meiosis (Figure 3.5A). The curve can be divided into five distinguishable parts. The first portion of the curve illustrates Pcp1 accumulation during meiotic prophase, when the bouquet is present and first SPB duplication is ongoing. The second part of the curve reveals a shoulder starting at the onset of MI. At this stage, SPB duplication has finished and segregation of the homologues is taking place on the first meiotic spindle. The shoulder stage is directly followed by a large and rapid increase starting at the onset of MII; this represents the second meiotic SPB duplication. The peak of the curve associated with MII spindles and segregation of the sister chromatids is followed by the gradual diminution of Pcp1 signal while cells finish meiosis and prepare for spore formation.

To normalise timing of all timecourses and superimpose the curves in one graph, we align all the peaks on X-axis (Figure 3.5B). We observed that each WT cell follows similar profile to that of Pcp1 accumulation with the same timing; this superimposability is most prominent in the first parts of the graph, as the reduction of Pcp1 signal at the end of MII appears to be more variable.

A WT Pcp1 intensity profil and the phases of meiosis



B Superimposition of 22 WT Pcp1 intensity profiles

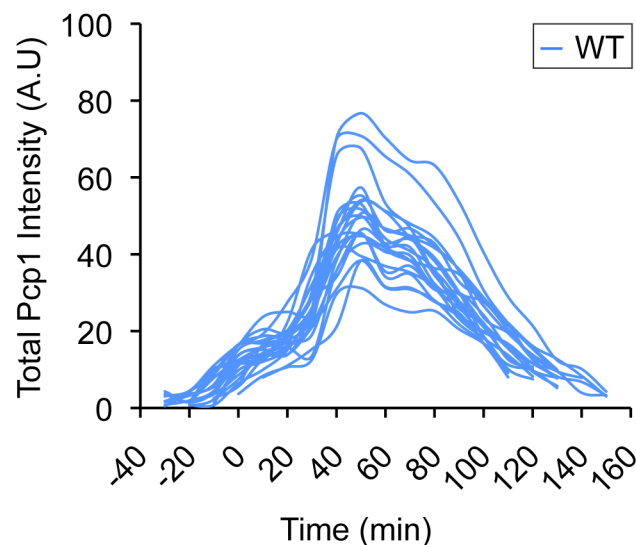


Figure 3.5 Pcp1 accumulation in WT meiosis is a dynamic process

(A) Example of a graph obtained for a WT cell after Pcp1 intensity measurement. The schematic cells in blue with magenta nucleus and green SPB dots illustrate the different phases of meiosis. From left to right: cell with an elongated nucleus horsetail stage in meiotic prophase, cell with two SPBs meiosis-I (M-I), cell with four SPBs meiosis-II (M-II). (B) Superimposition of 22 WT cells curves of Pcp1 intensity measurement. The characteristics shared by each curve are from left to right a small increase, a shoulder followed by a rapid and large increase and then diminution of the signal. 0 min represent the onset of M-I. Curves were superimposed by alignment of all the peaks on X-axis (50min).

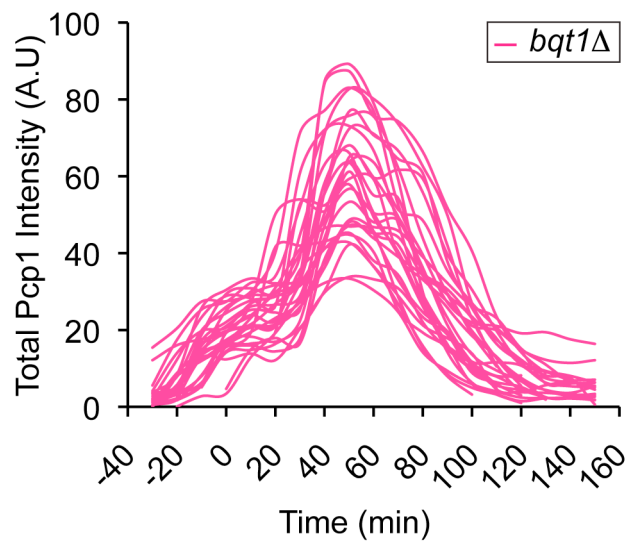
Proper SPB maturation is essential for successful behaviour of the SPB and the spindle later on during chromosomes segregation (Jin et al., 2005). Our observations illustrate how tightly controlled this phenomenon is throughout meiosis and provide the first quantitation of a SPB component through meiosis in fission yeast.

3.3.2 Bouquet disruption results in mildly altered Pcp1 levels but does not affect its timing of accumulation

To determine whether or not an over-accumulation of SPB components exists in bouquet deficient cells compared to WT, we carried out the same approach for 29 *bqt1Δ* cells with a dysfunctional SPB (Figure 3.6A). As for WT cells, to superimpose the curves in one graph, we align all the peaks on X-axis. We directly compared Pcp1 intensity profiles in WT and in *bqt1Δ* cells (Figure 3.6B) and calculated the average curves for both 22 WT and 29 *bqt1Δ* cells (Figure 3.9A).

We observed that the shape of the curve of all the *bqt1Δ* cells quantified is similar to that of WT cells. We can distinguish the same phases as in WT cells (small increase, shoulder followed by a rapid and large increase and then diminution of the signal). The timing of Pcp1 recruitment to the SPB seems therefore unaffected. After comparison of the value at each time-point throughout meiosis, we noticed a mild difference in Pcp1 level in WT *versus* *bqt1Δ*. The major differences are observed at the shoulder and at the peak of the curve, i.e. at MI and MII division, respectively. To verify if the mild difference detected is significant, we calculated the P-value using a t-test, tails 2 for three time-points at the shoulder of the curve and the peak (Table 3.1). The P-value calculated for the chosen time points in MI and in MII indicates no differences between the groups, we conclude that the variations observed are statistically significant.

A
Superimposition of 29 *bqt1* Δ Pcp1 intensity profiles



B
Comparison of WT and *bqt1* Δ Pcp1 intensity profile

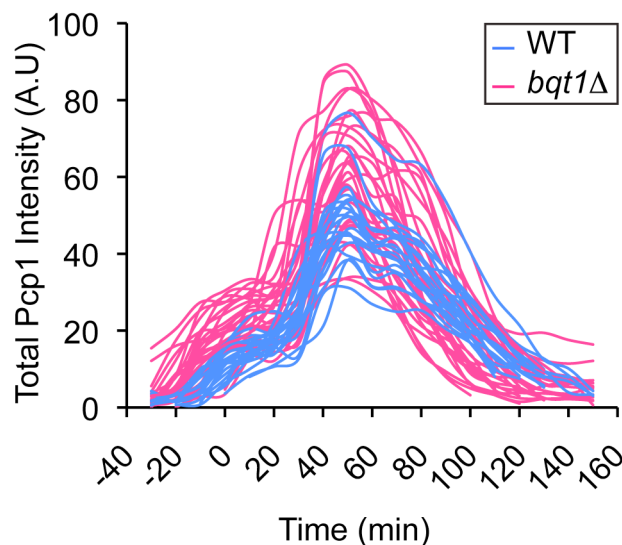


Figure 3.6 Pcp1 levels changes with the same timing in WT and *bqt1* Δ cells

(A) Superimposition of Pcp1 intensity measurement of 29 *bqt1* Δ cells with a dysfunctional SPB. (B) Superimposition of Pcp1 intensity graphs of 22 WT cells (blue) and 29 *bqt1* Δ cells (magenta). The characteristics shared by each curve are similar to WT from left to right a small increase, a shoulder followed by a rapid and large increase and then diminution of the signal. 0 min represent the onset of MI. Curves were superimposed by alignment of all the peaks on X-axis (50min).

3. Measurement of SPB component intensities in live cells

	Meiosis-I			Meiosis-II
	0min	10min	20min	Peak of the curve
P-value	3.94E-06	2.64E-07	3.68E-04	9.13E-03

Table 3.1 P- value comparing Pcp1 intensity of WT and *bqt1*Δ cells at several key points of meiosis

P-values are based on the comparison of 22 WT and 29 *bqt1*Δ cells with a dysfunctional SPB. Peak of the curve, compare the highest value of every WT and *bqt1*Δ cells.

To examine the duplication process more precisely, we tabulated the number of distinguishable SPB dots throughout meiosis in both WT and *bqt1Δ* cells. In this manuscript, “SPB duplication” will be referring to duplication of the signal being viewed. Whether or not this reflects, real SPB duplication or SPB maturation is a process that we are currently investigating. It is important to note that observation of four distinguishable dots at only one time point (i.e. in only one frame) at anytime throughout meiosis, was enough to be categorised as four distinguishable dots. Our resolution often allowed us to distinguish duplicated but yet un-separated dots. The results for 116 WT cells and 57 *bqt1Δ* cells that have a dysfunctional SPB (i.e. disorganised SPB signal that does not follow the WT pattern) are summarised in (Table 3.2). We observed that indeed 73.7% of the cells with a dysfunctional SPB do have in turn, one, two and then four discernible SPB dots (Figure 4.1-3). We believe that the category where we can count only two or three SPB dots (19.3%) is more a reflection of the large lapse time between frames (10 min) than an illustration of defective SPB duplication. Indeed one might think that in 10 min one might miss the time where the duplicated SPBs are actually distinguishable. In addition, given that we perform this analysis on 2D projection of the 3D images, we must consider that if we were to look at the 3D images we might be able to discriminate dots on top of each other. The last category, where we can count more than four SPB dots (7%) is also present in WT cells to a similar extent (6%) meaning that it is not a phenotype specific to bouquet mutant cells.

In conclusion, these data illustrate how despite obvious SPB disorganisation and chromosome segregation defects, direct comparison of Pcp1 levels throughout meiosis in WT cells and *bqt1Δ* cells does not reveal a defect in timing of Pcp1 accumulation/duplication. Nonetheless, these observations allowed us to observe a statistically significant difference in Pcp1 level at MI and MII anaphases, we therefore, next addressed whether such difference could be biologically significant. Furthermore, we gather important insights into the behaviour of SPBs in WT and *bqt1Δ* cells – these will be expanded upon in the next chapter.

Number of distinguishable dots	% of WT cells (n=116)	% of <i>bqt1Δ</i> cells (n=57)
4	93.1 (108)	73.7 (42)
3 or 2	0.9 (1)	19.3 (11)
More than 4	6 (7)	7 (4)

Table 3.2 SPB duplication is not significantly affected in bouquet deficient cells

Phenotypes were observed on WT and *bqt1Δ* meiosis movies acquired by fluorescence microscopy in live cell. SPB and chromosomes were observed via endogenously tagged Pcp1-GFP and Hht1-mRFP. 116 WT cells and 57 *bqt1Δ* cells that have a dysfunctional SPB were categorised in 3 levels. It is important to note that observation of four distinguishable dots at only one time point (i.e. in only one frame) at anytime throughout meioses, was enough to be categorised as four distinguishable dots. The percentage of cells exhibiting each phenotype is shown with the number of observed cells in parentheses.

3.4 Pcp1 level manipulation

In order to determine whether the small difference of Pcp1 intensity observed between WT and *bqt1Δ* is biologically significant or not, we wanted to re-create this Pcp1 increase in a bouquet proficient background and ask if this confers bouquet phenotypes.

3.4.1 Choice of Pcp1 over-expression strategy

To over-express Pcp1 we envisaged two different strategies. The first one was to place *pcp1* under the control of a strong foreign promoter (Maundrell, 1990) while the second was to add an extra copy of the *pcp1* gene into the genome.

3.4.1.1 Pcp1 over-expression strategy N°1 = strong foreign promoter

The most commonly used expression system in fission yeast is the *nmt* promoter, which stand for no message in thiamine promoter (*Pnmt*). Three versions exist, the full strength promoter (*Pnmt1*), and two attenuated versions (Basi et al., 1993) (*Pnmt41* and *Pnmt81*) with reduced activity. However, the strength of the promoter is highly dependent on the gene being expressed, and *Pnmt1* being a very robust promoter, it is often not possible to achieve full repression in the presence of thiamine (repress state). Hence even under repressed conditions, the protein of interest could be over-expressed.

Over-expression of Pcp1 using construct in which *pcp1* is under the control of *nmt1* promoter confers SPB and spindle defects (Jin et al., 2005). Therefore, we constructed GFP tagged versions of *Pnmt1-GFP-pcp1*, *Pnmt41-GFP-pcp1* and *Pnmt81-GFP-pcp1*. Before embarking on Pcp1-GFP quantitation, we first characterised the strains by imaging Pcp1-GFP signals and the end product of meiosis (the number of spores per ascus) under repressed conditions (presence of thiamine). For each genotype, the number of spores per ascus for two hundred asci were counted, and the experiment was repeated a minimum of 5 times

3. Measurement of SPB component intensities in live cells

(Figure 3.7A). Cells were classified in five categories: four normal spores, four abnormal spores, three, two or one spore. Abnormal spores are of uneven size and shape compared to normal spores, which are uniformly round and have the same size. In these experiments we are underestimating the percentage of deficient asci, as we cannot include those that fail to form spores since they are indistinguishable from zygotes. On the one hand, the proportion of asci with one or two spores is similar between *bqt1Δ* and *Pnmt1-GFP-pcp1* strains, while the proportion of asci with three spores increases in the latter, suggesting that defects in MII are more common in cells overexpressing Pcp1 than in cells lacking the bouquet. In addition, images of *Pnmt1-GFP-pcp1* cells under repressed conditions, from cycling cells (Figure 3.7B_h) or from cells undergoing meiosis (Figure 3.7B_e) reveal that Pcp1-GFP signal is more disorganised than in WT (Figure 3.7B_a and f) and *bqt1Δ* cells (Figure 3.7B_b and g). Hence, even under repressed conditions, *nmt1*-controlled Pcp1 leads to greater or different defects than in *bqt1Δ* cells. On the other hand, under repressed condition, *Pnmt41-GFP-pcp1* and *Pnmt81-GFP-pcp1* constructs behave like WT (Figure 3.7A). Moreover, as suggested by the proportion of asci with four spores, Pcp1-GFP signal behaviour in *Pnmt41-GFP-pcp1* and *Pnmt81-GFP-pcp1* cells appears WT-like (Figure 3.7B). Hence, these promoters fail to produce enough Pcp1 to recapitulate the Pcp1 elevation seen in the absence of the bouquet. Therefore, none of these three systems seems appropriate to recapitulate the mildly elevated levels of Pcp1 seen in *bqt1Δ* cells.

From simultaneous experiments I was performing at the time (described above) we also knew that Pcp1 accumulation is a highly dynamic process tightly regulated through meiosis; hence, choosing a constant Pcp1 overexpression level seemed unlikely to reproduce the *bqt1Δ* Pcp1-elevation phenotype. Therefore, we thought that it would be more judicious to use a system where Pcp1 is under the control of its own promoter and terminator.

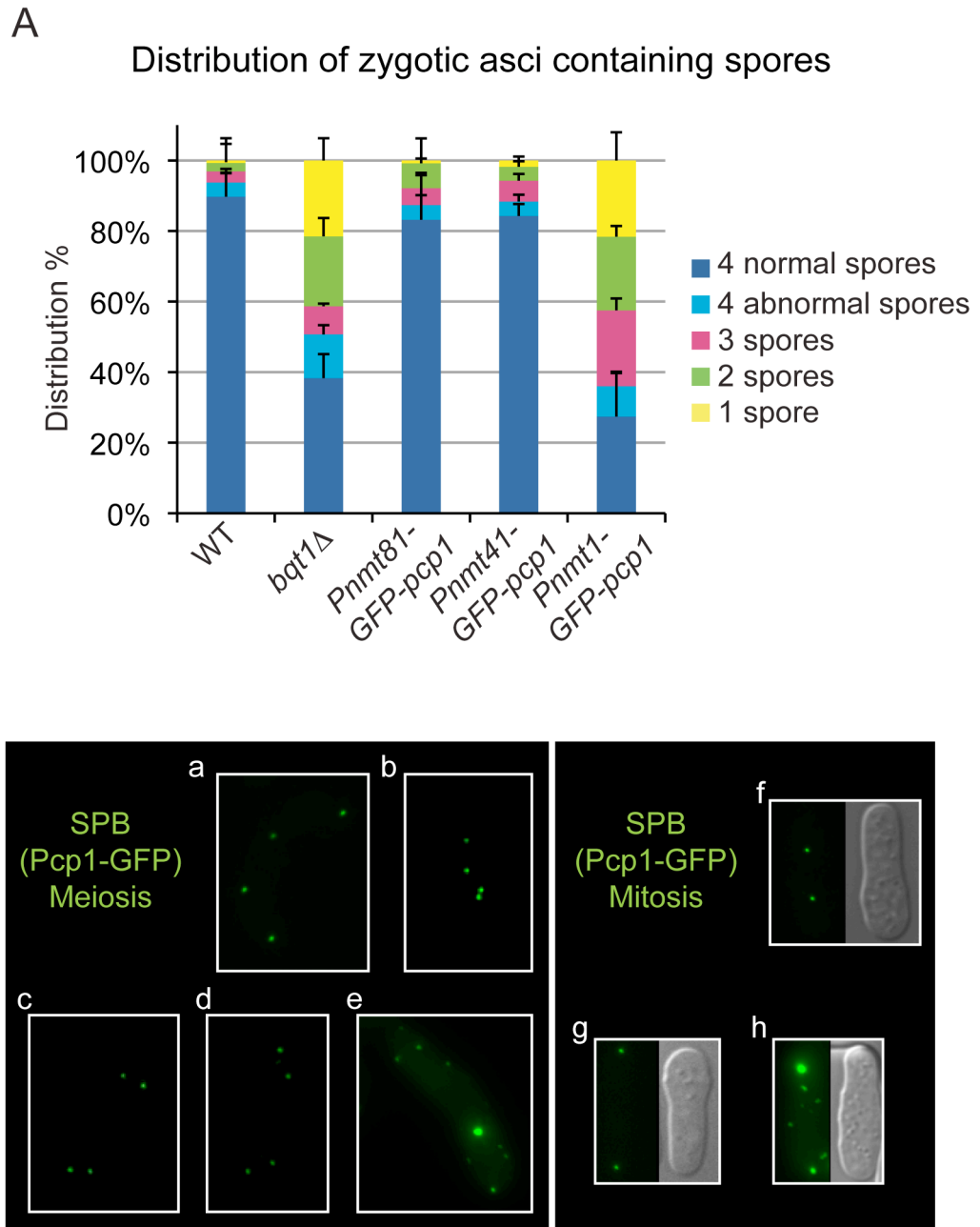


Figure 3.7 Pcp1 over-expression

(A-B) Experiments were performed in the presence of thiamine (condition where the *nmt* promoter is repressed) (A) Distribution of categories of asci. Asci from zygotic meiosis were scored under light microscopy. 200 asci per genotype were counted in each experiment. Data represent the average of five experiments. Error bars indicate standard deviation. (B) Images taken on the same day from endogenously tagged Pcp1-GFP in meiosis (a-b) and in mitosis (f-g) or Pcp1-GFP under the control of a foreign promoter in meiosis (c-e) and in mitosis (h). (a and f) WT cell, (b and g) *bqt1*Δ cell, (c) *Pnmt81-GFP-pcp1* (d) *Pnmt41-GFP-pcp1* (e and h) *Pnmt1-GFP-pcp1*.

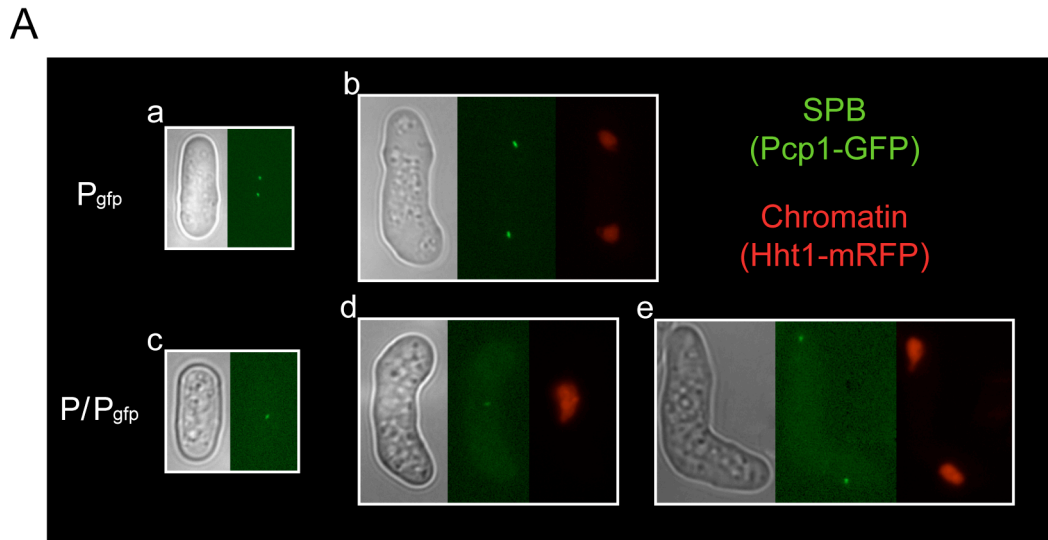
3.4.1.2 *Pcp1* over-expression strategy N° 2 = two *pcp1* copies in the genome

We created strains containing a second copy of the *pcp1* gene under the control of its own promoter and terminator at the aureobasidin locus (*aur1*) (hereafter referred to as *pcp1-2copies*). We inserted a *pcp1-GFP* construct into strains harbouring either a *WT-pcp1* (*pcp1-2copies* P/P_{gfp}) or a *pcp1-GFP* copy at the endogenous locus (*pcp1-2copies* P_{gfp}/P_{gfp}). To check that *pcp1-GFP* inserted at *aur1* locus is expressed, we looked for GFP signal in a strain with *WT-pcp1*.

<i>pcp1-2copies</i> Strains name	<i>pcp1</i> endogenous locus	<i>aur1</i> locus
P/P _{gfp}	<i>pcp1</i>	<i>pcp1-GFP</i>
P _{gfp} /P _{gfp}	<i>pcp1-GFP</i>	<i>pcp1-GFP</i>

The strains used in this experiment as well as those generally used for imaging are h⁹⁰, and their meiotic synchronisation is not straightforward due to the limiting step that the conjugation process represent. Therefore, Western blot analyses were performed on extracts from exponentially growing cells (Figure 3.8B). We suspected that if the construct is expressed in cycling cells, it is most likely also expressed in meiosis as it is under the control of its own promoter. Anti-Pcp1 antibody was designed to recognise the N-terminal region of Pcp1 (Fong et al., 2010), and is thus able to detect both Pcp1 (141 kDa) and Pcp1-GFP (161 kDa). Because we detected two bands representing Pcp1 with and without the GFP tag in extracts from P/P_{gfp}, we concluded that the construct inserted at the *aur1* locus is correctly expressing Pcp1-GFP, although we did not quantify its levels rigorously. Moreover, fluorescence microscopy of meiotic cells confirmed expression of the ectopic GFP-tagged copy when endogenously not tagged, as a GFP dot appeared at the SPB in these strains (Figure 3.8A).

These experiments demonstrate that the *pcp1-GFP* construct at the *aur1* locus is expressed and localised to both mitotic and meiotic SPBs.



B

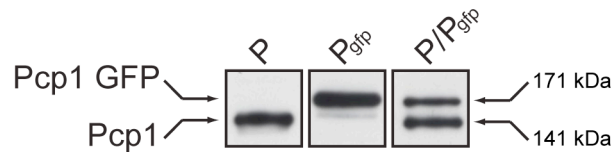


Figure 3.8 Expression of 2 copies of *pcp1*

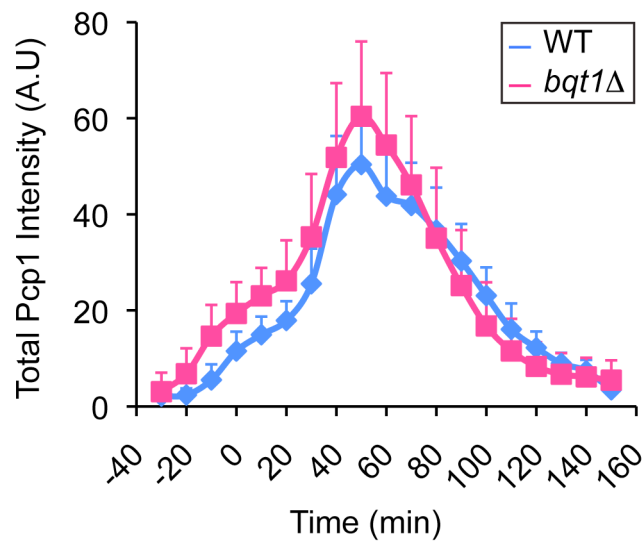
(A) Pcp1-GFP images from (a-b) WT cells where Pcp1 is GFP tagged at its endogenous locus (P_{gfp}) in (a) mitosis and (b) after MI we can start to detect *pcp1* signal duplication prior MII. (c-e) *pcp1-2copies* P/P_{gfp} (P/P_{gfp}) where Pcp1 is untagged at its endogenous locus and GFP tagged at the ectopic locus in (c) mitosis (d) meiotic prophase I (e) meiosis-I. (B) Western blot using anti-Pcp1 antibody on TCA extract from cycling cells from WT cells where Pcp1 is untagged (P), WT cells where Pcp1 is GFP tagged (P_{gfp}), *pcp1-2copies* P/P_{gfp} (P/P_{gfp}) cells where Pcp1 is untagged at its endogenous locus and GFP tagged at the ectopic locus.

3.4.2 Can the small difference in Pcp1 intensity between WT and *bqt1Δ* cells explain the *bqt1Δ* phenotypes?

We quantified and compared Pcp1-GFP signal levels in the *pcp1-2copies* P_{gfp}/P_{gfp} strain versus WT (Figure 3.9B). The difference in Pcp1 intensity between WT and *pcp1-2copies* is of a very similar magnitude to the difference in Pcp1 level between WT and *bqt1Δ* strains (Figure 3.9). Nonetheless, this mild elevation in Pcp1 level failed to induce any bouquet-deficient phenotypes in bouquet-proficient strains (Figure 3.10 and Figure 3.11). Indeed, the numbers of spores per ascus were similar for *pcp1-2copies* P_{gfp}/P_{gfp} and control strains. For both, the results obtained are similar to WT, in contrast to *bqt1Δ* strains, which show low levels of normal asci (Chikashige et al., 2006, Tomita and Cooper, 2007) (Figure 3.10). In addition, our live analysis of *2copies* strains failed to reveal defects in chromosome segregation at MI or MII (Figure 3.11). Nevertheless, we observed small supernumerary Pcp1 dots, appearing during SPB separation (Figure 3.12). Although these supernumerary Pcp1 dots do not confer any phenotypes, they are reminiscent of the aberrant microtubule organisation centres (AMTOCs) characterised in *dot2* mutants (Jin et al., 2005). However, these supernumerary Pcp1 dots were not included in the quantitation since we found their contribution to the total intensity to be negligible compared to the main foci.

We conclude that a subtle over-expression of Pcp1 (i.e. of a very similar magnitude to the difference in Pcp1 level between WT and *bqt1Δ* strains) does not present any bouquet phenotypes while it reproduces previously described strong-overexpression phenotypes (Jin et al., 2005), albeit to a smaller extent. Consequently, we have shown that the small difference of Pcp1 intensity observed between WT and *bqt1Δ* is not responsible for spindle and SPB defects observed in bouquet deficient strains.

A
Average curves of WT and *bqt1* Δ Pcp1 intensity profiles



B
Average curves of WT and *pcp1-2copies* Pcp1 intensity profiles

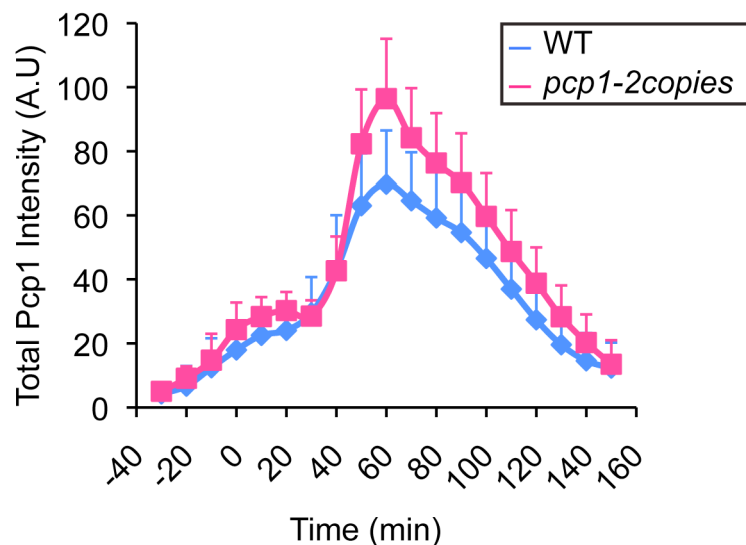


Figure 3.9 WT versus *bqt1* Δ present the same difference of Pcp1 intensity than WT versus *pcp1-2copies*

(A) Average curve of 22 WT Pcp1 intensity measurements (blue) and 29 *bqt1* Δ (magenta). Error bars represent standard deviation. (B) Average curve of 13 WT Pcp1 intensity measurements (blue) and 13 *pcp1-2copies* (magenta). Error bars represent standard deviation. It is important to note that we cannot compare directly the absolute values of the two sets of experiments, as they were not performed using the exact same conditions. 0 min represent the onset MI.

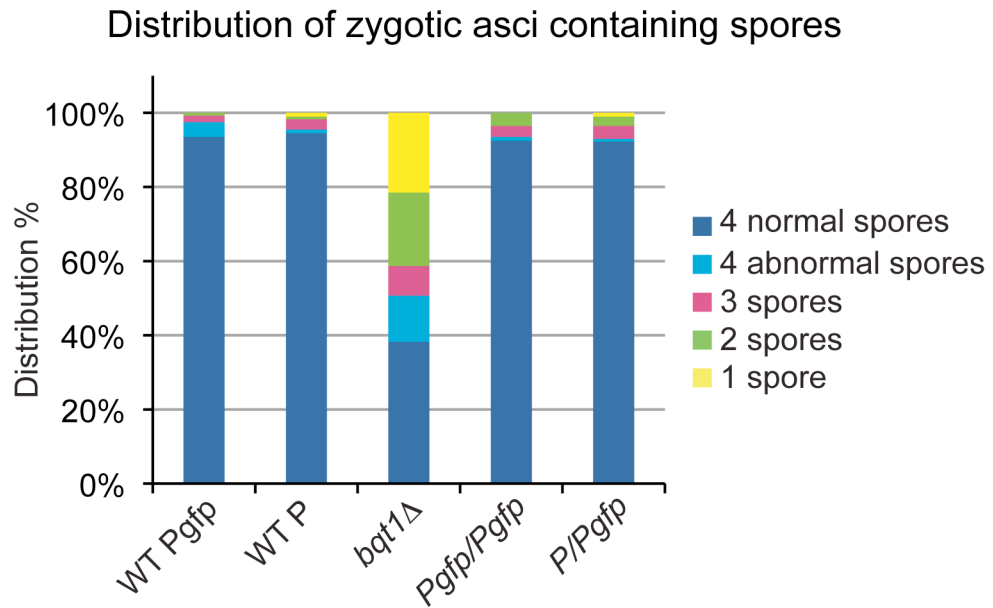


Figure 3.10 *pcp1-2copies* has no defect in meiosis sporulation

Distribution of categories of asci. Asci from zygotic meiosis were scored under light microscopy. 200 asci per genotype were counted in the experiment. WT cells where Pcp1 is GFP tagged (WT Pgfp), WT cells where Pcp1 is untagged (WT P), *pcp1-2copies* P_{gfp}/P_{gfp} cells where Pcp1 is GFP tagged at its endogenous locus and GFP tagged at the ectopic locus (Pgfp/Pgfp), *pcp1-2copies* P/P_{gfp} cells where Pcp1 is untagged at its endogenous locus and GFP tagged at the ectopic locus (P/Pgfp).

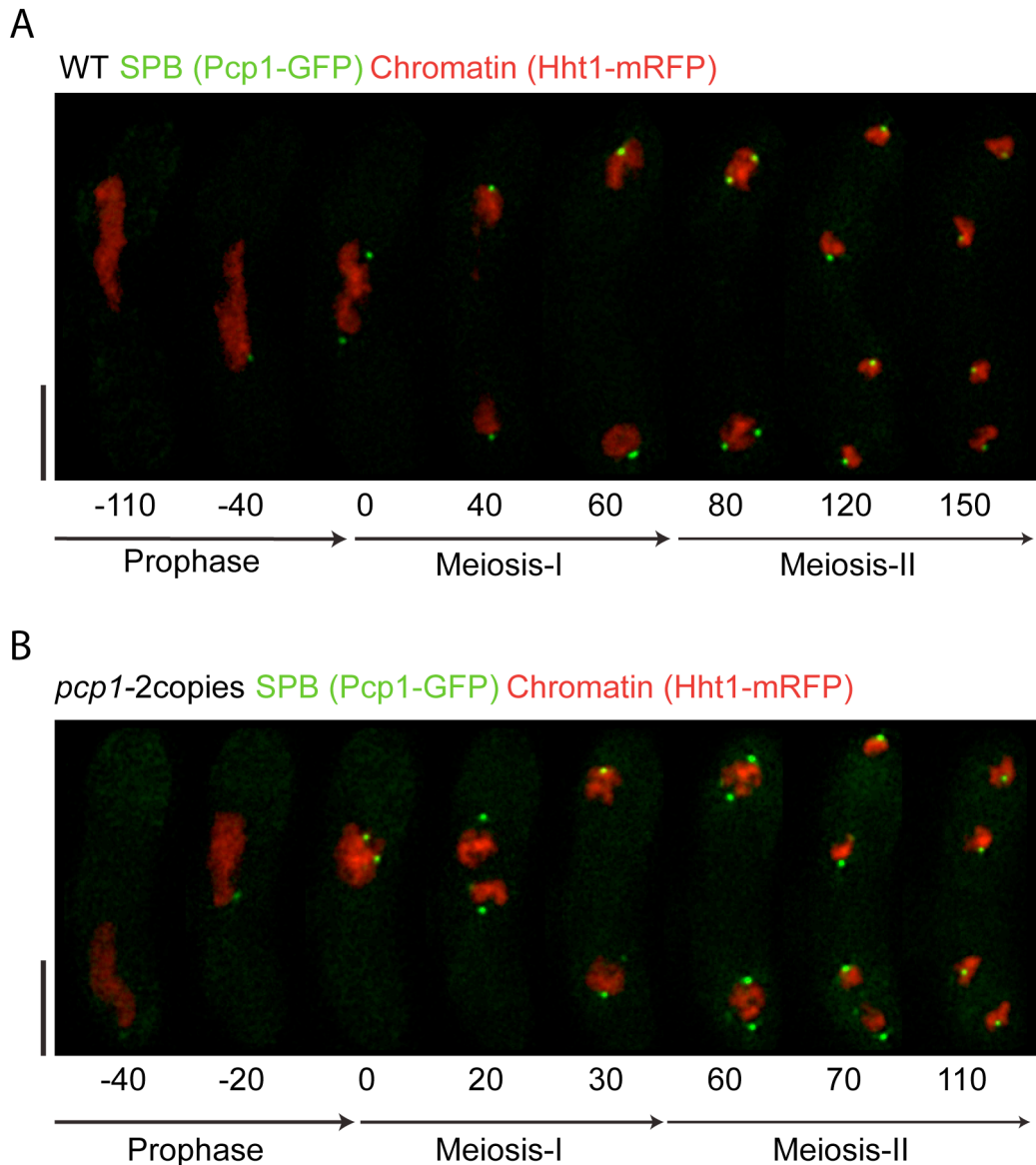


Figure 3.11 The small difference of Pcp1 intensity between WT and *bqt1Δ* is not biologically significant

Series of frames from meiosis movies acquired by fluorescence microscopy in live cell and used for Pcp1 quantitation. (A) WT cell SPB and chromosomes were observed via endogenously tagged Pcp1-GFP and Hht1-mRFP respectively. (B) *pcp1-2copies* SPB was observed via endogenously tagged Pcp1-GFP and ectopically tagged Pcp1-GFP, chromosomes were observed via endogenously tagged Hht1-mRFP. Numbers under the frames represent the time in minutes. The stages of meiosis are indicated below. 0 min is the onset of MI. Scale bars equal 5 μ m.

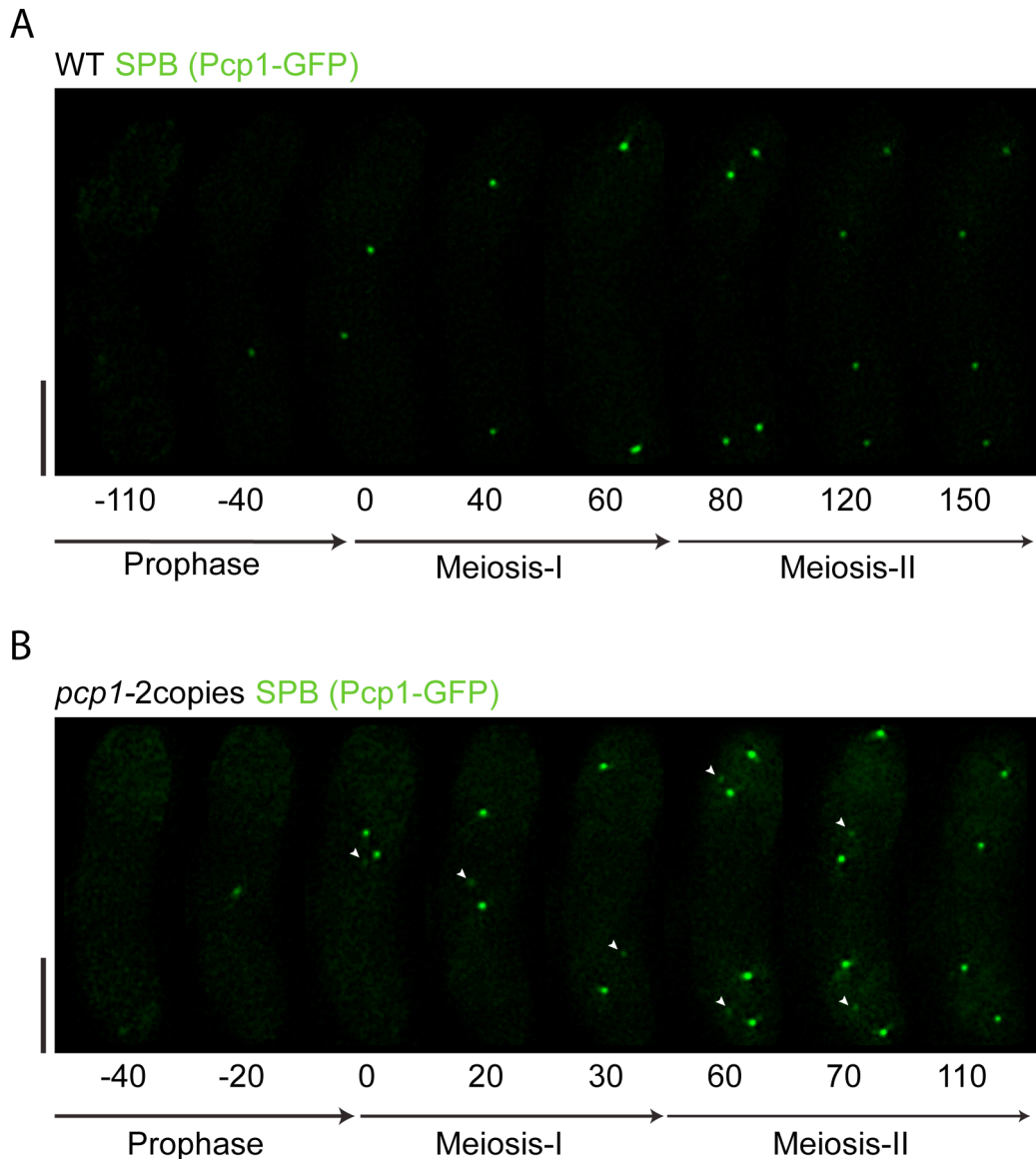


Figure 3.12 *pcp1-2copies* displays small supernumerary Pcp1 dots during SPB separation

GFP channel of the same merge images as Figure 3.9. Series of frames from meiosis movies acquired by fluorescence microscopy in live cell and used for Pcp1 quantitation. (A) WT cell SPB was observed via endogenously tagged Pcp1-GFP. (B) *pcp1-2copies* SPB was observed via endogenously tagged Pcp1-GFP and ectopically tagged Pcp1-GFP. Numbers under the frames represent the time in minutes. The stages of meiosis are indicated below. 0 min is the onset of MI. White arrowhead indicates supernumerary Pcp1 dot. Scale bars equal 5 μ m.

All the conclusions drawn so far have been made by studying Pcp1. Before going any further in our investigations, we decided to verify that Pcp1 is representative of overall SPB behaviour.

3.5 Pcp1 is representative of SPB behaviour

The SPB being a multiprotein complex, we wanted to determine if our characterisation of Pcp1 could be considered representative of the SPB complex, or if the phenotypes observed are component specific. Previous studies from the lab describing SPB defects in bouquet deficient backgrounds revealed that several SPB components present the same cytological behaviour (Tomita and Cooper, 2007) suggesting that the defects observed are not component specific. In order to explore this more precisely, we assessed the colocalisation of Pcp1 with Sid4, another SPB core component, as well as determining its accumulation profile, in WT and *bqt1Δ* cells.

3.5.1 Pcp1 and Sid4 colocalise throughout meiosis in *bqt1Δ* cells

To determine if Pcp1 is representative of SPB behaviour, we analysed SPB behaviour in strains where Pcp1 and Sid4 are respectively tagged with GFP and mRFP at their endogenous locus. Sid4 is a scaffold protein that anchors the septation initiation network (SIN) complex to the SPB (Chang and Gould, 2000). The settings used to image Sid4 and Pcp1 localisation (Z sections first, wavelength second), prevent us from being able to determine with precision if Pcp1 and Sid4 colocalise or are just juxtaposed very closely. Nonetheless, we observed that Pcp1 and Sid4 localise very close to each other in 100% of cells from prophase to the end of meiosis, whether in a WT (Figure 3.13) or a *bqt1Δ* (Figure 3.14) background. However, we noticed some differences, in both WT and *bqt1Δ* cells Sid4 emerge as a core SPB components that stay at the SPB throughout the meiotic differentiation (very low at the timing of mating and gradually increase

toward the onset of MI) whereas Pcp1 localisation at the SPB dramatically increase at the onset of MI (Figure 3.13 at -60 min and Figure 3.14A at -70 min and 3.14B at -60 min). In addition, while both Pcp1 and Sid4 signals appear clearly as two dots at the onset of MI and MII, this separation into 2 dots occurs earlier for Pcp1 than Sid4 (Figure 3.13B, 3.13A enlarged frames). These observations demonstrate that Pcp1 is representative of general SPB behaviour, and provide an illustration of how subtle fine-tuning of SPB maturation is performed in a component specific manner. It also reiterates the idea that the SPB is not completely disorganised in bouquet deficient cells.

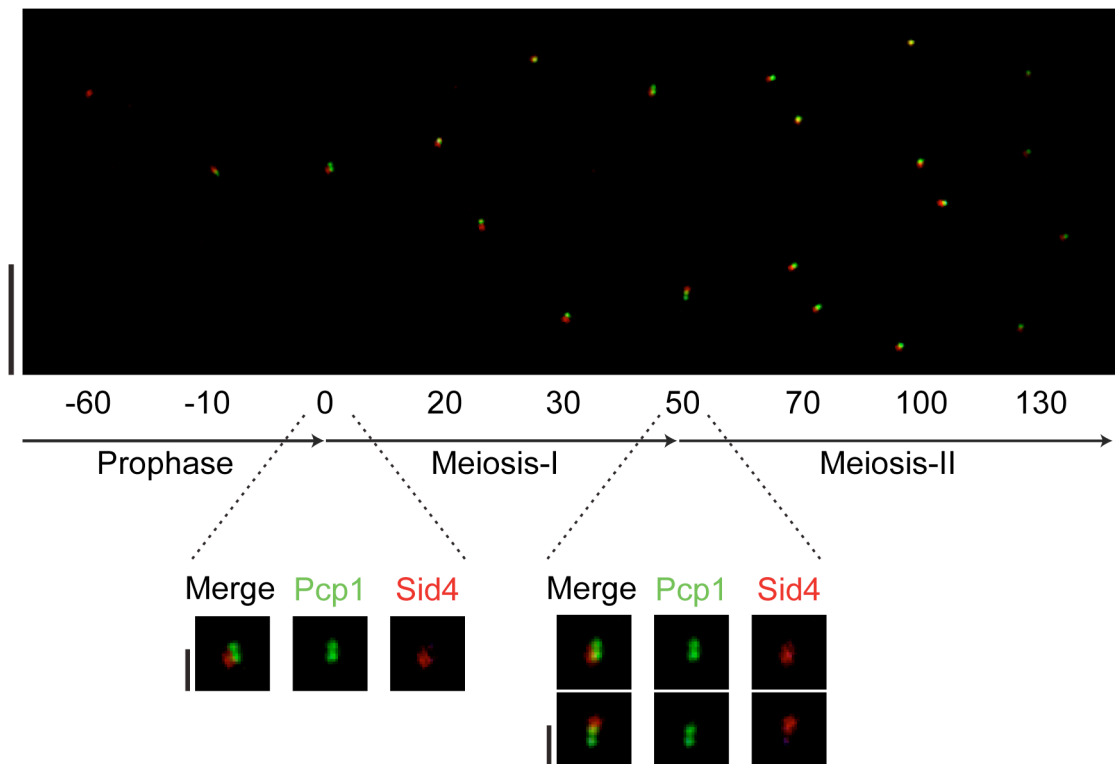
3.5.2 Pcp1 and Sid4 accumulation profiles are similar in *bqt1Δ* cells

Using the same method as for Pcp1 investigation, we determined the profile of Sid4 accumulation at the SPB in WT and *bqt1Δ* cells. Because WT and *bqt1Δ* movies were filmed with different lamps and far apart in time, the data collected cannot be compared directly in terms of values. As this experiment aimed to determine only whether the timing of Sid4 accumulation matches that of Pcp1 and whether it is roughly maintained in the absence of the bouquet, we determined the profile of only three representative WT and *bqt1Δ* cells (Figure 3.15).

First, we compared WT and *bqt1Δ* Sid4-GFP accumulation profiles. For the three cells quantified, the shape of the curve is for the most part similar between WT and *bqt1Δ* cells, with minor differences toward the end of the curve. In all cases, the signal first accumulates slowly at MI and drastically at MII before gradually decreasing after the peak; however, the timing with which the signal decreases after the peak appears slightly delayed in the absence of the bouquet. Having determined the profile of only three representative cells and with different settings, we do not know at this point whether this is a feature of *bqt1Δ* cells. In order to answer to this question, we would need to repeat the experiment with both WT and *bqt1Δ* movies under the same conditions in more cells.

A

WT SPB (Pcp1-GFP) SPB (Sid4-mRFP)



B

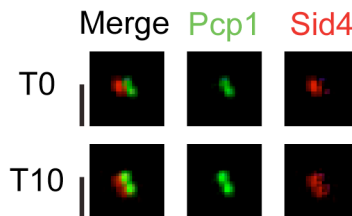


Figure 3.13 Pcp1 and Sid4 colocalise at the SPB throughout meiosis in WT
 Series of frames from WT meiosis movies acquired by fluorescence microscopy in live cell. Pcp1 and Sid4 SPB components were observed via endogenously tagged Pcp1-GFP and Sid4-mRFP respectively. (A) This movie illustrates Pcp1 and Sid4 colocalisation throughout meiosis. Numbers under the frames represent the time in minutes and stages of meiosis are indicated below. 0 min represent the onset of MI. Scale bar equals 5 μ m. SPB at the onset of MI (0 min) and MII (50 min) are shown as enlarged views on separate channels and illustrate delays between Pcp1 and Sid4 duplication. Scale bars equal 1 μ m. (B) Onset of MI time points shown as enlarged views on separate channels, number next to the frames indicate the time in minutes. Scale bars equal 1 μ m. These frames illustrate delays between Pcp1 (0 min) and Sid4 (10 min) duplication.

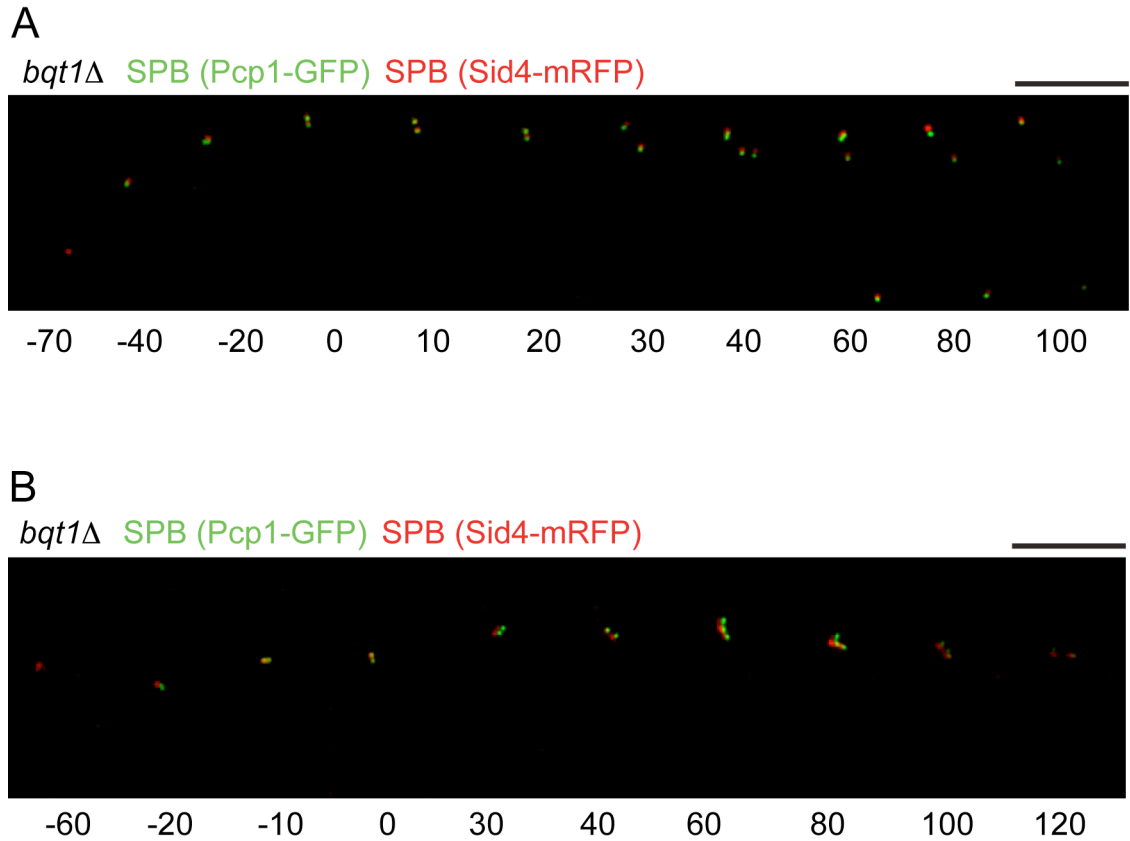
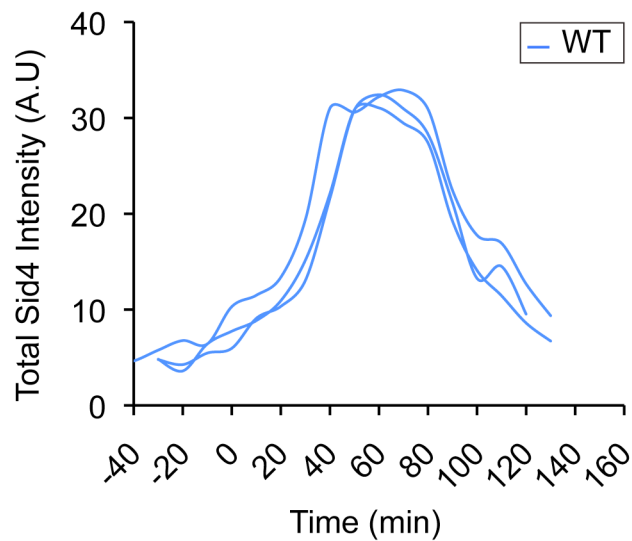


Figure 3.14 Pcp1 and Sid4 colocalise at the SPB throughout meiosis in *bqt1Δ* cells

Series of frames from *bqt1Δ* meiosis movies acquired by fluorescence microscopy in live cell. Pcp1 and Sid4 SPB components were observed via endogenously tagged Pcp1-GFP and Sid4-mRFP respectively. Numbers under the frames represent the time in minutes. 0 min represent the onset of MI. Scale bars equal 5 μ m. This movie illustrates Pcp1 and Sid4 colocalisation throughout meiosis while aberrant SPB separation occurs. (A) Duplicated SPBs are sticky and separate poorly only after MII duplication occurred (60 min). (B) SPBs duplicate in MI (30 min) and in MII (60 min) but do not separate at all.

A
Superimposition of 3 WT Sid4 intensity profiles



B
Superimposition of 3 *bqt1* Δ Sid4 intensity profiles

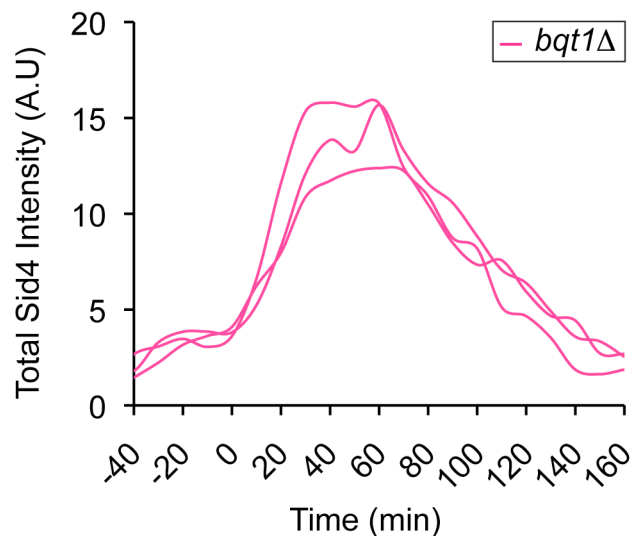


Figure 3.15 Shape of Sid4 intensity profile is similar in WT and *bqt1* Δ cells

(A) Superimposition of Sid4 intensity measurement of 3 WT curves. (B) Superimposition of Sid4 intensity measurement of 3 *bqt1* Δ curves. The characteristics shared by each curve are similar between WT and *bqt1* Δ from left to right, a small increase, followed by a rapid and large increase and then diminution of the signal. 0 min represent the onset of MI. Quantitation of the signal was not performed before -40 min in prophase even if though Sid4 signal is present (Figure 3.13 & 3.14) in order to compare better Sid4 and Pcp1 profiles. We cannot compare directly the absolute values of the two sets of experiments, as they were not performed using the exact same conditions.

Second, we compared Sid4-GFP and Pcp1-GFP accumulation profiles. While some of the characteristics described for Pcp1 such as the shoulder at MI appear less pronounced, the curve is quite reminiscent of that of Pcp1 (Figure 3.9A). This correlates with our previous observation that Sid4 appears as two distinguishable dots later than Pcp1 at the onset of MI and MII and the fact that Sid4 is present at the SPB and increase gradually throughout meiotic prophase as opposed to Pcp1, which seems to be recruited to the SPB in late prophase, at the onset of MI (Figure 3.13, 3.14). Collectively, these data suggest that each SPB component is subjected to a different maturation progression, but that the duplication process itself is not the target of bouquet-dependent regulation. They also suggest that Pcp1 is reasonably representative of SPB behaviour.

3.6 Overview

In this chapter, we have shown that while loss of the bouquet leads to defective SPB behaviour, the duplication of the SPB is largely normal as monitored by quantitative live analysis of Pcp1 as well as Sid4. We have also shown that although a small difference in total Pcp1 signal intensity exists between WT and *bqt1Δ* cells, such a small difference is not responsible for *bqt1Δ* phenotypes, since reproducing the same difference in a bouquet proficient background does not confer bouquet phenotypes. Therefore, these results point toward more subtle defects rather than a total disorganisation of the SPB. It should be noted that we cannot rule out the possibility that subtle over-expression of several SPB components would confer the bouquet phenotypes; other analyses, however, have pointed us in other directions.

Chapter 4. Separation of the duplicated SPB is abnormal in bouquet deficient cells

4.1 Aim

By analogy with the chromosome cycle, the centrosome/SPB cycle involves SPB duplication followed by SPB separation. In addition, like the systems ensuring that genome doubling take place only once per cell cycle, specific regulatory systems exist to insure that centrosomes duplicate only once per cell cycle thus maintaining a stable number of centrosomes per cell (Tsou and Stearns, 2006). Centrosome and chromosome cycles are tightly coordinated to ensure faithful cell cycle progression (Doxsey et al., 2005b).

The results presented in the preceding chapter imply that SPB duplication is largely intact in bouquet deficient cells. Thorough examinations of Pcp1 signal throughout meiosis using high quality 3D movies allowed us to closely monitor SPB behaviour. In this chapter, I will present how such meticulous analysis gave us insight into SPB separation, a fundamental events of the SPB cycle as well as into the coupling of the SPB and chromosome cycles.

4.2 Separation of the duplicated SPB is abnormal in bouquet deficient cells

After duplication, maturation and subsequent insertion in the nuclear envelope, SPBs separate along with the formation of the meiotic spindle. However, while analysing Pcp1 behaviour in live cells, we noticed that the SPBs appear to have difficulties separating from one another in the absence of the bouquet (Figure 4.1-4.3). Separation defects range from SPB signals separating for several frames and then coming back together (Figure 4.1, 4.2), behaviour we refer to as being sticky to SPB dots that do not separate at all (Figure 4.3).

To explore these separation defects further, we examined the timing of SPB separation with respect to the timing of meiosis (Table 4.1). As chromosome segregation is often defective in *bqt1Δ* cells, we could not use it as a criterium to assess timing of meiosis. Duplication however, is not significantly affected therefore we used the number of SPB dots to discriminate between the different phases of meiosis.

Similarly to the analysis conducted to assess SPB duplication (Table 3.2), here in order to characterise the SPB separation defect, we took in consideration and classified in different categories only the cells that have a dysfunctional SPB. We observed that most of the cells (63.2%) tend to show separation of the duplicated SPB only at the time where MII spindle should be forming (Figure 4.2), while a small percentage (12.3%) fail to show any sign of separation (Figure 4.3). Separation of the duplicated SPB hence appears to fail most of the time in MI, although it is not a MI specific event as 17.5% of the cells show SPB separation in MI but not in MII (Figure 4.1).

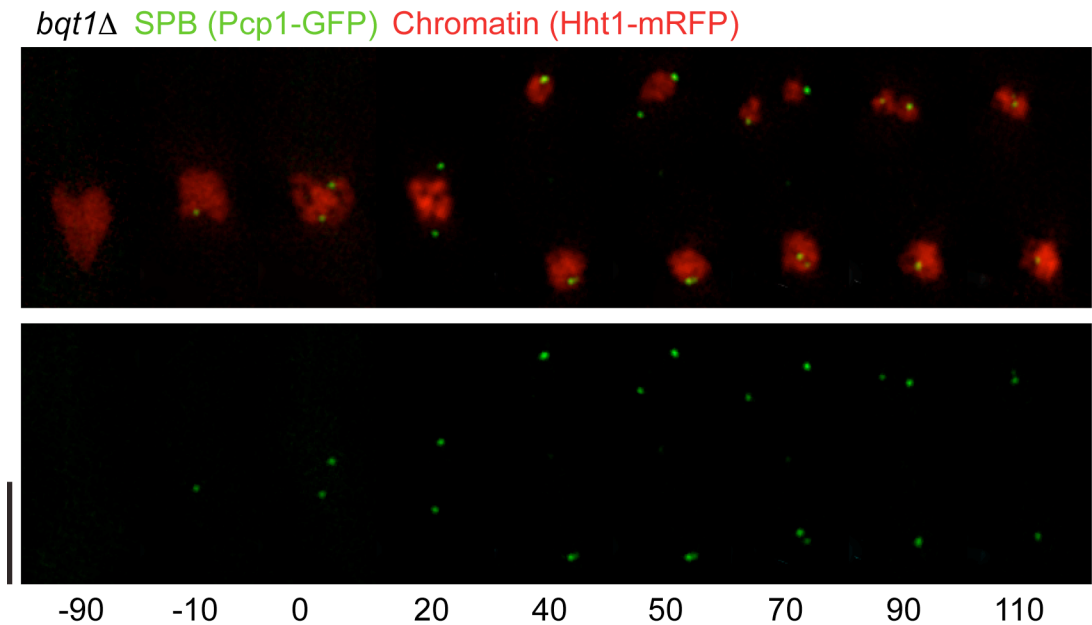


Figure 4.1 Example of SPB separation at MI but not at MII

Series of frames from *bqt1* Δ meiosis movie acquired by fluorescence microscopy in live cell. SPB and chromosomes were observed via endogenously tagged Pcp1-GFP and Hht1-mRFP respectively. Numbers under the frames represent the time in minutes. 0 min represent the onset of MI. Scale bar equals 5 μ m. The lower panel shows only the green channel (SPB signal) of the upper panel. This movie illustrates aberrant SPB separation in *bqt1* Δ cells in which duplicated SPBs separate in MI (0-40 min) but do not separate properly or are sticky in MII (50-90 min).

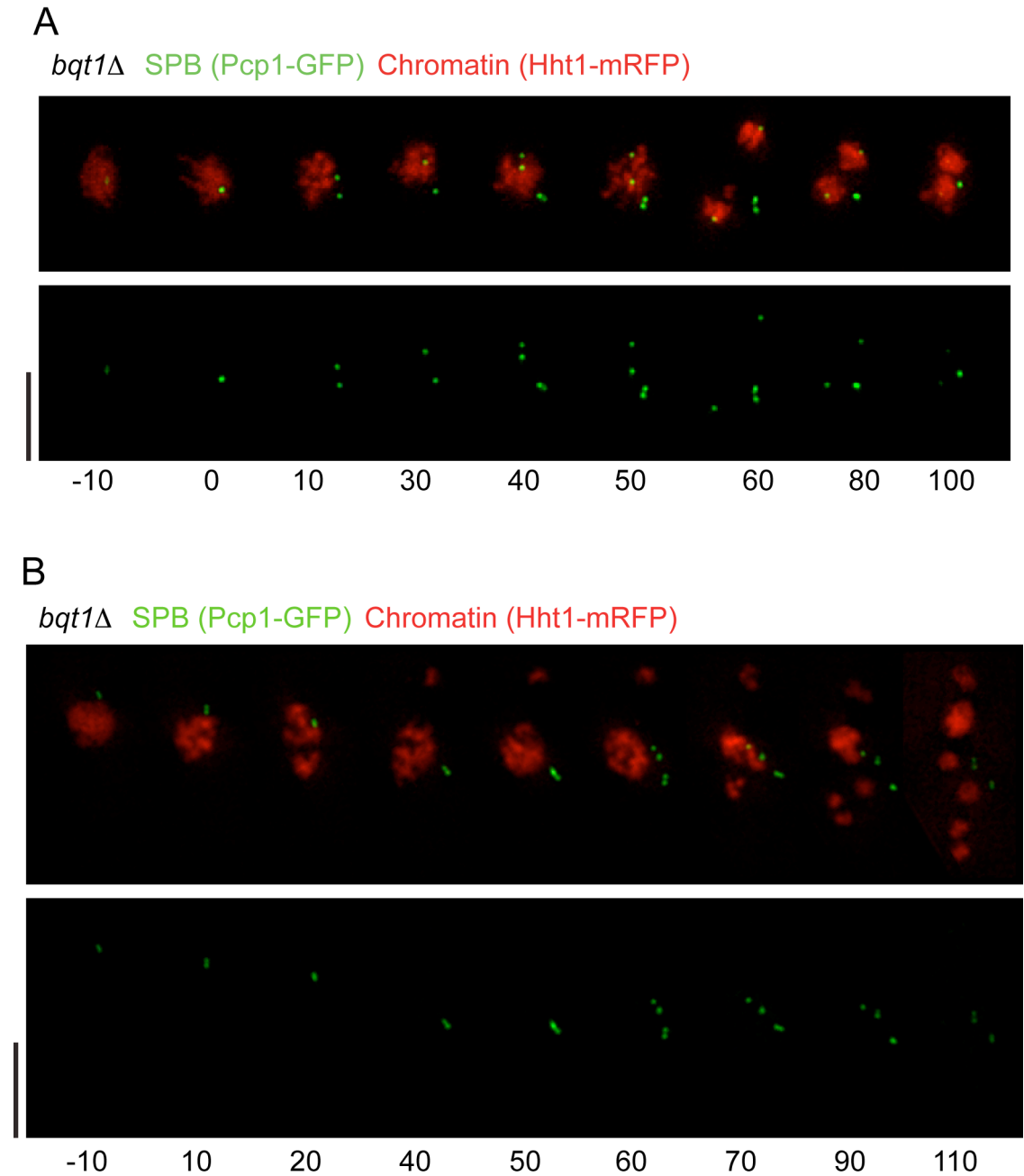


Figure 4.2 Examples of SPB separation at MII only

Series of frames from *bqt1* Δ meiosis movies acquired by fluorescence microscopy in live cell. SPB and chromosomes were observed via endogenously tagged Pcp1-GFP and Hht1-mRFP respectively. Numbers under the frames represent the time in minutes. 0 min represent the onset of MI. Scale bars equal 5 μ m. The lower panel shows only the green channel (SPB signal) of the upper panel. (A) Aberrant SPB separation in *bqt1* Δ cells in which duplicated SPBs are sticky and separate slightly in MI (10-30 min) and better in MII (60 min). (B) Aberrant SPB separation in *bqt1* Δ cells in which SPBs are sticky and separate poorly only after MII duplication occurred (60 min).

bqt1 Δ SPB (Pcp1-GFP) Chromatin (Hht1-mRFP)

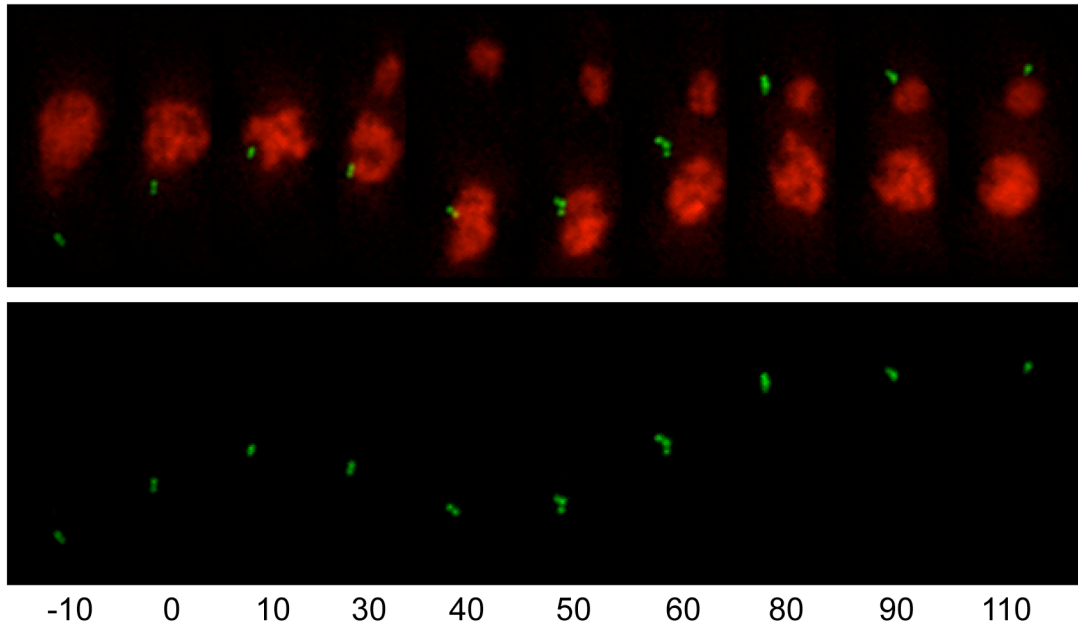


Figure 4.3 Example of SPB that do not separate at all

Series of frames from *bqt1* Δ meiosis movie acquired by fluorescence microscopy in live cell. SPB and chromosomes were observed via endogenously tagged Pcp1-GFP and Hht1-mRFP respectively. Numbers under the frames represent the time in minutes. 0 min represent the onset of MI. Scale bar equals 5 μ m. The lower panel shows only the green channel (SPB signal) of the upper panel. This movie illustrates aberrant SPB separation in *bqt1* Δ cells in which SPBs duplicate in MI (30 min) in MII (50-60 min) but do not separate at all.

4. Separation of the duplicated SPB is abnormal in bouquet deficient cells

SPB Separation	% of cells (n=57)
Separate in MI and MII	7 (4)
Separate in MI but not in MII	17.5 (10)
Separate in MII only	63.2 (36)
Do no separate at all	12.3 (7)

Table 4.1 Separation of the duplicated SPB is abnormal in bouquet deficient cells

Phenotypes were observed on *bqt1Δ* meiosis movies acquired by fluorescence microscopy in live cell. SPB and chromosomes were observed via endogenously tagged Pcp1-GFP and Hht1-mRFP respectively. 57 cells, which do have a dysfunctional SPB, were categorised in 4 levels. The percentage of cells exhibiting each phenotype is shown with the number of observed cells in parentheses.

Therefore, we conclude that a major defect of *bqt1Δ* cells lies in their inability to separate the duplicated SPBs. In addition, analysis of the SPB separation defect led us to uncover additional important characteristics of *bqt1Δ* cells. Firstly, we noticed that a functional MI does not guarantee a functional MII. Conversely, if MI is defective, it does not necessarily mean that MII will be defective. Hence, we propose that the role of the bouquet is to leave some mark(s) on the SPB that persists through MII and act as a prerequisite to successful separation of the duplicated SPB at both MI and MII. A deficiency of this mark would reduce the probability of proper separation at either MI and MII. Secondly, we realised that just as SPB duplication progresses with WT timing through the meiotic cell cycle regardless of SPB separation and chromosome segregation defects, SPB separation is initiated twice during meiosis independently of the fate of MI segregation. Indeed, *bqt1Δ* cells do not arrest in MI when MI segregation fails. Moreover, as seen in Pcp1 accumulation profiles (Figure 3.6, 3.9A), Pcp1 signals drop at the same rate in WT and *bqt1Δ* cells, illustrating that there is not a conspicuous delay in meiotic exit.

4.3 Overview

In this chapter, we closely monitor SPB separation, a key event of the SPB cycle. Using high quality 3D movies collected for Pcp1 quantitation, we find that while SPB duplication is fairly normal in the absence of the bouquet, SPB separation is aberrant. We next naturally focused on the investigation of the factors implicated in SPB separation.

Chapter 5. The bouquet is required for γ -TuC localisation to SPBs

5.1 Aim

Results presented in the preceding chapters imply that the major defect at the SPB level in bouquet deficient cells is the separation of the duplicated SPBs. In agreement with the idea that elongating spindles effect SPB separation by pushing the duplicated SPBs apart (Lim et al., 2009), we observed by fluorescence microscopy in live cells that separation of the SPBs is concomitant with spindle formation. It is well established that a key player in nucleating cytoplasmic microtubules as well as spindles is the γ -tubulin complex (γ -TuC) (Job et al., 2003). We therefore wondered about the whereabouts and functionality of the γ -TuC in bouquet-deficient cells. This chapter presents our investigation of these issues.

5.2 In absence of the bouquet, the γ -TuC localises unevenly between duplicated SPB

To examine the localisation of the γ -TuC throughout meiosis, we examined Alp4, an essential component of the γ -TuC and among the most studied (Vardy and Toda, 2000). Using strains with both the SPB (Sid4) and the γ -TuC (Alp4) endogenously tagged with mRFP and GFP respectively, we assessed their colocalisation in WT and *bqt1* Δ cells.

As described in the literature (Tanaka et al., 2005), we observed that Alp4 localises perfectly to the SPB throughout meiosis from beginning of prophase until the end of MII in WT cells (Figure 5.1). However, we noticed that at the very end of MII, when the SPB signal (Sid4 or Pcp1) decreases, Alp4 signal does not follow the same pattern. Instead, Alp4 signal disperses and an increased number of small, dynamic, and variably sized Alp4 foci are visible throughout the cell (Figure 5.1 140 min and 5.6 140 min). This phenomenon seems to coincide with forespore membrane and spore formation, as the signal persists until approximately 2 hours after SPB signal disappearance. We did not further investigate the mechanisms behind, or the role of, this intriguing pattern.

In *bqt1* Δ cells, we observed defects in γ -TuC localisation. We divided these defects into several categories based on their severity (Table 5.1). Defects range from unequal separation of Alp4 signal between the two SPBs at MII only (25%) (Figure 5.2 and 5.6A) to defects at both MI and MII (26%) (Figure 5.3 and 5.6B) to a complete loss of Alp4 at the SPB (8%) (Figure 5.4 and 5.6C). Defects arise with the earliest onset at MI, meaning that we never saw Alp4 mislocalising during prophase. This latter observation is interesting since in the absence of the bouquet, we observe SPB defects starting at the onset of MI but never in prophase. These data indicate that the stabilisation and/or recruitment of the γ -TuC at the meiotic SPB are imperfect starting from the onset of MI only and augment previous observations that Alp4 localisation is regulated differently during

prophase than during the rest of meiosis (Tanaka et al., 2005). We will address this question in the next chapters. Alp4 thus represents the first SPB component examined in this study that does not follow the same behaviour as the rest of the SPB. Considering that SPB separation rely on spindle formation and therefore on proper microtubule nucleation by the γ -TuC, these results collectively suggest that SPB separation defects observed in the absence of the bouquet could be a consequence of altered localisation of the γ -TuC to the SPB.

In order to determine if such a connection exists, first we categorised the movies of Sid4 and the γ -TuC according to SPB separation defects (Table 5.2). The Sid4-mRFP behaviour we observe corroborates nicely with our data using Pcp1-GFP as SPB marker (Table 4.1). Second, we arrange each of the SPB separation categories depending on their γ -TuC localisation with the SPB and compare the two rankings (Table 5.2). 70% of the cells whose SPBs show signs of separation only at MII are SPBs that have uneven separation of the γ -TuC at both MI and MII, while 100 % of the SPBs that separate at MI but not at MII have defects in γ -TuC localisation only at MII and 87.5% of the SPBs that fail completely to separate have an apparent loss of γ -TuC from the SPB. This comparison allowed us to establish a very interesting correlation between Alp4 uneven localisation to the SPB and the extent of SPB separation defects, reinforcing the idea that the SPB separation defects are consequences of altered localisation of the γ -TuC to the SPB. However, having monitored only one component of the γ -TuC, we cannot state that the whole complex is unevenly localised at the SPB in the absence of the bouquet. One continuing avenue would be to repeat the experiment with other γ -TuC components. Instead, since the γ -TuC is the nucleation point of the microtubule, we decided to verify the activity of the complex. Thus, we next asked whether the SPBs that do colocalise with Alp4 are the ones able to nucleate a spindle.

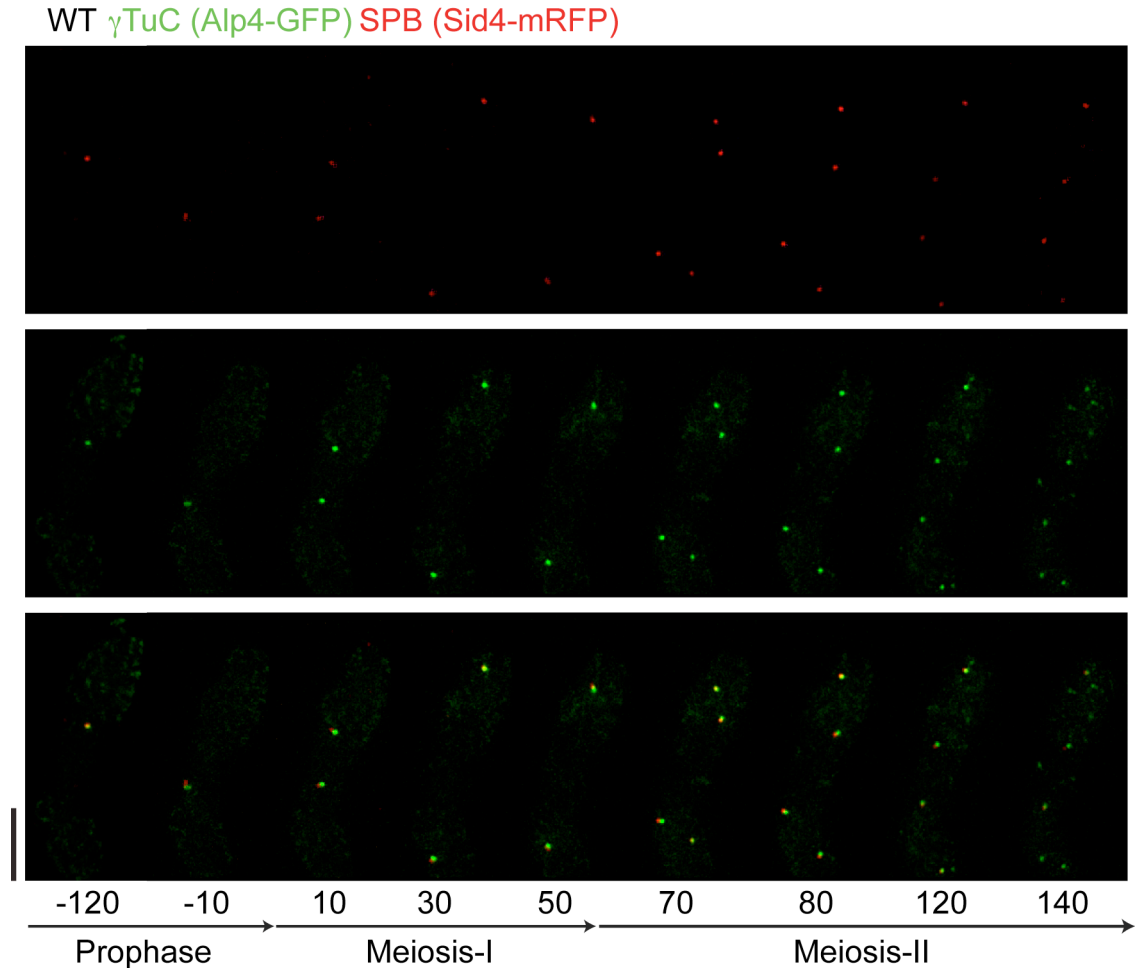


Figure 5.1 Example of γ -TuC localisation throughout WT meiosis

Series of frames from a WT meiosis movie acquired by fluorescence microscopy in live cell. SPB and γ -TuC were observed via endogenously tagged Sid4-mRFP and Alp4-GFP respectively. Numbers under the frames represent the time in minutes. The stages of meiosis are indicated below. 0 min represents the onset of MI. Scale bar equals 5 μ m. SPB and γ -TuC colocalise from prophase to the end of MII until Alp4 signal disperses and an increased number of small, dynamic, and variables in size Alp4 foci are visible throughout the cell 140 min.

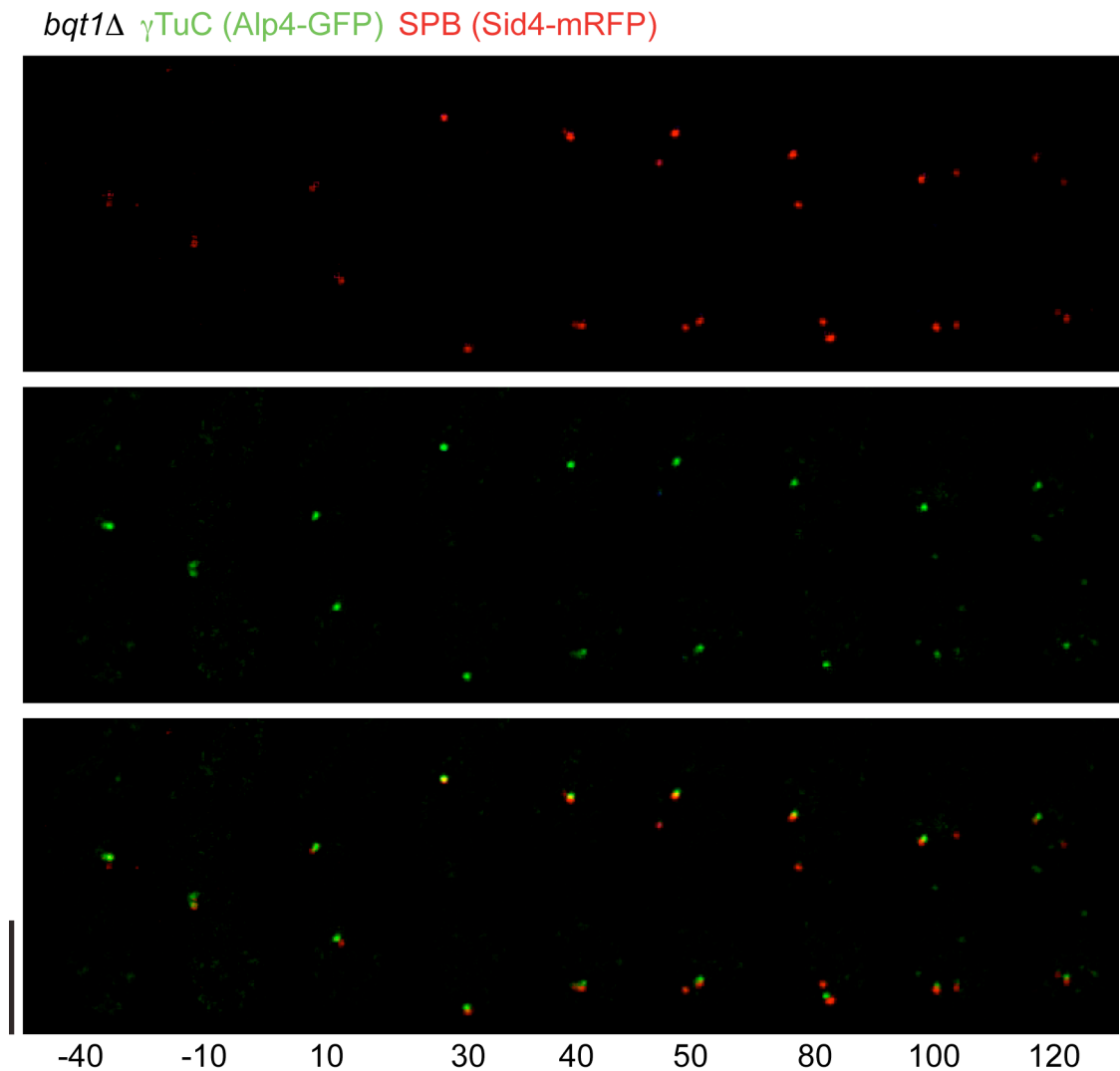


Figure 5.2 Example of γ -TuC unequal separation at MII only

Series of frames from a *bqt1* Δ meiosis movie acquired by fluorescence microscopy in live cell. SPB and γ -TuC were observed via endogenously tagged Sid4-mRFP and Alp4-GFP respectively. Numbers under the frames represent the time in minutes. 0 min represents the onset of MI. Scale bar equals 5 μ m. The movie illustrates γ -TuC unequal separation at MII only (50-120 min) and aberrant SPB separation in which duplicated SPBs separate in MI (10-40 min) but do not separate properly or are sticky in MII 50-120 min.

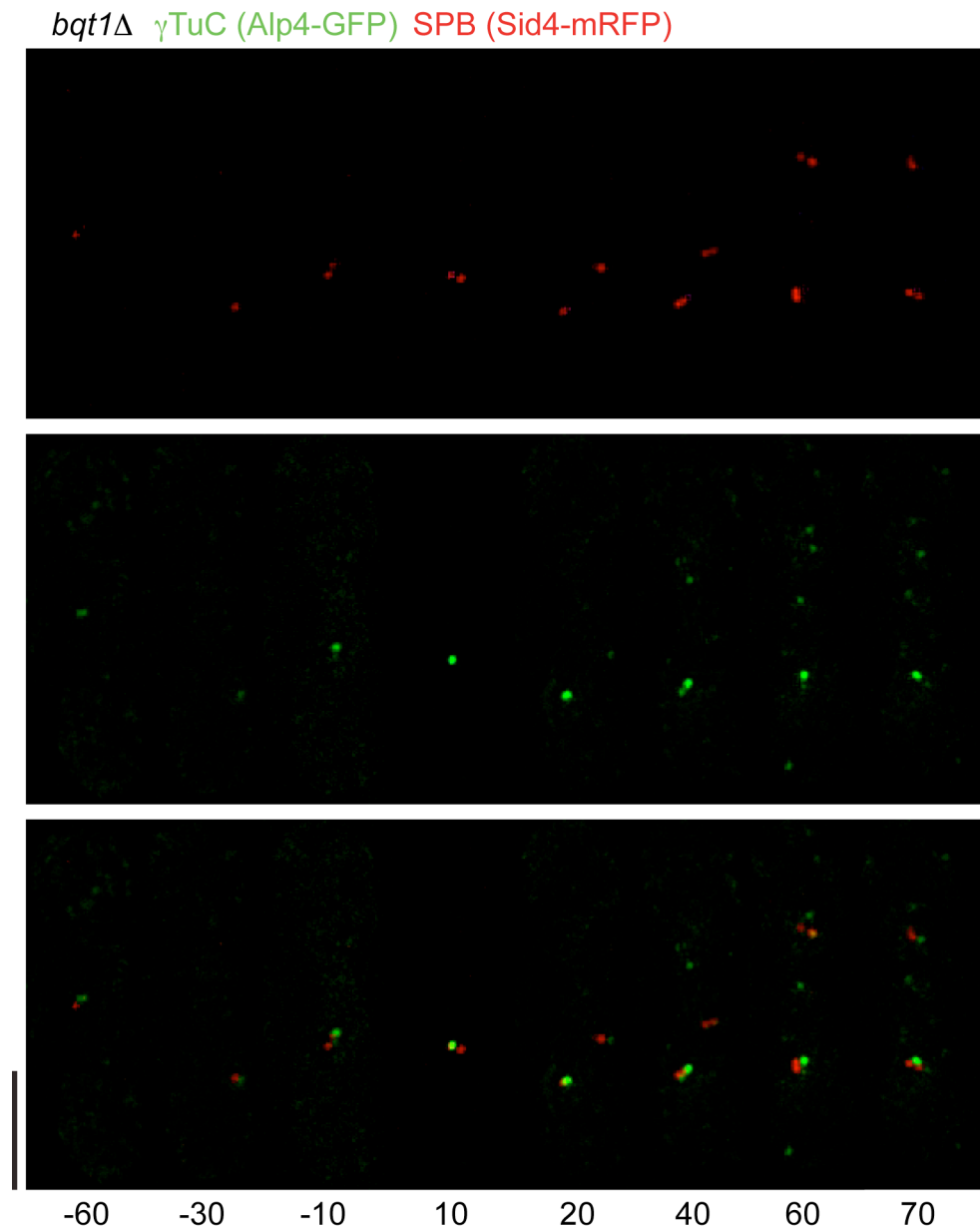


Figure 5.3 Example of γ -TuC unequal separation at MI and MII

Series of frames from a *bqt1* Δ meiosis movie acquired by fluorescence microscopy in live cell. SPB and γ -TuC were observed via endogenously tagged Sid4-mRFP and Alp4-GFP respectively. Numbers under the frames represent the time in minutes. 0 min represents the onset of MI. Scale bar equals 5 μ m. The movie illustrates γ -TuC unequal separation at MI (-10-20 min) and MII (40-80 min) and aberrant SPB separation in which duplicated SPBs are sticky.

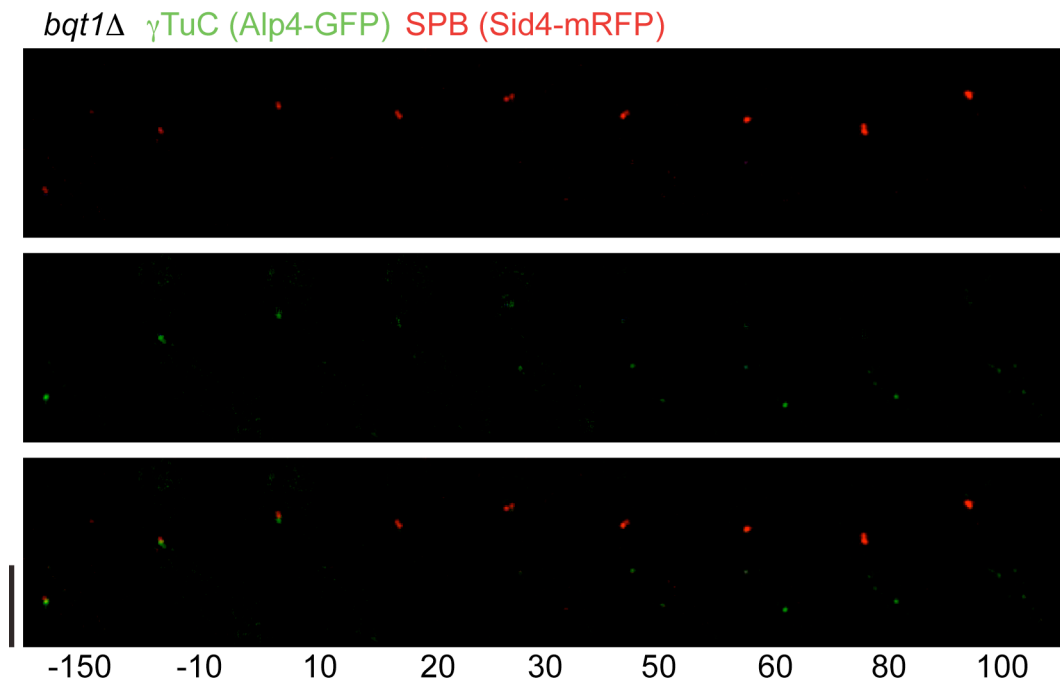


Figure 5.4 Example of γ -TuC signal leaving the SPB

Series of frames from a *bqt1* Δ meiosis movie acquired by fluorescence microscopy in live cell. SPB and γ -TuC were observed via endogenously tagged Sid4-mRFP and Alp4-GFP respectively. Numbers under the frames represent the time in minutes. 0 min represents the onset of MI. Scale bar equals 5 μ m. The movie illustrates γ -TuC unequal separation at MI (-10-20 min) and MII (40-80 min) and aberrant SPB separation in which duplicated SPBs are sticky.

Alp4 signal distribution to SPBs	% of cells (n=100)
WT-like	41
Unequal distribution at MII only	25
Unequal distribution at MI and MII	26
Leave/Decrease	8

Table 5.1 Alp4 localises unequally between duplicated SPBs in bouquet mutant

Phenotypes were observed on *bqt1* Δ meiosis movies acquired by fluorescence microscopy in live cell. SPB and γ -TuC were observed via endogenously tagged Sid4-mRFP and Alp4-GFP respectively. 100 cells were categorised in 4 levels.

SPB \ Alp4	Leave/Decrease	Unequal separation at MI and MII	Unequal separation at MII only
Do not Separate at all	12% (7)	-	-
Separate in MII only	1.5% (1)	40% (23)	15% (9)
Separate in MI but not in MII	-	-	13.5% (8)
Separate in MI and MII	-	3% (2)	15% (9)

Table 5.2 Correlation between Alp4 unequal localisation to the SPB and SPB separation defects

Phenotypes were observed on *bqt1* Δ meiosis movies acquired by fluorescence microscopy in live cell. SPB and γ -TuC were observed via endogenously tagged Sid4-mRFP and Alp4-GFP respectively. 59 cells, which do have unequal distribution of Alp4 signal between duplicated SPBs (horizontal categories) were cross categorised depending on their SPB separation defects (vertical categories). The percentage of cells exhibiting each phenotype is shown with the number of observed cells in parentheses. Numbers in red represent the highest match between each one of the SPB separation defect categories and the categories of Alp4 unequal distribution at SPB.

5.3 Presence of γ -TuC at the SPB correlates with spindle formation

Our observation that SPBs, which fail to separate lack Alp4 suggests that the spindle formation defect seen in the absence of the bouquet, stems from γ -TuC mislocalisation. To address this explicitly, we monitored the γ -TuC (Alp4-GFP), the SPB (Sid4-mRFP) and the microtubules (mRFP-Atb2) (Figure 5.5 and 5.6). We observed that the vast majority of spindles were indeed nucleated from an SPB that colocalises with Alp4, thereby providing a straightforward explanation for the correlation between SPB separation defects and Alp4 mislocalisation to the SPB (Figure 5.6). In addition, this investigation allowed us to understand the different flavours of phenotypes previously described (Tomita and Cooper, 2007). A monopolar spindle can be explained by a severely unequal separation of the γ -TuC between two SPBs (Figure 5.6B 0 and 30 min), while a collapsing spindle can originate from two SPBs with low levels of γ -TuC (Figure 5.6B 50-60 min). A weak or absent spindle can be the consequence of the loss of the γ -TuC from all SPBs (Figure 5.6C).

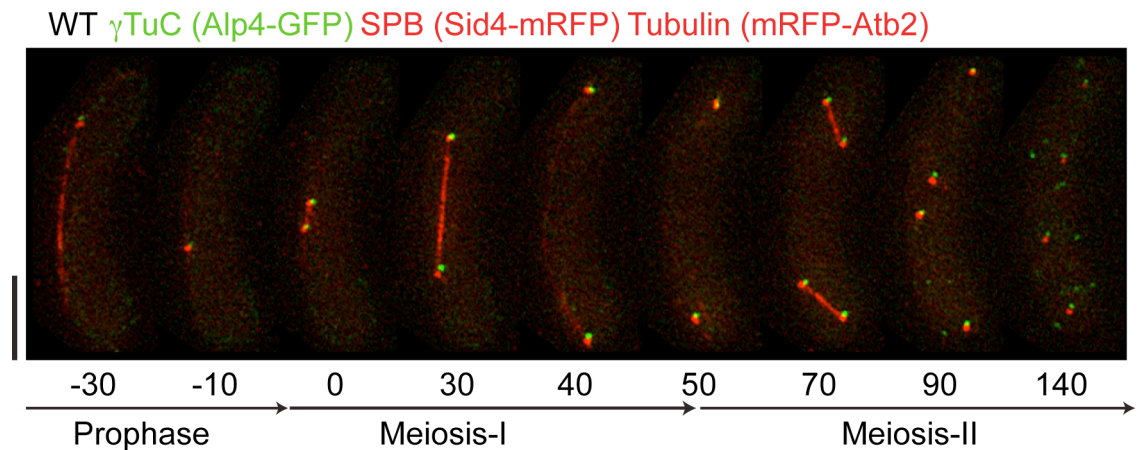
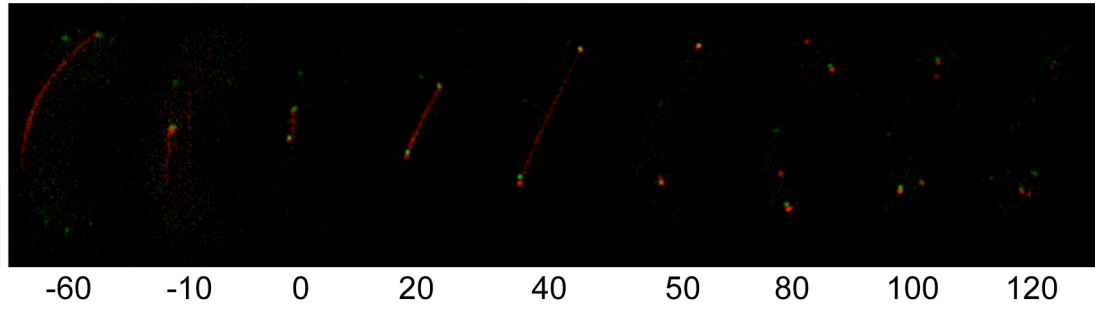


Figure 5.5 Example of spindle formation and γ -TuC localisation throughout WT meiosis

Series of frames from a WT meiosis movie acquired by fluorescence microscopy in live cell. SPB and γ -TuC were observed via endogenously tagged Sid4-mRFP and Alp4-GFP respectively. Tubulin was observed by ectopically expressed mRFP-Atb2. Numbers under the frames represent the time in minutes. The stages of meiosis are indicated below. 0 min represents the onset of MI. Scale bar equals 5 μ m. SPB and γ -TuC colocalise from prophase to the end of MII until Alp4 signal disperses and an increased number of small, dynamic, and variables in size Alp4 foci are visible throughout the cell 140 min with spindle formation at MI and MII.

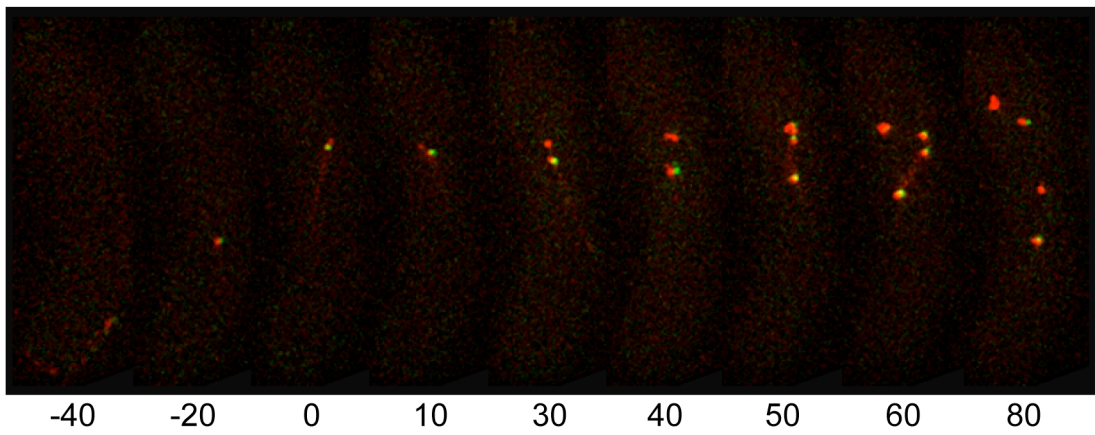
A

bqt1 Δ γ TuC (Alp4-GFP) SPB (Sid4-mRFP) Tubulin (mRFP-Atb2)



B

bqt1 Δ γ TuC (Alp4-GFP) SPB (Sid4-mRFP) Tubulin (mRFP-Atb2)



C

bqt1 Δ γ TuC (Alp4-GFP) SPB (Sid4-mRFP) Tubulin (mRFP-Atb2)

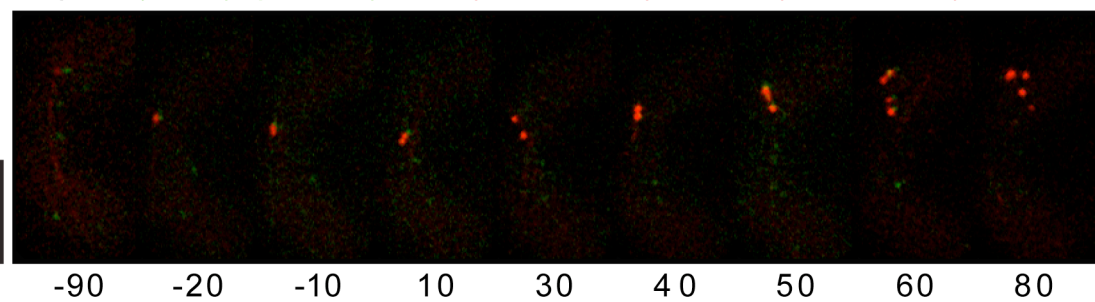


Figure 5.6 Examples of γ -TuC unequal localisation to duplicated SPBs

Series of frames from *bqt1 Δ* meiosis movies acquired by fluorescence microscopy in live cell. SPB and γ -TuC were observed via endogenously tagged Sid4-mRFP and Alp4-GFP respectively. Tubulin was observed by ectopically expressed mRFP-Atb2. Numbers under the frames represent the time in minutes. 0 min represents the onset of MI. Scale bars equal 5 μ m.

(A) The movie illustrates γ -TuC unequal separation at MII only (50-120 min) and aberrant SPB separation in which duplicated SPBs separate in MI (0-50 min) but do not separate properly or are sticky in MII (50-120 min). Correct spindle formation at MI correlates with equal segregation of Alp4 between duplicated SPB (20-40 min) while there is no spindle formation at MII (50-100 min) when Alp4 is unequally distributed between SPBs.

(B) The movie illustrates γ -TuC unequal separation at MI (0-30 min) and MII (40-60 min) and aberrant SPB separation in which duplicated SPBs are sticky. Monopolar spindle at MI correlates with severe unequal segregation of Alp4 between duplicated SPB (0 and 30 min) and very weak and collapsing spindle at MII correlates with unequal Alp4 distribution between SPBs (50-60 min).

(C) The movie illustrates γ -TuC leaving the SPB at MI (10 min) and aberrant SPB separation in which SPBs duplicate in MI (10-30 min) and in MII (50-60 min) but do not separate at all it correlates with no spindle formation.

5.4 Alp4 over-expression does not rescue bouquet phenotypes

In the preceding sections, we showed that stabilisation and/or recruitment of the γ -TuC at the meiotic SPB are imperfect. If deficient recruitment of the γ -TuC to the SPB triggers the bouquet deficient phenotypes, they might be rescued by γ -TuC overexpression. The γ -TuC function as a complex to nucleate microtubule therefore, it primary seem important to overexpress all γ -TuC components. However, since previous study has shown that mild overexpression of Alp4 alone is enough to rescue γ -TuC localisation to SPB in a Pcp1 mutant defective in γ -TuC recruitment (Fong et al., 2010) we decided to overexpress only Alp4.

5.4.1 Plasmid based Alp4 over-expression

Knowing from the literature that Alp4 is essential and that over-expression of any of the γ -TuC components can be lethal (Vardy and Toda, 2000, Masuda et al., 2006), we needed a system that would allow mild over-expression of Alp4. In order to achieve such mild over-expression and keep the *alp4* endogenous copy intact, we used a plasmid where *alp4* is under the control of *nmt1* promoter (*p-nmt1*) and performed experiments under repressed conditions (presence of thiamine). As previously reported in the literature, even under repressed conditions a significant level of expression can be detected (Forsburg, 1993). In addition, since the number of plasmid copies within a cell is not controllable, this system slightly increases the possibility of Alp4 being over-expressed even under repressed conditions. We scored the end product of meiosis (number of spores per ascus) in WT and *bqt1* Δ cells transformed with either an empty vector or the *p-nmt1-alp4* vector (Figure 5.7). To verify the presence of the plasmid within the cell, at the same time as we patched the cells for meiotic induction, we re-streaked the cells in inducing conditions and checked for cell elongation, one of Alp4 over-expression phenotypes (Masuda et al., 2006). Under repressing conditions, we did not observe any differences between WT empty vector and WT *alp4*⁺, meaning that *alp4* over-expression is mild enough to support cell

viability. However, we also failed to observe rescue of the bouquet phenotypes by *bqt1* Δ *alp4*⁺.

Although it seems that Alp4 over-expression does not rescue bouquet phenotypes, we cannot state that Alp4 is really over-expressed in this experiment. This would require the use of a plasmid where Alp4 is tagged and detectable by western blot. We also cannot be certain that plasmids are kept during conjugation and meiosis. Moreover, since here we assessed rescue of bouquet phenotypes by looking at the end product of meiosis, we could be missing subtler rescue. For all these reasons we decided to adjust our strategy.

5.4.2 Genomic integration based Alp4 over-expression

To verify the results obtained with the first strategy, we over-expressed Alp4 in strains where chromosomes and SPB (Pcp1) are tagged with mRFP and GFP respectively. Under these conditions, one can directly observe SPB separation and detect a more subtle rescue of bouquet phenotypes. In addition, instead of using plasmid-based expression, we used strains where *nmt1* promoter replaces *alp4* endogenous promoter. These strains are hereafter referred to as WT *nmt1-alp4* and *bqt1* Δ *nmt1-alp4*.

5.4.2.1 Repressed conditions

As in the previous experiment, we first filmed WT-*nmt1-alp4* and *bqt1* Δ -*nmt1-alp4* cells under repressed conditions. We observed that WT-*nmt1-alp4* accomplish meiosis just like WT strains (Figure 5.8A), as 30 out of the 32 cells observed have perfect SPB separation (the same numbers are seen for WT). Hence, *alp4* expression in this system is both sufficient and mild enough to support meiosis. As in the previous experiment, repressed *bqt1* Δ -*nmt1-alp4* did not rescue the bouquet phenotypes (Figure 5.8B and C), as only 5 out of 30 cells exhibit proper SPB separation.

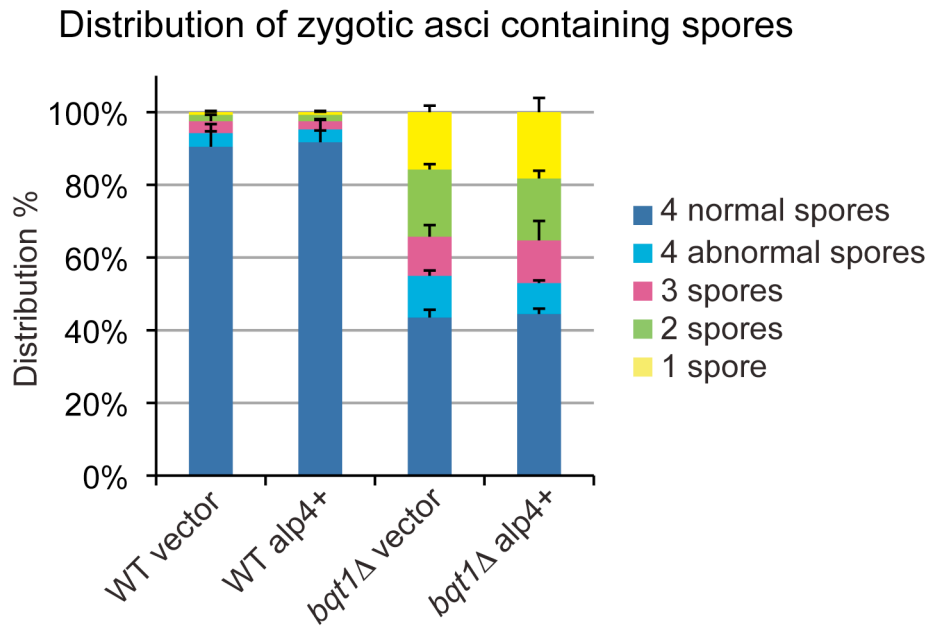


Figure 5.7 Alp4 expression under the control of *nmt1* promoter in repressed conditions does not rescue bouquet SPB defects

Distribution of categories of asci. Asci from zygotic meiosis were scored under light microscopy. 200 asci per genotype were counted in the experiment. Cells were grown under repressed conditions (presence of thiamine) prior meiotic induction. Data represent the average of two experiments. Error bars indicate standard deviation. WT or *bqt1Δ* cells containing empty vector (WT vector, *bqt1Δ* vector), WT or *bqt1Δ* cells containing vector with *alp4* under the control of *nmt1* promoter (WT alp4+, *bqt1Δ* alp4+).

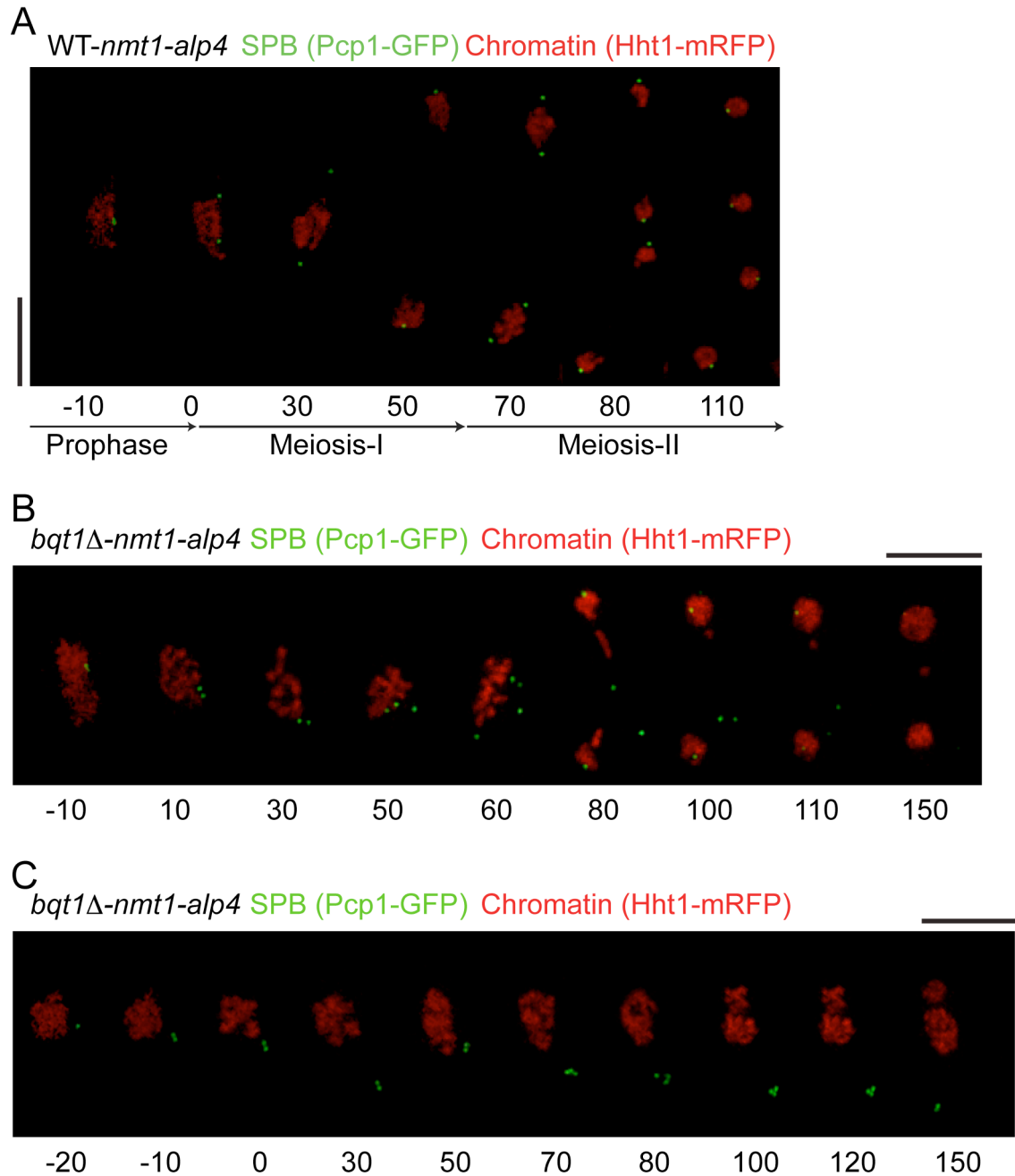


Figure 5.8 *Alp4* expression under the control of *nmt1* promoter in repressed conditions does not rescue bouquet SPB defects

Series of frames from WT-*nmt1-alp4* (A) *bqt1Δ-nmt1-alp4* (B-C) meiosis movies acquired by fluorescence microscopy in live cell. Cells were grown in presence of thiamine prior meiotic induction. SPB and chromosomes were observed via endogenously tagged Pcp1-GFP and Hht1-mRFP respectively. Numbers under the frames represent the time in minutes. 0 min is the onset of MI. Scale bars equal 5 μ m. (A) WT-like SPB separation at MI and MII. (B-C) Aberrant SPB separation reminiscent of *bqt1Δ* cells (B) SPBs are sticky and separate only after MII duplication occurred (80 min). (C) SPBs duplicate in MI (0 min) in MII (70-80 min) but do not separate at all.

5.4.2.2 *Induced conditions*

The timing with which the *nmt1* promoter is activated after removal of thiamine is variable but the steady state is thought to be reached after 16h. It has also been shown that lower levels of thiamine can be used to set intermediate level of expression (Javerzat et al., 1996). We thus tested two different conditions. Cells were grown in the presence of thiamine, then re-streaked for either 16 hours without thiamine or 24 hours with a low level of thiamine and finally patched for meiotic induction. However, for both *WT-nmt1-alp4* and *bqt1 Δ -nmt1-alp4*, the phenotypes observed were similar in the presence of low level of thiamine or without thiamine. We concluded that with these conditions we were not able to adjust Alp4 expression level and we did not further attempt to fine-tune the system. For the rest of the analysis, the two sets of experiments were considered as one.

By contrast, *WT-nmt1-alp4* meiosis in induced conditions (no thiamine) appears very defective (Figure 5.9). Only 8 cells out of 40 were able to produce asci with 3 or 4 spores. Phenotypes vary and are difficult to interpret. Nonetheless, we noticed cells that were conjugating but did not pursue meiosis, or cells where meiosis seems to stop after MI (i.e. no second round of SPB duplication visible) (Figure 5.9A) as well as cells with two consecutive SPB duplications but inefficient chromosome segregation (Figure 5.9B). We believe that the variation in the phenotypes observed could be attributed to differences in *alp4* expression level among the cells.

Under these conditions, Alp4 over-expression does not seem to rescue bouquet phenotypes, as only 2 of 50 cells produce asci with 4 spores. Meiosis appears very defective (Figure 5.10), and phenotypes extremely difficult to interpret as they are additive with those of *WT-nmt1-alp4* under induced conditions. For example (Figure 5.10A) we observed cells like in *WT-nmt1-alp4* (Figure 5.9A), where SPB duplication occurs only once during meiosis but with sticky SPB as

opposed to more separated SPB in WT-*nmt1-alp4*. We did not categorise further the phenotypes, as it was clear that there was no rescue of bouquet defects.

However, the system has many flaws and does not allow us to conclude with confidence. We believe that under repressed conditions, Alp4 over-expression is too subtle while it is too over-expressed in absence of thiamine to obtain clear phenotypes. The next experiment would be to try to over-express Alp4 using the attenuated version of *nmt1* promoter *nmt41* and *nmt81* in absence of thiamine or alternatively to use the same system as *pcp1-2copies* and add a second copy of the *alp4* gene in the genome. Another very different strategy to test if Alp4 recruitment and/or stabilisation are causative of bouquet defects would be to artificially tether Alp4 to the SPB by inserting a SPB targeting sequence. Spindle microtubule nucleation occurs in the nucleoplasm; hence, Alp4 should be targeted to the inner plaque of the SPB. However, while artificial targeting to the cytoplasmic side of the SPB has already been described (Morrell et al., 2004, Tomlin et al., 2002), artificial targeting to the nucleoplasmic side has not yet been reported so we would have to develop such a system *de novo*. However, while Alp4 may be an indicator of the γ -TuC it might very well be insufficient and more γ -tubulin itself may be needed.

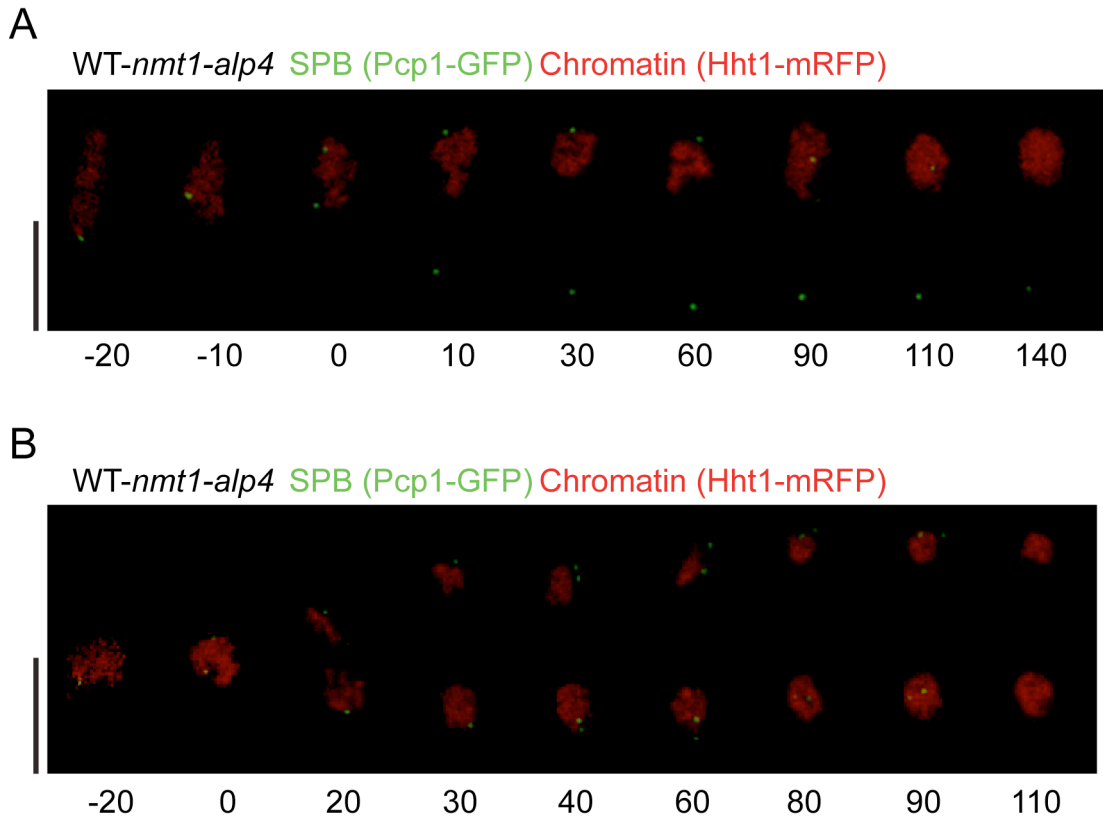


Figure 5.9 Strong *Alp4* over-expression in WT cells shows severe meiotic defects

Series of frames from WT-*nmt1-*alp4** meiosis movies acquired by fluorescence microscopy in live cell. *Alp4* over-expression was induced by the absence of thiamine for 16 hours prior meiosis induction. SPB and chromosomes were observed via endogenously tagged Pcp1-GFP and Hht1-mRFP respectively. Numbers under the frames represent the time in minutes. 0 min is the onset of MI. Scale bars equal 5 μ m. (A) Aberrant SPB duplication, SPB duplicates only once (0min) (B) SPB duplicates twice (0min and 40 min) but chromosomes segregation is abnormal.

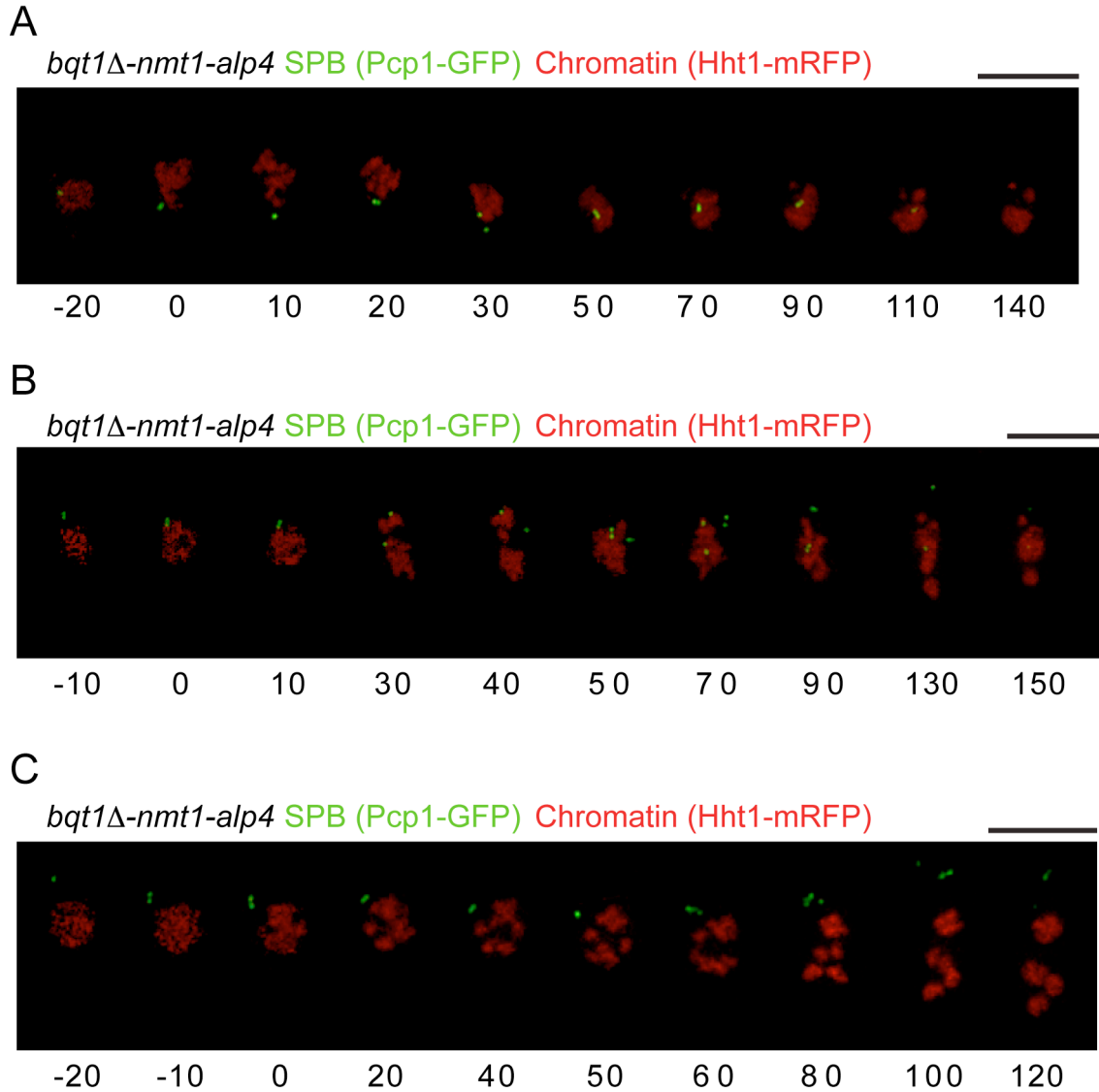


Figure 5.10 Strong Alp4 over-expression does not rescue bouquet SPB separation defects

Series of frames from *bqt1 Δ -nmt1-alp4* meiosis movies acquired by fluorescence microscopy in live cell. Alp4 over-expression was induced by the absence of thiamine for 16 hours prior meiosis induction. SPB and chromosomes were observed via endogenously tagged Pcp1-GFP and Hht1-mRFP respectively. Numbers under the frames represent the time in minutes. 0 min is the onset of MI. Scale bars equal 5 μ m. (A) Aberrant SPB duplication and separation, SPB duplicates only once and are sticky. (B-C) Aberrant SPB separation reminiscent of *bqt1 Δ* cells (B) SPBs are sticky and separate poorly only after MII duplication occurred (70 min). (C) SPBs duplicate in MI (0 min) in MII (50-60 min) but do not separate at all.

5.5 Overview

In this chapter, by following γ -TuC and SPB behaviour in WT and *bqt1* Δ cells we found that in the absence of the bouquet, γ -TuC localises unevenly between the duplicated SPBs from the onset of MI and that SPB separation defects tightly correlate with this defective localisation. These results led us to consider the possibility that the major defect in bouquet deficient cell lies in the stabilisation and/or recruitment of the γ -TuC to the meiotic SPB. In the following chapters, we focus on the analysis of events that could be involved in Alp4 stabilisation and/or the recruitment to the meiotic SPB, such as the relationship between SPB insertion in the nuclear envelope and post-translational modifications of candidate SPB components.

Chapter 6. γ -TuC recruitment to the meiotic SPB

6.1 Aim

In the preceding chapter, we have shown that the bouquet is required for proper γ -TuC localisation to the meiotic SPB, and that successful SPB separation and subsequent chromosome segregation depend on its even distribution between duplicated SPBs. Here we investigate the mechanisms involved in γ -TuC recruitment.

As presented in the introduction, γ -TuC recruitment in cycling cells depends on its localisation (cytoplasm vs. nucleoplasm) and cell cycle stage (interphase microtubules vs. spindle microtubules) (Samejima et al., 2010, Fong et al., 2010). γ -TuC recruitment in meiosis is less well understood. Reports in the literature suggest that, like in cycling cells, the γ -TuC is recruited by different means for cytoplasmic microtubule nucleation during prophase versus spindle nucleation at meiosis-I and II (Tanaka et al., 2005). Indeed, it has been shown that in prophase Alp4 localisation to the cytoplasmic side of the SPB depends on Hrs1, a meiotic specific SPB component involved in horsetail nuclear movement (Tanaka et al., 2005). In *hrs1 Δ* cells, Alp4 is delocalised from the SPB in prophase; however, its localisation to the SPB is recovered at the onset of MI (Tanaka et al., 2005). Thus, Alp4 is recruited to the meiotic SPB by distinct mechanisms in prophase and during the rest of meiosis. Consistently, we observed uneven localisation of Alp4 only from the onset of MI onwards and never in prophase. Therefore, we became interested in the mechanisms involved in Alp4 recruitment specifically at the onset of MI.

Several reports in the literature highlight the role of pericentrin in γ -TuC recruitment to the centrosome/SPB in various species (Flory et al., 2002, Zimmerman et al., 2004) (Zhang and Megraw, 2007). In *S.pombe*, a recent study reveals the importance of Pcp1 (Pericentrin-like protein) in γ -TuC recruitment specifically to the mitotic SPB (Fong et al., 2010). Pcp1 localises to the inner

plaque of the SPB throughout the cell cycle (Flory et al., 2002) and hence recruits the γ -TuC during mitosis when the SPB is inserted in the nuclear envelope (NE) to nucleate spindle microtubules. Pcp1 thus emerges as a good candidate for involvement in γ -TuC recruitment at the meiotic SPB for nucleation of meiotic spindle microtubules. Here we explore the role of Pcp1 as well as the step of SPB insertion in the NE in meiosis.

6.2 Pcp1 participates in γ -TuC recruitment to the meiotic SPB

In order to study the role of Pcp1 in γ -TuC recruitment to the meiotic SPB, we took advantage of a published temperature sensitive allele of Pcp1, *pcp1-15* (Fong et al., 2010). *pcp1-15* has been shown to be defective in Alp4 recruitment to the mitotic SPB at restrictive temperature. To test whether Pcp1 is also involved in Alp4 recruitment to the meiotic SPB, we performed live cell imaging and analysed spindle formation and SPB separation in *pcp1-15* strains where the SPB (Sid4) is endogenously tagged with mRFP and the tubulin observed via ectopically expressed GFP-Atb2.

pcp1-15 has been characterised in mitosis at its restrictive temperature 36°C and semi restrictive temperature 34°C (Fong et al., 2010). However, meiosis is most efficient between 25 and 30°C. We thus decided to test *pcp1-15* meiosis at different temperatures. Cells were grown at 25°C (permissive temperature) to avoid mitotic defects, induced to undergo meiosis and filmed at 25, 27 30 or 32°C. We ranked the cells depending on faithful formation of spindle at MI and MII and subsequent SPB separation (Figure 6.1-6.2 and Table 6.1). As the temperature increases, the percentage of *pcp1-15* cells with defective meiosis increases, with the percentage MI plus MII defects (Figure 6.2B) rising from 0% at 25°C to 15.6% at 32°C and the percentage of MII defects without MI defects rising from 2.7% at 25°C to 20.8% at 32°C. We observed monopolar and collapsing spindle reminiscent of the defects described in mitosis (Fong et al., 2010). The

phenotypes seen at 32°C are specific for the *pcp1-15* allele as WT cells at 32°C show 100% successful meiosis. We concluded from these experiments that even though the penetrance of the phenotypes is limited at 32°C, this temperature is sufficient to detect significant phenotypes in *pcp1-15* meiosis.

As the meiotic *pcp1-15* phenotypes are similar to their reported mitotic phenotypes, we suspected that Pcp1 is also involved in the recruitment of the γ -TuC to the meiotic SPB. Moreover, the defects observed in *pcp1-15* meiosis (defective spindle, sticky SPBs) are comparable to *bqt1 Δ* phenotypes, recalling our finding that *bqt1 Δ* defects are associated with faulty γ -TuC recruitment. However, *bqt1 Δ* and *pcp1-15* meioses are not strictly identical; for instance, the percentages of functional SPBs at MI differs between the two strains 37% in *pcp1-15* and only 17.5% in *bqt1 Δ* (Chapter 2). These differences could be attributed to weak penetrance of the phenotypes at 32°C, or could indicate that Alp4 localisation to the SPB, albeit very important for spindle formation and proper SPB separation, is not the primary defect in *bqt1 Δ* cells. To address issues of cause and consequence, we decided to investigate the insertion of the SPB in the NE, which is often compromised in bouquet mutants and whose failure could be envisioned to lie upstream of problems with Alp4 localisation.

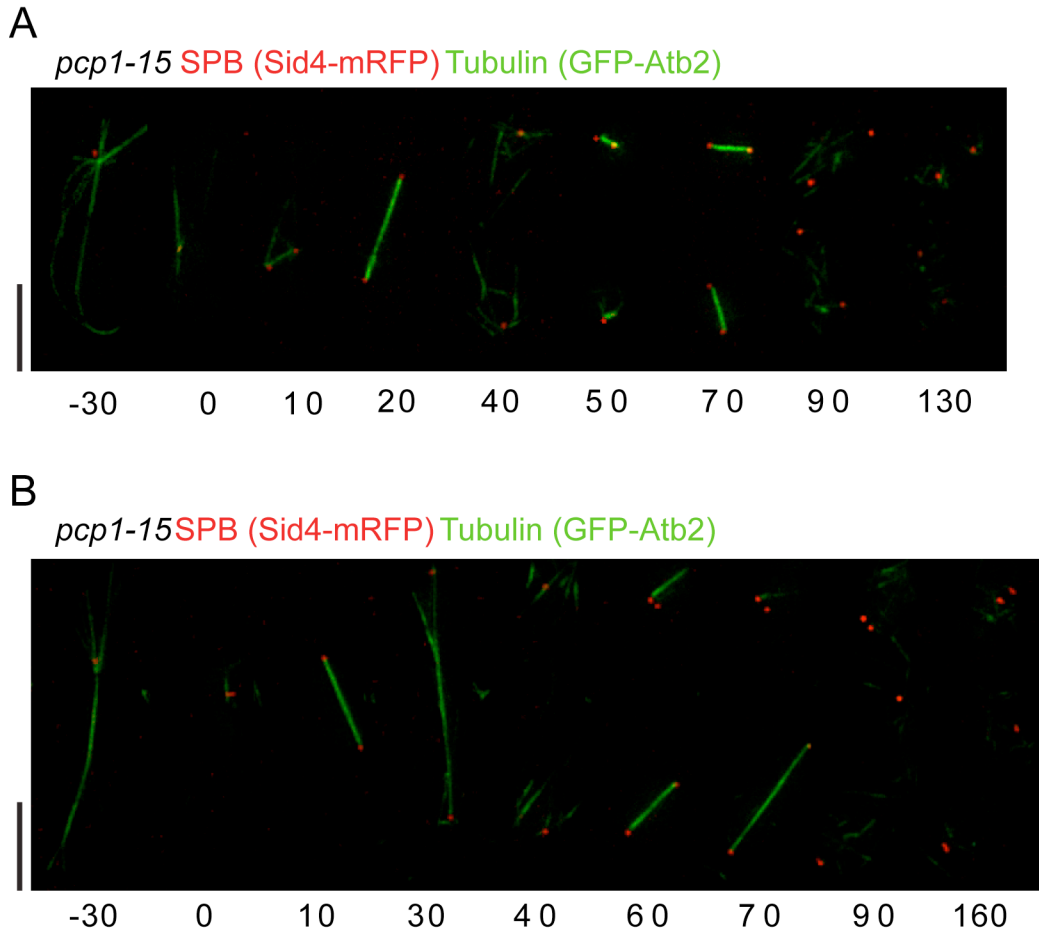


Figure 6.1 Mild phenotypes of *pcp1-15* meiosis at 32°C

Series of frames from *pcp1-15* meiosis movies acquired by fluorescence microscopy in live cell at 32°C. SPB and Spindle were observed via endogenously tagged Sid4-mRFP and ectopically expressed GFP-Atb2 respectively. Numbers under the frames represent the time in minutes. 0 min represents the onset of MI. Scale bars equal 5 μ m. (A) SPB separates and spindle forms properly in MI and MII (WT-like meiosis) (B) SPB separates and spindle forms properly in MI but in MII instead of two bipolar spindles we observed one bipolar and one monopolar spindle (60 min).

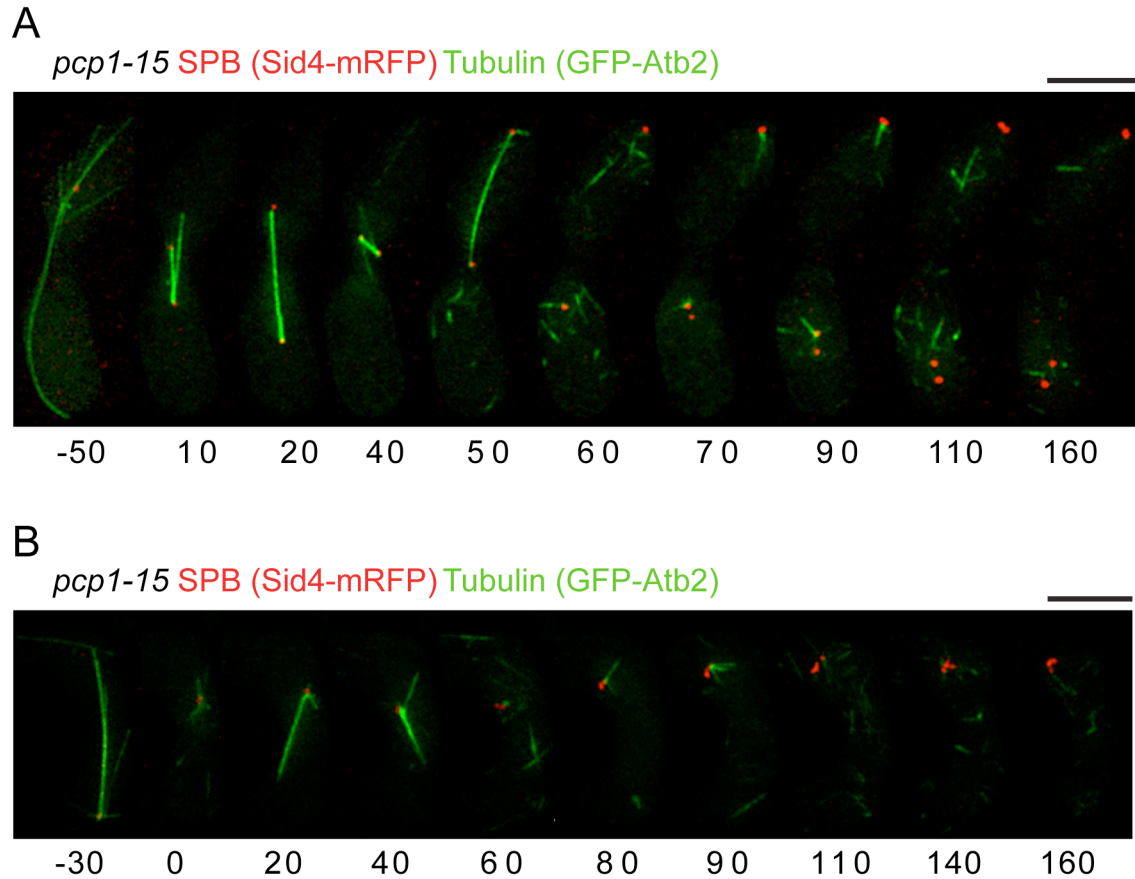


Figure 6.2 Strong phenotypes of *pcp1-15* meiosis at 32°C

Series of frames from *pcp1-15* meiosis movies acquired by fluorescence microscopy in live cell. SPB and Spindle were observed via endogenously tagged Sid4-mRFP and ectopically expressed GFP-Atb2 respectively. Numbers under the frames represent the time in minutes. 0 min represents the onset of MI. Scale bars equal 5 μ m (A) SPB separates and spindle forms properly in MI but in MII SPBs are sticky and we observed only small monopolar spindle (70-90 min). (B) Aberrant SPB separation and spindle formation where SPBs duplicate in MI and (20-40 min) and in MII (90-110 min) but do not separate at all and produce only monopolar spindle (20-40 min) and (80-90 min).

	<i>pcp1-15</i>				WT
	% of cells 25°C (n=37)	% of cells 27°C (n=35)	% of cells 30°C (n=39)	% of cells 32°C (n=96)	% of cells 32°C (n=25)
WT-like MI✓ MII✓✓	83.8 (31)	77.2 (27)	51.3 (20)	46.9 (45)	100 (25)
MI✓ MII✓X	13.5 (5)	11.4 (4)	23.1 (9)	16.7 (16)	-
MI✓ MIIXX	2.7 (1)	5.7 (2)	23.1 (9)	20.8 (20)	-
MIX MIIXX	-	5.7 (2)	2.5 (1)	15.6 (15)	-

Table 6.1 Pcp1 is involved in Alp4 recruitment at the meiotic SPB

Phenotypes were observed on *pcp1-15* meiosis movies acquired by fluorescence microscopy in live cell. SPB and Spindle were observed via endogenously tagged Sid4-mRFP and ectopically expressed GFP-Atb2 respectively. For each temperature, the number of observed cells is in parentheses and cells categorised in 4 levels. ✓ means successful SPB separation and spindle formation and X means defective SPB separation and spindle formation. In MII both spindle formation where considered. The percentage of cells exhibiting each phenotype is shown with the number of observed cells in parentheses.

6.3 SPBs fail to interact properly with the membrane in absence of bouquet

As mentioned in the Introduction, electron microscopy (EM) data have shown that in cycling cells, the SPB inserts in the NE via formation of a fenestra at the time of mitotic entry and returns to the cytoplasmic side of the NE at the end of mitosis (anaphase) (Ding et al., 1997). The main proteins implicated in this process are Cut11 and Cut12. Cut11 is a constitutive component of the nuclear pore complex (NPC) that localises to the mitotic as well as the meiotic SPB (Figure 6.3) (West et al., 1998). Its localisation to the mitotic SPB coincides with the time between SPB entry and exit from the NE (West et al., 1998). Cut12 is an SPB component (Bridge et al., 1998). Since mitotic SPB duplication occurs prior to fenestra formation and subsequent membrane insertion, it seems reasonable to think that meiotic SPB duplication precedes NE insertion both at MI and MII. We presume that the SPB detaches from the NE between anaphase-I and metaphase-II; indeed, live analysis of Cut11-GFP reveals that Cut11 localises to the SPB in metaphase-I but not in late anaphase-I, and re-colocalises with the SPB in metaphase II before leaving again at anaphase-II (Figure 6.3).

Knowing from previous studies in the lab that SPBs frequently detach from the NE in *bqt1 Δ* cells (Tomita and Cooper, 2007), we wished to explore this observation further along with its relationship to SPB behaviour. As a membrane marker, we used Cut11-GFP, whose localisation both to the NPCs and the SPB at some time points can be confusing; we have also initiated a search for more suitable membrane markers. We first noticed that as in WT cells, Cut11 signals appear at the SPB in MI at the onset of metaphase in *bqt1 Δ* cells, leave the SPB at the MI/MII transition, and reappear in MII before leaving again during MII anaphase (Figure 6.3-6.4). This pattern reinforces the idea that the SPB cycle continues throughout meiosis and is not affected by bouquet disruption-induced defects in chromosome segregation, spindle formation and SPB separation.

Most importantly, despite intermittent obstruction of the SPB signal by Cut11 signals, we noticed a direct correlation between the severity of SPB separation defects and SPB positioning with respect to the NE in *bqt1 Δ* cells. In WT cells, we never detected SPBs detaching from the NE. However, in *bqt1 Δ* cells, we observed different scenarios. For example, when separation of the duplicated SPB occurs only at MII, it is usually the case that after MI duplication, one SPB appeared to be inserted in the NE while the other was not; the inserted SPB duplicates and separates in MII, while the SPB whose MI insertion failed duplicates but does not separate (Figure 6.4A, arrowhead). When the SPBs do not separate at all, it seems that all four duplicated but not separated SPBs detach from the NE (Figure 6.4B). Because of the punctate nature of Cut11 signal and the intermittent colocalisation with the SPB it is not always straightforward to determine whether the SPB is first inserted in the NE and then detached or is never inserted properly and then eventually detaches from the cytoplasmic side of the NE. In addition, when the SPB does appear clearly detached, we do not know if it is completely disconnected or if it somehow remains connected to some membrane. The best way to address these questions would be to perform EM analyses, although use of this approach would require solutions to two major limitations. The first one is the poor synchrony (Chapter 7) and the second is the weak proportion of cells that present strong phenotypes (only slightly more than 50% of *bqt1 Δ* cells show SPB and spindle defects, and those 50% are again divided in four categories depending on the strength of the phenotypes). As our preliminary results are interesting, it could be informative to repeat the same experiment with another NE marker that would not colocalise with the SPB and have a less punctate signal, such as *Ish1* (Taricani et al., 2002).

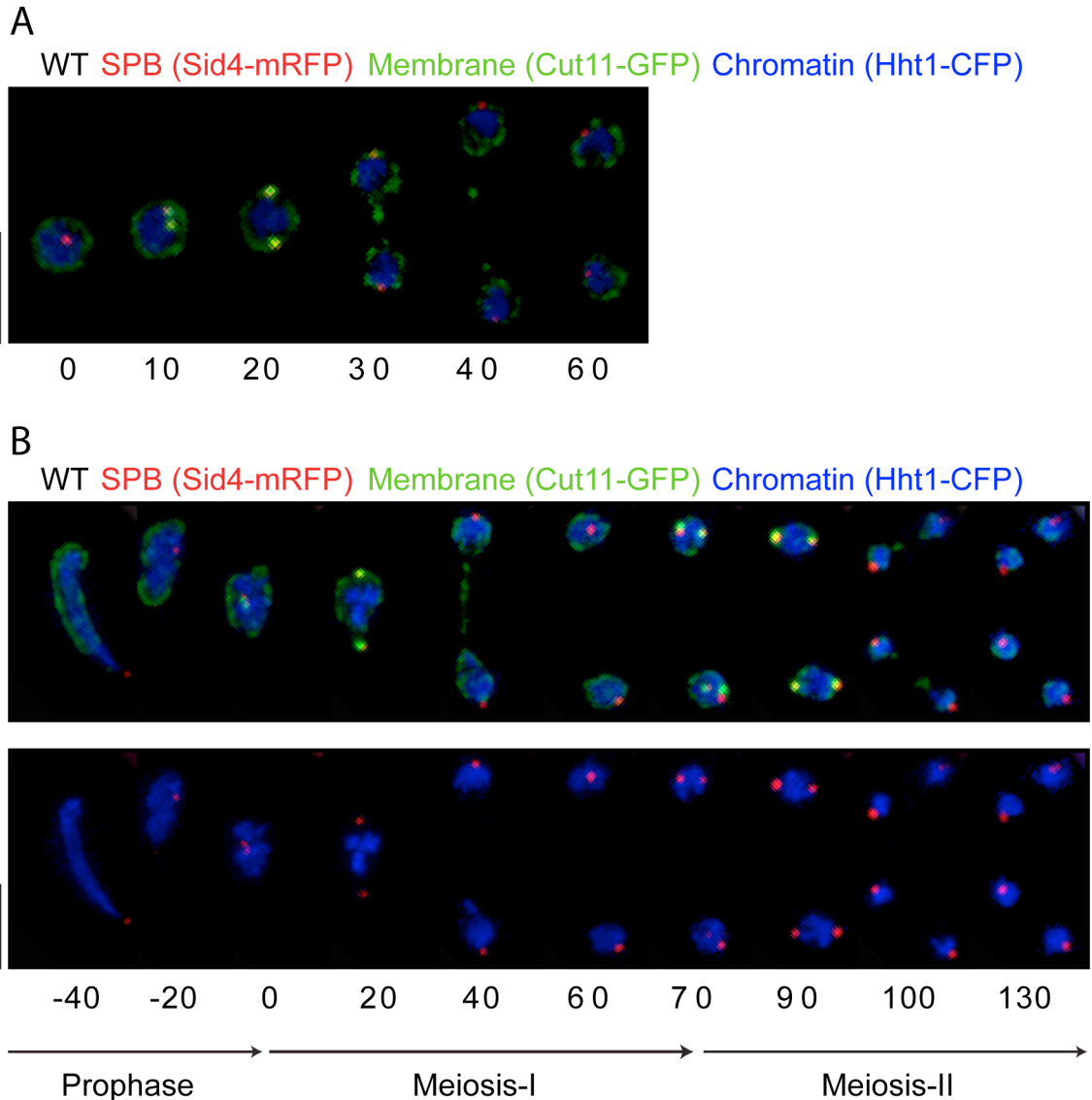


Figure 6.3 Example of SPB insertion in the nuclear envelop in WT mitosis and meiosis

(A-B) Series of frames from WT movie acquired by fluorescence microscopy in live cell. SPB, membrane and chromosomes were observed via endogenously tagged Sid4-mRFP, Cut11-GFP and Hht1-CFP respectively. Numbers under the frames represent the time in minutes. Scale bars equal 2 μ m. (A) Mitotic division. 0 min is the beginning of mitosis (B) Meiotic division. The stages of meiosis are indicated below. 0 min is the onset of MI. The lower panel shows only the red and blue channels (SPB and chromosomes signals) of the upper panel. (A-B) Cut11 signal in addition to be at the NPC also localises transiently to the mitotic SPB in metaphase (10-20 min) and to the meiotic SPB in MI metaphase (0-20min) and MII metaphase (70-90min).

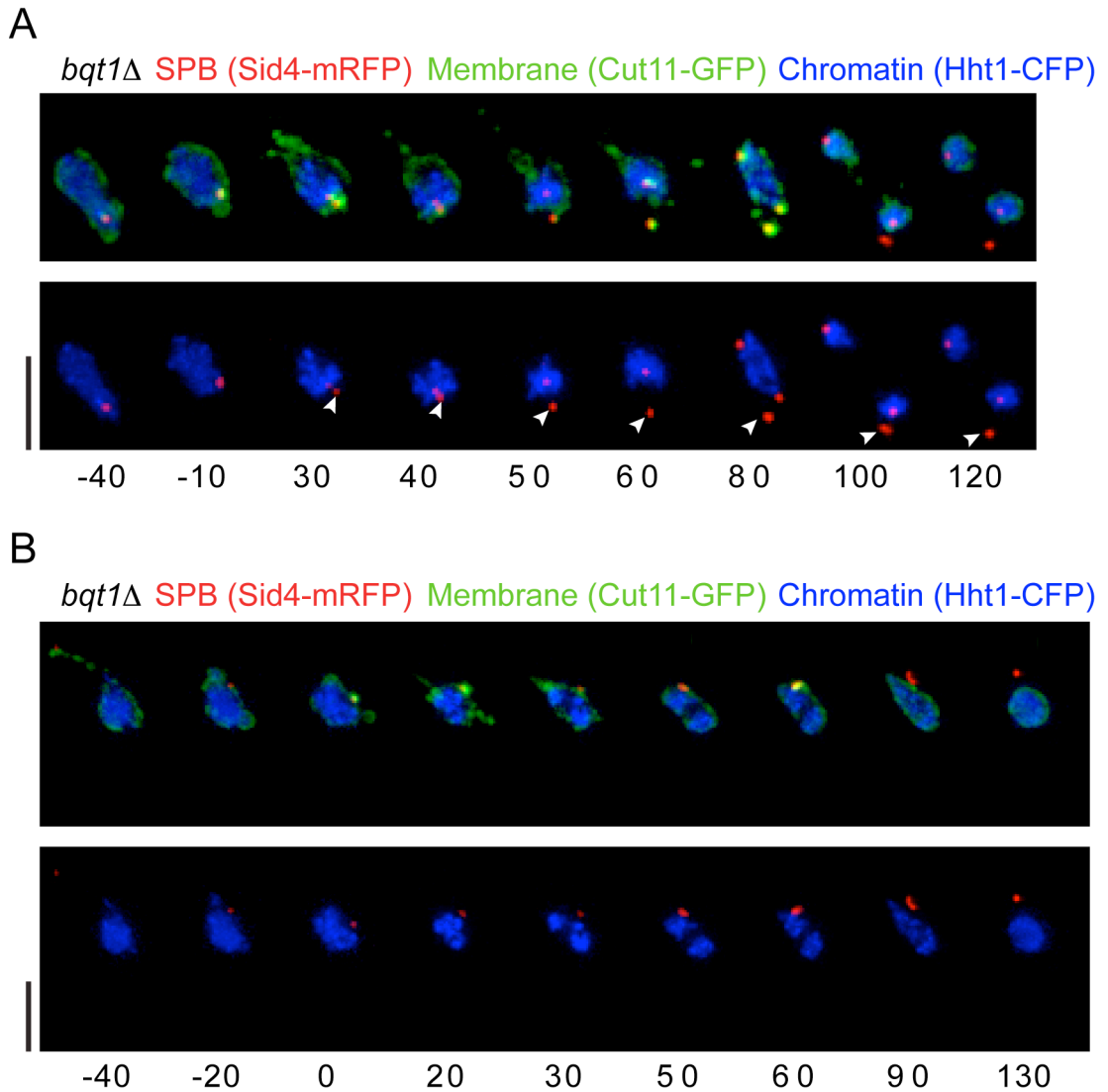


Figure 6.4 SPB detaches from the nuclear envelop in bouquet deficient cells

Series of frames from *bqt1* Δ meiosis movies acquired by fluorescence microscopy in live cell. SPB, membrane and chromosomes were observed via endogenously tagged Sid4-mRFP, Cut11-GFP and Hht1-CFP respectively. Numbers under the frames represent the time in minutes. The stages of meiosis are indicated below. 0 min is the onset of MI. Scale bars equal 2 μ m. The lower panel shows only the red and blue channels (SPB and chromosomes signals) of the upper panel. (A-B) As in WT Cut11 signal in addition to be at the NPC also localises transiently to the meiotic SPB in MI (A) -10-30 min (B) 0-20 min and MII 60-80 min (B) 60 min. (A-B) Illustrates aberrant SPB separation in *bqt1* Δ cells (A) SPBs are sticky and separate poorly only after MII duplication occurred (60 min). The SPB that separated in MII seems inside the NE while the one that does not separate (white arrowhead) seems outside the NE (B) SPBs duplicate in MI (20 min) in MII (50-60 min) but do not separate at all. All the SPBs seem detached from the NE.

In conclusion, we have uncovered a strong correlation between detachment of the SPB from the NE and severity of SPB defects. If all defective SPBs are detached from the NE, we would propose that NE detachment is the proximal bouquet-controlled trigger for SPB dysfunction. To be certain about this relationship, we are developing better NE markers and intend to use a more sophisticated 3D analysis of SPB position with respect to the NE. The hypothesis that the SPB has to insert twice during meiosis could explain why MI and MII appear as two sequential events independent from each other in terms of SPB dysfunction. Nonetheless, the data presented here do not allow us to discriminate between cause and consequence. We still do not know whether Alp4 is not recruited properly to the SPB because of detachment from the NE, or if there is a yet unknown event that affects both SPB detachment and Alp4 recruitment, or whether Alp4 recruitment is a prerequisite for detachment.

6.4 Overview

In this chapter, we investigated the mechanisms involved in Alp4 recruitment to the SPB at the onset of meiosis. We determined that both robust Pcp1 function and NE insertion are important. It is tempting to hypothesise a model where the role of the bouquet would be to leave a mark at the SPB during prophase that is essential for NE insertion, and that the absence of this mark leads to insertion defects that prevent Pcp1 from recruiting Alp4. To test this model, it would be interesting to look in mutants defective for SPB insertion and investigate Alp4 localisation and determine if the meiotic phenotypes are similar to *bqt1 Δ* cells. It could also be informative to look in *bqt1 Δ* cells at the localisation of other proteins involved in SPB insertion. Alternatively, we could try to rescue bouquet phenotypes by promoting SPB insertion.

Chapter 7. Biochemical approach to assess modification of SPB components in meiosis

7.1 Aim

The principal objective throughout this work was to determine the difference(s) at the SPB level in presence or absence of bouquet function. Using live cell imaging, we presented in the previous chapters that *bqt1Δ* phenotypes encompass defects in the stabilisation/recruitment of Alp4 at the meiotic SPB. Knowing that SPB components are highly post-translationally modified (Keck et al., 2011) we sought to compare post-translational modification profiles of WT and *bqt1Δ* cells. We took a candidate approach, considering that Pcp1 is known to be involved in Alp4 recruitment and attempting to detect alterations in Pcp1 modification in the absence of the bouquet.

7.2 Meiosis synchronisation

Our analyses of SPB components by live cell imaging reveals how dynamic SPB component accumulation is throughout meiosis. Moreover, Alp4 seems to be differentially regulated during prophase compared with the rest of meiosis (chapter 5). Consequently we sought to perform two-dimensional protein gel electrophoresis (2D-PGE) experiments on extracts from synchronised meiotic cultures in order to compare samples from different stages; note that perfect synchrony is not necessary here, as modification changes in the presence versus absence of the bouquet can in principle be assessed quantitatively.

7.2.1 Strategy

Live cell imaging presented in previous chapters was performed on zygotic meiosis where in response to nitrogen starvation, the pheromone pathway is activated and cells of opposite mating type conjugate to form a diploid zygote that will then undergo meiosis and sporulation. Because of the conjugation step, zygotic meiosis has a very poor synchrony. However, 2D-PGE experiments were performed on extract from azygotic meiotic time courses (Material and Methods).

In order to estimate the level of synchrony, for each time point (every hour for 12 hours) two hundred cells were counted and the percentage of cells with one, two and more than two nuclei determined by DAPI staining (Figure 7.1A). For the last category, cells with more than two nuclei rather than cells with strictly four nuclei were counted to compensate for defective chromosome segregation in the *bqt1Δ* background. An example of the curves of number of nuclei *versus* time is shown Figure 7.1B. After nitrogen starvation (-N), cells are finishing the cell cycle as illustrated by the peak of cells with two nuclei at one hour. They then reach G1 and prepare for meiotic prophase. From one to six hours the proportion of cells with two nuclei (dividing cells) decreases while the proportion of cells with one nucleus (cells in G1 and meiotic prophase) reaches its maximum between five and six hours. After six hours, MI progression can be followed by the appearance

7. Biochemical approach to assess modification of SPB components in meiosis

of cells with two nuclei. However, MI is transient since cells progress through MII as illustrated by the rapid increase (starting at seven hours) of the 'more than two nuclei' curve. Although the synchrony is not perfect, only 15-20% as followed by the nuclear division at MI, after twelve hours almost 80% of cells with more than two nuclei are observed. The remaining 20% are cells with only one nucleus and represent a population that was arrested in G1 but failed to undergo meiosis. Another indicator of the level of synchrony of the experiment is the slopes of the curves representing the appearance of one or ≥ 2 nuclei; the steeper the slope, the better the synchrony. Under the conditions we use, we can attain moderate level of synchrony, but because for these experiments, the presence or absence of a modification is being scored rather than the timing of its appearance, perfect synchrony is not crucial.

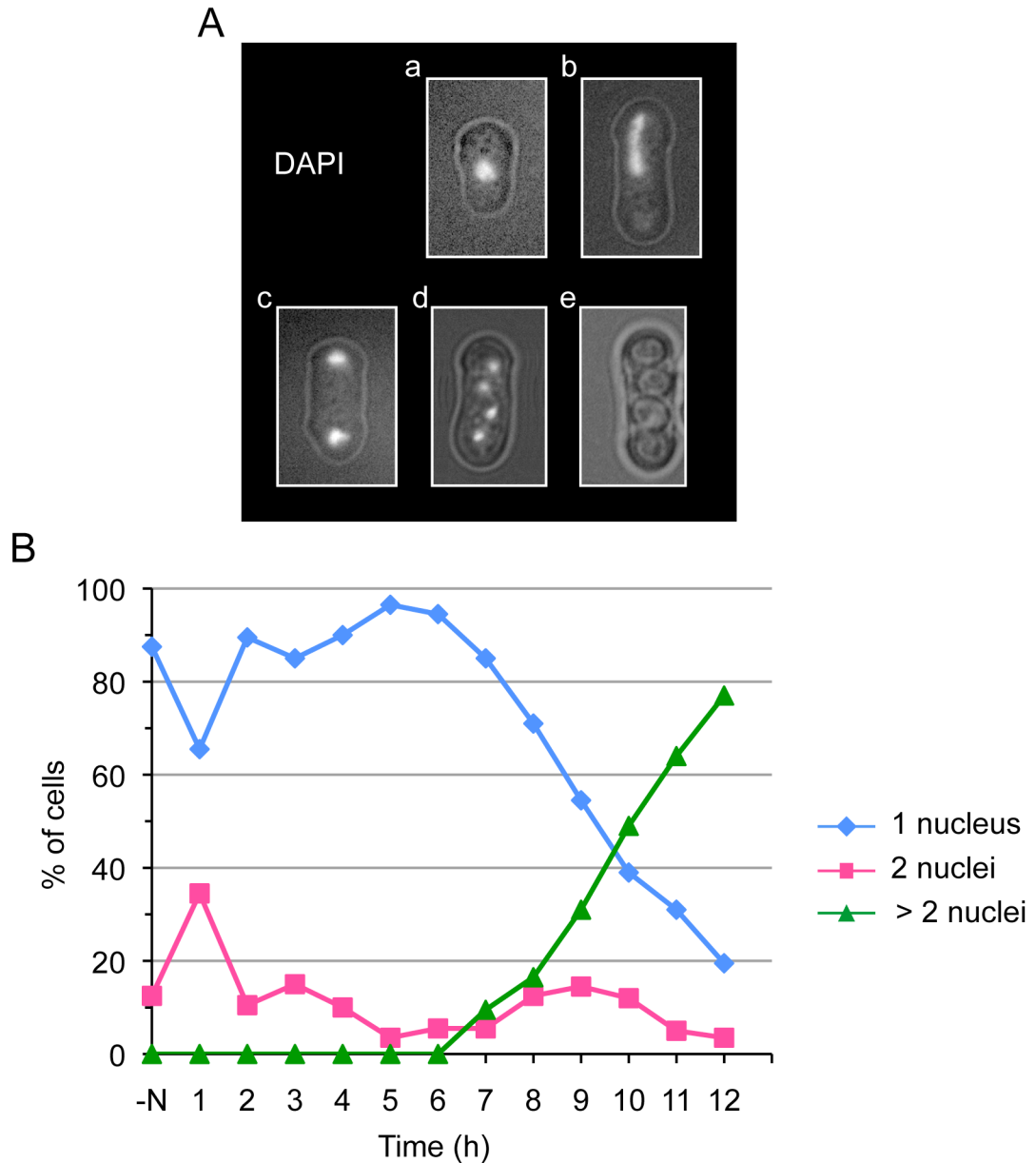


Figure 7.1 Example of meiosis synchronisation profile

(A) Images from diploid cells collected from synchronised meiotic culture, fixed and stained with DAPI. (a) Cell arrested in G1 with a round nucleus (b) Cell with a nucleus adopting the horsetail shape characteristic of meiotic prophase (c) Cell with two nuclei after MI (d) Cell with four nuclei after MII (e) Cell with asci with four spores. (B) Samples from cultures synchronised in meiosis were harvested every hours, fixed, stained with DAPI and the number of nuclei per cell counted for 200 cells. % of cells with one nucleus (blue curve), two nuclei (pink curve) and more than two nuclei (green curve) were plotted over time. (-N) represents the time when the cultures were switched to nitrogen starvation media to induce meiosis. The inclination of the one and more than two nuclei curves gives an indication of the level of synchrony of the experiment, the steeper the slope the better the synchrony.

7.2.2 Bouquet phenotypes are similar in azygotic and zygotc meiosis

Since all the results presented in preceding chapters were obtained from zygotc meiosis, before embarking on post-translational modification analyses from azygotc meiosis we needed to verify that *bqt1Δ* presents the same SPB and spindle defects in azygotc meiosis. Indeed, one might imagine that since the telomere bouquet is already formed in conjugating cells, passage through the conjugation step without the bouquet in *bqt1Δ* cells could somehow participate in the phenotypes observed in zygotc meioses. Therefore, live cells imaging on azygotc meiosis from *bqt1Δ^{-/-}* diploids where chromosomes (histone H3) and SPBs (Sid4) are endogenously tagged with mRFP and GFP, respectively, and microtubules are observed by ectopically expressed GFP-Atb2, was performed. Unlike zygotc meiosis, azygotc meiosis occurs in a rod-shaped cell instead of the classic banana-like shape. By consequence, spindles are shorter at both MI and MII (Figure 7.2). Nonetheless, the exact same phenotypes as in *bqt1Δ* zygotc meiosis were observed, formation of bipolar spindle at MI but sticky SPB at MII (Figure 7.3A), collapsing spindle and SPB that separates very poorly at MI and MII (Figure 7.3B), and cells with SPB separation failure and monopolar or no apparent spindle (Figure 7.3C). For each genotype, the number of spores per ascus was determined from a population of two hundred cells (Figure 7.4), and the distribution obtained is comparable between azygotc and zygotc meiosis. Therefore, biochemical experiments from azygotc meiosis were carried on.

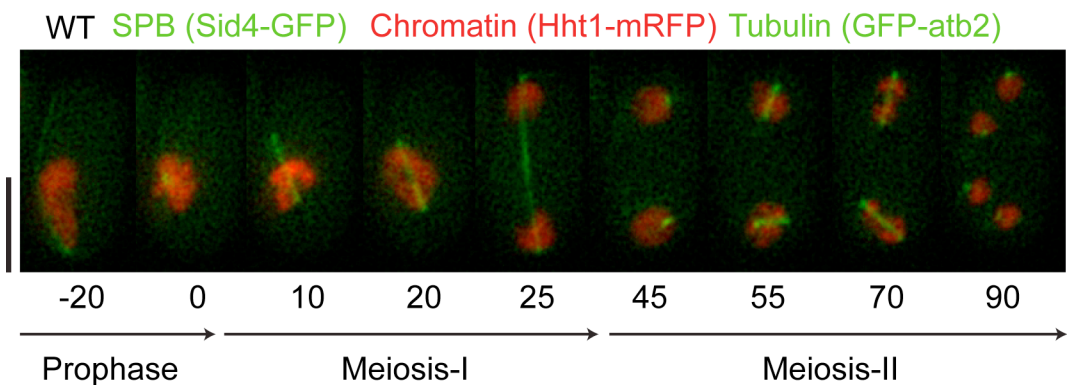


Figure 7.2 Example of WT azygotic meiosis

Series of frames from WT azygotic meiosis movie acquired by fluorescence microscopy in live cell. SPB and chromosomes were observed via endogenously tagged Sid4-GFP and Hht1-mRFP respectively and spindle via ectopically expressed GFP-Atb2. Numbers under the frames represent the time in minutes. The stages of meiosis are indicated below. 0 min is the onset of MI. Scale bar equals 5 μ m. Azygotic meiosis occurs in a rod-shaped cell instead of the classic banana-like shape of zygotc meiosis and then produces shorter spindle than the ones observed in zygotc meiosis at both MI (25 min) and MII (70 min).

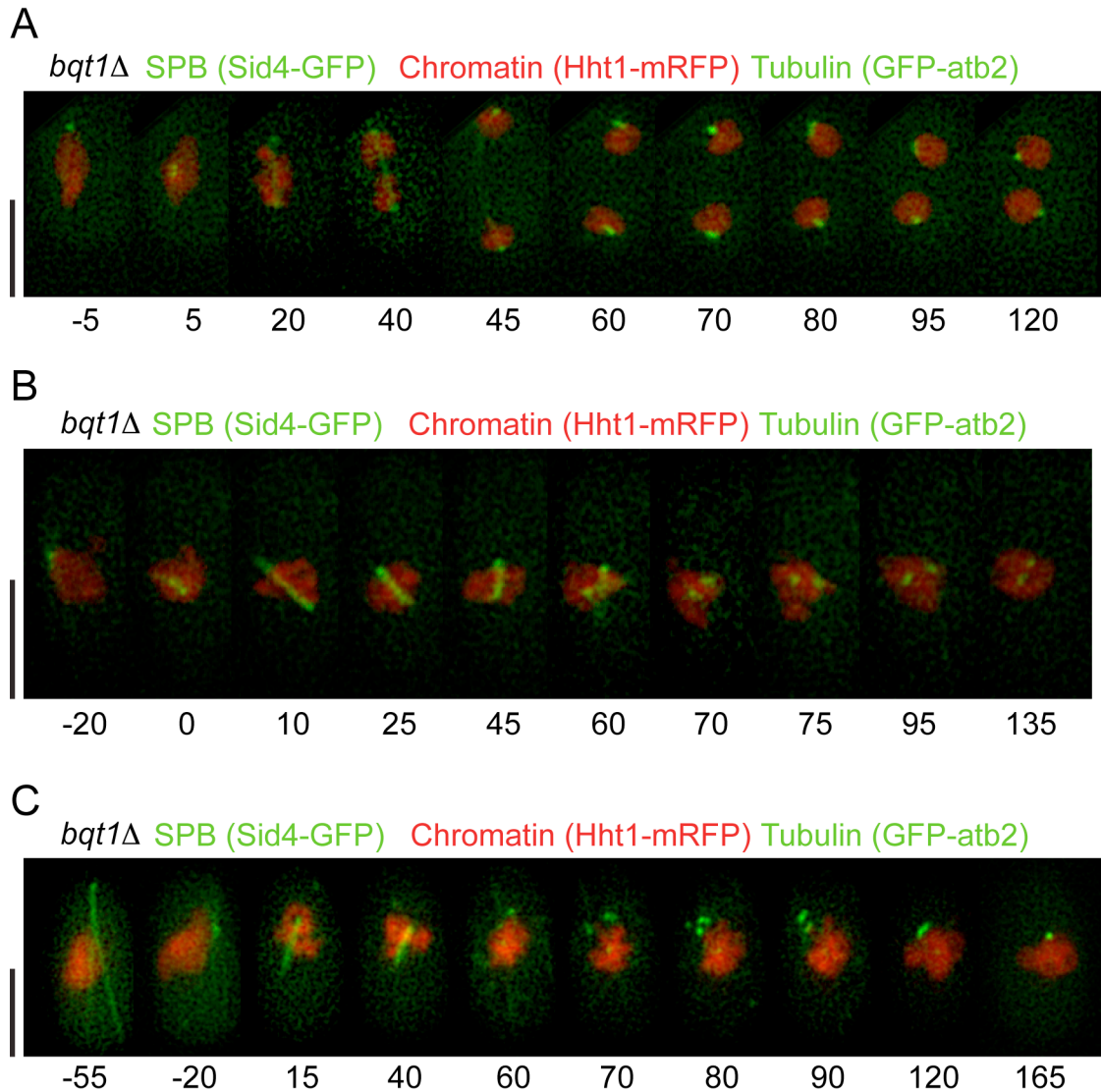


Figure 7.3 Aberrant spindle formation and SPB separation in bouquet deficient azygotic meiosis

Series of frames from *bqt1* Δ azygotic meiosis movies acquired by fluorescence microscopy in live cell. SPB and chromosomes were observed via endogenously tagged Sid4-GFP and Hht1-mRFP respectively and spindle via ectopically expressed GFP-Atb2. Numbers under the frames represent the time in minutes. The stages of meiosis are indicated below. 0 min is the onset of MI. Scale bars equal 5 μ m. (A) SPB separates and spindle forms properly in MI but not in MII instead SPB are sticky (60-80 min) and no spindle forms. (B) At MI SPB separates poorly and a weak collapsing spindle forms, at MII SPB does not separate and no spindle forms. (C) At MI SPB does not separate and a monopolar spindle forms (15-40 min) at MII SPB does not separate and no spindle forms.

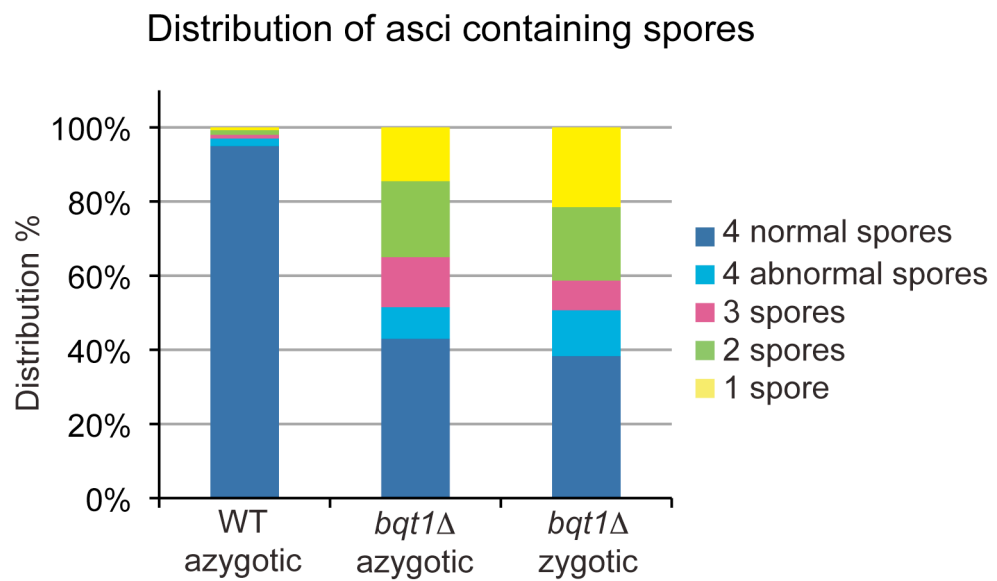


Figure 7.4 Comparison of zygotic and azygotic asci containing spores in bouquet deficient background.

Distribution of categories of asci. Asci from zygotic and azygotic meiosis were scored under light microscopy. 200 asci per genotype were counted in the experiment.

7.3 Pcp1 characterisation

The first candidate we wanted to characterise biochemically was Pcp1 since it has been implicated in Alp4 recruitment to the mitotic SPB (Fong et al., 2010) but also because our own experiments implicated Pcp1 in Alp4 recruitment to the meiotic SPB (Chapter 6).

The strategy was to perform western blot experiments in parallel with 2D-PGE, in order to have an overview of how Pcp1 progresses through meiosis and to analyse its post-translational modifications. Samples from synchronised azygotic meiotic cultures were collected in duplicate every hour over twelve hours. The first half of each sample after TCA extractions was run on a 4-12% Bis-Tris polyacrylamide gel while the second half was prepared for 2D-PGE using 2D-PGE extraction protocol and the 2D clean-up kit (discussed below). Some problems of protein degradation in meiotic extracts were encountered.

7.3.1 Improvement of protein extraction from meiotic samples

Experiments were performed on strains where *pcp1* is endogenously tagged with 13-Myc at its C-terminus (Pcp1-Myc). Pcp1 signal after western blot can thus either be detected with anti-Pcp1 antibody (kind gift from Takashi Toda's lab) or anti-Myc antibody (Figure 7.5A). At first, western blot analysis using anti-Pcp1 antibody revealed one band at the expected size for Pcp1-Myc (161 kDa) and a very low level of Pcp1 degradation were obtained (Figure 7.5B). However, in meiotic extracts, a second band at 100 kDa appeared; this band appeared both in TCA extracts and extracts for 2D-PGE (Figure 7.5B). Anti-Pcp1 antibody recognises the N-terminal of the protein (Fong et al., 2010), so if the 100 kDa band truly represents the N-terminus of Pcp1 and is not a non specific protein recognised by anti-Pcp1 antibody specifically in meiosis, the Pcp1 C-terminus at 61 kDa should also be detectable. Using anti-Myc antibody, both Pcp1 and a smaller band at 61 kDa, were indeed detected. Thus, a cleavage of Pcp1 that is not detectable in cycling cells was observed in meiotic extracts. Because the

appearance of this cleavage was reproducible, obtained after different protocols of protein extraction, and detectable in strains where Pcp1 is untagged (Figure 7.5B*) we initially believed that this cleavage could be a specific meiotic product with a biological significance. However, addition of PMSF and protease cocktail inhibitor to the initial wash buffer and protein extraction buffer resulted in the appearance of only a single band of 161 kDa, representing full-length Pcp1 (Figure 7.5C). We concluded that in meiosis Pcp1 is particularly sensitive to proteases, and that the cleavage first observed happens during protein extraction and not *in vivo*. Because the site of degradation was at least to some extent reproducible, the structure of Pcp1 must render this site accessible to proteases.

Having determined that in meiosis as in mitosis, Pcp1 exists *in vivo* only in its full size, western blot experiments as well as 2D-PGE were performed with untagged Pcp1 using samples from synchronised azygotic meiotic culture after protein extractions using the improved protocol.

7.3.2 Pcp1 profile analysed by western blot through meiosis

Samples from synchronised azygotic meiosis cultures were collected every hour for twelve hours, TCA extracted, run on 4-12% Bis-Tris polyacrylamide gel and immunoblotted with anti-Pcp1 antibody. Cdc2 was used as loading control. As many genes are differentially regulated throughout meiosis, it is not easy to find a gene product that is constant in quantity (Mata et al., 2002). Therefore, the loading control was used to compare the ratio of Pcp1 to loading control in WT versus *bqt1Δ* samples rather than Pcp1 signal over time. Obvious differences between WT and *bqt1Δ* profiles were not observed (Figure 7.6). However, this result was not surprising since as mentioned previously, the synchrony is not perfect (Figure 7.6) and the penetrance of *bqt1Δ* phenotypes only slightly over 50%. Therefore, aiming for better resolution the analysis was instead pursued by 2D-PGE.

7. Biochemical approach to assess modification of SPB components in meiosis

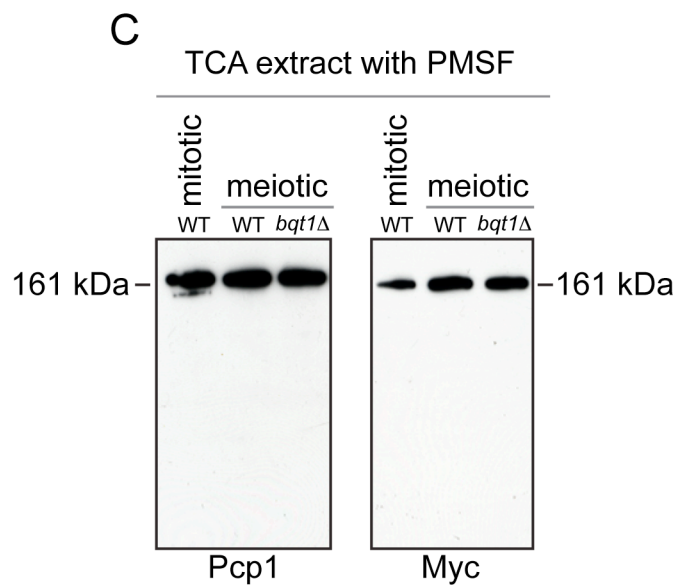
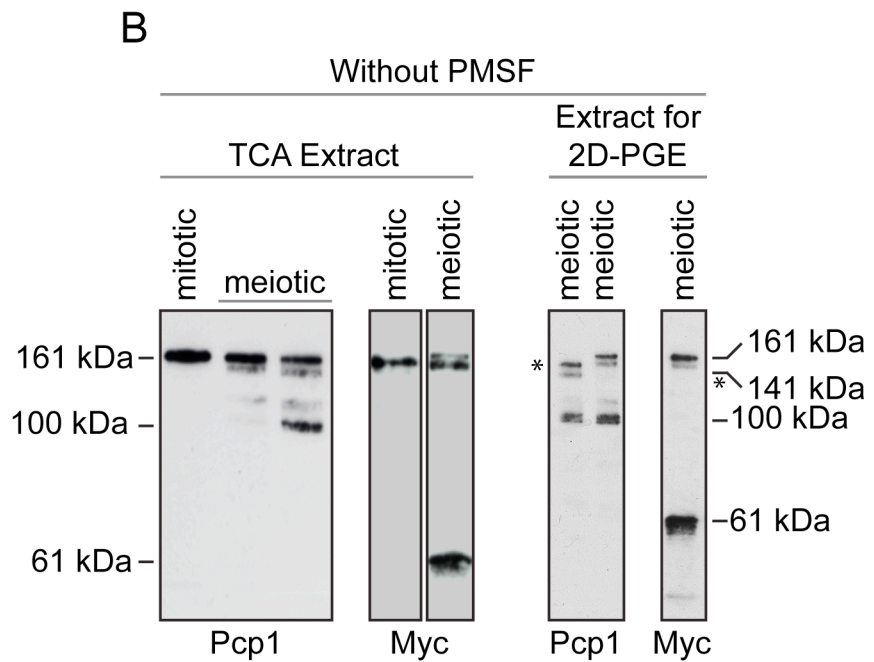
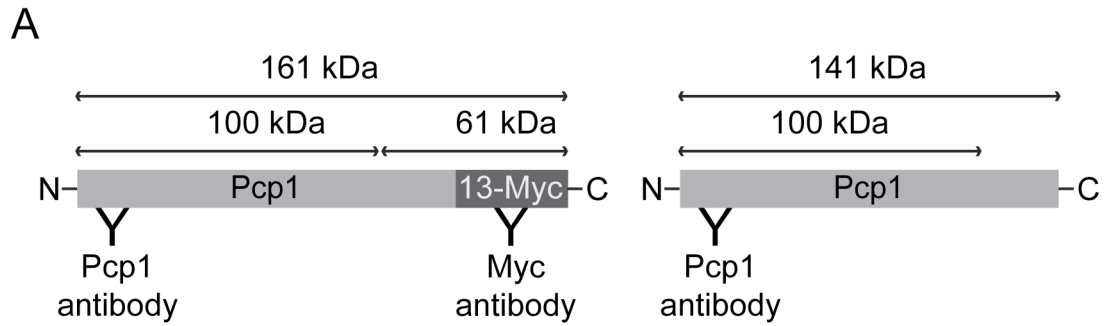


Figure 7.5 Pcp1 is hypersensitive to proteases in meiotic extract

(A) Schematic representation of Pcp1, Pcp1-Myc and of the Pcp1 fragments detected by western blot and illustrating the portions of the protein recognised by anti-Pcp1 and anti-Myc antibody respectively. N- and -C represent the N- and C- Terminal of the protein respectively.

(B-C) Experiments were performed with protein extract from strains where Pcp1 is endogenously tagged with 13-Myc (Pcp1-Myc) except from one sample (*) where Pcp1 is untagged note the difference in the running size (141 kDa vs 161 kDa). Samples from WT and *bqt1Δ* cycling diploid cells (mitotic) and WT and *bqt1Δ* azygotic synchronised meiosis (meiotic) after TCA extraction or extraction for 2D-PGE performed without or with PMSF were run on 4-12% bis-tris polyacrylamide gel and revealed with anti-Pcp1 antibody (Pcp1) or anti-Myc antibody (Myc).

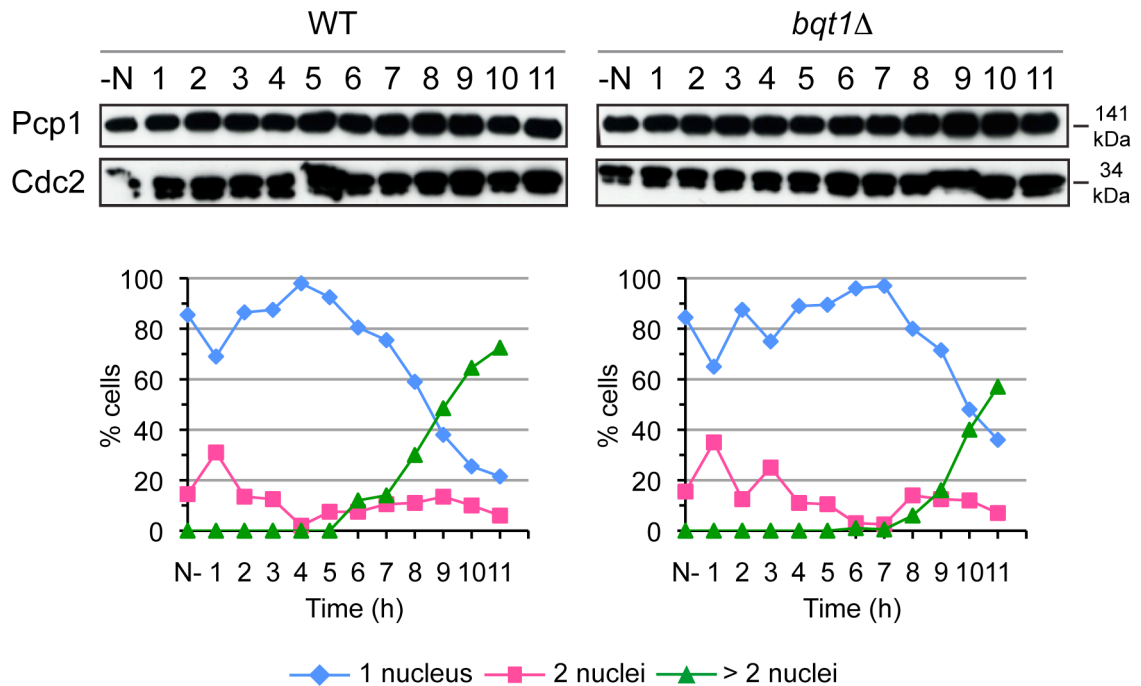


Figure 7.6 Pcp1 analysis by western blot does not reveal differences between WT and bouquet deficient cells

After TCA extraction samples from WT and *bqt1Δ* azygotic synchronised meiosis were run on 4-12% bis-tris polyacrylamide gel and revealed with anti-Pcp1 antibody (Ppc1) and anti-Cdc2 for the loading control (Cdc2). The relevant profiles of meiotic synchronisation are presented under the respective blot. (N) represents the time when the cultures were switched to nitrogen starvation media to induce meiosis. Lane number represents the time in hour after nitrogen starvation and refers to the time of the meiotic time course.

7.3.3 Pcp1 post-translational modifications analysed by 2D -PGE

2D-PGE were performed using samples from the same time course as for Pcp1 western blots (Figure 7.6). After 2D-PGE extraction and use of the 2D clean-up kit, 40 μ g of each sample was run for the first dimension on a 24 cm long gel strip of pH range 4 to 7 (the predicted pI of Pcp1 is 5) (Figure 7.7A). The second dimension was run on 4-12% Bis-Tris polyacrylamide gel and revealed with anti-Pcp1 antibody.

The profiles obtained for both WT and *bqt1 Δ* samples gave a Pcp1 specific signal at the expected size (141 kDa) and pI (5) (Figure 7.7B and 7.7C). However, the signal obtained did not focus well, despite the fact that we could obtain reliably good focusing with another fission yeast protein (data not shown). Poor focusing is often a problem encountered with proteins of high molecular weight. Nonetheless, the profiles obtained were to some extent reproducible in both WT and *bqt1 Δ* extracts (Figure 7.7B). Therefore, WT and *bqt1 Δ* profiles were compared at two time points of the same time course, six hours (prophase) and nine hours (meiotic division) (Figure 7.7C). On the one hand, no major differences between WT and *bqt1 Δ* profiles at any of the two time points chosen were observed. On the other hand, some differences between prophase (6 hours) and meiotic division (9 hours) were noticed. Such differences could indicate a distinct regulation of Pcp1 between prophase and meiotic division, which could be interesting. However, the quality of the patterns obtained does not give a good enough resolution to detect subtle differences. Assuming that most of the post-translational modifications are phosphorylation, treatment with phosphatase could improve the quality resolution of other modifications and may be able to highlight differences between WT and *bqt1 Δ* cells. However, thus far we cannot discern any obvious differences between WT and *bqt1 Δ* Pcp1 post-translational profiles.

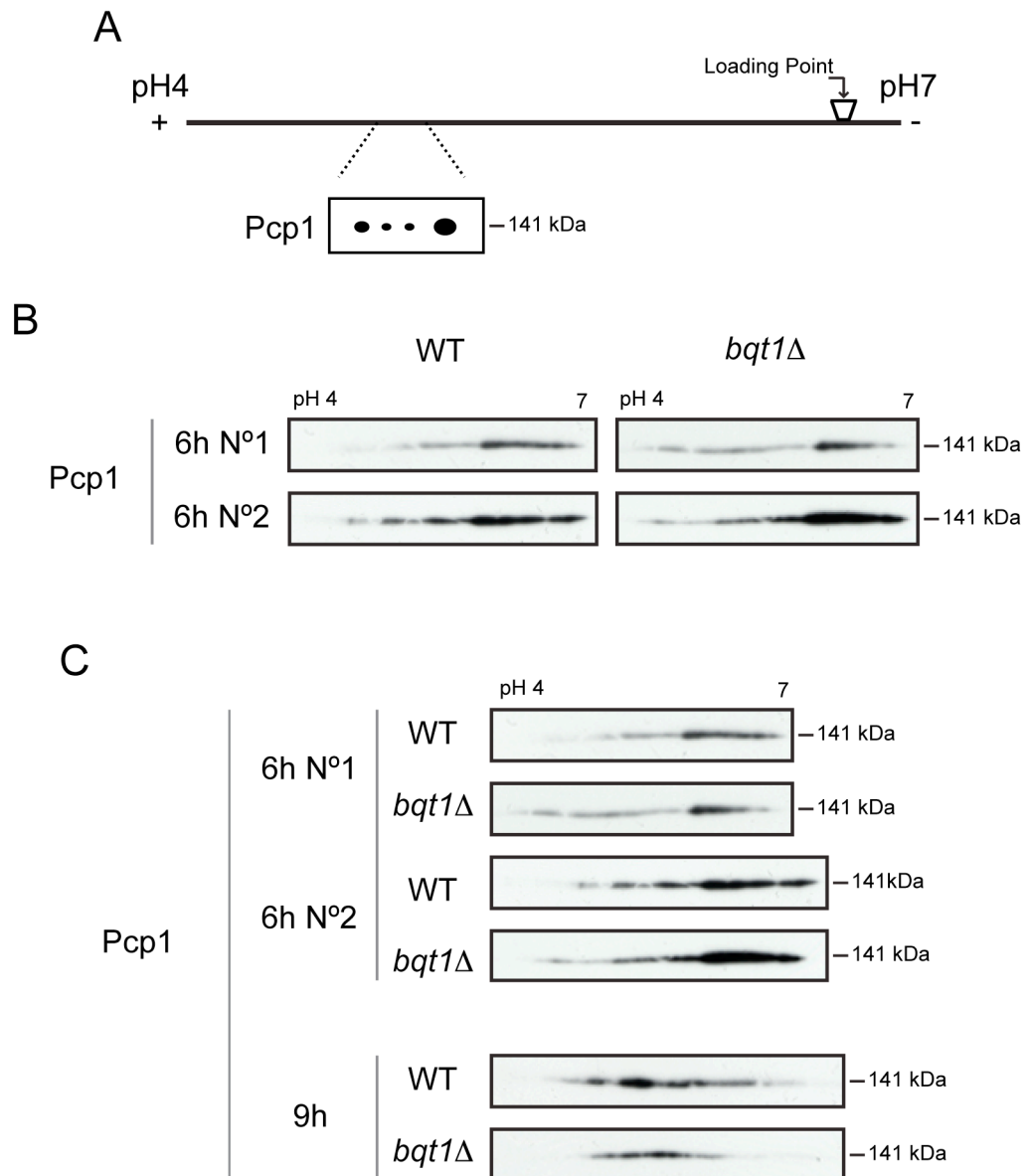


Figure 7.7 Pcp1 analysis by 2D-PGE does not reveal post-translational differences between WT and bouquet deficient cells

(A) Schematic representation of a 24 cm long gel strip of pH range 4 to 7 used for 2D-PGE. The (+) side is the acidic side (pH4) where the protein negatively charged will focus while the (-) side is the basic side (pH7) where the protein positively charged will focus. Protein extract is loaded on the strip for the first dimension the further away (loading point) from the predicted pI of the protein of interest (Pcp1 predicted pI = 5). The approximate area of the strip where Pcp1 focuses and migrates after the second dimension is also represented on a schematic view.

(B-C) After 2D-PGE extraction and 2D clean-up kit 40 μ g of samples from WT and *bqt1Δ* azygotic synchronised meiosis (6 and 9 hours) were run for the first dimension on 24 cm long strip of pH range 4 to 7, for the second dimension on 4-12% bis-tris polyacrylamide gel, and revealed with anti-Pcp1 antibody (Pcp1).

7.4 Alp4 characterisation

The second candidate we wanted to analyse by western blot and 2D-PGE is Alp4 since we found that in the absence of the bouquet, Alp4 localises unevenly between duplicated SPBs and that this defect correlates well with the spindle defects characterised in *bqt1Δ* cells (Chapter 3).

7.4.1 Alp4 profile analysed by western blot throughout meiosis

Strains in which Alp4 is endogenously tagged with 3-HA (Alp4-HA) were used, and the experiments performed as described for Pcp1. Samples from synchronised azygotic meiosis culture were collected every hour for twelve hours (Figure 7.8), TCA extracted, run on 4-12% Bis-Tris polyacrylamide gels and immunoblotted with anti-HA antibody and Cdc2 as loading control. Examination of the first gel (gel N°1) revealed a diminution of Alp4-HA signal between five and seven hours in *bqt1Δ* while the signal for the loading control was constant (Figure 7.8). The experiment was thus repeated with the same samples (gel N°2). The second gel does not show such diminution of Alp4-HA signal, but on the contrary reduction of the signal of the loading control at six and seven hours in the WT and at five and six hours in *bqt1Δ* (Figure 7.8). As the decreases observed on both gels are not similar, we believe that they stemmed from technical issues in the transfer step. Thus, as for Pcp1, no major differences in the Alp4 migration patterns exist between WT and *bqt1Δ*. In order to reach better resolution, post-translational modifications were analysed by 2D -PGE.

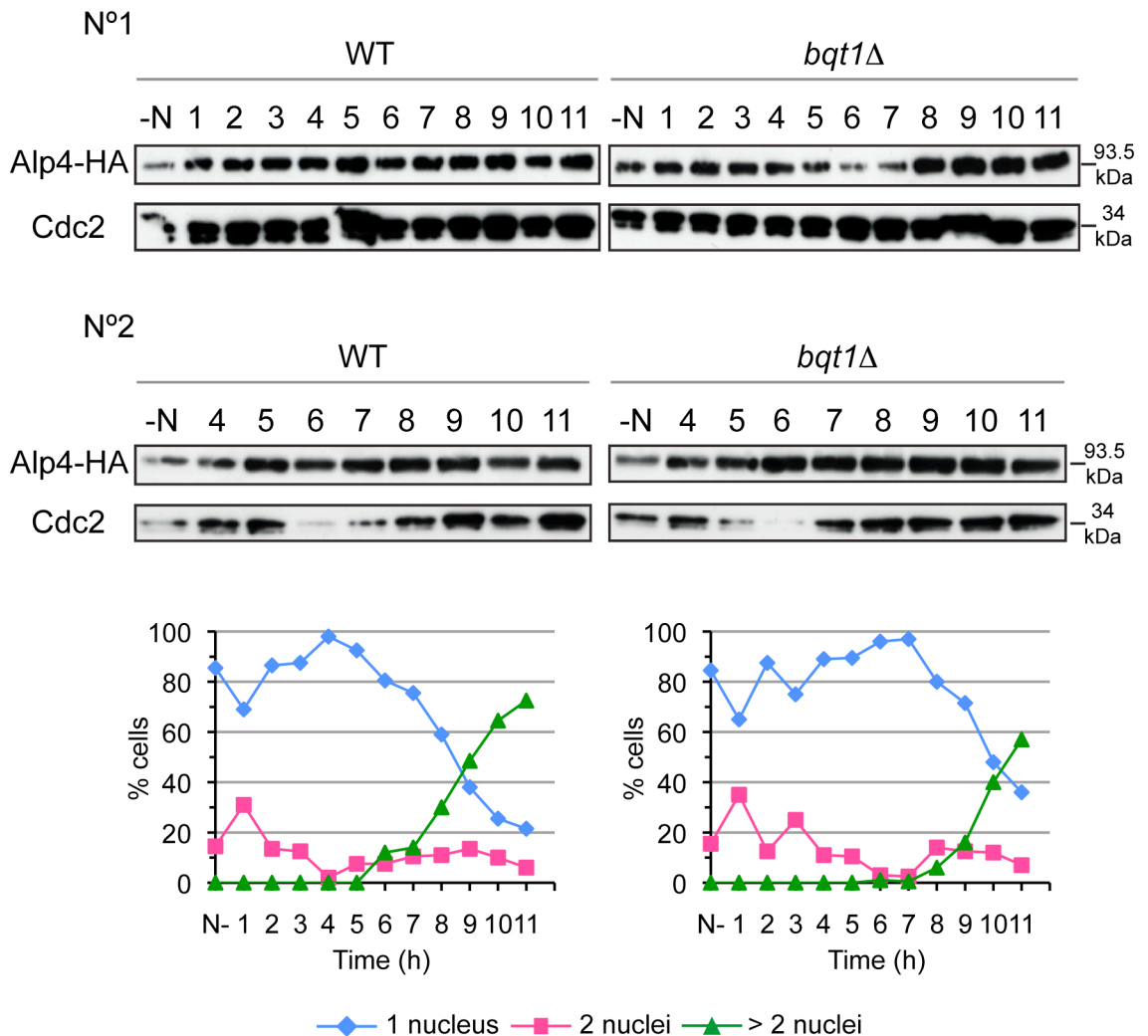


Figure 7.8 Alp4 analysis by western blot does not reveal differences between WT and bouquet deficient cells

After TCA extraction samples from WT and *bqt1Δ* azygotic synchronised meiosis where Alp4 is endogenously tagged with 3HA (Alp4-HA) were run on 4-12% bis-tris polyacrylamide gel and revealed with anti-HA antibody (Alp4-HA) and anti-Cdc2 for the loading control (Cdc2). The relevant profiles of meiotic synchronisation are presented under the respective blot. N°1 and N°2 are two independent run performed under the same conditions of the same samples. N represents the time when the cultures were switched to nitrogen starvation media to induce meiosis. Lane number represents the time in hour after nitrogen starvation and refers to the time of the meiotic time course.

7.4.2 Alp4 post-translational modifications analysed by 2D -PGE

Alp4-HA runs at a lower molecular weight (93.5 kDa) than Pcp1 (161 kDa) but nonetheless, all attempts of Alp4 analysis by 2D-PGE failed to detect Alp4-HA signal. I will present in this section the changes of parameters carried out. A summary can be found Table 7.1.

Sample for Alp4 2D-PGE were obtained from WT synchronised azygotic meiosis culture (Figure 7.8). Protein extraction was performed in presence of PMSF following the protocol for 2D-PGE extractions. Samples were cleaned with 2D clean-up kit before the first dimension unless stated otherwise. Since the predicted pI for Alp4 is 5, the first Alp4 2D-PGE (Table 7.1_1) was performed on a 24 cm long gel strip of pH rang 4 to 7. After the second dimension, no signal at the expected size (93.5 kDa) was detected. We assumed the protein concentration was too low to permit Alp4 detection. The second Alp4 2D-PGE (Table 7.1_2) was run under the exact same conditions as the first but with twice as much protein. Again, after the second dimension no signal at the expected size was detected. In combination with our ability to detect Alp4 by 1D Westerns, we concluded that protein concentration is probably not the issue. The experiment was repeated with the same extract but using strips with a broader pH range (24 cm strip of pH 3 to 11) in order to obtain a better overview and improve protein distribution in the first dimension (Table 7.1_3). Yet, after the second dimension no signal at the expected size (93.5 kDa) was detected. However, a rather focused signal migrating between 50 and 75kDa was detected (Figure 7.9A). To determine if the problem was specific to Alp4-HA detection or a more general issue, the same blot was immuno-blotted with anti-Pcp1 antibody. A very strong signal at the expected size and pI for Pcp1 was observed, and no Pcp1 signals indicative of protein degradation were detected. Hence, the inability to detect Alp4 by 2D-PGE is not due to protein degradation or incorrect pH range and appears to be specific to Alp4.

Since the problem seemed specific to Alp4-HA detection, we wondered whether strong protein denaturation, which could abolish recognition of the HA epitope by the anti-HA antibody as occurs during 2D-PGE protein extractions and treatment with the 2D clean-up kit and rehydration buffer. Therefore, extracts resuspended into rehydration buffer after 2D clean-up kit (Table 7.1_4) or directly after protein extraction (Table 7.1_5) were run on a 4-12% Bis-Tris polyacrylamide gel and Alp4-HA detected with anti-HA antibody. We observed that on a one-dimensional gel, Alp4-HA is detectable by anti-HA antibody whether protein extractions are performed using TCA extraction or the 2D-PGE extraction protocol, and whether or not extracts are cleaned with the 2D clean-up kit and resuspended in rehydration buffer (Figure 7.9B). Hence, neither strong denaturation nor the cleaning step appear as drawbacks for Alp4-HA detection. However, we noticed that the signal is stronger before than after the cleaning step. Thus, a fourth Alp4 2D-PGE was performed on a 24 cm strip of pH range 3 to 11NL using protein extract that was not subjected to the 2D clean-up kit, but rather was loaded in rehydration buffer directly after protein extraction for the first dimension (Table 7.1_6). Nonetheless, we again failed to detect signals at the expected size (93.5 kDa) although we did detect signal between 50 and 75 kDa (Figure 7.9A). Thus, the cleaning step appears not to be the impediment to detection of full-length Alp4.

The signal detected between 50 and 75 kDa is reproducible under the different running conditions tested for Alp4-HA 2D-PGE. In addition, it cannot be detected when using anti-Pcp1 antibody instead of anti-HA antibody therefore, it seems of interest to clarify its origin. Performing a 2D-PGE with a different HA tagged protein than Alp4-HA could allow us to determine whether it is a background band detected by the anti-HA antibody or if it is somehow specific of Alp4-HA that runs anomalously with respect to its size. If it was specific of Alp4-HA we could envisage to perform 2D-PGE experiments from both WT and *bqt1Δ* cells and compare the profiles. Alternatively, we could try to perform Alp4 2D-PGE using a different tag to detect Alp4.

Protein extract resuspended in sample preparation solution for 2D-PGE			
2D clean-up kit resuspended into rehydration buffer		+ Protein buffer	+ rehydration buffer
1st Dimension 4-7 stripe with 80µg Protein extract	1st Dimension 3-11NL stripe with 100 µg protein extract		1st Dimension 3-11NL stripe with 100 µg protein extract
2nd Dimension 4-12% bis-tris anti-HA antibody	2nd Dimension 4-12% bis-tris anti-HA antibody	western blot 4-12% bis-tris anti-HA antibody	2nd Dimension 4-12% bis-tris anti-HA antibody
No Alp4 signal	Unspecific Signal Fig 7.9A anti-Pcp1 antibody Good Pcp1 signal	Fig 7.9B	Unspecific Signal Fig 7.9A
2	3	4	5
- Concentration	- pH range - Degradation - Alp4 specificity	- Effect of strong protein denaturation on HA epitope recognition by anti-HA antibody - 2D clean-up kit	- 2D clean-up kit
1			6

Table 7.1 Summary of the experimental changes to try to detect Alp4 by 2D-PGE

From left to right each column numbered from 1 to 6 represent an experiment. From top to bottom experimental condition details are given for protein extraction, 2D-PGE first dimension and protein concentration, 2D-PGE second dimension or alternatively 1D-PGE and signal detection. The outcome of each individual experiment is highlighted in red and the parameter tested in the experiment in green.

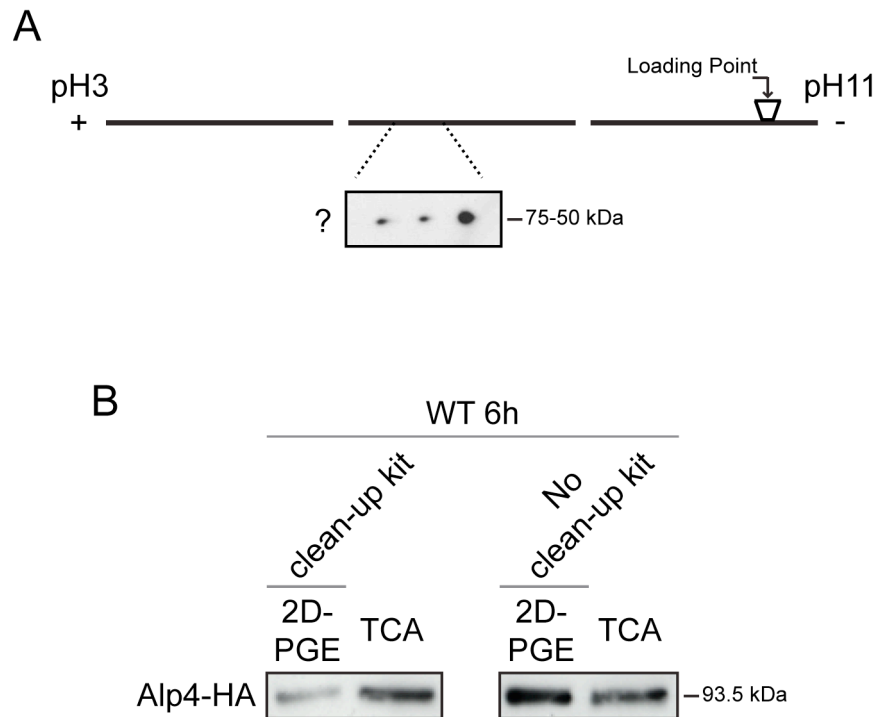


Figure 7.9 Alp4-HA can be detected after 1D-PGE but not after 2D-PGE

(A) Schematic representation of a 24 cm long gel strip of pH range 3 to 11NL used for 2D-PGE. The (+) side is the acidic side (pH3) where the protein negatively charged will focus while the (-) side is the basic side (pH11) where the protein positively charged will focus. Protein extract is loaded on the strip for the first dimension the further away (loading point) from the predicted pI of the protein of interest (Alp4 predicted pI = 5.5). Profile after the second dimension of the unspecific signal (Table 7.1_3 and 7.1_6) as well as the approximate size and area of the strip where the signal focuses are also indicated. The specific profile shown was obtained as follow: after 2D-PGE extraction 100 µg of samples from WT azygotic synchronised meiosis (6 hours) where Alp4 is endogenously tagged with 3HA was run into rehydration buffer for the first dimension on 24 cm long strip of pH range 3 to 11NL, for the second dimension on 4-12% bis-tris polyacrylamide gel, and revealed with anti-HA antibody. (?) Represents the unspecific signal that does not run at Alp4-HA predicted size (93.5 kDa) but between (50 and 75 kDa) (Table 7.1_6).

(B) Samples from WT azygotic synchronised meiosis (6 hours) where Alp4 is endogenously tagged with 3HA (Alp4-HA) were prepared by TCA extraction or extraction for 2D-PGE followed by 2D clean-up kit or not and run on 4-12% bis-tris polyacrylamide gel and revealed with anti-HA antibody (Alp4-HA) (Table 7.1_4 and 7.1_5).

7.5 Overview

In this chapter, we aimed to investigate Pcp1 and Alp4 post-translational profiles to determine whether there were any differences between WT and *bqt1Δ* cells. Unfortunately, we have not been able to generate data providing strong evidence for one or the other, as in addition to the issues of imperfect synchrony and weak penetrance of *bqt1Δ* phenotypes, technical problems were encountered. Indeed, Pcp1 post-translational modification profiles obtained by 2D-PGE were not of high enough resolution to allow full use of the sensitivity of the technique and did not reveal strong differences between WT and *bqt1Δ* cells. Alp4 signal could not be detected by 2D-PGE even after multiple trials. Therefore, we concluded that 2D-PGE is not the best approach to give a clear answer to the question raised. We are next envisaging the pursuit of the analysis by protein purification and mass spectrometry techniques.

Chapter 8. Discussion and future perspectives

The major goal of this study was to determine and characterise the differences at the SPB level in presence or absence of bouquet function, in order to understand how the telomere bouquet is controlling the meiotic spindle. Using quantitative live analysis, we found that SPB duplication and the dynamics of the SPB cycle are not substantially altered in the absence of the bouquet. Rather, physical separation of the duplicated SPBs is strongly affected. We have determined that the SPB separation defects as well as the spindle defects observed in bouquet deficient cells correlate with uneven localisation of the γ -TuC to the duplicated SPBs. Therefore, we postulate that the telomere bouquet controls γ -TuC localisation to the meiotic SPB. In addition, we have found a correlation between the detachment of the SPB from the NE and the severity of the SPB defects and are aiming to investigate further the relationship between NE detachment and the localisation of the γ -TuC to the SPB. We hypothesise a model in which the telomere bouquet leaves a “mark” on the SPB that persists through MII and acts as a prerequisite to anchor the SPB to the NE at MI and MII onset, thereby promoting proper SPB insertion and proper γ -TuC localisation to the SPB. Considering the role of Pcp1 in SPB insertion (Fong et al., 2010) and recruitment of the γ -TuC to the mitotic (Fong et al., 2010) and possibly meiotic SPB (Chapter 6), we first envisage that the “mark” left by the bouquet at the SPB could be a post-translational modification of Pcp1 itself. However, our biochemical analyses performed so far do not provide evidences strong enough to argue against or for such hypothesis (Chapter 7). Naturally, the bouquet could also be modifying any another protein involved directly or indirectly in SPB insertion and/or γ -TuC recruitment to the SPB. Alternatively, the “mark” left by the bouquet could also be the recruitment of specific factors required for efficient progression of the downstream events of meiosis.

8.1 Implications of the similarities of the SPB cycle in presence and absence of the bouquet

Our analysis represents the first quantitation of SPB component levels throughout meiosis in fission yeast and highlights the dynamics of the SPB maturation cycle. We can directly follow SPB duplication and progression, allowing us to make several surprising observations. First, comparison of Pcp1 and Sid4 accumulation profiles, allowed us to determine that while the general trend is similar, the fine-tuning of the SPB maturation is performed in a component specific manner. On the one hand, Sid4 is recruited to the SPB earlier than Pcp1 during prophase and on the other hand, after SPB duplication Pcp1 appears as two distinguishable dots before Sid4 signal does (Chapter 3, Figure 3.13 and comparing Figure 3.9A with 3.15). Second, we noticed that while the SPB duplicates twice during the course of meiosis, the quantity of SPB components doubles between prophase and MI but roughly triples between MI and MII (Chapter 3, Figure 3.9). This surprising observation could be an illustration of the different roles of the MI SPBs, which nucleate the spindle in charge of homologue separation, and the MII SPBs, which nucleate the spindle in charge of the separation of the sisters. The most unexpected observation was that there were no major differences between WT and bouquet deficient cell Pcp1 (or Sid4) profiles. Therefore, the SPB cycle progresses independently of SPB separation and chromosome segregation defects. This raises the question of the role of the bouquet in checkpoint activation. Similarly to mitosis where the spindle assembly checkpoint (SAC) ensures that the cell does not proceed through anaphase with unattached chromosomes (Musacchio and Hardwick, 2002), in fission yeast meiosis the SAC can also be activated and delay anaphase-I and anaphase-II onset (Yamamoto et al., 2008). Strains defective in recombination or sister chromatid cohesion are able to trigger the checkpoint and significantly delay meiotic progression (Yamamoto et al., 2008). Therefore, it could be of interest to further characterise this aspect of the bouquet by looking more directly at the metaphase to anaphase transition and

also to assess the genetic interactions between the components of the SAC such as Mad2 (Musacchio and Hardwick, 2002).

8.2 Implications of SPB separation defects

Using live cell imaging, we established a strong correlation between the extent of SPB separation defects and uneven localisation of the γ -TuC to the SPBs. Nevertheless, it is possible to imagine that more than one factor participates in the SPB separation defects observed. Because SPB separation and spindle formation involve severing of the inter-SPB bridge, it could be informative to monitor the behaviour of components of the half-bridge such as Cdc31 and Sfi1 (Paoletti et al., 2003, Kilmartin, 2003).

In addition, similarly to the centrosome where the mother centriole is mature before the daughter centriole (Piel et al., 2000) the yeast SPBs also present some asymmetry in maturation between old and new SPBs (Grallert et al., 2004). Because we are observing asymmetrical localisation of the γ -TuC between the duplicated SPBs, we are wondering if this uneven localisation could be attributed to the maturation status of the SPB. It is tempting to assume that the old SPB would be the one with the highest capacity to recruit the γ -TuC. Several reports in the literature where the old SPB is more functional than the new SPB support this hypothesis (Fong et al., 2010, Tallada et al., 2009, West et al., 1998). Moreover, we have observed that SPB separation takes place after MII duplication has occurred in 63% of the cells that do have a defective meiosis. Moreover, after the second duplication at MII, one could consider that there are 3 generations of SPBs (at MII the mother from MI is becoming a grandmother while the daughter is becoming a mother, and each duplicates to give rise to two new daughters). Therefore, one could argue that the presence of more “mature” SPBs increases the chances of faithful γ -TuC localisation and SPB separation. To discriminate between old and new SPB in cycling cells, the slow folding fluorescent proteins

(Grallert et al., 2004) or factors known to localise asymmetrically such as the Cdc7 kinase involved in the septation initiation network (Sohrmann et al., 1998) are commonly used. However, there is to our knowledge no report of components localising asymmetrically between old and new SPB in fission yeast meiosis. Moreover, the slow folding fluorescent protein system requires a prolonged phase where the cells are arrested in order to provide enough time for the protein to fold and become visible by fluorescence microscopy. We would thus need to use a system that would allow arrest of the cells prior to MI duplication as well as efficient release.

8.3 How can the bouquet influence γ -TuC localisation?

Simultaneous analysis of the NE and the SPB allowed us to propose that the uneven localisation of the γ -TuC to the SPB in the absence of the bouquet is a direct consequence of the detachment defect of the SPB from the NE. To further test this model, we envisage repeating the experiment with another NE marker, Ish1 (Taricani et al., 2002), that seems to give a better resolution than Cut11 and also to develop EM analysis. Furthermore, in mitosis, SPB insertion in the NE requires both a physical step mediated by Cut11 and an activation step mediated by Cut12 and Plo1, where the recruitment of Plo1 to the SPB is key (Tallada et al., 2009). We know from previous studies that neither Cut11 ((Tomita and Cooper, 2007) and this study) nor Cut12 (Tomita and Cooper, 2007) are mis-localised in bouquet deficient meiosis therefore, it could be of interest to carefully monitor Plo1 localisation throughout meiosis. Alternatively the absence of the bouquet could alter Plo1 activity rather than its localisation. It would not be surprising if Plo1 was also implicated in meiosis progression since in addition to its role in the G2/M transition, Polo kinases have been reported to play important roles in meiosis in various organisms (Lee and Amon, 2003, Ishiguro et al., 2010)

Alternatively, the bouquet could directly influence γ -TuC localisation to the SPB by recruiting and/or modifying a factor required for γ -TuC recruitment or the γ -TuC itself. The candidate approach we took to compare by 2D-PGE analyses post-

translational profiles of SPB components of WT and *bqt1Δ* cells failed to reveal any clear differences. Protein purification followed by mass spectrometry could be a more unbiased way to address these questions and provide valuable insight into the role of the bouquet.

In mitotic interphase, the γ -TuC is recruited to the nuclear periphery beneath the SPB in the nucleoplasm by a yet undefined mechanism (Ding et al., 1997, Fong et al., 2010). It is assumed that the close proximity between the nucleoplasmic pool of γ -TuC and the SPB assists the recruitment of the γ -TuC by Pcp1 to the mitotic SPB upon insertion (Fong et al., 2010). In meiosis, studies have shown that like in mitosis, the γ -TuC is differentially recruited to the cytoplasmic and the nucleoplasmic side of the SPB (Tanaka et al., 2005). Therefore, considering that in bouquet deficient cells, localisation of the γ -TuC to the SPB is defective from the onset of MI and assuming that a nucleoplasmic pool of γ -TuC also exists beneath the SPB during meiotic prophase, it is tempting to speculate that the bouquet plays a role in maintaining the nucleoplasmic pool of the γ -TuC in the vicinity of the SPB to facilitate its recruitment to the meiotic SPB. Moreover, given that like the telomeres in meiosis, the centromeres are clustered at the SPB during vegetative growth (Funabiki et al., 1993), it is also tempting to extrapolate and infer a similar role for mitotic centromeres. Unfortunately, the mechanisms by which the centromeres are clustered at the SPB are not fully understood. The lack of centromere mutant that specifically disrupts the centromere/SPB contact without affecting centromere architecture prevents us from unambiguously addressing the question of the role of the centromere clustering. Nevertheless, this provocative idea that chromatin plays a role in spindle formation is supported by several reports in the literature showing that in the absence of centrosomes, spindle microtubules are organised from within the chromatin by a system that requires the presence of the γ -TuC (Mahoney et al., 2006, Heald et al., 1996). It also raises the question of what aspects of the telomere bouquet are necessary to control the meiotic spindle.

8.4 What is/are the feature(s) of the telomere bouquet necessary to control the meiotic spindle?

Understanding the aspects of the telomere bouquet necessary to control the meiotic spindle is key to uncover the molecular requirements governing bouquet functions and the potential “mark” left by the bouquet.

Tomita and Cooper have previously determined that the bouquet controls the meiotic spindle independently of its function in recombination and nuclear movements, since mutants where recombination or the movements are impaired do not confer any SPB or spindle defects. They also showed that spindle formation requires both the telomeric proteins and the telomeric chromatin, since a mutant allele of Taz1 that fails to bind DNA but yet locates to the SPB confers defective spindle formation.

If association with telomeric chromatin (and not just telomere proteins) is required for SPB separation, is the clustering of all the telomeres needed for proficient meiotic spindle formation or could a single telomere assume bouquet function? To answer to these questions, we took advantage of a unique property of fission yeast, its ability to survive complete telomere loss by circularisation of its three chromosomes by intrachromosomal fusion (Figure 8.1). Such ‘circular strains’ completely devoid of telomeres have a defective meiosis in part because of the lack of bouquet formation (Naito et al., 1998) (Figure 8.2A). We added a single internal telomere tract to one of the chromosomes of a circular strain completely devoid of telomeres (Figure 8.1) and asked whether this internal telomere is enough to ensure efficient spindle formation. Initial analyses conducted by Tomita.K in the laboratory and further live imaging that I performed revealed that the presence of only one internal telomere is enough to confer to a strain otherwise devoid of telomeres efficient spindle formation and SPB separation (Figure 8.2B). Therefore, clustering of the telomeres *per se* is not required for bouquet function regarding spindle formation. This very interesting observation

automatically raises the question: What is/are the properties of this single internal telomere tract that is/are required for efficient spindle formation?

Next we aim to determine which feature(s) of the telomeric chromatin is/are required. Is it specific to telomeres or is it the heterochromatic nature of telomeres, or could any chromatin-SPB association assure the same function? One way to address these questions would be to artificially tether another heterochromatic or euchromatic region of the chromosomes in a bouquet deficient background and ask whether it can play the role of the bouquet. Alternatively, another fission yeast specific tool, a mutant strain in which both centromeres and telomeres are clustered at the SPB during meiotic prophase, could be used (Chikashige et al., 2004). Analyses of the progression of meiosis in such strains in a bouquet deficient background could also determine if telomeres and centromeres are interchangeable for controlling faithful meiotic spindle formation. Furthermore, interesting observations in line with the idea of a function for chromatin in general in spindle formation came from the analysis of bouquet deficient cells that do have a functional spindle. We had been wondering why only 60% of the cells observed present defects in spindle formation. Is there a compensatory mechanism that is taking over when the bouquet is not present? We have often observed that while the SPB/telomere contact is abolished in the 40% of bouquet deficient strains that construct a functional spindle, "accidental" contacts between SPB and chromatin seem to occur. Preliminary data from Fennell.A in the laboratory are indeed showing a strong correlation between chromatin/SPB contacts during meiotic prophase and spindle recovery. He is currently investigating the nature of the chromatin seen associated with the SPB in the bouquet deficient background.

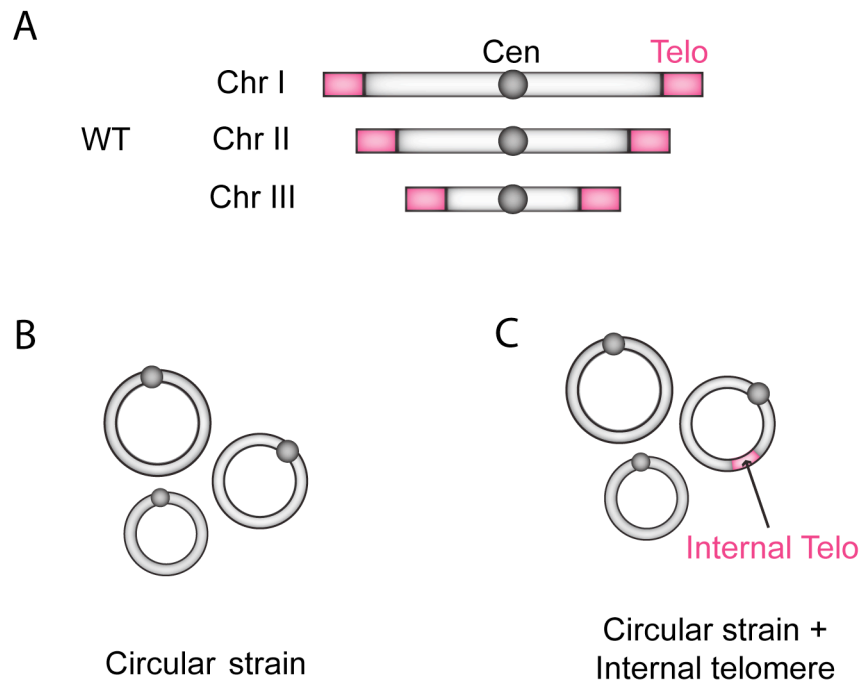


Figure 8.1 Schematic representation of WT, circular and circular with internal telomere strains

(A) Schematic representation of a WT strain with three linear chromosomes with the telomeres depicted in pink at the end of the chromosomes. (B) Circular strain devoid of telomeres, where after complete telomeres loss each individual chromosome has intrachromosomally fused. (C) Circular strain devoid of telomeres where we have artificially inserted an internal telomere tract depicted in pink in one of the chromosomes.

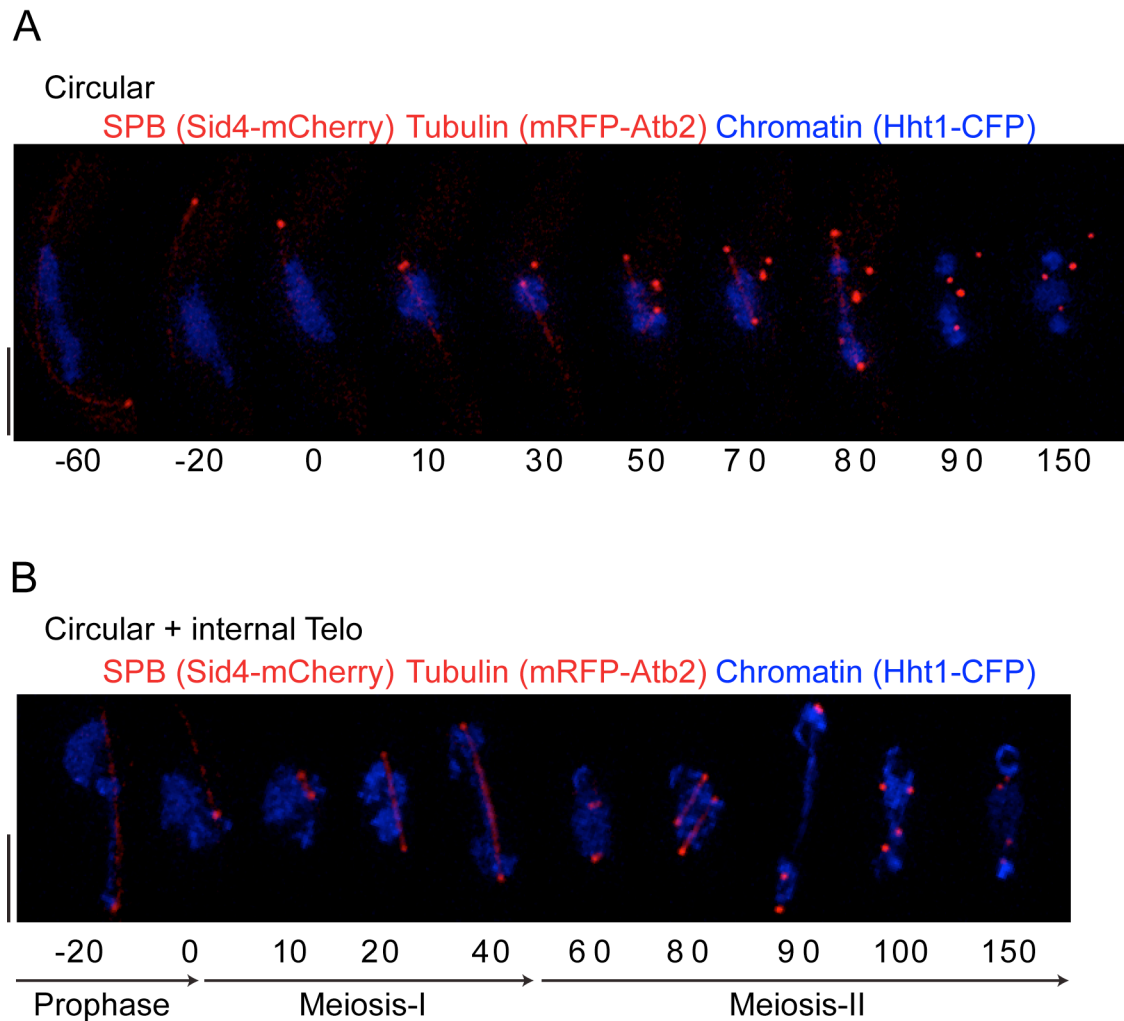


Figure 8.2 Telomere clustering is not required for bouquet function

Series of frames from movies acquired by fluorescence microscopy in live cell of circular meiosis (A) and circular meiosis with the presence of an internal telomere tract (B). SPB, and chromosomes were observed via endogenously tagged Sid4-mRFP Hht1-CFP respectively. Tubulin was observed by ectopically expressed mRFP-Atb2. Numbers under the frames represent the time in minutes. The stages of meiosis are indicated below. 0 min is the onset of MI. Scale bars equal 2 μ m. (A) Aberrant spindle formation and SPB separation in circular strain. SPB do not separate at MI (10-30 min) and form a monopolar spindle (10-30 min) SPBs separate only after MII duplication had occur (50-80 min) but remain sticky (50-70min). (B) Rescue of spindle formation and SPB separation in circular strain with an internal telomere tract. Bipolar spindle at MI (10-40 min) and at MII (80 min). Chromosome segregation remains aberrant because of the nature of the circular strain.

Moreover, we are also wondering about the role of the telomeric protein Pot1, which binds the single stranded region of the telomeres, in meiosis. As presented in the Introduction (see 1.1.4), telomeres are composed of a double stranded region bound by the double strand binding complex Taz1/Rap1, which in meiosis plays a role in bouquet formation, but also of a single stranded 3' overhang bound by the single strand binding complex Pot1/Tpz1; the double strand and single strand complexes are bridged by protein/protein interactions. The single strand complex is required for telomere protection, and deletion of Pot1 results in telomere loss, senescence and survival by chromosome circularisation (Baumann and Cech, 2001). Therefore, the role of the single strand complex has never been addressed in meiosis. We already know from the experiment where we add an internal telomere tract to a circular strain that the single-stranded 3' overhang is not needed for bouquet function; however, the proteins of the single strand complex are still present in the cell and could be recruited to the internal telomere by protein/protein interactions with the double strand telomere binding proteins (Miyoshi et al., 2008). Therefore, we are planning to delete Pot1 in the circular strain containing an internal telomere tract and repeat the experiment.

The data presented in this work, taken together, have not only established methods to monitor meiotic SPBs and provided initial characterisation of basic meiotic SPB biology, but also have uncovered the beginnings of the mechanism by which the chromosomes control the SPB behaviour and thereby spindle formation.

References

- ADAMS, I. R. & KILMARTIN, J. V. 1999. Localization of core spindle pole body (SPB) components during SPB duplication in *Saccharomyces cerevisiae*. *J Cell Biol*, 145, 809-23.
- ADAMS, I. R. & KILMARTIN, J. V. 2000. Spindle pole body duplication: a model for centrosome duplication? *Trends Cell Biol*, 10, 329-35.
- ANDERS, A., LOURENCO, P. C. & SAWIN, K. E. 2006. Noncore components of the fission yeast gamma-tubulin complex. *Mol Biol Cell*, 17, 5075-93.
- ANDERS, A. & SAWIN, K. E. 2011. Microtubule stabilization in vivo by nucleation-incompetent gamma-tubulin complex. *J Cell Sci*, 124, 1207-13.
- ARAI, K., SATO, M., TANAKA, K. & YAMAMOTO, M. 2010. Nuclear compartmentalization is abolished during fission yeast meiosis. *Curr Biol*, 20, 1913-8.
- ARAKI, Y., LAU, C. K., MAEKAWA, H., JASPERSEN, S. L., GIDDINGS, T. H., JR., SCHIEBEL, E. & WINEY, M. 2006. The *Saccharomyces cerevisiae* spindle pole body (SPB) component Nbp1p is required for SPB membrane insertion and interacts with the integral membrane proteins Ndc1p and Mps2p. *Mol Biol Cell*, 17, 1959-70.
- ASAKAWA, H., HAYASHI, A., HARAGUCHI, T. & HIRAOKA, Y. 2005. Dissociation of the Nuf2-Ndc80 complex releases centromeres from the spindle-pole body during meiotic prophase in fission yeast. *Mol Biol Cell*, 16, 2325-38.
- ASAKAWA, H., KOJIDANI, T., MORI, C., OSAKADA, H., SATO, M., DING, D. Q., HIRAOKA, Y. & HARAGUCHI, T. 2010. Virtual breakdown of the nuclear envelope in fission yeast meiosis. *Curr Biol*, 20, 1919-25.
- BAHE, S., STIERHOF, Y. D., WILKINSON, C. J., LEISS, F. & NIGG, E. A. 2005. Rootletin forms centriole-associated filaments and functions in centrosome cohesion. *J Cell Biol*, 171, 27-33.
- BAHLER, J., WU, J. Q., LONGTINE, M. S., SHAH, N. G., MCKENZIE, A., 3RD, STEEVER, A. B., WACH, A., PHILIPPSSEN, P. & PRINGLE, J. R. 1998. Heterologous modules for efficient and versatile PCR-based gene targeting in *Schizosaccharomyces pombe*. *Yeast*, 14, 943-51.
- BAHLER, J., WYLER, T., LOIDL, J. & KOHLI, J. 1993. Unusual nuclear structures in meiotic prophase of fission yeast: a cytological analysis. *J Cell Biol*, 121, 241-56.
- BASI, G., SCHMID, E. & MAUNDRELL, K. 1993. TATA box mutations in the *Schizosaccharomyces pombe* nmt1 promoter affect transcription efficiency but not the transcription start point or thiamine repressibility. *Gene*, 123, 131-6.

- BASTO, R., LAU, J., VINOGRADOVA, T., GARDIOL, A., WOODS, C. G., KHODJAKOV, A. & RAFF, J. W. 2006. Flies without centrioles. *Cell*, 125, 1375-86.
- BAUMANN, P. & CECH, T. R. 2001. Pot1, the putative telomere end-binding protein in fission yeast and humans. *Science*, 292, 1171-5.
- BEAUDOUIN, J., GERLICH, D., DAIGLE, N., EILS, R. & ELLENBERG, J. 2002. Nuclear envelope breakdown proceeds by microtubule-induced tearing of the lamina. *Cell*, 108, 83-96.
- BETTENCOURT-DIAS, M. & GLOVER, D. M. 2007. Centrosome biogenesis and function: centrosomics brings new understanding. *Nat Rev Mol Cell Biol*, 8, 451-63.
- BETTENCOURT-DIAS, M., RODRIGUES-MARTINS, A., CARPENTER, L., RIPARBELLI, M., LEHMANN, L., GATT, M. K., CARMO, N., BALLOUX, F., CALLAINI, G. & GLOVER, D. M. 2005. SAK/PLK4 is required for centriole duplication and flagella development. *Curr Biol*, 15, 2199-207.
- BLANGY, A., LANE, H. A., D'HERIN, P., HARPER, M., KRESS, M. & NIGG, E. A. 1995. Phosphorylation by p34cdc2 regulates spindle association of human Eg5, a kinesin-related motor essential for bipolar spindle formation in vivo. *Cell*, 83, 1159-69.
- BOBINNEC, Y., KHODJAKOV, A., MIR, L. M., RIEDER, C. L., EDDE, B. & BORNENS, M. 1998. Centriole disassembly in vivo and its effect on centrosome structure and function in vertebrate cells. *J Cell Biol*, 143, 1575-89.
- BORDE, V., GOLDMAN, A. S. & LICHTEN, M. 2000. Direct coupling between meiotic DNA replication and recombination initiation. *Science*, 290, 806-9.
- BORNENS, M. 2002. Centrosome composition and microtubule anchoring mechanisms. *Curr Opin Cell Biol*, 14, 25-34.
- BRIDGE, A. J., MORPHEW, M., BARTLETT, R. & HAGAN, I. M. 1998. The fission yeast SPB component Cut12 links bipolar spindle formation to mitotic control. *Genes Dev*, 12, 927-42.
- BROWN, N. & COSTANZO, V. 2009. An ATM and ATR dependent pathway targeting centrosome dependent spindle assembly. *Cell Cycle*, 8, 1997-2001.
- BULLITT, E., ROUT, M. P., KILMARTIN, J. V. & AKEY, C. W. 1997. The yeast spindle pole body is assembled around a central crystal of Spc42p. *Cell*, 89, 1077-86.
- BUONOMO, S. B., CLYNE, R. K., FUCHS, J., LOIDL, J., UHLMANN, F. & NASMYTH, K. 2000. Disjunction of homologous chromosomes in meiosis I depends on proteolytic cleavage of the meiotic cohesin Rec8 by separin. *Cell*, 103, 387-98.
- BURNS, R. G. 1995. Analysis of the gamma-tubulin sequences: implications for the functional properties of gamma-tubulin. *J Cell Sci*, 108 (Pt 6), 2123-30.
- BYERS, B. & GOETSCH, L. 1974. Duplication of spindle plaques and integration of the yeast cell cycle. *Cold Spring Harb Symp Quant Biol*, 38, 123-31.

- BYERS, B. & GOETSCH, L. 1975a. Behavior of spindles and spindle plaques in the cell cycle and conjugation of *Saccharomyces cerevisiae*. *J Bacteriol*, 124, 511-23.
- BYERS, B. & GOETSCH, L. 1975b. Electron microscopic observations on the meiotic karyotype of diploid and tetraploid *Saccharomyces cerevisiae*. *Proc Natl Acad Sci U S A*, 72, 5056-60.
- CHANG, L. & GOULD, K. L. 2000. Sid4p is required to localize components of the septation initiation pathway to the spindle pole body in fission yeast. *Proc Natl Acad Sci U S A*, 97, 5249-54.
- CHENG, J., TURKEL, N., HEMATI, N., FULLER, M. T., HUNT, A. J. & YAMASHITA, Y. M. 2008. Centrosome misorientation reduces stem cell division during ageing. *Nature*, 456, 599-604.
- CHIKASHIGE, Y., DING, D. Q., FUNABIKI, H., HARAGUCHI, T., MASHIKO, S., YANAGIDA, M. & HIRAOKA, Y. 1994. Telomere-led premeiotic chromosome movement in fission yeast. *Science*, 264, 270-3.
- CHIKASHIGE, Y., DING, D. Q., IMAI, Y., YAMAMOTO, M., HARAGUCHI, T. & HIRAOKA, Y. 1997. Meiotic nuclear reorganization: switching the position of centromeres and telomeres in the fission yeast *Schizosaccharomyces pombe*. *EMBO J*, 16, 193-202.
- CHIKASHIGE, Y. & HIRAOKA, Y. 2001. Telomere binding of the Rap1 protein is required for meiosis in fission yeast. *Curr Biol*, 11, 1618-23.
- CHIKASHIGE, Y., KUROKAWA, R., HARAGUCHI, T. & HIRAOKA, Y. 2004. Meiosis induced by inactivation of Pat1 kinase proceeds with aberrant nuclear positioning of centromeres in the fission yeast *Schizosaccharomyces pombe*. *Genes Cells*, 9, 671-84.
- CHIKASHIGE, Y., TSUTSUMI, C., YAMANE, M., OKAMASA, K., HARAGUCHI, T. & HIRAOKA, Y. 2006. Meiotic proteins bqt1 and bqt2 tether telomeres to form the bouquet arrangement of chromosomes. *Cell*, 125, 59-69.
- CHIKASHIGE, Y., YAMANE, M., OKAMASA, K., TSUTSUMI, C., KOJIDANI, T., SATO, M., HARAGUCHI, T. & HIRAOKA, Y. 2009. Membrane proteins Bqt3 and -4 anchor telomeres to the nuclear envelope to ensure chromosomal bouquet formation. *J Cell Biol*, 187, 413-27.
- CHRETIEN, D., BUENDIA, B., FULLER, S. D. & KARSENTI, E. 1997. Reconstruction of the centrosome cycle from cryoelectron micrographs. *J Struct Biol*, 120, 117-33.
- COLAIACOVO, M. P., MACQUEEN, A. J., MARTINEZ-PEREZ, E., MCDONALD, K., ADAMO, A., LA VOLPE, A. & VILLENEUVE, A. M. 2003. Synaptonemal complex assembly in *C. elegans* is dispensable for loading strand-exchange proteins but critical for proper completion of recombination. *Dev Cell*, 5, 463-74.
- CONRAD, M. N., LEE, C. Y., CHAO, G., SHINOHARA, M., KOSAKA, H., SHINOHARA, A., CONCHELLO, J. A. & DRESSER, M. E. 2008. Rapid telomere movement in meiotic prophase is promoted by NDJ1, MPS3, and CSM4 and is modulated by recombination. *Cell*, 133, 1175-87.

- COOPER, J. P., NIMMO, E. R., ALLSHIRE, R. C. & CECH, T. R. 1997. Regulation of telomere length and function by a Myb-domain protein in fission yeast. *Nature*, 385, 744-7.
- COOPER, J. P., WATANABE, Y. & NURSE, P. 1998. Fission yeast Taz1 protein is required for meiotic telomere clustering and recombination. *Nature*, 392, 828-31.
- CRASTA, K., HUANG, P., MORGAN, G., WINEY, M. & SURANA, U. 2006. Cdk1 regulates centrosome separation by restraining proteolysis of microtubule-associated proteins. *EMBO J*, 25, 2551-63.
- CRASTA, K., LIM, H. H., GIDDINGS, T. H., JR., WINEY, M. & SURANA, U. 2008. Inactivation of Cdh1 by synergistic action of Cdk1 and polo kinase is necessary for proper assembly of the mitotic spindle. *Nat Cell Biol*, 10, 665-75.
- CUNHA-FERREIRA, I., BENTO, I. & BETTENCOURT-DIAS, M. 2009. From zero to many: control of centriole number in development and disease. *Traffic*, 10, 482-98.
- DAGA, R. R. & JIMENEZ, J. 1999. Translational control of the cdc25 cell cycle phosphatase: a molecular mechanism coupling mitosis to cell growth. *J Cell Sci*, 112 Pt 18, 3137-46.
- DE GRAMONT, A., BARBOUR, L., ROSS, K. E. & COHEN-FIX, O. 2007. The spindle midzone microtubule-associated proteins Ase1p and Cin8p affect the number and orientation of astral microtubules in *Saccharomyces cerevisiae*. *Cell Cycle*, 6, 1231-41.
- DE LA ROCHE SAINT-ANDRE, C. 2008. Alternative ends: telomeres and meiosis. *Biochimie*, 90, 181-9.
- DE VEAUX, L. C., HOAGLAND, N. A. & SMITH, G. R. 1992. Seventeen complementation groups of mutations decreasing meiotic recombination in *Schizosaccharomyces pombe*. *Genetics*, 130, 251-62.
- DEHE, P. M. & COOPER, J. P. 2010. Fission yeast telomeres forecast the end of the crisis. *FEBS Lett*, 584, 3725-33.
- DERNBURG, A. F., MCDONALD, K., MOULDER, G., BARSTEAD, R., DRESSER, M. & VILLENEUVE, A. M. 1998. Meiotic recombination in *C. elegans* initiates by a conserved mechanism and is dispensable for homologous chromosome synapsis. *Cell*, 94, 387-98.
- DING, D. Q., CHIKASHIGE, Y., HARAGUCHI, T. & HIRAOKA, Y. 1998. Oscillatory nuclear movement in fission yeast meiotic prophase is driven by astral microtubules, as revealed by continuous observation of chromosomes and microtubules in living cells. *J Cell Sci*, 111 (Pt 6), 701-12.
- DING, D. Q., YAMAMOTO, A., HARAGUCHI, T. & HIRAOKA, Y. 2004. Dynamics of homologous chromosome pairing during meiotic prophase in fission yeast. *Dev Cell*, 6, 329-41.
- DING, R., WEST, R. R., MORPHEW, D. M., OAKLEY, B. R. & MCINTOSH, J. R. 1997. The spindle pole body of *Schizosaccharomyces pombe* enters and

- leaves the nuclear envelope as the cell cycle proceeds. *Mol Biol Cell*, 8, 1461-79.
- DOXSEY, S., MCCOLLUM, D. & THEURKAUF, W. 2005a. Centrosomes in cellular regulation. *Annu Rev Cell Dev Biol*, 21, 411-34.
- DOXSEY, S., ZIMMERMAN, W. & MIKULE, K. 2005b. Centrosome control of the cell cycle. *Trends Cell Biol*, 15, 303-11.
- EKWALL, K., NIMMO, E. R., JAVERZAT, J. P., BORGSTROM, B., EGEL, R., CRANSTON, G. & ALLSHIRE, R. 1996. Mutations in the fission yeast silencing factors *clr4+* and *rik1+* disrupt the localisation of the chromo domain protein *Swi6p* and impair centromere function. *J Cell Sci*, 109 (Pt 11), 2637-48.
- FAVA, F., RAYNAUD-MESSINA, B., LEUNG-TACK, J., MAZZOLINI, L., LI, M., GUILLEMOT, J. C., CACHOT, D., TOLLON, Y., FERRARA, P. & WRIGHT, M. 1999. Human 76p: A new member of the gamma-tubulin-associated protein family. *J Cell Biol*, 147, 857-68.
- FERREIRA, M. G. & COOPER, J. P. 2001. The fission yeast *Taz1* protein protects chromosomes from Ku-dependent end-to-end fusions. *Mol Cell*, 7, 55-63.
- FLORY, M. R., MORPHEW, M., JOSEPH, J. D., MEANS, A. R. & DAVIS, T. N. 2002. *Pcp1p*, an *Spc110p*-related calmodulin target at the centrosome of the fission yeast *Schizosaccharomyces pombe*. *Cell Growth Differ*, 13, 47-58.
- FONG, C. S., SATO, M. & TODA, T. 2010. Fission yeast *Pcp1* links polo kinase-mediated mitotic entry to gamma-tubulin-dependent spindle formation. *EMBO J*, 29, 120-30.
- FONG, K. W., CHOI, Y. K., RATTNER, J. B. & QI, R. Z. 2008. *CDK5RAP2* is a pericentriolar protein that functions in centrosomal attachment of the gamma-tubulin ring complex. *Mol Biol Cell*, 19, 115-25.
- FORSBURG, S. L. 1993. Comparison of *Schizosaccharomyces pombe* expression systems. *Nucleic Acids Res*, 21, 2955-6.
- FUJITA, A., VARDY, L., GARCIA, M. A. & TODA, T. 2002. A fourth component of the fission yeast gamma-tubulin complex, *Alp16*, is required for cytoplasmic microtubule integrity and becomes indispensable when gamma-tubulin function is compromised. *Mol Biol Cell*, 13, 2360-73.
- FUNABIKI, H., HAGAN, I., UZAWA, S. & YANAGIDA, M. 1993. Cell cycle-dependent specific positioning and clustering of centromeres and telomeres in fission yeast. *J Cell Biol*, 121, 961-76.
- GEISER, J. R., SUNDBERG, H. A., CHANG, B. H., MULLER, E. G. & DAVIS, T. N. 1993. The essential mitotic target of calmodulin is the 110-kilodalton component of the spindle pole body in *Saccharomyces cerevisiae*. *Mol Cell Biol*, 13, 7913-24.
- GEISLER, S., PEREIRA, G., SPANG, A., KNOP, M., SOUES, S., KILMARTIN, J. & SCHIEBEL, E. 1996. The spindle pole body component *Spc98p* interacts with the gamma-tubulin-like *Tub4p* of *Saccharomyces cerevisiae* at the sites of microtubule attachment. *EMBO J*, 15, 3899-911.

- GERACE, L. & BLOBEL, G. 1980. The nuclear envelope lamina is reversibly depolymerized during mitosis. *Cell*, 19, 277-87.
- GIROUX, C. N., DRESSER, M. E. & TIANO, H. F. 1989. Genetic control of chromosome synapsis in yeast meiosis. *Genome*, 31, 88-94.
- GOLUBOVSKAYA, I. N., HARPER, L. C., PAWLOWSKI, W. P., SCHICHNES, D. & CANDE, W. Z. 2002. The pam1 gene is required for meiotic bouquet formation and efficient homologous synapsis in maize (*Zea mays* L.). *Genetics*, 162, 1979-93.
- GOTTSCHLING, D. E., APARICIO, O. M., BILLINGTON, B. L. & ZAKIAN, V. A. 1990. Position effect at *S. cerevisiae* telomeres: reversible repression of Pol II transcription. *Cell*, 63, 751-62.
- GOTTSCHLING, D. E. & ZAKIAN, V. A. 1986. Telomere proteins: specific recognition and protection of the natural termini of *Oxytricha* macronuclear DNA. *Cell*, 47, 195-205.
- GOULD, R. R. & BORISY, G. G. 1977. The pericentriolar material in Chinese hamster ovary cells nucleates microtubule formation. *J Cell Biol*, 73, 601-15.
- GRALLERT, A., KRAPP, A., BAGLEY, S., SIMANIS, V. & HAGAN, I. M. 2004. Recruitment of NIMA kinase shows that maturation of the *S. pombe* spindle pole body occurs over consecutive cell cycles and reveals a role for NIMA in modulating SIN activity. *Genes Dev*, 18, 1007-21.
- GROMLEY, A., JURCZYK, A., SILLIBOURNE, J., HALILOVIC, E., MOGENSEN, M., GROISMAN, I., BLOMBERG, M. & DOXSEY, S. 2003. A novel human protein of the maternal centriole is required for the final stages of cytokinesis and entry into S phase. *J Cell Biol*, 161, 535-45.
- HAGAN, I., HAYLES, J. & NURSE, P. 1988. Cloning and sequencing of the cyclin-related *cdc13+* gene and a cytological study of its role in fission yeast mitosis. *J Cell Sci*, 91 (Pt 4), 587-95.
- HAGAN, I. & YANAGIDA, M. 1990. Novel potential mitotic motor protein encoded by the fission yeast *cut7+* gene. *Nature*, 347, 563-6.
- HAGAN, I. & YANAGIDA, M. 1992. Kinesin-related *cut7* protein associates with mitotic and meiotic spindles in fission yeast. *Nature*, 356, 74-6.
- HAGAN, I. & YANAGIDA, M. 1995. The product of the spindle formation gene *sad1+* associates with the fission yeast spindle pole body and is essential for viability. *J Cell Biol*, 129, 1033-47.
- HAGAN, I. M. 2008. The spindle pole body plays a key role in controlling mitotic commitment in the fission yeast *Schizosaccharomyces pombe*. *Biochem Soc Trans*, 36, 1097-101.
- HAREN, L., REMY, M. H., BAZIN, I., CALLEBAUT, I., WRIGHT, M. & MERDES, A. 2006. NEDD1-dependent recruitment of the gamma-tubulin ring complex to the centrosome is necessary for centriole duplication and spindle assembly. *J Cell Biol*, 172, 505-15.
- HARPER, L., GOLUBOVSKAYA, I. & CANDE, W. Z. 2004. A bouquet of chromosomes. *J Cell Sci*, 117, 4025-32.

- HEALD, R., TOURNEBIZE, R., BLANK, T., SANDALTZOPOULOS, R., BECKER, P., HYMAN, A. & KARSENTI, E. 1996. Self-organization of microtubules into bipolar spindles around artificial chromosomes in *Xenopus* egg extracts. *Nature*, 382, 420-5.
- HEITZ, M. J., PETERSEN, J., VALOVIN, S. & HAGAN, I. M. 2001. MTOC formation during mitotic exit in fission yeast. *J Cell Sci*, 114, 4521-32.
- HENTGES, P., VAN DRIESSCHE, B., TAFFOREAU, L., VANDENHAUTE, J. & CARR, A. M. 2005. Three novel antibiotic marker cassettes for gene disruption and marker switching in *Schizosaccharomyces pombe*. *Yeast*, 22, 1013-9.
- HIRAOKA, Y. & DERNBURG, A. F. 2009. The SUN rises on meiotic chromosome dynamics. *Dev Cell*, 17, 598-605.
- HIRAOKA, Y., MAEKAWA, H., ASAKAWA, H., CHIKASHIGE, Y., KOJIDANI, T., OSAKADA, H., MATSUDA, A. & HARAGUCHI, T. 2011. Inner nuclear membrane protein Ima1 is dispensable for intranuclear positioning of centromeres. *Genes Cells*, 16, 1000-11.
- HIRATA, A. & SHIMODA, C. 1994. Structural modification of spindle pole bodies during meiosis II is essential for the normal formation of ascospores in *Schizosaccharomyces pombe*: ultrastructural analysis of *spo* mutants. *Yeast*, 10, 173-83.
- HIRATA, A. & TANAKA, K. 1982. Nuclear behavior during conjugation and meiosis in the fission yeast *Schizosaccharomyces pombe*. *J Gen Appl Microbiol*, 28, 263-274.
- HORIE, S., WATANABE, Y., TANAKA, K., NISHIWAKI, S., FUJIOKA, H., ABE, H., YAMAMOTO, M. & SHIMODA, C. 1998. The *Schizosaccharomyces pombe* *mei4+* gene encodes a meiosis-specific transcription factor containing a forkhead DNA-binding domain. *Mol Cell Biol*, 18, 2118-29.
- HORIO, T., UZAWA, S., JUNG, M. K., OAKLEY, B. R., TANAKA, K. & YANAGIDA, M. 1991. The fission yeast gamma-tubulin is essential for mitosis and is localized at microtubule organizing centers. *J Cell Sci*, 99 (Pt 4), 693-700.
- HUGHES, S. E., BEELER, J. S., SEAT, A., SLAUGHTER, B. D., UNRUH, J. R., BAUERLY, E., MATTHIES, H. J. & HAWLEY, R. S. 2011. Gamma-Tubulin Is Required for Bipolar Spindle Assembly and for Proper Kinetochores Microtubule Attachments during Prometaphase I in *Drosophila* Oocytes. *PLoS Genet*, 7, e1002209.
- IINO, Y. & YAMAMOTO, M. 1985. Negative control for the initiation of meiosis in *Schizosaccharomyces pombe*. *Proc Natl Acad Sci U S A*, 82, 2447-51.
- ISHIGURO, T., TANAKA, K., SAKUNO, T. & WATANABE, Y. 2010. Shugoshin-PP2A counteracts casein-kinase-1-dependent cleavage of Rec8 by separase. *Nat Cell Biol*, 12, 500-6.
- JAIN, D. & COOPER, J. P. 2010. Telomeric strategies: means to an end. *Annu Rev Genet*, 44, 243-69.

- JASPERSEN, S. L. & WINEY, M. 2004. The budding yeast spindle pole body: structure, duplication, and function. *Annu Rev Cell Dev Biol*, 20, 1-28.
- JAVERZAT, J. P., CRANSTON, G. & ALLSHIRE, R. C. 1996. Fission yeast genes which disrupt mitotic chromosome segregation when overexpressed. *Nucleic Acids Res*, 24, 4676-83.
- JIN, Y., MANCUSO, J. J., UZAWA, S., CRONEMBOLD, D. & CANDE, W. Z. 2005. The fission yeast homolog of the human transcription factor EAP30 blocks meiotic spindle pole body amplification. *Dev Cell*, 9, 63-73.
- JOB, D., VALIRON, O. & OAKLEY, B. 2003. Microtubule nucleation. *Curr Opin Cell Biol*, 15, 111-7.
- KAKUI, Y., SATO, M., TANAKA, K. & YAMAMOTO, M. 2011. A novel fission yeast mei4 mutant that allows efficient synchronization of telomere dispersal and the first meiotic division. *Yeast*, 28, 467-79.
- KAN, F., DAVIDSON, M. K. & WAHLS, W. P. 2011. Meiotic recombination protein Rec12: functional conservation, crossover homeostasis and early crossover/non-crossover decision. *Nucleic Acids Res*, 39, 1460-72.
- KANO, H. & ISHIKAWA, F. 2001. spRap1 and spRif1, recruited to telomeres by Taz1, are essential for telomere function in fission yeast. *Curr Biol*, 11, 1624-30.
- KANO, H., SADAIE, M., URANO, T. & ISHIKAWA, F. 2005. Telomere binding protein Taz1 establishes Swi6 heterochromatin independently of RNAi at telomeres. *Curr Biol*, 15, 1808-19.
- KAWAGUCHI, S. & ZHENG, Y. 2004. Characterization of a Drosophila centrosome protein CP309 that shares homology with Kendrin and CG-NAP. *Mol Biol Cell*, 15, 37-45.
- KECK, J. M., JONES, M. H., WONG, C. C., BINKLEY, J., CHEN, D., JASPERSEN, S. L., HOLINGER, E. P., XU, T., NIEPEL, M., ROUT, M. P., VOGEL, J., SIDOW, A., YATES, J. R., 3RD & WINEY, M. 2011. A cell cycle phosphoproteome of the yeast centrosome. *Science*, 332, 1557-61.
- KEENEY, S., GIROUX, C. N. & KLECKNER, N. 1997. Meiosis-specific DNA double-strand breaks are catalyzed by Spo11, a member of a widely conserved protein family. *Cell*, 88, 375-84.
- KILMARTIN, J. V. 2003. Sfi1p has conserved centrin-binding sites and an essential function in budding yeast spindle pole body duplication. *J Cell Biol*, 162, 1211-21.
- KILMARTIN, J. V., DYOS, S. L., KERSHAW, D. & FINCH, J. T. 1993. A spacer protein in the Saccharomyces cerevisiae spindle pole body whose transcript is cell cycle-regulated. *J Cell Biol*, 123, 1175-84.
- KILMARTIN, J. V. & GOH, P. Y. 1996. Spc110p: assembly properties and role in the connection of nuclear microtubules to the yeast spindle pole body. *EMBO J*, 15, 4592-602.
- KING, M. C., DRIVAS, T. G. & BLOBEL, G. 2008. A network of nuclear envelope membrane proteins linking centromeres to microtubules. *Cell*, 134, 427-38.

- KITAJIMA, T. S., MIYAZAKI, Y., YAMAMOTO, M. & WATANABE, Y. 2003. Rec8 cleavage by separase is required for meiotic nuclear divisions in fission yeast. *EMBO J*, 22, 5643-53.
- KITAJIMA, T. S., SAKUNO, T., ISHIGURO, K., IEMURA, S., NATSUME, T., KAWASHIMA, S. A. & WATANABE, Y. 2006. Shugoshin collaborates with protein phosphatase 2A to protect cohesin. *Nature*, 441, 46-52.
- KNOP, M., PEREIRA, G., GEISLER, S., GREIN, K. & SCHIEBEL, E. 1997. The spindle pole body component Spc97p interacts with the gamma-tubulin of *Saccharomyces cerevisiae* and functions in microtubule organization and spindle pole body duplication. *EMBO J*, 16, 1550-64.
- KNOP, M. & SCHIEBEL, E. 1997. Spc98p and Spc97p of the yeast gamma-tubulin complex mediate binding to the spindle pole body via their interaction with Spc110p. *EMBO J*, 16, 6985-95.
- KNOP, M. & SCHIEBEL, E. 1998. Receptors determine the cellular localization of a gamma-tubulin complex and thereby the site of microtubule formation. *EMBO J*, 17, 3952-67.
- KOHLI, J. & BAHLER, J. 1994. Homologous recombination in fission yeast: absence of crossover interference and synaptonemal complex. *Experientia*, 50, 295-306.
- KOLLMAN, J. M., POLKA, J. K., ZELTER, A., DAVIS, T. N. & AGARD, D. A. 2010. Microtubule nucleating gamma-TuSC assembles structures with 13-fold microtubule-like symmetry. *Nature*, 466, 879-82.
- KOSZUL, R., KIM, K. P., PRENTISS, M., KLECKNER, N. & KAMEOKA, S. 2008. Meiotic chromosomes move by linkage to dynamic actin cables with transduction of force through the nuclear envelope. *Cell*, 133, 1188-201.
- KRAMER, A., MAILAND, N., LUKAS, C., SYLJUASEN, R. G., WILKINSON, C. J., NIGG, E. A., BARTEK, J. & LUKAS, J. 2004. Centrosome-associated Chk1 prevents premature activation of cyclin-B-Cdk1 kinase. *Nat Cell Biol*, 6, 884-91.
- KUPKE, T., DI CECCO, L., MULLER, H. M., NEUNER, A., ADOLF, F., WIELAND, F., NICKEL, W. & SCHIEBEL, E. 2011. Targeting of Nbp1 to the inner nuclear membrane is essential for spindle pole body duplication. *EMBO J*, 30, 3337-52.
- KURIYAMA, R. & BORISY, G. G. 1981. Centriole cycle in Chinese hamster ovary cells as determined by whole-mount electron microscopy. *J Cell Biol*, 91, 814-21.
- KUTAY, U. & HETZER, M. W. 2008. Reorganization of the nuclear envelope during open mitosis. *Curr Opin Cell Biol*, 20, 669-77.
- LANE, H. A. & NIGG, E. A. 1996. Antibody microinjection reveals an essential role for human polo-like kinase 1 (Plk1) in the functional maturation of mitotic centrosomes. *J Cell Biol*, 135, 1701-13.
- LEE, B. H. & AMON, A. 2003. Polo kinase--meiotic cell cycle coordinator. *Cell Cycle*, 2, 400-2.

- LENART, P., RABUT, G., DAIGLE, N., HAND, A. R., TERASAKI, M. & ELLENBERG, J. 2003. Nuclear envelope breakdown in starfish oocytes proceeds by partial NPC disassembly followed by a rapidly spreading fenestration of nuclear membranes. *J Cell Biol*, 160, 1055-68.
- LIM, H. H., ZHANG, T. & SURANA, U. 2009. Regulation of centrosome separation in yeast and vertebrates: common threads. *Trends Cell Biol*, 19, 325-33.
- LIU, B., JOSHI, H. C., WILSON, T. J., SILFLOW, C. D., PALEVITZ, B. A. & SNUSTAD, D. P. 1994. gamma-Tubulin in Arabidopsis: gene sequence, immunoblot, and immunofluorescence studies. *Plant Cell*, 6, 303-14.
- LIU, H., JANG, J. K., KATO, N. & MCKIM, K. S. 2002. mei-P22 encodes a chromosome-associated protein required for the initiation of meiotic recombination in *Drosophila melanogaster*. *Genetics*, 162, 245-58.
- LOFFLER, H., BOCHTLER, T., FRITZ, B., TEWS, B., HO, A. D., LUKAS, J., BARTEK, J. & KRAMER, A. 2007. DNA damage-induced accumulation of centrosomal Chk1 contributes to its checkpoint function. *Cell Cycle*, 6, 2541-8.
- LUDERS, J., PATEL, U. K. & STEARNS, T. 2006. GCP-WD is a gamma-tubulin targeting factor required for centrosomal and chromatin-mediated microtubule nucleation. *Nat Cell Biol*, 8, 137-47.
- MACIVER, F. H., TANAKA, K., ROBERTSON, A. M. & HAGAN, I. M. 2003. Physical and functional interactions between polo kinase and the spindle pole component Cut12 regulate mitotic commitment in *S. pombe*. *Genes Dev*, 17, 1507-23.
- MACQUEEN, A. J., PHILLIPS, C. M., BHALLA, N., WEISER, P., VILLENEUVE, A. M. & DERNBURG, A. F. 2005. Chromosome sites play dual roles to establish homologous synapsis during meiosis in *C. elegans*. *Cell*, 123, 1037-50.
- MAHONEY, N. M., GOSHIMA, G., DOUGLASS, A. D. & VALE, R. D. 2006. Making microtubules and mitotic spindles in cells without functional centrosomes. *Curr Biol*, 16, 564-9.
- MANANDHAR, G., SCHATTEN, H. & SUTOVSKY, P. 2005. Centrosome reduction during gametogenesis and its significance. *Biol Reprod*, 72, 2-13.
- MARTIN-CASTELLANOS, C., BLANCO, M., ROZALEN, A. E., PEREZ-HIDALGO, L., GARCIA, A. I., CONDE, F., MATA, J., ELLERMEIER, C., DAVIS, L., SAN-SEGUNDO, P., SMITH, G. R. & MORENO, S. 2005. A large-scale screen in *S. pombe* identifies seven novel genes required for critical meiotic events. *Curr Biol*, 15, 2056-62.
- MARTINI, E., DIAZ, R. L., HUNTER, N. & KEENEY, S. 2006. Crossover homeostasis in yeast meiosis. *Cell*, 126, 285-95.
- MASUDA, H., SEVIK, M. & CANDE, W. Z. 1992. In vitro microtubule-nucleating activity of spindle pole bodies in fission yeast *Schizosaccharomyces pombe*: cell cycle-dependent activation in xenopus cell-free extracts. *J Cell Biol*, 117, 1055-66.
- MASUDA, H., TODA, T., MIYAMOTO, R., HARAGUCHI, T. & HIRAOKA, Y. 2006. Modulation of Alp4 function in *Schizosaccharomyces pombe* induces

- novel phenotypes that imply distinct functions for nuclear and cytoplasmic gamma-tubulin complexes. *Genes Cells*, 11, 319-36.
- MATA, J., LYNE, R., BURNS, G. & BAHLER, J. 2002. The transcriptional program of meiosis and sporulation in fission yeast. *Nat Genet*, 32, 143-7.
- MATA, J., WILBREY, A. & BAHLER, J. 2007. Transcriptional regulatory network for sexual differentiation in fission yeast. *Genome Biol*, 8, R217.
- MAUNDRELL, K. 1990. nmt1 of fission yeast. A highly transcribed gene completely repressed by thiamine. *J Biol Chem*, 265, 10857-64.
- MCCOLLUM, D. & GOULD, K. L. 2001. Timing is everything: regulation of mitotic exit and cytokinesis by the MEN and SIN. *Trends Cell Biol*, 11, 89-95.
- MCKIM, K. S., GREEN-MARROQUIN, B. L., SEKELSKY, J. J., CHIN, G., STEINBERG, C., KHODOSH, R. & HAWLEY, R. S. 1998. Meiotic synapsis in the absence of recombination. *Science*, 279, 876-8.
- MIKI, F., KURABAYASHI, A., TANGE, Y., OKAZAKI, K., SHIMANUKI, M. & NIWA, O. 2004. Two-hybrid search for proteins that interact with Sad1 and Kms1, two membrane-bound components of the spindle pole body in fission yeast. *Mol Genet Genomics*, 270, 449-61.
- MIKI, F., OKAZAKI, K., SHIMANUKI, M., YAMAMOTO, A., HIRAOKA, Y. & NIWA, O. 2002. The 14-kDa dynein light chain-family protein Dlc1 is required for regular oscillatory nuclear movement and efficient recombination during meiotic prophase in fission yeast. *Mol Biol Cell*, 13, 930-46.
- MIRZAYAN, C., COPELAND, C. S. & SNYDER, M. 1992. The NUF1 gene encodes an essential coiled-coil related protein that is a potential component of the yeast nucleoskeleton. *J Cell Biol*, 116, 1319-32.
- MITCHISON, T. & KIRSCHNER, M. 1984. Dynamic instability of microtubule growth. *Nature*, 312, 237-42.
- MITCHISON, T. J. 1993. Localization of an exchangeable GTP binding site at the plus end of microtubules. *Science*, 261, 1044-7.
- MIYOSHI, T., KANO, J., SAITO, M. & ISHIKAWA, F. 2008. Fission yeast Pot1-Tpp1 protects telomeres and regulates telomere length. *Science*, 320, 1341-4.
- MOENS, P. B. & RAPPORT, E. 1971. Spindles, spindle plaques, and meiosis in the yeast *Saccharomyces cerevisiae* (Hansen). *J Cell Biol*, 50, 344-61.
- MORELLI, M. A., WERLING, U., EDELMANN, W., ROBERSON, M. S. & COHEN, P. E. 2008. Analysis of meiotic prophase I in live mouse spermatocytes. *Chromosome Res*, 16, 743-60.
- MORENO, S., KLAR, A. & NURSE, P. 1991. Molecular genetic analysis of fission yeast *Schizosaccharomyces pombe*. *Methods Enzymol*, 194, 795-823.
- MORITZ, M., BRAUNFELD, M. B., GUENEBAUT, V., HEUSER, J. & AGARD, D. A. 2000. Structure of the gamma-tubulin ring complex: a template for microtubule nucleation. *Nat Cell Biol*, 2, 365-70.

- MORITZ, M., BRAUNFELD, M. B., SEDAT, J. W., ALBERTS, B. & AGARD, D. A. 1995. Microtubule nucleation by gamma-tubulin-containing rings in the centrosome. *Nature*, 378, 638-40.
- MORRELL, J. L., TOMLIN, G. C., RAJAGOPALAN, S., VENKATRAM, S., FEOKTISTOVA, A. S., TASTO, J. J., MEHTA, S., JENNINGS, J. L., LINK, A., BALASUBRAMANIAN, M. K. & GOULD, K. L. 2004. Sid4p-Cdc11p assembles the septation initiation network and its regulators at the *S. pombe* SPB. *Curr Biol*, 14, 579-84.
- MULLER, E. G., SNYDSMAN, B. E., NOVIK, I., HAILEY, D. W., GESTAUT, D. R., NIEMANN, C. A., O'TOOLE, E. T., GIDDINGS, T. H., JR., SUNDIN, B. A. & DAVIS, T. N. 2005. The organization of the core proteins of the yeast spindle pole body. *Mol Biol Cell*, 16, 3341-52.
- MULVIHILL, D. P., PETERSEN, J., OHKURA, H., GLOVER, D. M. & HAGAN, I. M. 1999. Plo1 kinase recruitment to the spindle pole body and its role in cell division in *Schizosaccharomyces pombe*. *Mol Biol Cell*, 10, 2771-85.
- MURAKAMI-TONAMI, Y., YAMADA-NAMIKAWA, C., TOCHIGI, A., HASEGAWA, N., KOJIMA, H., KUNIMATSU, M., NAKANISHI, M. & MURAKAMI, H. 2007. Mei4p coordinates the onset of meiosis I by regulating cdc25+ in fission yeast. *Proc Natl Acad Sci U S A*, 104, 14688-93.
- MURPHY, S. M., PREBLE, A. M., PATEL, U. K., O'CONNELL, K. L., DIAS, D. P., MORITZ, M., AGARD, D., STULTS, J. T. & STEARNS, T. 2001. GCP5 and GCP6: two new members of the human gamma-tubulin complex. *Mol Biol Cell*, 12, 3340-52.
- MURPHY, S. M., URBANI, L. & STEARNS, T. 1998. The mammalian gamma-tubulin complex contains homologues of the yeast spindle pole body components spc97p and spc98p. *J Cell Biol*, 141, 663-74.
- MUSACCHIO, A. & HARDWICK, K. G. 2002. The spindle checkpoint: structural insights into dynamic signalling. *Nat Rev Mol Cell Biol*, 3, 731-41.
- NAITO, T., MATSUURA, A. & ISHIKAWA, F. 1998. Circular chromosome formation in a fission yeast mutant defective in two ATM homologues. *Nat Genet*, 20, 203-6.
- NAKAMURA, T., ASAKAWA, H., NAKASE, Y., KASHIWAZAKI, J., HIRAOKA, Y. & SHIMODA, C. 2008. Live observation of forespore membrane formation in fission yeast. *Mol Biol Cell*, 19, 3544-53.
- NAKAYAMA, J., RICE, J. C., STRAHL, B. D., ALLIS, C. D. & GREWAL, S. I. 2001. Role of histone H3 lysine 9 methylation in epigenetic control of heterochromatin assembly. *Science*, 292, 110-3.
- NICCOLI, T., YAMASHITA, A., NURSE, P. & YAMAMOTO, M. 2004. The p150-Glued Ssm4p regulates microtubular dynamics and nuclear movement in fission yeast. *J Cell Sci*, 117, 5543-56.
- NIGG, E. A. 2006. Cell biology: a licence for duplication. *Nature*, 442, 874-5.

- NIMMO, E. R., CRANSTON, G. & ALLSHIRE, R. C. 1994. Telomere-associated chromosome breakage in fission yeast results in variegated expression of adjacent genes. *EMBO J*, 13, 3801-11.
- NIMMO, E. R., PIDOUX, A. L., PERRY, P. E. & ALLSHIRE, R. C. 1998. Defective meiosis in telomere-silencing mutants of *Schizosaccharomyces pombe*. *Nature*, 392, 825-8.
- NIWA, O., SHIMANUKI, M. & MIKI, F. 2000. Telomere-led bouquet formation facilitates homologous chromosome pairing and restricts ectopic interaction in fission yeast meiosis. *EMBO J*, 19, 3831-40.
- NOGALES, E., WHITTAKER, M., MILLIGAN, R. A. & DOWNING, K. H. 1999. High-resolution model of the microtubule. *Cell*, 96, 79-88.
- NURSE, P. 1985. Mutants of the fission yeast *Schizosaccharomyces pombe* which alter the shift between cell proliferation and sporulation. *Mol. Gen. Genet*, 198, 497-502.
- NURSE, P. 1990. Universal control mechanism regulating onset of M-phase. *Nature*, 344, 503-8.
- O'TOOLE, E. T., WINEY, M. & MCINTOSH, J. R. 1999. High-voltage electron tomography of spindle pole bodies and early mitotic spindles in the yeast *Saccharomyces cerevisiae*. *Mol Biol Cell*, 10, 2017-31.
- OAKLEY, B. R., OAKLEY, C. E., YOON, Y. & JUNG, M. K. 1990. Gamma-tubulin is a component of the spindle pole body that is essential for microtubule function in *Aspergillus nidulans*. *Cell*, 61, 1289-301.
- OAKLEY, C. E. & OAKLEY, B. R. 1989. Identification of gamma-tubulin, a new member of the tubulin superfamily encoded by *mipA* gene of *Aspergillus nidulans*. *Nature*, 338, 662-4.
- OEGEMA, K., WIESE, C., MARTIN, O. C., MILLIGAN, R. A., IWAMATSU, A., MITCHISON, T. J. & ZHENG, Y. 1999. Characterization of two related *Drosophila* gamma-tubulin complexes that differ in their ability to nucleate microtubules. *J Cell Biol*, 144, 721-33.
- PAOLETTI, A., BORDES, N., HADDAD, R., SCHWARTZ, C. L., CHANG, F. & BORNENS, M. 2003. Fission yeast *cdc31p* is a component of the half-bridge and controls SPB duplication. *Mol Biol Cell*, 14, 2793-808.
- PETERS, N., PEREZ, D. E., SONG, M. H., LIU, Y., MULLER-REICHERT, T., CARON, C., KEMPHUES, K. J. & O'CONNELL, K. F. 2010. Control of mitotic and meiotic centriole duplication by the Plk4-related kinase ZYG-1. *J Cell Sci*, 123, 795-805.
- PETERSEN, J. & HAGAN, I. M. 2005. Polo kinase links the stress pathway to cell cycle control and tip growth in fission yeast. *Nature*, 435, 507-12.
- PETERSEN, J., HEITZ, M. J. & HAGAN, I. M. 1998. Conjugation in *S. pombe*: identification of a microtubule-organising centre, a requirement for microtubules and a role for Mad2. *Curr Biol*, 8, 963-6.
- PIEL, M., MEYER, P., KHODJAKOV, A., RIEDER, C. L. & BORNENS, M. 2000. The respective contributions of the mother and daughter centrioles to

- centrosome activity and behavior in vertebrate cells. *J Cell Biol*, 149, 317-30.
- PIEL, M., NORDBERG, J., EUTENEUER, U. & BORNENS, M. 2001. Centrosome-dependent exit of cytokinesis in animal cells. *Science*, 291, 1550-3.
- ROBINOW, C. F. & MARAK, J. 1966. A fiber apparatus in the nucleus of the yeast cell. *J Cell Biol*, 29, 129-51.
- ROMANIENKO, P. J. & CAMERINI-OTERO, R. D. 2000. The mouse Spo11 gene is required for meiotic chromosome synapsis. *Mol Cell*, 6, 975-87.
- SAITO, T. T., TOUGAN, T., OKUZAKI, D., KASAMA, T. & NOJIMA, H. 2005. Mcp6, a meiosis-specific coiled-coil protein of *Schizosaccharomyces pombe*, localizes to the spindle pole body and is required for horsetail movement and recombination. *J Cell Sci*, 118, 447-59.
- SAKUNO, T. & WATANABE, Y. 2009. Studies of meiosis disclose distinct roles of cohesion in the core centromere and pericentromeric regions. *Chromosome Res*, 17, 239-49.
- SALINA, D., BODOOR, K., ECKLEY, D. M., SCHROER, T. A., RATTNER, J. B. & BURKE, B. 2002. Cytoplasmic dynein as a facilitator of nuclear envelope breakdown. *Cell*, 108, 97-107.
- SAMEJIMA, I., LOURENCO, P. C., SNAITH, H. A. & SAWIN, K. E. 2005. Fission yeast mto2p regulates microtubule nucleation by the centrosomin-related protein mto1p. *Mol Biol Cell*, 16, 3040-51.
- SAMEJIMA, I., MILLER, V. J., RINCON, S. A. & SAWIN, K. E. 2010. Fission yeast Mto1 regulates diversity of cytoplasmic microtubule organizing centers. *Curr Biol*, 20, 1959-65.
- SATO, M., DHUT, S. & TODA, T. 2005. New drug-resistant cassettes for gene disruption and epitope tagging in *Schizosaccharomyces pombe*. *Yeast*, 22, 583-91.
- SAUNDERS, W., LENGYEL, V. & HOYT, M. A. 1997. Mitotic spindle function in *Saccharomyces cerevisiae* requires a balance between different types of kinesin-related motors. *Mol Biol Cell*, 8, 1025-33.
- SAWIN, K. E., LOURENCO, P. C. & SNAITH, H. A. 2004. Microtubule nucleation at non-spindle pole body microtubule-organizing centers requires fission yeast centrosomin-related protein mod20p. *Curr Biol*, 14, 763-75.
- SAWIN, K. E. & TRAN, P. T. 2006. Cytoplasmic microtubule organization in fission yeast. *Yeast*, 23, 1001-14.
- SCHERTHAN, H. 2001. A bouquet makes ends meet. *Nat Rev Mol Cell Biol*, 2, 621-7.
- SCHERTHAN, H. 2007. Telomere attachment and clustering during meiosis. *Cell Mol Life Sci*, 64, 117-24.
- SCHMIDT, A. E., MILLER, T., SCHMIDT, S. L., SHIEKHATTAR, R. & SHILATIFARD, A. 1999. Cloning and characterization of the EAP30 subunit of the ELL complex that confers derepression of transcription by RNA polymerase II. *J Biol Chem*, 274, 21981-5.

- SCHRAMM, C., ELLIOTT, S., SHEVCHENKO, A. & SCHIEBEL, E. 2000. The Bbp1p-Mps2p complex connects the SPB to the nuclear envelope and is essential for SPB duplication. *EMBO J*, 19, 421-33.
- SCHUH, M. & ELLENBERG, J. 2007. Self-organization of MTOCs replaces centrosome function during acentrosomal spindle assembly in live mouse oocytes. *Cell*, 130, 484-98.
- SHEEHAN, M. J. & PAWLOWSKI, W. P. 2009. Live imaging of rapid chromosome movements in meiotic prophase I in maize. *Proc Natl Acad Sci U S A*, 106, 20989-94.
- SHIMANUKI, M., MIKI, F., DING, D. Q., CHIKASHIGE, Y., HIRAOKA, Y., HORIO, T. & NIWA, O. 1997. A novel fission yeast gene, kms1+, is required for the formation of meiotic prophase-specific nuclear architecture. *Mol Gen Genet*, 254, 238-49.
- SHIMODA, C. 2004. Forespore membrane assembly in yeast: coordinating SPBs and membrane trafficking. *J Cell Sci*, 117, 389-96.
- SHIMODA, C., HIRATA, A., KISHIDA, M., HASHIDA, T. & TANAKA, K. 1985. Characterization of meiosis-deficient mutants by electron microscopy and mapping of four essential genes in the fission yeast *Schizosaccharomyces pombe*. *Mol Gen Genet*, 200, 252-7.
- SOHRMANN, M., SCHMIDT, S., HAGAN, I. & SIMANIS, V. 1998. Asymmetric segregation on spindle poles of the *Schizosaccharomyces pombe* septum-inducing protein kinase Cdc7p. *Genes Dev*, 12, 84-94.
- SPANG, A., GEISLER, S., GREIN, K. & SCHIEBEL, E. 1996. gamma-Tubulin-like Tub4p of *Saccharomyces cerevisiae* is associated with the spindle pole body substructures that organize microtubules and is required for mitotic spindle formation. *J Cell Biol*, 134, 429-41.
- STARR, D. A. & FISCHER, J. A. 2005. KASH 'n Karry: the KASH domain family of cargo-specific cytoskeletal adaptor proteins. *Bioessays*, 27, 1136-46.
- STAVRU, F., HULSMANN, B. B., SPANG, A., HARTMANN, E., CORDES, V. C. & GORLICH, D. 2006. NDC1: a crucial membrane-integral nucleoporin of metazoan nuclear pore complexes. *J Cell Biol*, 173, 509-19.
- STEARNS, T., EVANS, L. & KIRSCHNER, M. 1991. Gamma-tubulin is a highly conserved component of the centrosome. *Cell*, 65, 825-36.
- STEARNS, T. & KIRSCHNER, M. 1994. In vitro reconstitution of centrosome assembly and function: the central role of gamma-tubulin. *Cell*, 76, 623-37.
- STIRLING, D. A., WELCH, K. A. & STARK, M. J. 1994. Interaction with calmodulin is required for the function of Spc110p, an essential component of the yeast spindle pole body. *EMBO J*, 13, 4329-42.
- SUNDBERG, H. A. & DAVIS, T. N. 1997. A mutational analysis identifies three functional regions of the spindle pole component Spc110p in *Saccharomyces cerevisiae*. *Mol Biol Cell*, 8, 2575-90.
- SUNDBERG, H. A., GOETSCH, L., BYERS, B. & DAVIS, T. N. 1996. Role of calmodulin and Spc110p interaction in the proper assembly of spindle pole body components. *J Cell Biol*, 133, 111-24.

- TAKAHASHI, M., YAMAGIWA, A., NISHIMURA, T., MUKAI, H. & ONO, Y. 2002. Centrosomal proteins CG-NAP and kendrin provide microtubule nucleation sites by anchoring gamma-tubulin ring complex. *Mol Biol Cell*, 13, 3235-45.
- TALLADA, V. A., BRIDGE, A. J., EMERY, P. A. & HAGAN, I. M. 2007. Suppression of the *Schizosaccharomyces pombe* cut12.1 cell-cycle defect by mutations in *cdc25* and genes involved in transcriptional and translational control. *Genetics*, 176, 73-83.
- TALLADA, V. A., TANAKA, K., YANAGIDA, M. & HAGAN, I. M. 2009. The *S. pombe* mitotic regulator Cut12 promotes spindle pole body activation and integration into the nuclear envelope. *J Cell Biol*, 185, 875-88.
- TANAKA, K. & HIRATA, A. 1982. Ascospore development in the fission yeasts *Schizosaccharomyces pombe* and *S. japonicus*. *J Cell Sci*, 56, 263-79.
- TANAKA, K. & KANBE, T. 1986. Mitosis in the fission yeast *Schizosaccharomyces pombe* as revealed by freeze-substitution electron microscopy. *J Cell Sci*, 80, 253-68.
- TANAKA, K., KOHDA, T., YAMASHITA, A., NONAKA, N. & YAMAMOTO, M. 2005. Hrs1p/Mcp6p on the meiotic SPB organizes astral microtubule arrays for oscillatory nuclear movement. *Curr Biol*, 15, 1479-86.
- TANENBAUM, M. E. & MEDEMA, R. H. 2010. Mechanisms of centrosome separation and bipolar spindle assembly. *Dev Cell*, 19, 797-806.
- TANG, X., JIN, Y. & CANDE, W. Z. 2006. Bqt2p is essential for initiating telomere clustering upon pheromone sensing in fission yeast. *J Cell Biol*, 173, 845-51.
- TANGE, Y., FUJITA, A., TODA, T. & NIWA, O. 2004. Functional dissection of the gamma-tubulin complex by suppressor analysis of *gtb1* and *alp4* mutations in *Schizosaccharomyces pombe*. *Genetics*, 167, 1095-107.
- TANGE, Y., HORIO, T., SHIMANUKI, M., DING, D. Q., HIRAOKA, Y. & NIWA, O. 1998. A novel fission yeast gene, *tht1+*, is required for the fusion of nuclear envelopes during karyogamy. *J Cell Biol*, 140, 247-58.
- TARICANI, L., TEJADA, M. L. & YOUNG, P. G. 2002. The fission yeast ES2 homologue, *Bis1*, interacts with the *Ish1* stress-responsive nuclear envelope protein. *J Biol Chem*, 277, 10562-72.
- THON, G. & VERHEIN-HANSEN, J. 2000. Four chromo-domain proteins of *Schizosaccharomyces pombe* differentially repress transcription at various chromosomal locations. *Genetics*, 155, 551-68.
- TOMITA, K. & COOPER, J. P. 2007. The telomere bouquet controls the meiotic spindle. *Cell*, 130, 113-26.
- TOMLIN, G. C., MORRELL, J. L. & GOULD, K. L. 2002. The spindle pole body protein Cdc11p links Sid4p to the fission yeast septation initiation network. *Mol Biol Cell*, 13, 1203-14.
- TRELLES-STICKEN, E., DRESSER, M. E. & SCHERTHAN, H. 2000. Meiotic telomere protein Ndj1p is required for meiosis-specific telomere distribution, bouquet formation and efficient homologue pairing. *J Cell Biol*, 151, 95-106.
- TSOU, M. F. & STEARNS, T. 2006. Mechanism limiting centrosome duplication to once per cell cycle. *Nature*, 442, 947-51.

- TUZON, C. T., BORGSTROM, B., WEILGUNY, D., EGEL, R., COOPER, J. P. & NIELSEN, O. 2004. The fission yeast heterochromatin protein Rik1 is required for telomere clustering during meiosis. *J Cell Biol*, 165, 759-65.
- TZUR, Y. B., WILSON, K. L. & GRUENBAUM, Y. 2006. SUN-domain proteins: 'Velcro' that links the nucleoskeleton to the cytoskeleton. *Nat Rev Mol Cell Biol*, 7, 782-8.
- UZAWA, S., LI, F., JIN, Y., MCDONALD, K. L., BRAUNFELD, M. B., AGARD, D. A. & CANDE, W. Z. 2004. Spindle pole body duplication in fission yeast occurs at the G1/S boundary but maturation is blocked until exit from S by an event downstream of *cdc10+*. *Mol Biol Cell*, 15, 5219-30.
- VARDY, L. & TODA, T. 2000. The fission yeast gamma-tubulin complex is required in G(1) phase and is a component of the spindle assembly checkpoint. *EMBO J*, 19, 6098-111.
- VENKATRAM, S., JENNINGS, J. L., LINK, A. & GOULD, K. L. 2005. Mto2p, a novel fission yeast protein required for cytoplasmic microtubule organization and anchoring of the cytokinetic actin ring. *Mol Biol Cell*, 16, 3052-63.
- VENKATRAM, S., TASTO, J. J., FEOKTISTOVA, A., JENNINGS, J. L., LINK, A. J. & GOULD, K. L. 2004. Identification and characterization of two novel proteins affecting fission yeast gamma-tubulin complex function. *Mol Biol Cell*, 15, 2287-301.
- VEROLLET, C., COLOMBIE, N., DAUBON, T., BOURBON, H. M., WRIGHT, M. & RAYNAUD-MESSINA, B. 2006. *Drosophila melanogaster* gamma-TuRC is dispensable for targeting gamma-tubulin to the centrosome and microtubule nucleation. *J Cell Biol*, 172, 517-28.
- VOGEL, S. K., PAVIN, N., MAGHELLI, N., JULICHER, F. & TOLIC-NORRELYKKE, I. M. 2009. Self-organization of dynein motors generates meiotic nuclear oscillations. *PLoS Biol*, 7, e1000087.
- VOGT, N., KOCH, I., SCHWARZ, H., SCHNORRER, F. & NUSSLEIN-VOLHARD, C. 2006. The gammaTuRC components Grip75 and Grip128 have an essential microtubule-anchoring function in the *Drosophila* germline. *Development*, 133, 3963-72.
- WADE, R. H. 2009. On and around microtubules: an overview. *Mol Biotechnol*, 43, 177-91.
- WANG, X., YANG, Y., DUAN, Q., JIANG, N., HUANG, Y., DARZYNKIEWICZ, Z. & DAI, W. 2008. sSgo1, a major splice variant of Sgo1, functions in centriole cohesion where it is regulated by Plk1. *Dev Cell*, 14, 331-41.
- WEST, R. R., VAISBERG, E. V., DING, R., NURSE, P. & MCINTOSH, J. R. 1998. *cut11(+)*: A gene required for cell cycle-dependent spindle pole body anchoring in the nuclear envelope and bipolar spindle formation in *Schizosaccharomyces pombe*. *Mol Biol Cell*, 9, 2839-55.
- WIESE, C. & ZHENG, Y. 2000. A new function for the gamma-tubulin ring complex as a microtubule minus-end cap. *Nat Cell Biol*, 2, 358-64.

- WINEY, M., HOYT, M. A., CHAN, C., GOETSCH, L., BOTSTEIN, D. & BYERS, B. 1993. NDC1: a nuclear periphery component required for yeast spindle pole body duplication. *J Cell Biol*, 122, 743-51.
- YAMAMOTO, A., KITAMURA, K., HIHARA, D., HIROSE, Y., KATSUYAMA, S. & HIRAOKA, Y. 2008. Spindle checkpoint activation at meiosis I advances anaphase II onset via meiosis-specific APC/C regulation. *J Cell Biol*, 182, 277-88.
- YAMAMOTO, A., WEST, R. R., MCINTOSH, J. R. & HIRAOKA, Y. 1999. A cytoplasmic dynein heavy chain is required for oscillatory nuclear movement of meiotic prophase and efficient meiotic recombination in fission yeast. *J Cell Biol*, 145, 1233-49.
- YAMAMOTO, M. 1996. Regulation of meiosis in fission yeast. *Cell Struct Funct*, 21, 431-6.
- YANG, J., ADAMIAN, M. & LI, T. 2006. Rootletin interacts with C-Nap1 and may function as a physical linker between the pair of centrioles/basal bodies in cells. *Mol Biol Cell*, 17, 1033-40.
- YOUDES, J. L., METS, D. G., MCILWRAITH, M. J., MARTIN, J. S., WARD, J. D., NJ, O. N., ROSE, A. M., WEST, S. C., MEYER, B. J. & BOULTON, S. J. 2010. RTEL-1 enforces meiotic crossover interference and homeostasis. *Science*, 327, 1254-8.
- ZHANG, J. & MEGRAW, T. L. 2007. Proper recruitment of gamma-tubulin and D-TACC/Msps to embryonic Drosophila centrosomes requires Centrosomin Motif 1. *Mol Biol Cell*, 18, 4037-49.
- ZHENG, Y., JUNG, M. K. & OAKLEY, B. R. 1991. Gamma-tubulin is present in Drosophila melanogaster and Homo sapiens and is associated with the centrosome. *Cell*, 65, 817-23.
- ZHENG, Y., WONG, M. L., ALBERTS, B. & MITCHISON, T. 1995. Nucleation of microtubule assembly by a gamma-tubulin-containing ring complex. *Nature*, 378, 578-83.
- ZIMMERMAN, W. C., SILLIBOURNE, J., ROSA, J. & DOXSEY, S. J. 2004. Mitosis-specific anchoring of gamma tubulin complexes by pericentrin controls spindle organization and mitotic entry. *Mol Biol Cell*, 15, 3642-57.
- ZYSS, D. & GERGELY, F. 2009. Centrosome function in cancer: guilty or innocent? *Trends Cell Biol*, 19, 334-46.